Secondary Metabolites from the Endophytic Fungus
Aplosporella javeedii

Inaugural dissertation

for the attainment of the title of doctor
in the Faculty of Mathematics and Natural Sciences
at the Heinrich Heine University Düsseldorf

presented by

Ying Gao

from Jiangxi, P. R. China

Düsseldorf, 12 2020

from the Institute of Pharmaceutical Biology and Biotechnology
at the Heinrich Heine University Düsseldorf

Declaration of academic honesty/Erklärung

Hiermit erkläre ich ehrenwörtlich, dass ich die vorliegende Dissertation mit dem Titel " Sekundärmetaboliten aus dem endophytischen Pilz *Aplosporella javeedii* " selbst angefertigt habe. Außer den angegebenen Quellen und Hilfsmitteln wurden keine weiteren verwendet. Diese Dissertation wurde weder in gleicher noch in abgewandelter Form in einem anderen Prüfungsverfahren vorgelegt. Weiterhin erkläre ich, dass ich früher weder akademische Grade erworben habe, noch dies versucht habe.

Düsseldorf, den 05.12.2020

Ying Gao

Content

Abstract

In the process of long-term coexistence and evolution between endophytic fungi and host plants, especially medicinal plants, endophytic fungi have evolved to produce a large number of various types of secondary metabolites with novel structures and prominent biological activities. Among them, unusual and rarely studied endophytic fungi can provide opportunities to discover new natural products that can be helpful in the discovery of lead structures. During our research on secondary metabolites from endophytic fungi, the endophyte *Aplosporella javeedii*, which had hardly been studied so far, was isolated from the traditional Chinese medicinal plant *Orychophragmus violaceus* (L.) O. E. Schul (Brassicaceae).The projects involved in this dissertation mainly focus on the isolation and identification of bioactive secondary metabolites from the axenic culture of *A. javeedii*, as well as from OSMAC fungal cultures aiming at enhancing the chemical diversity of fungal secondary metabolites. The structures of the isolated secondary metabolites were elucidated by 1D, 2D NMR spectroscopy and by mass spectrometry, as well as by DFT-NMR, TDDFT-ECD and SOR calculations. The pure compounds were investigated for their cytotoxicity against the L5178Y tumor cell line, as well as against human Jurkat J16 and Ramos tumor cells. Moreover, their antimicrobial activities were tested against *Candida albicans*, *Mycobacterium tuberculosis* H37Rv, *Staphylococcus aureus*, *Acinetobacter baumannii* and other strains.

In summary, 13 natural products including 9 new compounds were isolated from the axenic fermentation of *A. javeedii*, whereas 12 natural products including 11 new compounds were isolated from the OSMAC fermentation of *A. javeedii* on solid rice medium in the presence of $NaNO_3$ or monosodium glutamate. This dissertation reflects the results from three manuscripts. The following abstracts are excerpts from the respective manuscripts:

Antifungal polyketide derivatives from the endophytic fungus Aplosporella javeedii (Ying Gao, Lin Wang, Rainer Kalscheuer, Zhen Liu, and Peter Proksch. *Bioorganic & Medicinal Chemistry*, 2020, 28, 115456.)

Six new polyketides aplojaveediins A–F (**1–6**) were isolated from the endophytic fungus *Aplosporella javeedii* associated with the host plant *Orychophragmus violaceus* (Brassicaceae). The structures of the new metabolites were elucidated by analysis of their NMR and MS data. Compound **1** exhibited antifungal activity against the hyphae form of *Candida albicans* strain ATCC 24433 in the agar plate diffusion assay and the microbroth dilution assay. The kinetic of killing of *C. albicans* cells for compound **1** was considerably faster than that of the positive control hygromycin B. Compounds **1** and **6** also exhibited moderate antibacterial activities against sensitive (ATCC 29213) and drug-resistant (ATCC 700699) strains of *Staphylococcus aureus*.

Sesterterpenes and macrolide derivatives from the endophytic fungus Aplosporella javeedii (Ying Gao, Fabian Stuhldreier, Laura Schmitt, Sebastian Wesselborg, Lin Wang, Werner E. G. Müller, Rainer Kalscheuer, Zhiyong Guo, Kun Zou, Zhen Liu, Peter Proksch. *Fitoterapia*, 2020, 146, 104652.)

Five sesterterpenes (**1–5**) including two new compounds (**1** and **2**), as well as a new (**6**) and a known macrolide (**7**) were isolated from the endophytic fungus *Aplosporella javeedii*. The structures of the new compounds were elucidated by analysis of their 1D and 2D NMR and HRMS data as well as by comparison with the literature. Compound **4** and its acetyl derivatives **4a**, **4b**, **4c** which were prepared by acetylation of **4** exhibited moderate cytotoxicity against the mouse lymphoma cell line L5178Y with IC_{50} values ranging from 6.2 to 12.8 μM, respectively. Moreover, **4a** and **4c** exhibited also cytotoxicity against human leukemia (Jurkat J16) and lymphoma (Ramos) cell lines. Compound **7** showed strong cytotoxicity against the L5178Y cell line, as well as against human Jurkat J16 and Ramos cells with IC_{50}

values of 0.4, 5.8, and 4.4 μM, respectively. Mechanistic studies indicated that **7** induces apoptotic cell death. In addition, compounds **3**, **4** and **7** showed low antibacterial activities against *Mycobacterium tuberculosis* H37Rv and compound **6** against *Staphylococcus aureus*, respectively, with MICs of 100 μM. Preliminary structure-activity relationships are discussed.

Induction of new lactam derivatives from the endophytic fungus Aplosporella javeedii through an OSMAC approach (Ying Gao, Fabian Stuhldreier, Laura Schmitt, Sebastian Wesselborg, Zhiyong Guo, Kun Zou, Attila Mándi, Tibor Kurtán, Zhen Liu, and Peter Proksch. *Frontiers in Microbiology*, 2020, 11, 600983.)

Fermentation of the endophytic fungus *Aplosporella javeedii* on solid rice medium in presence of either 3.5% $NaNO_3$ or 3.5% monosodium glutamate caused a significant change of the fungal metabolite pattern compared to fungal controls grown only on rice. Chemical investigation of the former fungal extracts yielded 11 new lactam derivatives, aplosporellins A–K (**2**–**12**), in addition to the known compound, pramanicin A (**1**). All of these compounds were not detected when the fungus was grown on rice medium without these activators thereby indicating the power of this OSMAC approach. The structures of the new compounds were elucidated by one- and two- dimensional NMR spectroscopy, DFT-NMR calculations and by mass spectrometry as well as by comparison with the literature whereas the absolute configuration of the lactam core was determined by TDDFT-ECD and OR calculations. Pramanicin A (**1**) showed strong cytotoxicity against human lymphoma (Ramos) and leukemia (Jurkat J16) cells with IC_{50} values of 4.7 and 4.4 μM, respectively. Mechanistic studies indicated that **1** activates caspase-3 and induces apoptotic cell death.

Zusammenfassung

Im Verlauf der langfristigen Koexistenz und Evolution zwischen endophytischen Pilzen und Wirtspflanzen, insbesondere Heilpflanzen, haben sich endophytische Pilze entwickelt, die eine große Anzahl verschiedener Arten von Sekundärmetaboliten mit neuartigen Strukturen und z. T. herausragenden biologischen Aktivitäten produzieren. Unter diesen bieten insbesondere ungewöhnliche und selten erforschte endophytische Pilze die Möglichkeit, neue Naturstoffe zu entdecken, die bei der Entdeckung von pharmazeutisch relevanten Leitstrukturen hilfreich sein können. Während unserer Forschung zu Sekundärmetaboliten aus endophytischen Pilzen wurde der bisher selten untersuchte Endophyt *Aplosporella javeedii* aus der traditionellen chinesischen Heilpflanze *Orychophragmus violaceus* (L.) O. E. Schul (Brassicaceae) isoliert. Die an dieser Dissertation beteiligten Projekte befassten sich schwerpunktmäßig mit der Isolierung und Identifizierung bioaktiver Sekundärmetaboliten aus der axenischen Kultur von *A. javeedii* sowie aus OSMAC Pilzkulturen mit dem Ziel, die chemische Vielfalt der sekundären Pilzmetaboliten zuerweitern. Die Strukturen der isolierten Sekundärmetaboliten wurden durch 1D, 2D NMR Spektroskopie und Massenspektrometrie sowie durch DFT-NMR, TDDFT-ECD und SOR Berechnungen aufgeklärt. Die isolierten Verbindungen wurden auf ihre Zytotoxizität gegen die L5178Y Tumorzelllinie sowie gegen humane Jurkat J16 und Ramos Tumorzellen untersucht. Darüber hinaus wurden ihre antimikrobiellen Aktivitäten gegen *Candida albicans*, *Mycobacterium tuberculosis* H37Rv, *Staphylococcus aureus*, *Acinetobacter baumannii* und andere Stämme getestet.

Zusammenfassend wurden 13 Naturstoffe, darunter 9 neue Verbindungen, aus der axenischen Fermentation von *A. javeedii* isoliert, während 12 Naturstoffe, darunter 11 neue Verbindungen aus der OSMAC Fermentation von *A. javeedii* auf

festem Reismedium in Gegenwart von NaNO₃ oder Mononatrium Glutamat isoliert wurden. Diese Dissertation spiegelt die Ergebnisse von drei Manuskripten wider:

Antifungal polyketide derivatives from the endophytic fungus Aplosporella javeedii (Ying Gao, Lin Wang, Rainer Kalscheuer, Zhen Liu, and Peter Proksch. *Bioorganic & Medicinal Chemistry*, 2020, 28, 115456.)

Six new polyketides aplojaveediins A–F (**1**–**6**) were isolated from the endophytic fungus *Aplosporella javeedii* associated with the host plant *Orychophragmus violaceus* (Brassicaceae). The structures of the new metabolites were elucidated by analysis of their NMR and MS data. Compound **1** exhibited antifungal activity against the hyphae form of *Candida albicans* strain ATCC 24433 in the agar plate diffusion assay and the microbroth dilution assay. The kinetic of killing of *C. albicans* cells for compound **1** was considerably faster than that of the positive control hygromycin B. Compounds **1** and **6** also exhibited moderate antibacterial activities against sensitive (ATCC 29213) and drug-resistant (ATCC 700699) strains of *Staphylococcus aureus*.

Sesterterpenes and macrolide derivatives from the endophytic fungus Aplosporella javeedii (Ying Gao, Fabian Stuhldreier, Laura Schmitt, Sebastian Wesselborg, Lin Wang, Werner E. G. Müller, Rainer Kalscheuer, Zhiyong Guo, Kun Zou, Zhen Liu, Peter Proksch. *Fitoterapia*, 2020, 146, 104652.)

Five sesterterpenes (**1**–**5**) including two new compounds (**1** and **2**), as well as a new (**6**) and a known macrolide (**7**) were isolated from the endophytic fungus *Aplosporella javeedii*. The structures of the new compounds were elucidated by analysis of their 1D and 2D NMR and HRMS data as well as by comparison with the literature. Compound **4** and its acetyl derivatives **4a**, **4b**, **4c** which were prepared by acetylation of **4** exhibited moderate cytotoxicity against the mouse lymphoma cell line L5178Y with IC₅₀ values ranging from 6.2 to 12.8 μM, respectively. Moreover, **4a** and **4c** exhibited also cytotoxicity against human leukemia (Jurkat J16)

and lymphoma (Ramos) cell lines. Compound **7** showed strong cytotoxicity against the L5178Y cell line, as well as against human Jurkat J16 and Ramos cells with IC_{50} values of 0.4, 5.8, and 4.4 μM, respectively. Mechanistic studies indicated that **7** induces apoptotic cell death. In addition, compounds **3**, **4** and **7** showed low antibacterial activities against *Mycobacterium tuberculosis* H37Rv and compound **6** against *Staphylococcus aureus*, respectively, with MICs of 100 μM. Preliminary structure-activity relationships are discussed.

Induction of new lactam derivatives from the endophytic fungus Aplosporella javeedii through an OSMAC approach (Ying Gao, Fabian Stuhldreier, Laura Schmitt, Sebastian Wesselborg, Zhiyong Guo, Kun Zou, Attila Mándi, Tibor Kurtán, Zhen Liu, and Peter Proksch. *Frontiers in Microbiology*, 2020, 11, 600983.)

Fermentation of the endophytic fungus *Aplosporella javeedii* on solid rice medium in presence of either 3.5% $NaNO_3$ or 3.5% monosodium glutamate caused a significant change of the fungal metabolite pattern compared to fungal controls grown only on rice. Chemical investigation of the former fungal extracts yielded 11 new lactam derivatives, aplosporellins A–K (**2**–**12**), in addition to the known compound, pramanicin A (**1**). All of these compounds were not detected when the fungus was grown on rice medium without these activators thereby indicating the power of this OSMAC approach. The structures of the new compounds were elucidated by one- and two- dimensional NMR spectroscopy, DFT-NMR calculations and by mass spectrometry as well as by comparison with the literature whereas the absolute configuration of the lactam core was determined by TDDFT-ECD and OR calculations. Pramanicin A (**1**) showed strong cytotoxicity against human lymphoma (Ramos) and leukemia (Jurkat J16) cells with IC_{50} values of 4.7 and 4.4 μM, respectively. Mechanistic studies indicated that **1** activates caspase-3 and induces apoptotic cell death.

Chapter 1 Introduction

1.1 Natural products in drug discovery

Natural products which are produced by organisms such as plants, animals, or microorganisms (also called small molecules) play an essential role in drug discovery. In the global medicine market, around 35% of these products originate from natural products (Calixto 2019). In a recent review on natural products as sources of new drugs approved by Food and Drug Administration (FDA) from 01/1981 to 09/2019, around 65% of all approved anticancer drugs originated from natural products, whereas most anti-infective drugs were either natural products or derivatives (Newman *et al.* 2020). Generally, natural products can be used as drugs directly, or alternatively they can be lead compounds for structural modification or total synthesis, or they can serve as raw materials to develop a library of analogues (Bérdy 2005, Cragg *et al.* 2013, Grabowski *et al.* 2008).

There are many famous and best-selling medicines that originate from natural products. For example, the discovery of the β-lactam antibiotic agent penicillin from *Penicillium notatum* is one of the most significant milestones in modern medical research. This finding opened up the era of exploring effective drugs from natural sources. Until now, there are a series of natural penicillins and semi-synthetic penicillins used in clinic treatment (Miller 2002, Lobanovska *et al.* 2017). Other important β-lactam antibiotics are cephalosporins, which were derived from the fungus *Acremonium chrysogenum* (Hameed *et al.* 2002). Through structural modification, cephalosporins can be grouped into five generations according to their antimicrobial properties. Each newer generation has significantly greater Gram-negative and lower Gram-positive antimicrobial properties than the preceding generation. It is considered that the fourth-generation cephalosporins exhibit a

broad-spectrum of antimicrobial activity (Chaudhry *et al.* 2019) and the fifth-generation, such as ceftobiprole exhibit anti-MRSA activity (Chahine *et al.* 2011).

Paclitaxel (Taxol), which was isolated from the plant *Taxus brevifolia* and the fungal endophyte *Taxomyces andreanae* is currently the most successful anticancer drug (Stierle *et al.* 1993). It can suppress the normal function of microtubules during cell division (Jordan *et al.* 2004) and is approved for the treatment of breast, pancreatic, ovarian, Kaposi's sarcoma, and non-small-cell lung cancers. Phenylahistin, which was isolated from *Aspergillus ustus* exhibits colchicine like anti-microtubule activity (Kanoh *et al.* 1997). Its synthetic derivative plinabulin is active against multidrug-resistant tumor cell lines (Nicholson *et al.* 2006) and is now in Phase III clinical trials for the treatment of non-small cell lung cancer since 2016 (Saxena *et al.* 2019).

Except for those antibacterial and anticancer agents, many other important drugs such as the lipid-lowering agents simvastatin (Kishore *et al.* 2018) and lovastatin (Tobert 2003), the antihypertensive agents captopril (Opie *et al.* 1995) and enalapril (Gomez *et al.* 1985), the antifungal agents griseofulvin (Araujo *et al.* 1990) and amphotericin B (Hamill 2013), as well as the antimalarial agent artemisinin (Klayman 1985) are all derived from natural sources.

In the process of searching for new chemical entities and target structures, research in bio-diversified areas, identification of the bioactive constituents of traditional remedies, and search for new compound templates can significantly broaden the sources of new natural products (Khan 2018). Moreover, with the emergence of novel technologies such as DNA sequencing, genomics/metagenomics, synthetic biology, genome editing technologies, big data, profiling techniques, computational biology techniques, and artificial intelligence, the discovery of target natural products and the development of new drugs are greatly accelerated (Thomford *et al.* 2018, Zhang *et al.* 2017, Chavali *et al.* 2017).
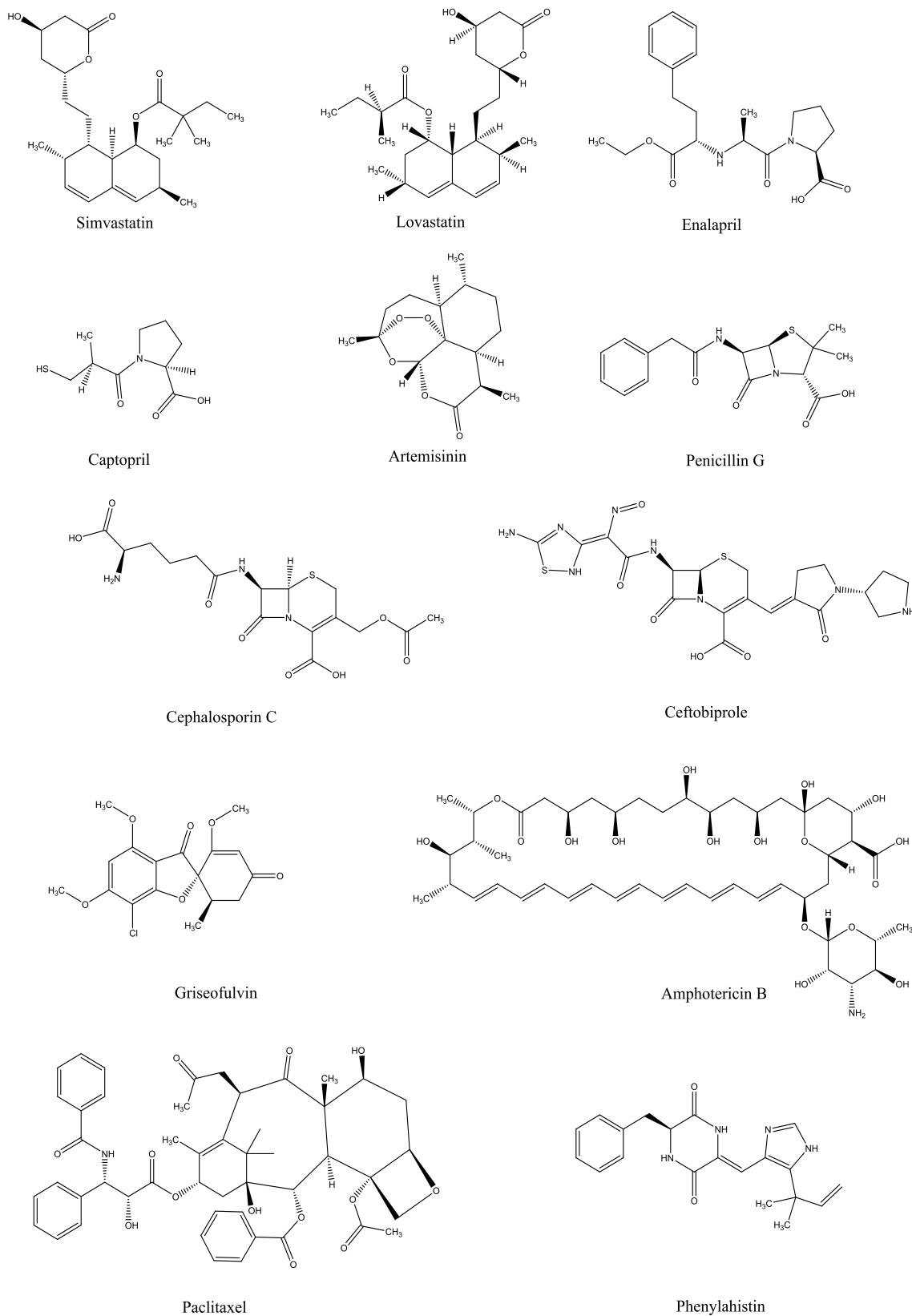
Simvastatin

Lovastatin

Enalapril

Captopril

Artemisinin

Penicillin G

Cephalosporin C

Ceftobiprole

Griseofulvin

Amphotericin B

Paclitaxel

Phenylahistin

Figure 1.1 Drugs and drug leads derived from natural products

1.2 Endophytic fungi as an important source of bioactive compounds

During drug discovery from natural sources, plants that served as the primary sources of natural products have been extensively explored for centuries. However, with environmental degradation and loss of biodiversity, more and more attention is now given to endophytes, especially endophytic fungi associated with plants rather than to plants themselves (Gouda *et al.* 2016). There are millions of different endophytic fungi that inhabit around 300,000 known species of higher plants. Still, less than 1% of them have been studied, suggesting that endophytic fungi represent abundant reservoirs for the discovery of novel bioactive agents (Patil *et al.* 2016, Fouda *et al.* 2015).

Endophytic fungi are fungi that colonize living plant tissues during a part or during all of their life cycle without causing any immediate, apparent disease to the host plants (Torres *et al.* 2012). With the long-term coexistence and evolution, endophytic fungi have developed mutually beneficial relationships with their host plants and play critical roles in preserving the natural balance, which can significantly influence the production of secondary metabolites. Endophytic fungi may improve the plant immune system, pathogen resistance, nutrient acquisition, and tolerance to biotic or abiotic stresses (Yan *et al.* 2019, Egamberdieva *et al.* 2017). Conversely, the host species and genotype, host developmental stage, the colonization area of the host, and environmental condition have also an impact on the population of endophytic fungi (Strobel *et al.* 2003, Khare *et al.* 2018). From these two aspects, endophytic fungi can produce a large number of various types of secondary metabolites, with many of them containing novel structures and showing excellent pharmacological and biological properties (Noor *et al.* 2020). These secondary metabolites can be categorized into different chemical groups, such as alkaloids, flavonoids, polyketides, quinones, steroids, peptides, terpenoids,

phenolics, saponins, tannins, tetralones, xanthones, and so on (Shukla *et al.* 2014, Patil *et al.* 2016, Gouda *et al.* 2016). Many of them show antimicrobial, anticancer, antioxidant, cytotoxic, antiparasitic, antileishmanial, immunomodulatory, antiproliferative, or antidiabetic activities (Strobel 2018, Khiralla *et al.* 2016, Saxena *et al.* 2019). Therefore, endophytic fungi show a significant potential for exploring pharmaceutical and biological agents.

Exploring endophytic fungi, which can produce bioactive metabolites, is always challenging. The first and most crucial step is the selection of plants. It is hypothesized that there are at least three strategies to select plants which are likely to harbor novel endophytes: plants growing in significant biodiversity areas of the world such as in the Amazon basin, in tropical rain forest; plants growing in extreme environments such as in the Arctic or Antarctic area, in geothermal, saline or alkaline soils, in deserts or plateaus, in the oceans or mangrove forests; or medicinal plants which are used as treatment materials in traditional folk medicines (Patil *et al.* 2016, Verma *et al.* 2009).

The human use of medicinal plants for the treatment of diseases can be traced back for millennia. Until now, plants still play an essential role in traditional medicine such as traditional Chinese medicine, Ayurveda, Kampo, traditional Korean medicine, and Unani, as well as in modern medicine for further drug discovery (Yuan *et al.* 2016). Plants contain a tremendous variety of bioactive compounds, which can deeply influence endophytic fungi. For one aspect, it is believed that some endophytic fungi can produce the same or similar bioactive metabolites as their host plants possibly due to gene transfer and recombination between hosts and endophytes (Patil *et al.* 2016, Venieraki *et al.* 2017, Aly *et al.* 2010). For example, paclitaxel was isolated from *Taxomyces andreanae,* which is a fungal endophyte of *Taxus brevifolia*. However, the host plant was the original source of this compound (Stierle *et al.* 1993). Vincristine which was originally

obtained from the plant *Catharanthus roseus* can be also detected in its endophytic fungus *Fusarium oxysporum* (Kumar *et al.* 2013). Camptothecin was initially described from the plant *Camptotheca acuminata*. Later, this compound and its analogues were also detected in the plant's endophytic fungus *Fusarium solani* (Kusari *et al.* 2009). Due to the high stress and chemical environment in medicinal plants, as well as the complex interspecies crosstalk between endophytes and hosts, endophytic fungi can produce various bioactive secondary metabolites which are important for their survival and beneficial. These metabolites are mostly different from those of host plants and feature unique structural characteristics (Aly *et al.* 2011, Jia *et al.* 2016). Thus, endophytic fungi of medicinal plants are a precious treasure house of bioactive and structurally novel natural products usually not found in plants.

Recent examples of bioactive compounds from endophytic fungi associated with medicinal plants include: the unusual chlorinated flavonoid chlorflavonin, which was isolated from the endophytic fungus *Mucor irregularis* of the Cameroonian medicinal plant *Moringa stenopetala*, exhibited strong antimycobacterial activity. Mapping of resistance-mediating mutations revealed the specific inhibition of acetohydroxyacid synthase catalytic subunit IlvB1 by chlorflavonin, causing combined auxotrophies to branched-chain amino acids and pantothenic acid. Moreover, it also displayed synergistic effects with isoniazid especially delamanid, leading to complete sterilization in liquid culture in combination treatment (Rehberg *et al.* 2018). Another example is the mycotoxin phomoxanthone A derived from the endophytic fungus *Phomopsis longicolla,* which was isolated from the medicinal mangrove plant *Sonneratia caseolaris* growing in South China. Phomoxanthone A disturbs the inner mitochondrial membrane within seconds and shows intense anticancer activity (Böhler *et al.* 2018, Wang *et al.* 2019, Rönsberg *et al.* 2013).
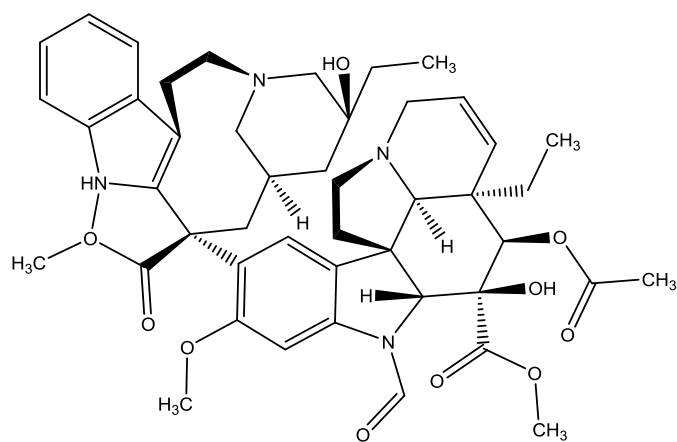
Vincristine
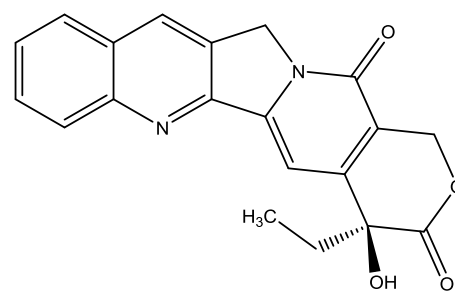
Camptothecin
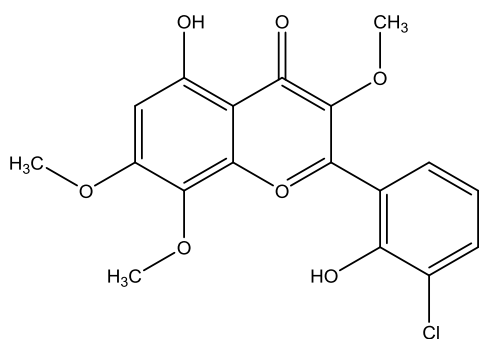
Chlorflavonin
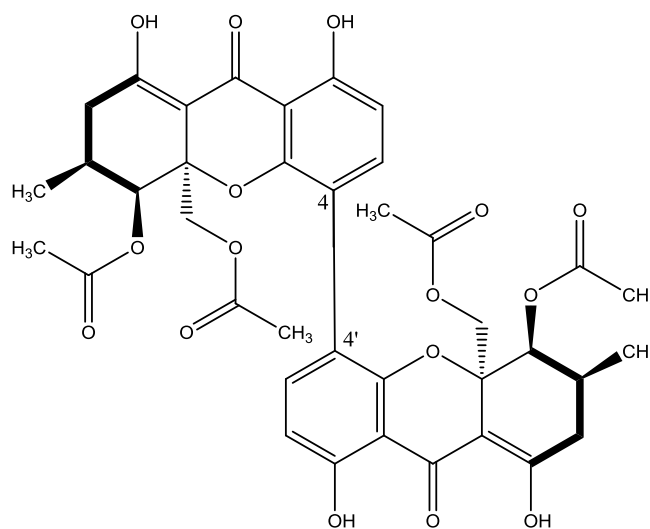
Phomoxanthone A

Figure 1.2 Bioactive metabolites isolated from endophytic fungi

1.3 OSMAC approach as an effective strategy for unlocking silent gene clusters and maximizing the diversity of fungal secondary metabolites

Conventional screening of endophytes that are cultivated under standard laboratory conditions often fails to express the full metabolic pathways of endophytes and leads to a limited chemical diversity of isolated compounds (Pan *et al.* 2019). Recent research of genome sequencing of fungi revealed that numerous biosynthetic gene clusters that can produce secondary metabolites are kept silent or cryptic under standard culturing conditions (Van Lanen *et al.* 2006). Therefore, the activation of silent or cryptic biosynthetic gene clusters can powerfully induce or maximize the diversity of fungal secondary metabolites (Yu *et al.* 2018). Nowadays, some useful strategies can be employed to activate silent biosynthetic gene clusters, such as the "One Strain MAny Compounds" (OSMAC) approach, co-cultivation of fungi with two or more microbes (Newman *et al.* 2017), epigenetic modulation (Zheng *et al.* 2008), or genetic modulation (Li *et al.* 2017).

The OSMAC approach is considered the simplest and most effective strategy for diversified fungal metabolic production by changing the cultivation parameters. These cultivation parameters can include: medium composition such as carbon/nitrogen ratio, salinity, metal ions, physical conditions such as temperature, pH, oxygen concentration, cultivation conditions such as solid or liquid, static or dynamic cultivation, addition of enzyme inhibitors/inducers or biosynthetic precursors (Bode *et al.* 2002, Pan *et al.* 2019, Yu *et al.* 2018). A large number of experiments have confirmed that the OSMAC strategy can provide a quick and powerful method to enhance the diversity of fungal secondary metabolites, thereby obtaining new drug leads and avoiding re-isolation of known compounds. Recent successful studies on OSMAC application can be used as examples.

Tran-Cong *et al.* added 2% tryptophan to rice medium which led to the isolation of a new strongly cytotoxic bismacrolactone from the endophytic fungus *Trichocladium sp.*, which had been isolated from roots of *Houttuynia cordata* (Tran-Cong *et al.* 2019). Li *et al.* used two different media, including solid rice medium and potato dextrose broth (PDB) which resulted in the isolation of two new compounds asperspin A and asperther A from the sponge-derived fungus *Aspergillus* sp. LS34 (Li *et al.* 2019). Ariantari *et al.* added a mixture of salts ($MgSO_4$, $NaNO_3$, and $NaCl$) to solid Czapek medium, thereby inducing the accumulation of nine new secondary metabolites from the endophytic fungus *Bulgaria inquinans* obtained from mistletoe (*Viscum album*) (Ariantari *et al.* 2019). Wang *et al.* added 3.5% $NaNO_3$ to solid rice medium, which caused a significant change of the metabolite pattern of the endophytic fungus *Aspergillus aculeatus* as indicated by HPLC analysis. Subsequent isolation yielded ten new substituted L-tryptophan-L-phenyllactic acid conjugates (Wang *et al.* 2018). Abdelwahab *et al.* cultured the endophytic fungus *Aspergillus versicolor* in liquid Wickerham medium containing 3.5% DMSO, which resulted in the isolation of an additional three known secondary metabolites that were not present in the fungal fermentation on rice medium (Abdelwahab *et al.* 2018).

1.4 The endophytic fungus *Aplosporella javeedii*

Aplosporella javeedii was first discovered and identified from healthy branches of *Celtis africana* Burm.f. (*Cannabaceae*) and *Searsia lancea* (L.f.) F.A. Barkley (*Anacardiaceae*) in South Africa in 2013. Its name is derived from the Persian phrase "Javeed Jami", meaning "long-lived" (Jami *et al.* 2014). *A. javeedii* belongs to the genus of *Aplosporella,* which comes from the family *Aplosporellaceae* in *Botryosphaeriales*. So far, around 300 species of this genus are listed in the Index Fungorum. Many members of this genus are associated with

canker and dieback disease on woody hosts, and nearly all of them were isolated from woody plants (Slippers *et al.* 2013, Ekanayaka *et al.* 2016). However, it is known that *aplospore* fungi can be isolated from both healthy and disease hosts since endophytic fungi may turn into pathogens once the host plant is subjected to severe stress or aging (Fan *et al.* 2015, Slippers *et al.* 2007).

Until now, there are limited reports on *A. javeedii*. Except for the first discovery in South Africa, other isolations and identifications were reported in China. In 2015, Fan *et al.* collected *A. javeedii* from branch cankers of five tree species, i.e. *Albizia julibrissin Durazz.* (Fabaceae Lindl.), *Broussonetia papyrifera* (L.) Vent. (Moraceae Gaudich.), *Gleditsia sinensis* Lam. (Fabaceae), *Juniperus chinensis* L. (Cupressaceae Gray), and *Styphnolobium japonicum* (L.) Schott (Fabaceae) (Fan *et al.* 2015). This report represents the first record of *A. javeedii* in China. Later, Zhu *et al.* did research on botryosphaerialean fungi associated with canker and dieback of tree hosts in Dongling Mountain of China and extended the host range of *A. javeedii* to *Rhus typhina* (Anacardiaceae) and *Ziziphus jujube* (Rhamnaceae) (Zhu *et al.* 2018). In 2019, Jia *et al*. identified *A. javeedii* from branches of mulberry (*Morus alba*) in China (Jia *et al.* 2019). These reports focus on fungal biology such as phylogenetic analyses, taxonomy, morphology, and so on. There is no report on secondary metabolites of *A. javeedii,* which prompted us to investigate this fungus.

1.5 Aims and significance of this study

Endophytic fungi play an essential role in exploring pharmaceutical and biological agents due to their sustainability to biosynthesize structurally diverse and bioactive molecules (Noor *et al.* 2020). An unusual and rarely researched endophytic fungus could provide more opportunity to discover new secondary metabolites. In this study, *Aplosporella javeedii* which had so far rarely been studied was isolated from healthy stem tissue of *Orychophragmus violaceus* (L.) O. E. Schul

(*Brassicaceae*) collected around Beijing. *O. violaceus* is an edible wild herb as well as a medicinal plant that is used in Traditional Chinese Medicine (TCM) for dissipating swelling and treating unknown pyrogenic infections (Hu *et al.* 2014, Zhou *et al.* 2011, Medicinal Plant Images Database 2007). In recent years, researchers also reported hepatoprotective effects for this plant (Huo *et al.* 2017). Besides, this study is the first record of *A. javeedii* isolated from a herbaceous plant.

The aims of this study mainly focused on the isolation and identification of bioactive secondary metabolites from the investigated endophytic fungus *Aplosporella javeedii*. Moreover, OSMAC approaches were used to enhance the chemical diversity of fungal secondary metabolites.

From the axenic culture of *A. javeedii* grown on solid rice medium, six new polyketide derivatives, five sesterterpenes including two new compounds, as well as a new and a known macrolide were isolated. One of the polyketide derivatives exhibited antifungal activity against the hyphae form of *Candida albicans* strain ATCC 24433 in the agar plate diffusion assay and in the microbroth dilution assay. Its kinetic of the killing of *C. albicans* cells was considerably faster than that of the positive control hygromycin B. A series of the isolated sesterterpenes and their acetyl derivatives exhibited moderate cytotoxicity against the mouse lymphoma cell line L5178Y, as well as against human leukemia (Jurkat J16) and lymphoma (Ramos) cell lines. Moreover, the know macrolide mutolide also displayed potent cytotoxicity against those three cell lines. Mechanistic studies indicated that mutolide induces apoptotic cell death. Besides, some of these compounds showed antibacterial activities against *Mycobacterium tuberculosis* H37Rv and *Staphylococcus aureus*. (Chapter 2 Publication 1 and Chapter 3 Publication 2)

Fermentation of *A. javeedii* on solid rice media in the presence of different halogen salts such as NaNO$_3$, NaI or monosodium glutamate induced the accumulation of very different natural product patterns as evident from HPLC

comparison of their crude extracts. The addition of either 3.5% $NaNO_3$ or 3.5% monosodium glutamate to rice medium induced the accumulation of a set of new lactam derivatives and the known lactam compound pramanicin A, all of which cannot be detected in axenic rice cultures lacking these activators. One- and two-dimensional NMR spectroscopy, DFT-NMR calculations, mass spectrometry as well as comparison with the literature were used for the structure elucidation of the new compounds. Moreover, TDDFT-ECD and OR calculations determined the absolute configuration of the lactam core. Among them, pramanicin A showed strong cytotoxicity against human lymphoma (Ramos) and leukemia (Jurkat J16) cells. Mechanistic studies indicated that pramanicin A activates caspase-3 and induces apoptotic cell death. (Chapter 4 Publication 3)

Chapter 2 Publication 1

Antifungal polyketide derivatives from the endophytic fungus *Aplosporella javeedii*

Published in: "Bioorganic & Medicinal Chemistry"

Impact factor: 3.073

Contribution: First authorship, contributed to 70% of this publication. The first author conducted most of the laboratory work including extraction, isolation, literature research, and manuscript preparation.

Reprinted by permission from "**Ying Gao**, Lin Wang, Rainer Kalscheuer, Zhen Liu, and Peter Proksch (2020) Antifungal polyketide derivatives from the endophytic fungus *Aplosporella javeedii*." *Bioorganic & Medicinal Chemistry*, **28**, 115456. Copyright © 2020 Elsevier Ltd.

.

Contents lists available at ScienceDirect

Bioorganic & Medicinal Chemistry

journal homepage: www.elsevier.com/locate/bmc

Antifungal polyketide derivatives from the endophytic fungus *Aplosporella javeedii*

Ying Gao[a], Lin Wang[a], Rainer Kalscheuer[a], Zhen Liu[a,*], Peter Proksch[a,b,*]

[a] *Institute of Pharmaceutical Biology and Biotechnology, Heinrich Heine University Düsseldorf, Universitätsstrasse 1, 40225 Düsseldorf, Germany*
[b] *Hubei Key Laboratory of Natural Products Research and Development, College of Biological and Pharmaceutical Sciences, China Three Gorges University, Yichang 443002, People's Republic of China*

ABSTRACT

Six new polyketides aplojaveediins A–F (**1–6**) were isolated from the endophytic fungus *Aplosporella javeedii* associated with the host plant *Orychophragmus violaceus* (Brassicaceae). The structures of the new metabolites were elucidated by analysis of their NMR and MS data. Compound **1** exhibited antifungal activity against the hyphae form of *Candida albicans* strain ATCC 24433 in the agar plate diffusion assay and the microbroth dilution assay. The kinetic of killing of *C. albicans* cells for compound **1** was considerably faster than that of the positive control hygromycin B. Compounds **1** and **6** also exhibited moderate antibacterial activities against sensitive (ATCC 29213) and drug-resistant (ATCC 700699) strains of *Staphylococcus aureus*.

1. Introduction

Endophytic fungi are firmly established as sources of new bioactive metabolites and have been shown to accumulate diverse groups of compounds such as alkaloids, terpenoids, steroids, phenols, quinones, xanthones, and peptides.[1,2,3,4,5] Due to this pronounced chemical diversity, endophytic fungi represent an important potential source of new medicinal and biotechnological agents. During our ongoing research on new bioactive secondary metabolites from endophytic fungi,[6,7] *Aplosporella javeedii* was isolated from stem tissue of *Orychophragmus violaceus* (L.) O. E. Schul (*Brassicaceae*) collected around Beijing. *O. violaceus* is an edible wild herb as well as a medicinal plant that is used in Traditional Chinese Medicine (TCM).[8,9] It is recorded in the TCM literature for dissipating swelling and for treating unknown pyrogenic infections.[10] In recent years, researchers also reported hepatoprotective effects for this plant.[11] *A. javeedii* is a member of the fungal family *Aplosporellaceae* and is usually associated with canker and dieback disease of woody plants. It was first isolated and identified from wood sections of *Celtis africana* Burm.f. (*Cannabaceae*) and *Searsia lancea* (L.f.) F.A. Barkley (*Anacardiaceae*) in South Africa in 2013.[12] Other records are from China and came from woody trees of the *Fabaceae*, *Cupressaceae*,[13] *Rhamnaceae*,[14] and *Moraceae*.[15] To our best knowledge, this is the first record of *A. javeedii* from a host plant of the *Brassicaceae*. Until now, there are no reports on secondary metabolites of *A. javeedii* which prompted us to investigate this fungus. When grown

on solid rice medium *A. javeedii* yielded six new polyketides (**1–6**) (Fig. 1). In this paper, we report the isolation and structure elucidation of these polyketides, as well as their antifungal and antibacterial activities.

2. Results and discussion

Compound **1** was obtained as colorless crystals, with UV absorptions at λ_{max} 208, 220 and 298 nm. Its molecular formula was established as $C_{13}H_{18}O_3$ on the basis of prominent pseudomolecular ion peaks at *m/z* 223.1332 $[M + H]^+$ and 221.1178 $[M - H]^+$ in the HRESIMS spectrum, indicating five degrees of unsaturation. The ^1H NMR data of **1** (Table 1) showed one aldehyde proton at δ_H 10.01 (s, H-7), one aromatic proton at δ_H 6.24 (s, H-5), one aromatic methyl group at δ_H 1.99 (s, Me-8). The ^{13}C NMR data of **1** (Table 1) displayed one aldehyde carbon at δ_C 194.1 (C-7) and six aromatic carbons at δ_C 165.2 (C-2), 165.0 (C-6), 147.9 (C-4), 112.7 (C-1), 110.2 (C-5), and 110.1 (C-3). The HMBC correlations (Fig. 2) from H-7 to C-1, C-2, and C-6, from Me-8 to C-2, C-3, and C-4, and from H-5 to C-1, C-3, and C-6 established the presence of a pentasubstituted benzene ring with an aldehyde group and a methyl group at C-1 and C-3, respectively. The remaining NMR data are characteristic signals of a *n*-pentyl chain, which was further confirmed by the COSY correlations between H$_2$-9 (δ_H 2.80)/H$_2$-10 (δ_H 1.61), H$_2$-10/H$_2$-11 (δ_H 1.35), H$_2$-12 (δ_H 1.36)/Me-13 (δ_H 0.91) as well as by the HMBC correlations from Me-13 to C-11 (δ_C 32.7) and C-12 (δ_C 23.5). In addition,

---
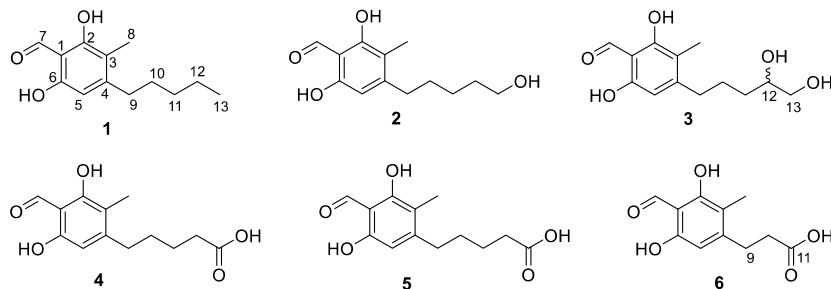
Fig. 1. Structures of new polyketides isolated from *A. javeedii.*

Table 1
^1H and ^{13}C NMR data for compounds **1–3** in methanol-d_4.

NO.	1[a]		2[a]		3[b]	
	δ_C, type	δ_H (*J* in Hz)	δ_C, type	δ_H (*J* in Hz)	δ_C, type[c]	δ_H (*J* in Hz)
1	112.7, C		112.7, C		112.7, C	
2	165.2, C		165.3, C		165.3, C	
3	110.1, C		110.1, C		110.1, C	
4	147.9, C		147.8, C		147.6, C	
5	110.2, CH	6.24, s	110.3, CH	6.25, s	110.3, CH	6.26, s
6	165.0, C		165.3, C		165.2, C	
7	194.1, C	10.01, s	194.1, C	10.03, s	194.2, C	10.05, s
8	7.1, CH₃	1.99, s	7.1, CH₃	1.99, s	7.1, CH₃	1.99, s
9	32.5, CH₂	2.80, m	32.5, CH₂	2.82, m	32.5, CH₂	2.88, ddd (13.9, 9.5, 6.1) 2.81, ddd (13.9, 9.3, 6.2)
10	33.7, CH₂	1.61, m	33.8, CH₂	1.64, m	30.0, CH₂	1.80, m 1.67, m
11	32.7, CH₂	1.35, m	26.7, CH₂	1.44, m	34.0, CH₂	1.59, m 1.43, m
12	23.5, CH₂	1.36, m	33.4, CH₂	1.56, m	72.9, CH	3.59, m
13	14.3, CH₃	0.91, t (6.9)	62.8, CH₂	3.55, t (6.4)	67.4, CH₂	3.45, dd (11.1, 4.8) 3.42, dd (11.1, 6.3)

[a] Recorded at 300 (^1H) and 75 MHz (^{13}C).
[b] Recorded at 600 (^1H) and 150 MHz (^{13}C).
[c] Data extracted from HSQC and HMBC spectra.

Fig. 2. COSY and key HMBC correlations for compound **1**.

the HMBC correlations from H-5 to C-9 (δ_C 32.5) and from H₂-9 to C-3, C-4, and C-5 indicated the location of the *n*-pentyl chain at C-4. The substitution of two hydroxy group at C-2 and C-6 of the benzene ring was suggested by the chemical shifts of C-2 and C-6 as well as the molecular formula of **1**. Thus, compound **1** was determined as 2,6-dihydroxy-3-methyl-4-pentylbenzaldehyde, for which the trivial name aplojaveediin A is proposed.

The molecular formula of **2** was determined as $C_{13}H_{18}O_4$ by the HRESIMS data, containing an additional oxygen atom when compared to **1**. The NMR data of **2** (Table 1) were similar to those of compound **1** except for the replacement of signals of the terminal methyl group in the side chain by signals of an oxygenated methylene resonating at δ_C 62.8 (C-13) and δ_H 3.55 (2H, t, *J* = 6.4 Hz, H₂-13). The COSY correlations between H₂-13/H₂-12 (δ_H 1.56), H₂-12/H₂-11 (δ_H 1.44), H₂-11/

H₂-10 (δ_H 1.64), H₂-10/H₂-9 (δ_H 2.82) together with the HMBC correlations from H₂-13 to C-11 (δ_C 26.7) and C-12 (δ_C 33.4) indicated the location of a hydroxy group at C-13 in the side chain of **2**. Detailed analysis of the 2D NMR spectra of **2** revealed that the remaining substructure of **2** was identical to that of **1**. Thus, the structure of **2** was elucidated as shown.

Compound **3** has the molecular formula $C_{13}H_{18}O_5$ as deduced from the HRESIMS data, containing an additional oxygen atom when compared to **2**. Comparison of the NMR data of **2** and **3** (Table 1) suggested that they are structurally similar. The major difference is the observation of an additional oxygenated methine at δ_C 72.9 (C-12) and δ_H 3.59 (H-12) in **3**. Besides, the protons of the oxygenated methylene at C-13 appeared as two dd peaks in **3** instead of two triplet peaks in **2**. The above finding suggested the attachment of an additional hydroxy group at C-12, which was further confirmed by the COSY correlations between H₂-13/H-12/H₂-11/H₂-10/H₂-9. Due to the limited amount, the absolute configuration at C-12 of **3** was not determined.

Aplojaveediin D (**4**) was found to have the molecular formula $C_{13}H_{16}O_5$ on the basis of the HRESIMS data, accounting for six degrees of unsaturation. Its ^1H NMR data (Table 2) were similar to those of **1** but lacked signals of the terminal methyl group in the side chain. Meanwhile, the ^{13}C NMR spectrum of **4** exhibited the signal of one additional carbonyl carbon at δ_C 178.0 (C-13). The HMBC correlations from H₂-12 (δ_H 2.32, t, *J* = 6.5 Hz) to C-13, C-11 (δ_C 25.9), and C-10 (δ_C 33.3), together with the COSY correlations between H₂-12/H₂-11 (δ_H 1.67) and between H₂-10 (δ_H 1.66)/H₂-9 (δ_H 2.84) indicated a terminal carboxylic acid group in the side chain that replaced the methyl substituent of compound **1**. The remaining substructure of **4** was

Table 2
^1H and ^{13}C NMR data for compounds **4–6** in methanol-d_4.

NO.	4[a]		5[a]		6[b]	
	δ_C, type	δ_H (*J* in Hz)	δ_C, type	δ_H (*J* in Hz)	δ_C, type	δ_H (*J* in Hz)
1	112.8, C		112.7, C		112.7, C	
2	165.3, C		165.3, C		165.4, C	
3	110.1, C		110.2, C		110.2, C	
4	147.5, C		147.3, C		147.2, C	
5	110.2, CH	6.26, s	110.3, CH	6.25, s	110.1, CH	6.28, s
6	164.8, C		165.0, C		165.2, C	
7	194.2, C	10.04, s	194.1, C	10.02, s	194.3, C	10.07, s
8	7.1, CH₃	1.99, s	7.1, CH₃	1.99, s	7.1, CH₃	1.97, s
9	32.2, CH₂	2.84, t (7.0)	32.1, CH₂	2.83, t (7.3)	28.9, CH₂	3.10, t (7.8)
10	33.3, CH₂	1.66, m	33.2, CH₂	1.65, m	41.2, CH₂	2.46, t (7.8)
11	25.9, CH₂	1.67, m	25.7, CH₂	1.67, m	181.8, C	
12	35.0, CH₂	2.32, t (6.5)	34.4, CH₂	2.36, t (7.0)		
13	178.0, C		175.7, C			
13-OMe			52.0, CH₃	3.65, s		

[a] Recorded at 300 (^1H) and 75 MHz (^{13}C).
[b] Recorded at 600 (^1H) and 150 MHz (^{13}C).

identical to that of **1** as confirmed by detailed analysis of the 2D NMR spectra of **4**.

Compound **5** exhibited the molecular formula $C_{14}H_{18}O_5$ as determined by the HRESIMS data. The ^1H and ^{13}C NMR data of **5** were similar to those of **4** (Table 2). Analysis of the 2D NMR spectra revealed that both compounds shared the same benzene ring core structure. Compound **5** was identified as the C-13*O*-methyl derivative of **4**, as evident from the presence of an additional methoxy group at δ_H 3.65 (3H, s) and δ_C 52.0, together with the HMBC correlations from the protons of this additional methoxy group and H$_2$-12 (δ_H 2.36, t, $J = 7.0$ Hz) to the carbonyl carbon at δ_C 175.7 (C-13), and from H$_2$-12 to C-10 (δ_C 33.2) and C-11 (δ_C 25.7). Compound **5** could already be detected in the HPLC chromatogram of the crude fungal extract which argues for **5** being a natural product and not an artefact arising from **4** in the presence of MeOH. Moreover, incubation of **4** in MeOH for several days at room temperature failed to yield **5**.

The molecular formula of aplojaveediin F (**6**) was established as $C_{11}H_{12}O_5$ from the HRESIMS data, requiring six degrees of unsaturation. Comparison of the NMR data (Table 2) indicated compound **6** to be closely related to compound **4** except for that the side chain of **6** lacked two methylene groups when compared to **4**. The HMBC correlations from H$_2$-10 (δ_H 2.46, t, $J = 7.8$ Hz) to C-11 (δ_C 181.8) and C-4 (δ_C 147.2), and from H$_2$-9 (δ_H 3.10, t, $J = 7.8$ Hz) to C-11, C-3, C-4 and C-5 as well as the COSY correlations between H$_2$-10 and H$_2$-9 indicated the presence of a *n*-propanoic acid side chain at C-4 in **6**. Thus, the structure of **6** was elucidated as shown.

Compounds **1–6** were tested for their antibacterial activity against a panel of bacterial strains. Compound **1** exhibited moderate antibacterial activity against the sensitive *Staphylococcus aureus* strain ATCC 29213, the methicillin-resistant and vancomycin intermediate sensitive (MRSA/VISA) *S. aureus* strain ATCC 700699 and *Bacillus subtilis* (ATCC 169) with minimal inhibitory concentrations (MICs) of 50, 50 and 25 µM, respectively. Compound **6** also exhibited moderate antibacterial activity against *S. aureus* ATCC 29213 and ATCC 700699 with MICs of 25 and 50 µM, respectively. No or only a very weak antibacterial effect was observed for compounds **1** and **6** against the other tested bacterial strains (Table S1). Compounds **2–5** showed no antibacterial activity.

In addition, compounds **1–6** were tested for their antifungal activity against *Candida albicans* grown in the yeast or the hyphae form. While compounds **2–6** were inactive, compound **1** exhibited antifungal activity against the hyphae form of *C. albicans* strain ATCC 24433 with an inhibition diameter of 8 mm in the agar plate diffusion assay at a concentration of 1 mM. The compound was also active against the yeast *Saccharomyces cerevisiae* resulting in an inhibition diameter of 18 mm (Fig. S44). The MIC of compound **1** against the hyphae form of *C. albicans* strain ATCC 24433 in liquid medium was 100 µM as determined by the microbroth dilution assay. Moreover, compound **1** showed no substantial cytotoxicity against the three tested human cell lines (HUH7, THP-1, CLS-54) up to a concentration of 100 µM (Fig. 3). As an extension of the antifungal assay, a time-kill assay was performed (Fig. 4). Incubation of cells of the hyphae form of *Candida albicans* strain ATCC 24,433 with compound **1** at 400 µM (= 4-fold MIC) resulted in a rapid decrease of viability by 3.5-log over a period of 6 h, after which a plateau was reached. In contrast, the positive control hygromycin B (474 µM = 4-fold MIC), which has antifungal activity against *C. candida*,[16,17] exhibited only a largely static growth inhibitory effect (Fig. 4). This finding highlights the fungicidal property of compound **1**. When comparing the antifungal activity of compounds **1–6**, it is obvious that addition of polar groups to the side chain (**2–5**) as well as shortening of the side chain (**6**) weakens the antifungal activity, which might be due to hindered uptake by the fungus. Based on its fungicidal activity and lack of cytotoxicity against human cells, compound **1** could be a promising candidate for the development of new antifungal agents.
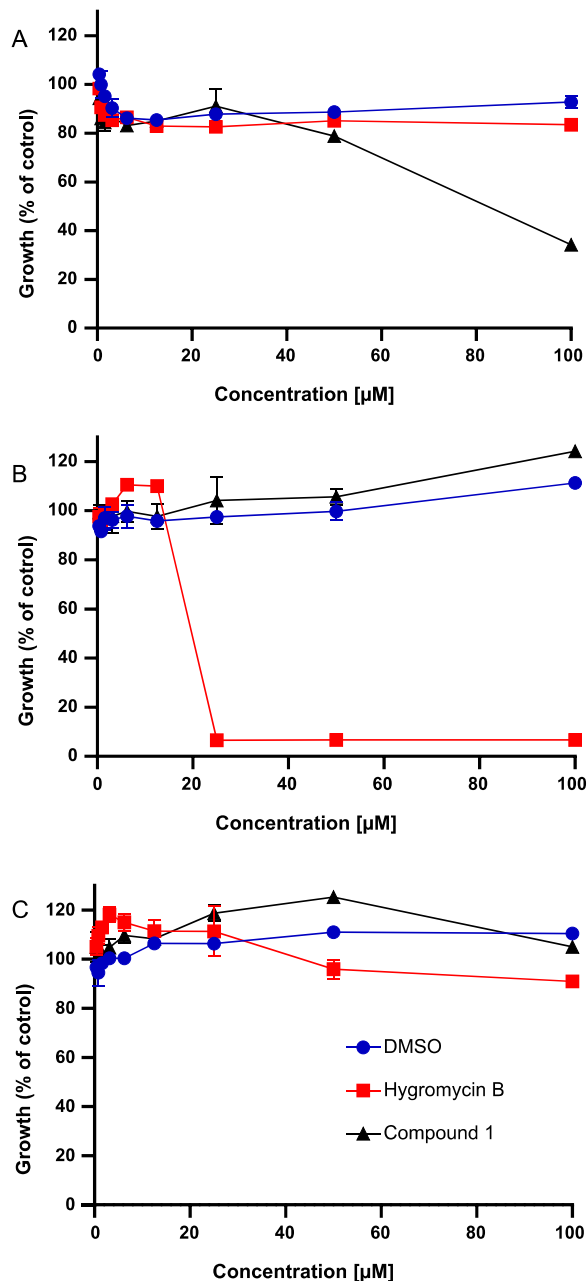
Fig. 3. Evaluation of cytotoxicity of compound **1** against different human cell lines. (A) Effect against the human liver cell line HUH7, (B) the human lung epithelial cell line CLS-54, and (C) the human monocytic leukemia cell line THP-1. DMSO was used as solvent control, the antifungal compound hygromycin B as reference. Data represent means from two replicates ± standard error.

3. Experimental

3.1. General experimental procedures

Optical rotations were measured with a Perkin-Elmer-241 MC polarimeter. NMR spectra were recorded at 25 °C on Bruker ARX 300 or 600 NMR spectrometers. Chemical shifts were referenced to the solvent residual peaks. Mass spectra (ESI) were recorded with a Finnigan LCQ
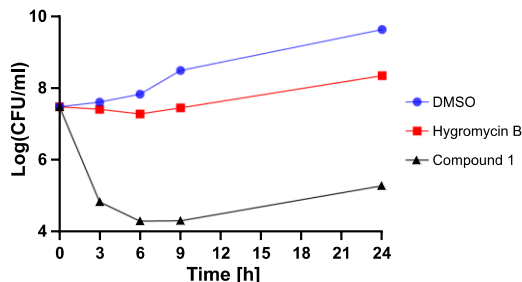
Fig. 4. Time-kill curve of compound **1** (400 μM, black) against the hyphae form of *Candida albicans* strain ATCC 24433. The antifungal compound hygromycin B (474 μM, red) was used as positive control; DMSO (blue) was used as the solvent control. Colony forming units (CFU) were quantified after the indicated time points of incubation. The medium was replaced after 6 h incubation with fresh medium containing compounds at the initial concentration to avoid effects by potential compound degradation.

Deca mass spectrometer while HRESIMS were recorded with a UHR-QTOF maXis 4G (Bruker Daltonics) mass spectrometer. HPLC analysis was performed with a Dionex UltiMate-3400SD system with a LPG-3400SD pump and a photodiode array detector (DAD 3000RS). The analytical column (125 × 4 mm) was prefilled with Eurosphere-10 C_{18} (Knauer, Germany). Semi-preparative HPLC was performed using a Merck Hitachi HPLC System (UV detector L7400; pump L7100; Eurosphere-100 C_{18}, 300 × 8 mm, Knauer, Germany). Normal phase column chromatography included Merck MN silica gel 60 M (0.04–0.063 mm) or Sephadex LH-20. TLC plates precoated with silica gel F_{254} (Merck, Germany) were used to monitor fractions following column chromatography with UV detection at 254 and 366 nm or by spraying the plates with anisaldehyde reagent followed by heating. Distilled and spectral grade solvents were used for column chromatography and spectroscopic measurements, respectively.

3.2. Fungal material and identification

The endophytic fungus was isolated from fresh, healthy stems of *O. violaceus* (L.) O. E. Schul (*Brassicaceae*), which were collected in April 2018 around Beijing, China. After 70% ethanol surface sterilization, the disinfected stems were dissected into small pieces of 0.5 cm length and placed on the fungal isolation medium (malt agar medium). The isolation of the fungal strain was achieved according to a standard procedure as described before.[18] It was identified as *Aplosporella javeedii* according to the DNA amplification and sequencing of the ITS region as described previously.[19] The sequence data were submitted to GenBank with the accession number MN720704. The fungal strain is kept in the Institute of Pharmaceutical Biology and Biotechnology, Heinrich-Heine University, Duesseldorf, Germany, with the ID code ZGB-B.

3.3. Cultivation, extraction and isolation

The fungus was cultivated on solid rice medium (100 g rice and 110 mL demineralized water) in ten Erlenmeyer flasks (1 L each). After autoclaving at 121 °C for 20 min and cooling down to room temperature, the fungal strain was added and cultivated for 20 days. After the fungus had completely overgrown the medium, the culture was extracted with 800 mL EtOAc followed by evaporation of the extract to dryness. The obtained brown extract (10.5 g) was subjected to a silica gel vacuum liquid chromatography column (VLC), using solvents in a gradient of increasing polarity (*n*-hexane, EtOAc, CH_2Cl_2, MeOH) to yield 12 fractions (V1 to V12). Fraction V3 (1.5 g) was subjected to a silica gel column with a gradient of *n*-hexane and EtOAc (20:1 to 0:100), affording eight subfractions (V3-S1 to V3-S8). Subfraction V3-S2 (80.2 mg) was purified by semi-preparative HPLC using MeOH-H_2O

(70:30 to 100:0) to give **1** (8.3 mg). Fraction V4 (1.1 g) was also separated on a silica gel column with a *n*-hexane-EtOAc gradient (20:1 to 0:100), affording ten subfractions (V4-S1 to V4-S10). Subfraction V4-S2 (51.1 mg) was purified by semi-preparative HPLC using MeOH-H_2O (30:70 to 70:30) to give **5** (4.3 mg). Fraction V5 (235.9 mg) was subjected to a Sephadex LH-20 column using CH_2Cl_2-MeOH (1:1) as eluent to obtain seven subfractions (V5-S1 to V5-S7). Subfraction V5-S4 (27.8 mg) was purified by semi-preparative HPLC using MeOH-H_2O (30:70 to 70:30) to give **2** (3.6 mg) and **4** (10.5 mg). Fractions V7 (206.4 mg) and V8 (100.2 mg) were combined and further fractionated using a Sephadex LH-20 column with CH_2Cl_2-MeOH (1:1) as eluent to give four subfractions (V7-S1 to V7-S4). Subfraction V8-S3 (119.6 mg) were subjected to a silica gel column with a CH_2Cl_2-MeOH gradient (20:1 to 0:100), followed by purification with semi-preparative HPLC using MeOH-H_2O (10:90 to70:30) as mobile phase to give **3** (2.0 mg). Fraction V9 (1.0 g) was separated on a Sephadex LH-20 column using CH_2Cl_2-MeOH (1:1) to yielded six subfractions (V9-S1 to V9-S6). Subfraction V9-S4 (18.2 mg) was further purified by semi-preparative HPLC using MeCN-H_2O (10:90 to 20:80) to give **6** (1.5 mg).

Aplojaveediin A (**1**): Colorless crystal; UV (MeOH) λ_{max} 208, 220 and 298 nm; ^{1}H and ^{13}C NMR data, see Table 1; HRESIMS $[M+H]^+$ *m/z* 223.1332 (calcd for $C_{13}H_{19}O_3$ 223.1334), $[M-H]^-$ *m/z* 221.1178 (calcd for $C_{13}H_{17}O_3$ 221.1178).

Aplojaveediin B (**2**): Brown homogeneous oil; UV (MeOH) λ_{max} 218 and 301 nm; ^{1}H NMR and ^{13}C NMR data, see Table 1; HRESIMS $[M+H]^+$ *m/z* 239.1280 (calcd for $C_{13}H_{19}O_4$ 239.1283), $[M-H]^-$ *m/z* 237.1130 (calcd for $C_{13}H_{17}O_4$ 237.1127).

Aplojaveediin C (**3**): Brown homogeneous oil; $[\alpha]_D^{20}$ + 6 (*c* 0.2, MeOH); UV (MeOH) λ_{max} 206, 220 and 297 nm; ^{1}H and ^{13}C NMR data, see Table 1; HRESIMS $[M-H]^-$ *m/z* 253.1084 (calcd for $C_{13}H_{17}O_5$ 253.1076).

Aplojaveediin D (**4**): Colorless crystal; UV (MeOH) λ_{max} 220 and 300 nm; ^{1}H and ^{13}C NMR data, see Table 2; HRESIMS $[M-H]^-$ *m/z* 251.0923 (calcd for $C_{13}H_{15}O_5$ 251.0919).

Aplojaveediin E (**5**): Colorless crystals; UV (MeOH) λ_{max} 208, 220 and 298 nm; ^{1}H and ^{13}C NMR data, see Table 2; HRESIMS $[M-H]^-$ *m/z* 265.1082 (calcd for $C_{14}H_{17}O_5$ 265.1076).

Aplojaveediin F (**6**): White amorphous solid; UV (MeOH) λ_{max} 220 and 297 nm; ^{1}H and ^{13}C NMR data, see Table 2; HRESIMS $[M-H]^-$ *m/z* 223.0607 (calcd for $C_{11}H_{11}O_5$ 223.0606).

3.4. Antibacterial assay

The antibacterial activities were tested by calculating the MICs against *Mycobacterium tuberculosis* H37Rv, *Staphylococcus aureus* ATCC 29213, *S. aureus* ATCC 700699, *Enterococcus faecalis* ATCC 29212, *E. faecalis* ATCC 51299, *E. faecium* ATCC 35667, *E. faecium* ATCC 700221, *Bacillus subtilis* ATCC 169 and *Escherichia coli* ATCC 25922. The MIC values were determined by the broth microdilution method following the recommendation of the Clinical and Laboratory Standards Institute (CLSI).[20]

3.5. Antifungal assay

Compounds were tested against the nosocomial pathogen *Candida albicans* both grown in the yeast form and the hyphae form. The microbroth dilution method was done as recommended by CLSI guidelines.[20] *Candida albicans* was inoculated in YPD medium (yeast extract 10 g/L, peptone 20 g/L, D-glucose 20 g/L) and incubated at 37 °C with shaking at 180 rpm overnight to obtain the yeast form. For the hyphae form, YP + Proline medium (yeast extract 10 g/L, peptone 20 g/L, proline 20 g/L) was used, and cells were incubated at 30 °C with shaking at 60 rpm overnight. Afterwards, cells were seeded at a density of 1 × 10^6 CFU/mL in 96 well microplate containing two fold serial dilutions of compounds at a concentration ranging from 100 to 0.78 μM in a total volume 100 μL. DMSO at a maximal concentration of 1% was

used as solvent control, while hygromycin B served as antifungal positive control.[16,17] The plates were incubated at 37 °C overnight aerobically as static cultures before being evaluated macroscopically. All tests were repeated twice.

The disc diffusion method was used as an additional sensitivity test. Briefly, a preculture of *Candida albicans* (hyphae form) was adjusted to 2×10^8 CFU/mL. Subsequently, 100 μL culture aliquots were plated out on the surface of YP + Proline agar plates. Then, 5 μL of compound **1** (1 mmol/L, 10MIC) was spotted onto a sterile filter disc. Hygromycin B (3.12 μg in 5 μL, 10MIC) was used as positive and DMSO (5 μL) as negative control. The plates were incubated at 30 °C overnight aerobically. Subsequently, the inhibition zones were measured by a caliper. All tests were repeated once.

3.6. Cytotoxicity assay

Cytotoxicity studies were conducted with three human cell lines THP-1 (human monocytic leukemia cell line), CLS-54 (human lung epithelial cell line), and HUH7 (liver cell line). The cells were cultured in RPMI 1640 medium containing 10% fetal bovine serum (FBS) at 37 °C in a humidified atmosphere of 5% CO_2 for 5 days. Afterwards, the cells were suspended and adjusted to a density of 1×10^6 cells/ml. For the adherent cell lines HUH7 and CLS-54, prior trypsinization was done for cell detachment. Cells were then seeded into a 96-well plate in a total volume of 100 μL containing 2-fold serial dilutions of the tested compounds in a concentration ranging from 100 to 0.78 μM. DMSO and hygromycin B were used as negative and positive controls, respectively. After 48 h incubation at 37 °C in a humidified atmosphere of 5% CO_2, 10 μL resazurin solution (100 μg/mL) was added to each well and incubated for a further 4 h. A microplate reader (excitation 545 nm, emission 590 nm) was used to measure the fluorescence. Residual growth was calculated relative to uninoculated (0% growth) and untreated (100% growth) controls, respectively.

3.7. Determination of time-kill kinetic

Time-kill kinetic was tested for compound **1** against the hyphae form of *Candida albicans*. A preculture grown in YP + Proline medium was adjusted to a density of 3×10^7 CFU/ml and split into three aliquots, which were treated either with 4-fold MIC (400 μM) of compound **1**, hygromycin B (474 μM) as an antifungal positive control or DMSO as the solvent control. After 0, 3, 6, 9 and 24 h incubation, 100 μL culture aliquots were taken and plated on YPD agar plates, and CFU were quantified after overnight incubation at 30℃ aerobically. In order to avoid the potential degradation of compounds, the medium was removed after 6 h incubation by centrifuging at 4000 rpm for 10 min and replaced with an equal volume of fresh medium containing the respective compound at the initial concentration.

Declaration of Competing Interest

The authors declare that they have no known competing financial interests or personal relationships that could have appeared to influence the work reported in this paper.

Acknowledgments

Appendix A. Supplementary material

Supplementary data to this article can be found online at https:// doi.org/10.1016/j.bmc.2020.115456.

References

1. Liu S, Zhao Y, Heering C, et al. Sesquiterpenoids from the Endophytic Fungus *Rhinocladiella similis*. *J Nat Prod.* 2019;82:1055–1062.
2. Harwoko H, Daletos G, Stuhldreier F, et al. Dithiodiketopiperazine derivatives from endophytic fungi *Trichoderma harzianum* and *Epicoccum nigrum*. *Nat Prod Res.* 2019;1–9.
3. Liu S, Dai H, Orfali RS, Lin W, Liu Z, Proksch P. New fusaric acid derivatives from the endophytic fungus *Fusarium oxysporum* and their phytotoxicity to barley leaves. *J Agric Food Chem.* 2016;64:3127–3132.
4. Patil RH, Patil MP, Maheshwari VL. Chapter 5 - Bioactive secondary metabolites from endophytic fungi: a review of biotechnological production and their potential applications. In: Atta ur R, ed. *Studies in Natural Products Chemistry*. Elsevier205; 2016:189.
5. Gouda S, Das G, Sen SK, Shin HS, Patra JK. Endophytes: a treasure house of bioactive compounds of medicinal importance. *Front Microbiol.* 2016;7:1538.
6. Liu S, Dai H, Makhloufi G, et al. Cytotoxic 14-membered macrolides from a mangrove-derived endophytic fungus *Pestalotiopsis microspora*. *J Nat Prod.* 2016;79:2332–2340.
7. Moussa M, Ebrahim W, El-Neketi M, et al. Tetrahydroanthraquinone derivatives from the mangrove-derived endophytic fungus *Stemphylium globuliferum*. *Tetrahedron Lett.* 2016;57:4074–4078.
8. Luo P, Lan ZQ, Li ZY. *Orychophragmus violaceus*, a potential edible-oil crop. *Plant Breed.* 1994;113:83–85.
9. Zhou LR, Wu J, Wang S. Orychophragmus. In: Kole C, ed. *Wild Crop Relatives: Genomic and Breeding Resources*. Berlin, Heidelberg: Springer Berlin Heidelberg; 2011:199–225.
10. Medicinal Plant Images Database. School of Chinese Medicine, Hong Kong Baptist University; 2007. http://libproject.hkbu.edu.hk/was40/detail?lang=en& channelid=1288&searchword=herb_id=D00879.
11. Huo X, Liu C, Gao L, Xu X, Zhu N, Cao L. Hepatoprotective effect of aqueous Extract from the seeds of *Orychophragmus violaceus* against liver injury in mice and HepG2 cells. *Int J Mol Sci.* 2017;18:1197.
12. Jami F, Slippers B, Wingfield MJ, Gryzenhout M. *Botryosphaeriaceae* species overlap on four unrelated, native South African hosts. *Fungal Biol.* 2014;118:168–179.
13. Fan XL, Yang Q, Cao B, Liang YM, Tian CM. New record of *Aplosporella javeedii* on five hosts in China based on multi-gene analysis and morphology. *Mycotaxon.* 2015;130:749–756.
14. Zhu HY, Tian CM, Fan XL. Studies of botryosphaerialean fungi associated with canker and dieback of tree hosts in Dongling Mountain of China. *Phytotaxa.* 2018;348:63–76.
15. Jia H, Liu Z, Sungbom O, et al. First report of *Aplosporella javeedii* causing branch blight disease of Mulberry (*Morus alba*) in China. *J Plant Dis Prot.* 2019;126(5):475–477. https://doi.org/10.1007/s41348-019-00245-5.
16. Basso Jr LR, Bartiss A, Mao Y, et al. Transformation of *Candida albicans* with a synthetic hygromycin B resistance gene. *Yeast.* 2010;27:1039–1048.
17. Ta CA, Guerrero-Analco JA, Roberts E, et al. Antifungal saponins from the Maya medicinal plant *Cestrum schlechtendahlii* G. Don (Solanaceae). *Phytother Res.* 2016;30:439–446.
18. Debbab A, Aly AH, Edrada-Ebel R, et al. Bioactive metabolites from the endophytic fungus *Stemphylium globuliferum* isolated from *Mentha pulegium*. *J Nat Prod.* 2009;72:626–631.
19. Kjer J, Debbab A, Aly AH, Proksch P. Methods for isolation of marine-derived endophytic fungi and their bioactive secondary products. *Nat Protoc.* 2010;5:479–490.
20. CLSI. *Methods for dilution antimicrobial susceptibility tests for bacteria that grow aerobically*. CLSI standard M07 11th ed. Wayne, PA: Clinical and Laboratory Standards Institute; 2018.

Support Information

Antifungal polyketide derivatives from the endophytic fungus *Aplosporella javeedii*

Ying Gao[a], Lin Wang[a], Rainer Kalscheuer[a], Zhen Liu[a,*], and Peter Proksch[a,b,*]

[a]Institute of Pharmaceutical Biology and Biotechnology, Heinrich Heine University Düsseldorf, Universitätsstrasse 1, 40225 Düsseldorf, Germany
[b]Hubei Key Laboratory of Natural Products Research and Development, College of Biological and Pharmaceutical Sciences, China Three Gorges University, Yichang 443002, People's Republic of China

[*]Corresponding authors.
E-mail address: zhenfeizi0@sina.com (Z. Liu); proksch@uni-duesseldorf (P. Proksch).

1

Table of Content

3

Fig. S1 Photo of *Orychophragmus. violaceus* (L.) O. E. Schul (*Brassicaceae*)
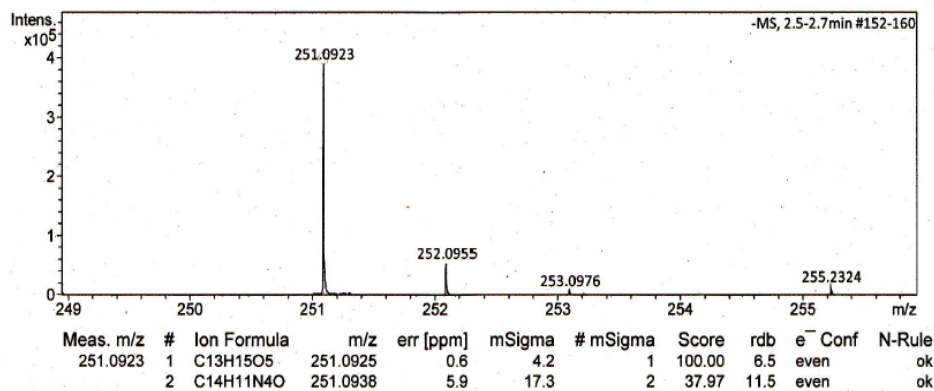

Fig. S2 Photo of *Aplosporella javeedii*

4

Fig. S3 HPLC chromatogram of compound **1**
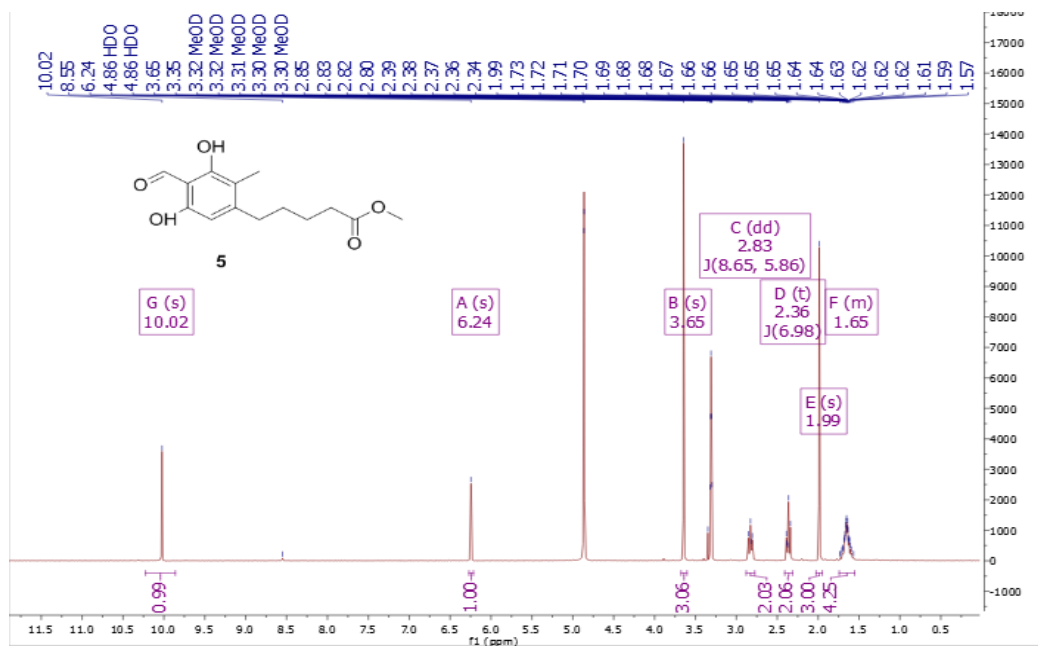

UV absorption of compound **1**

5

Fig. S4 ^{1}H-NMR (300 MHz, methanol-d_4) spectrum of compound **1**

Fig. S5 ^{13}C-NMR (75 MHz, methanol-d_4) spectrum of compound **1**

6

Fig. S6 COSY spectrum of compound **1**

Fig. S7 HSQC spectrum of compound **1**

7

Fig. S8 HMBC spectrum of compound **1**
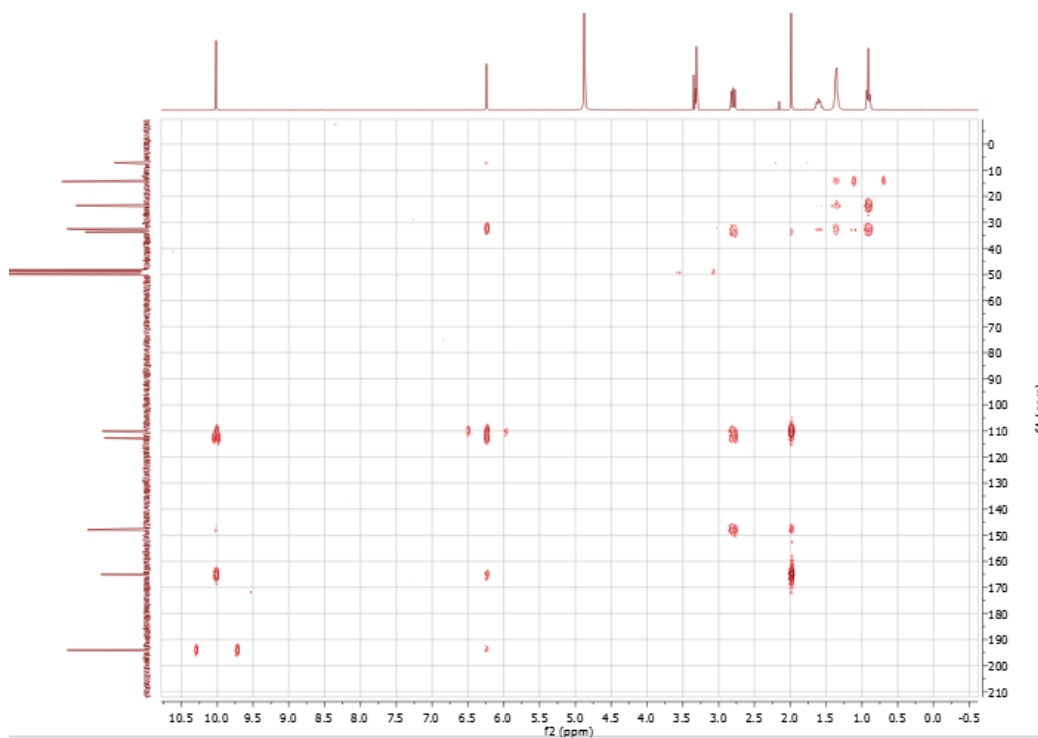
Fig. S9 HRESIMS of compound **1**

8
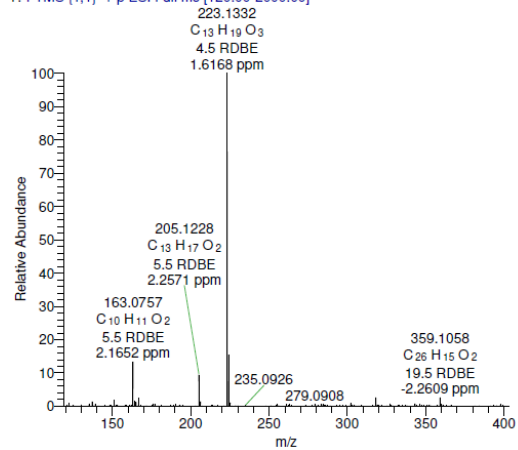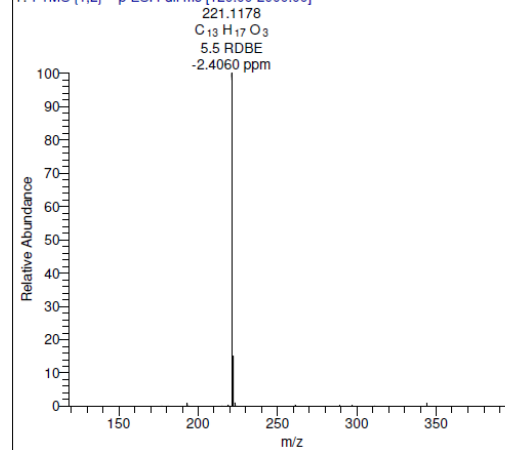
Fig. S10 HPLC chromatogram of compound **2**

UV absorption of compound **2**

9
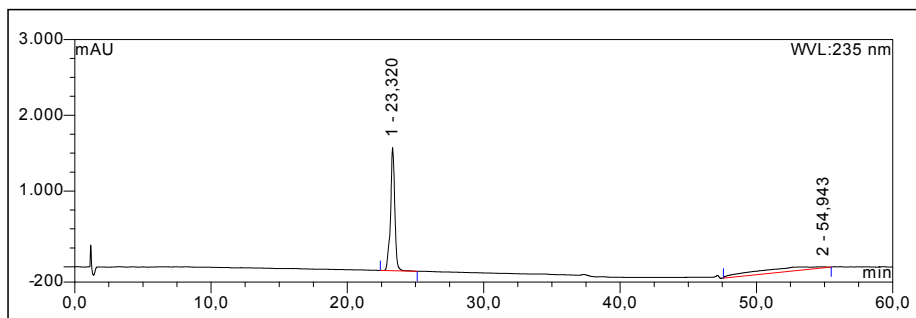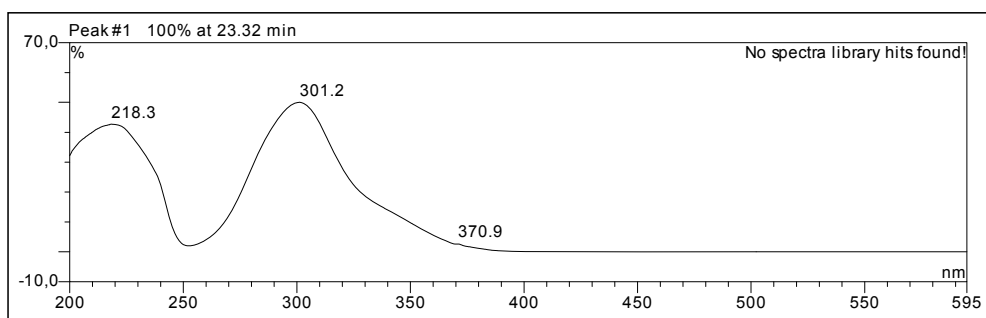
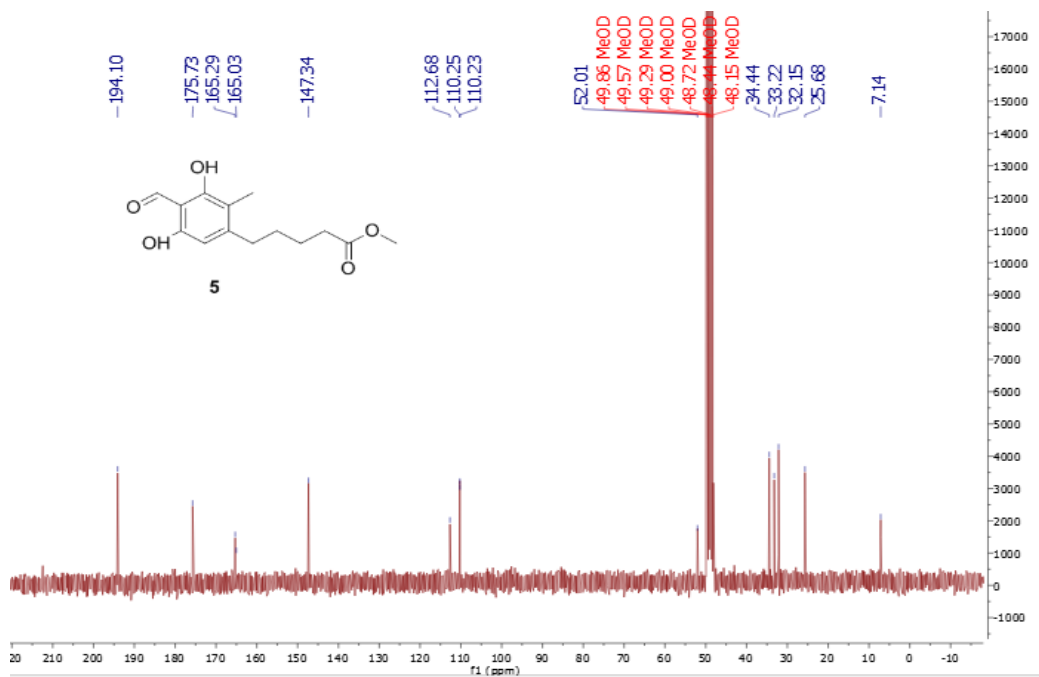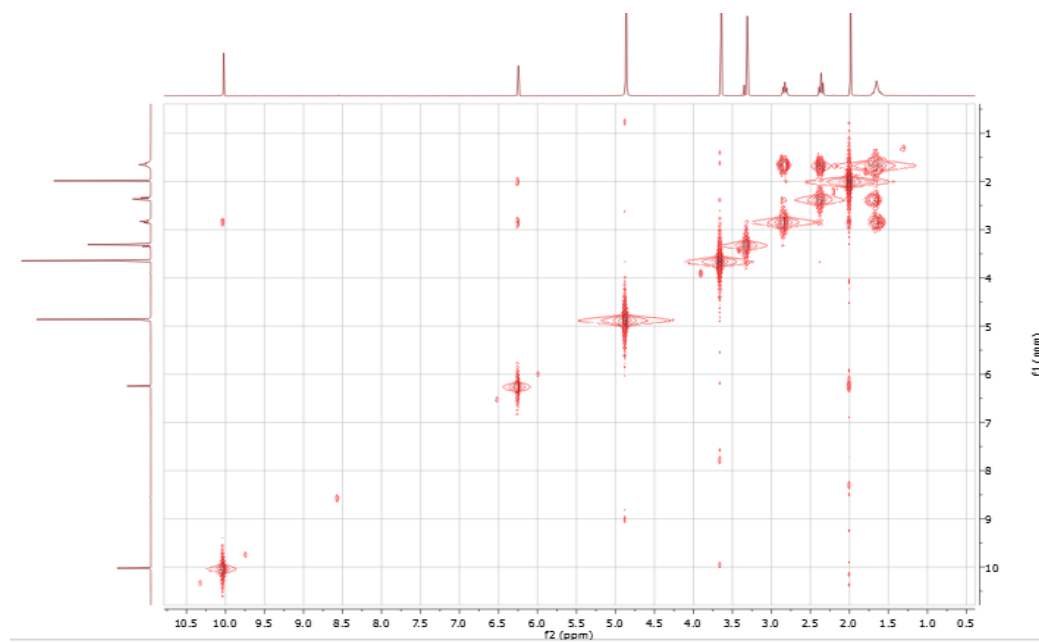**Fig. S11** ¹H-NMR (300 MHz, methanol-d_4) spectrum of compound **2**
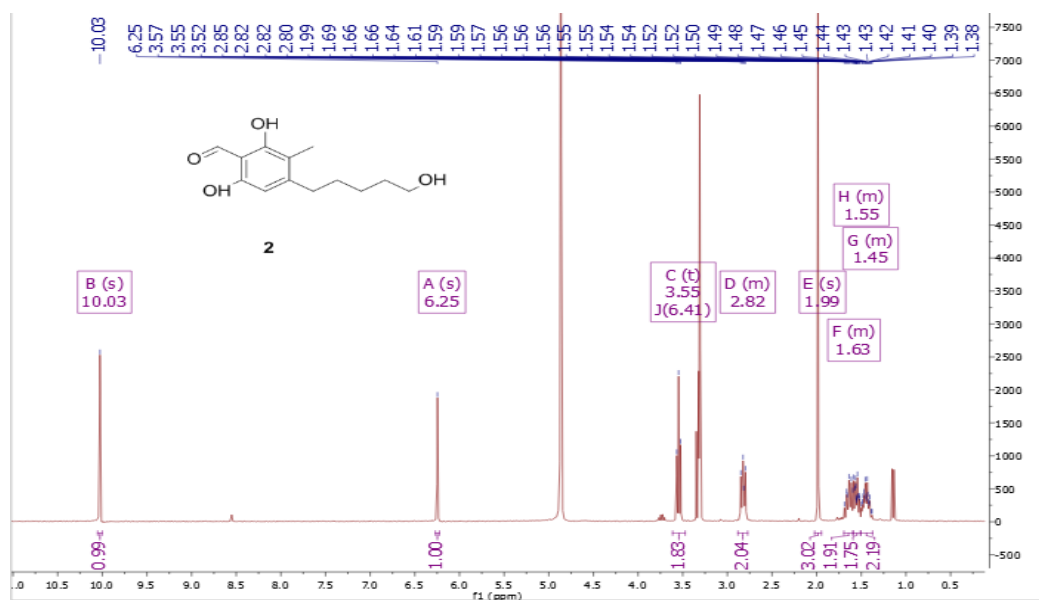
Fig. S12 ¹³C-NMR (75 MHz, methanol-d_4) spectrum of compound **2**
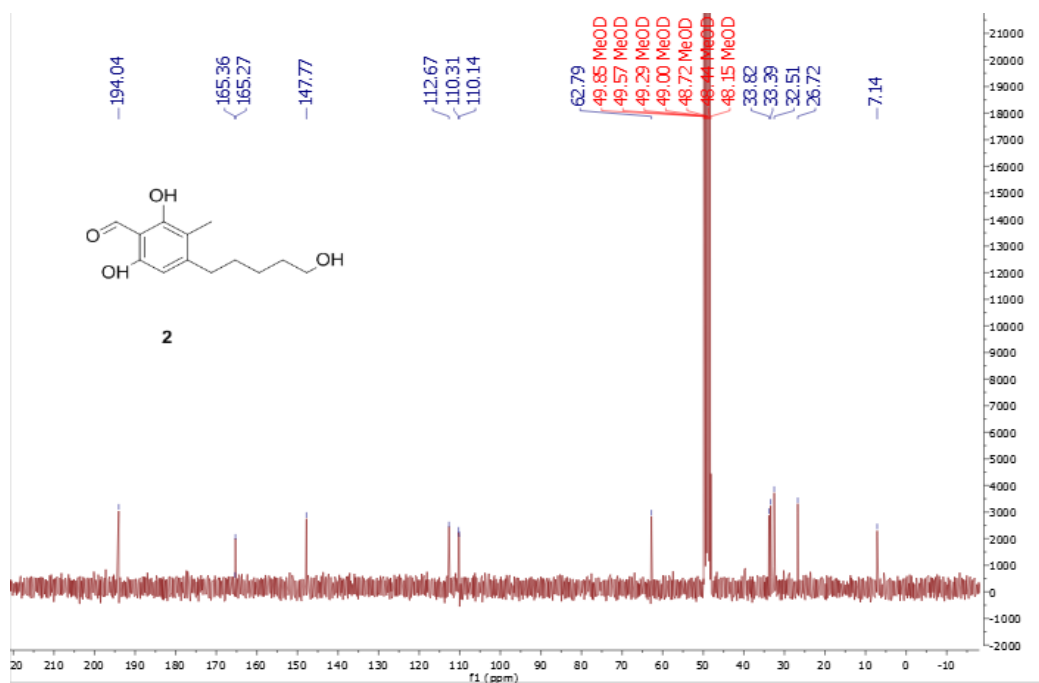
Fig. S13 COSY spectrum of compound **2**
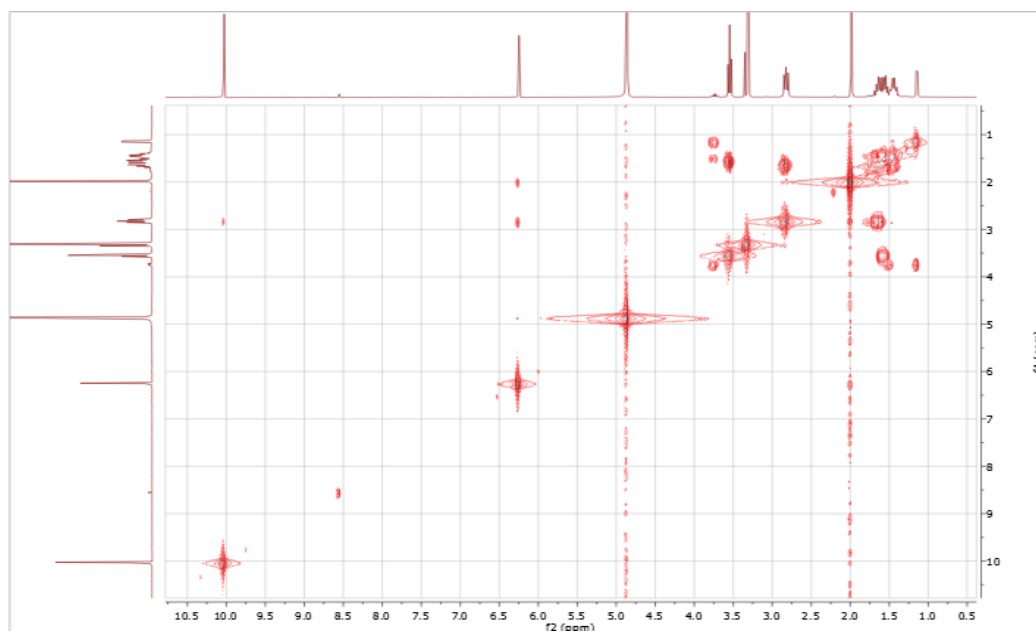
Fig. S14 HSQC spectrum of compound **2**

11
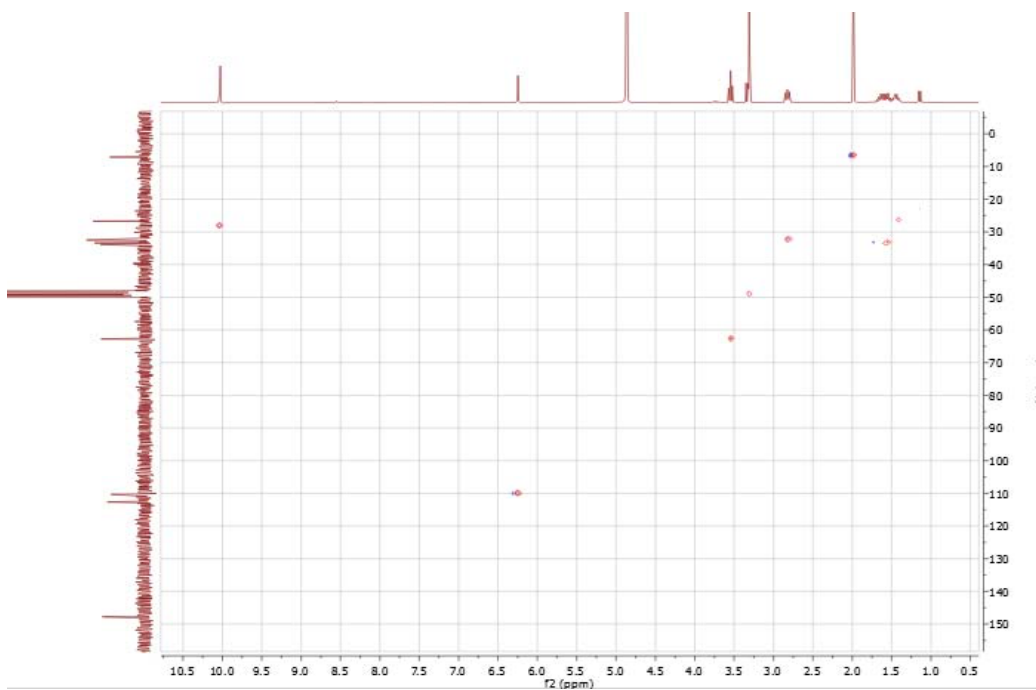
Fig. S15 HMBC spectrum of compound **2**
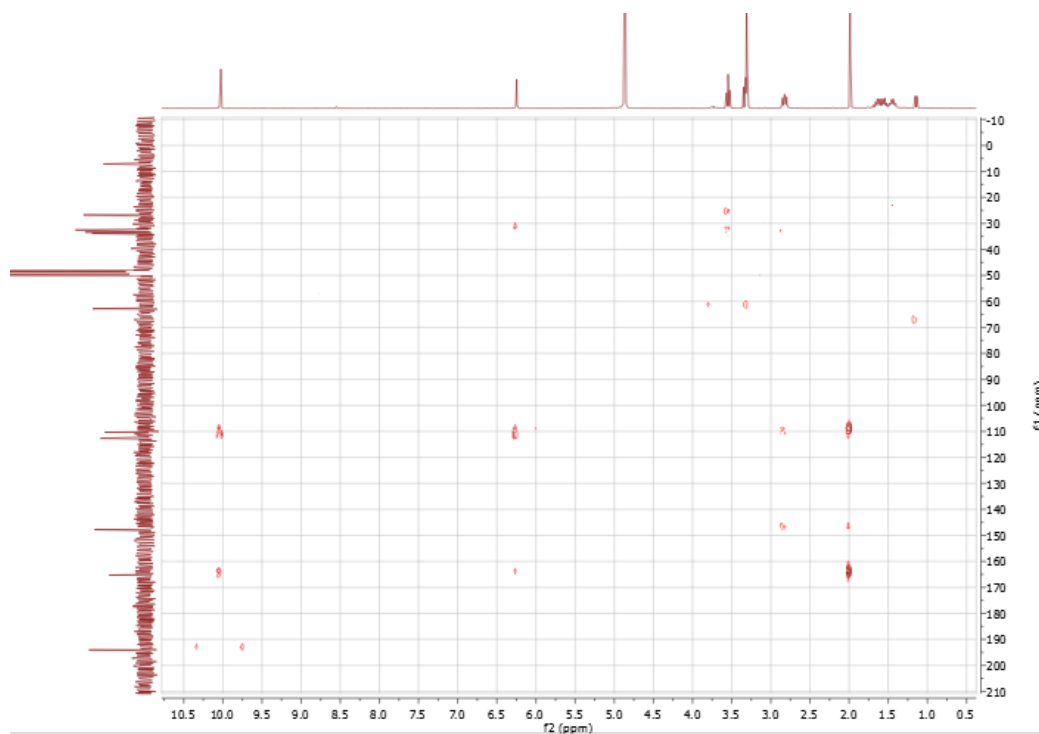
Fig. S16 HRESIMS of compound **2**
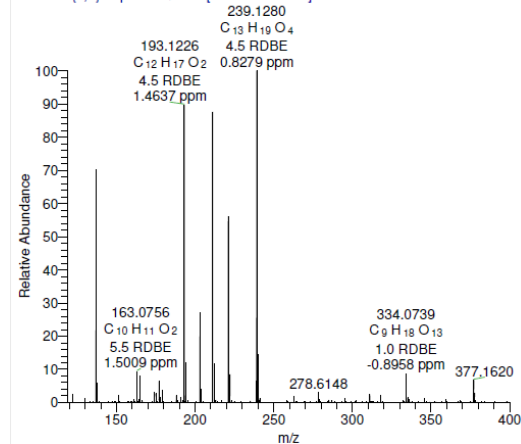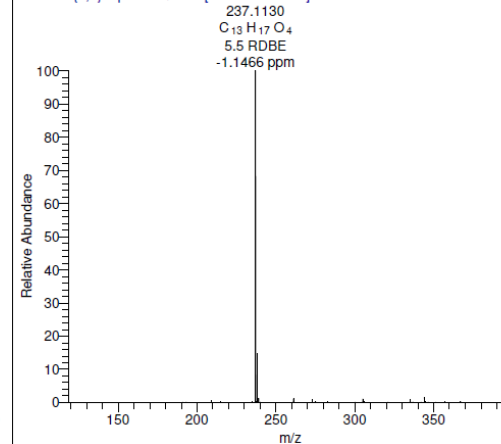
Fig. S17 HPLC chromatogram of compound **3**
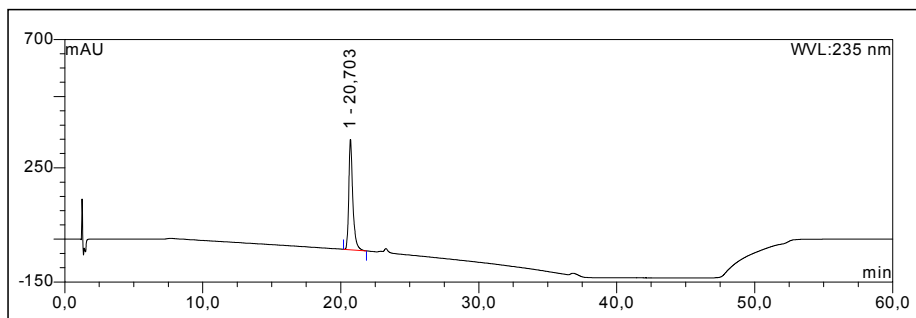
UV absorption of compound **3**

13
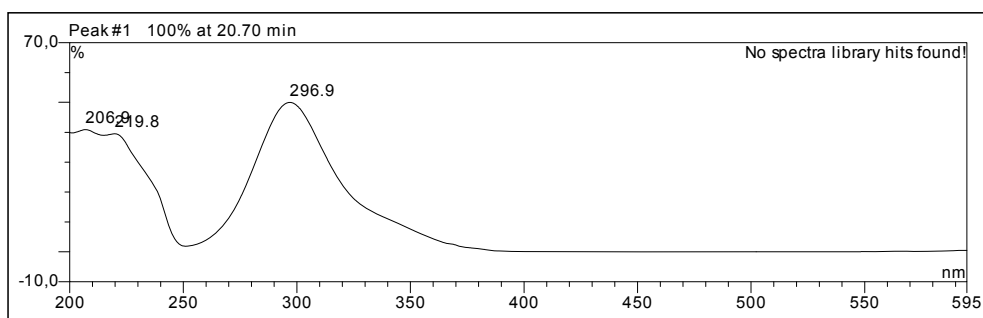
Fig. S18 ^{1}H-NMR (600 MHz, methanol-d_4) spectrum of compound **3**
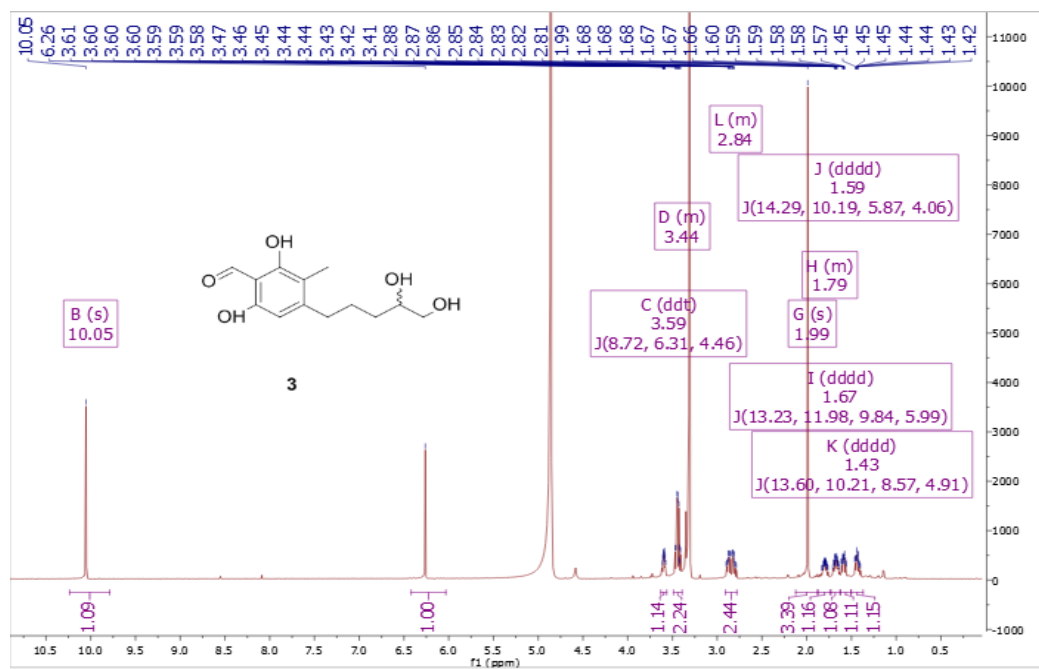
Fig. S19 COSY spectrum of compound **3**
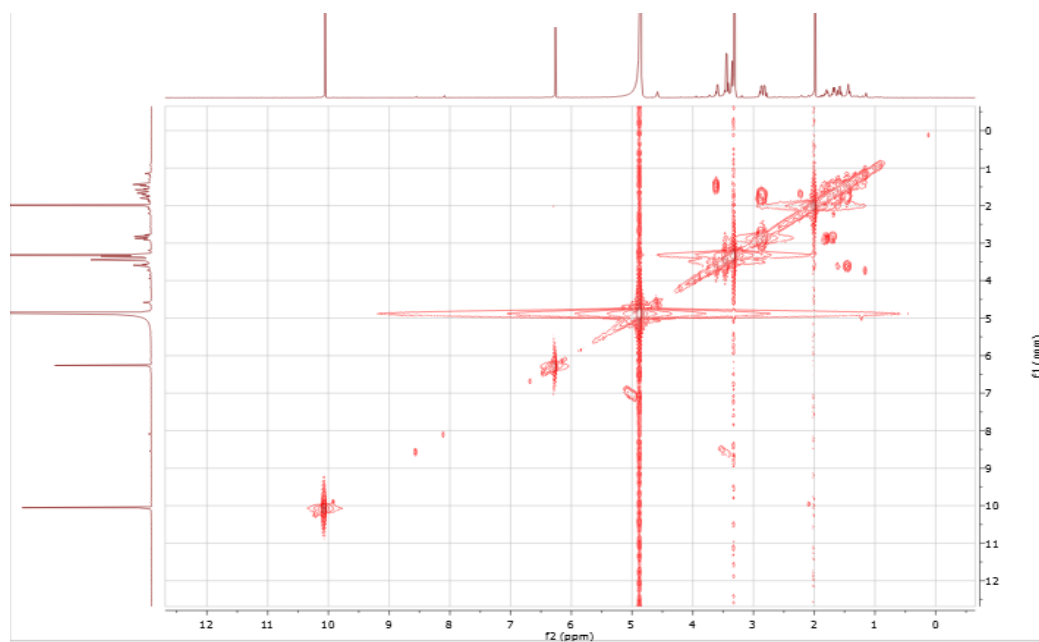
Fig. S20 HSQC spectrum of compound **3**

Fig. S21 HMBC spectrum of compound **3**
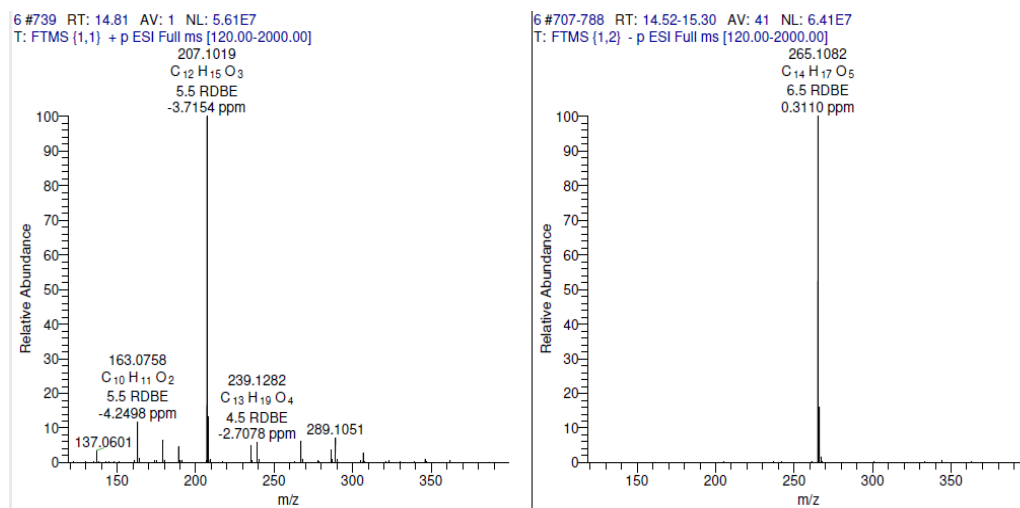

15
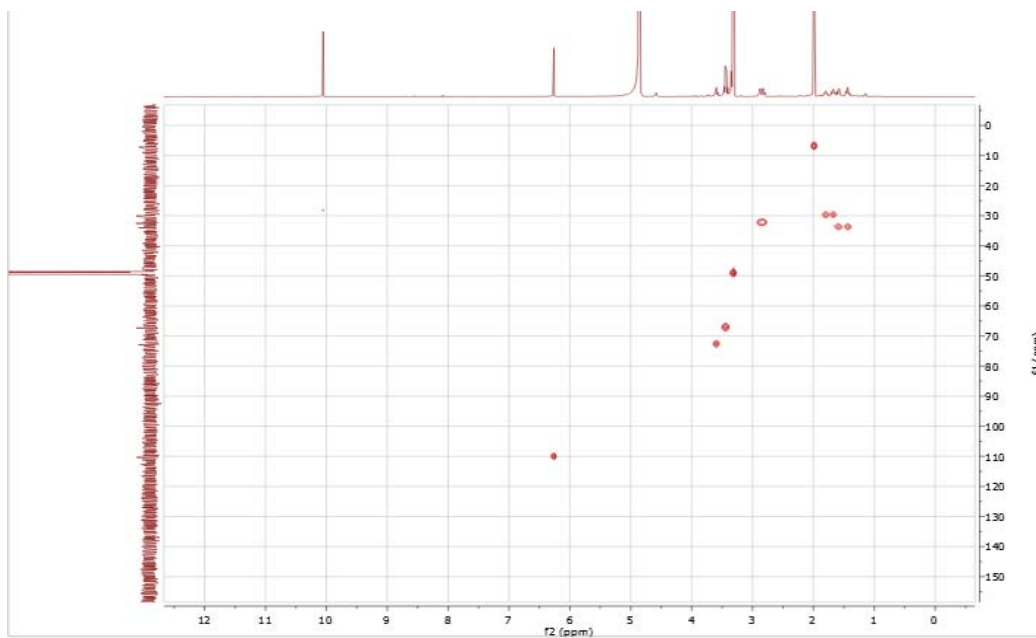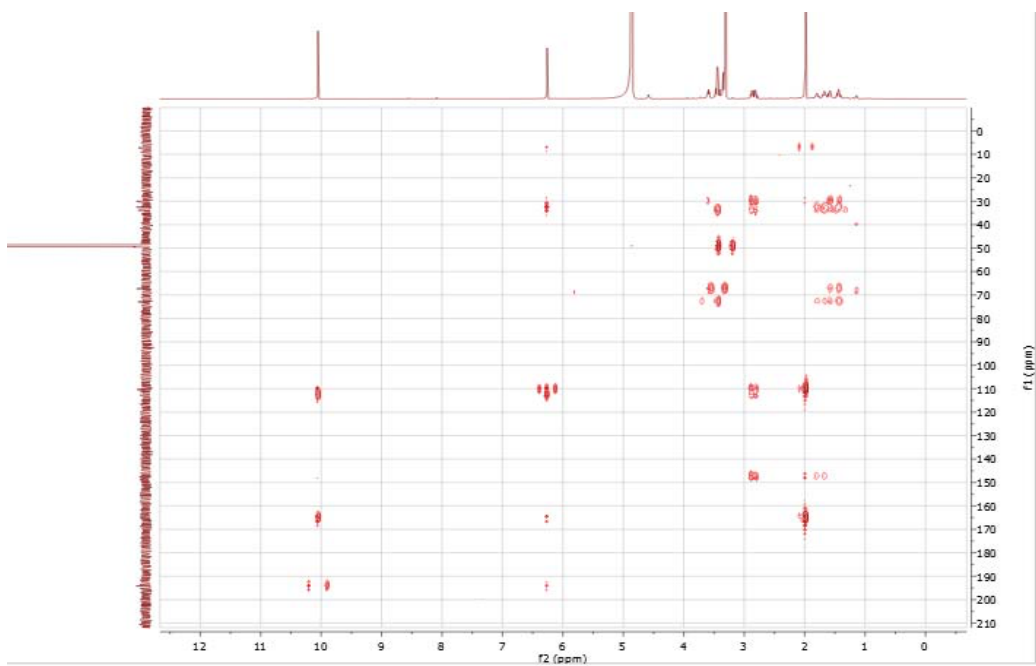
Fig. S22 HRESIMS of compound **3**
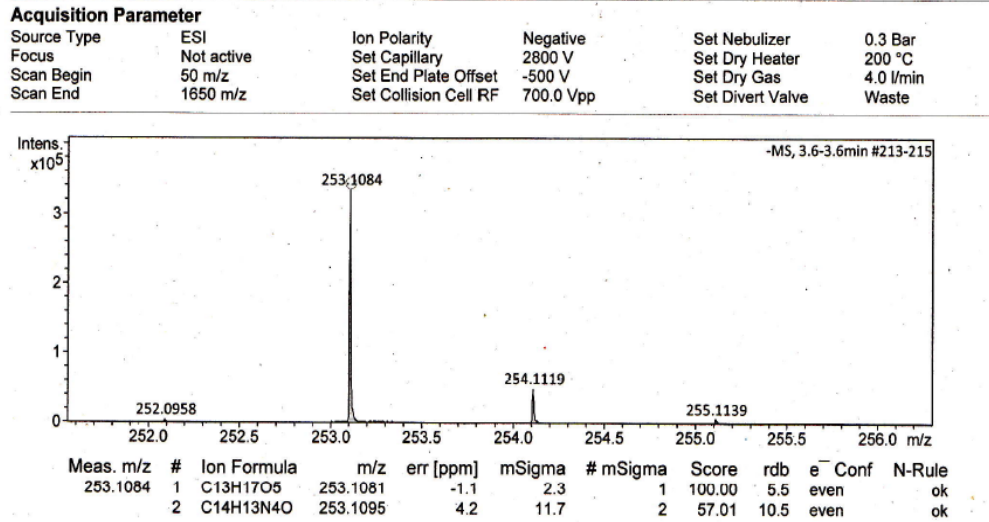
Fig. S23 HPLC chromatogram of compound **4**
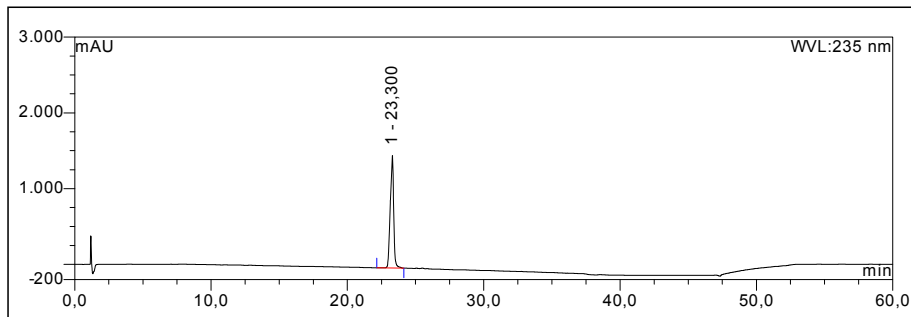
UV absorption of compound **4**
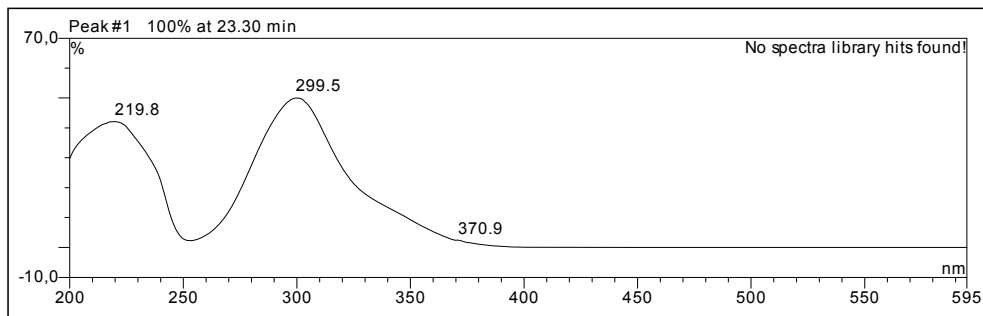
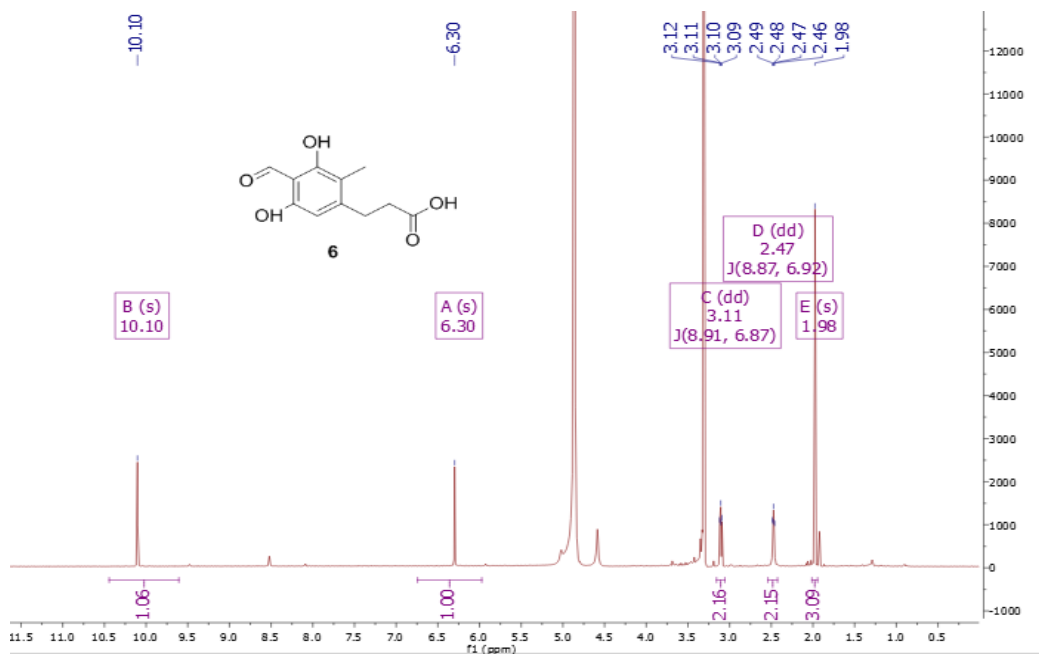**Fig. S24** ^{1}H-NMR (300 MHz, methanol-d_4) spectrum of compound **4**
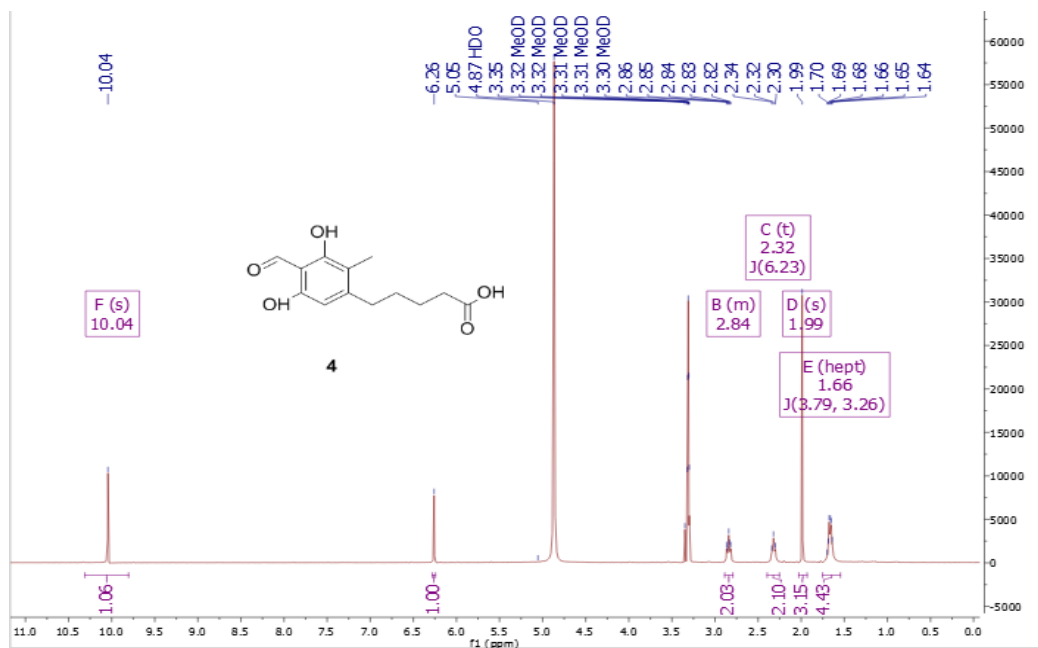
Fig. S25 ^{13}C-NMR (75 MHz, methanol-d_4) spectrum of compound **4**

17
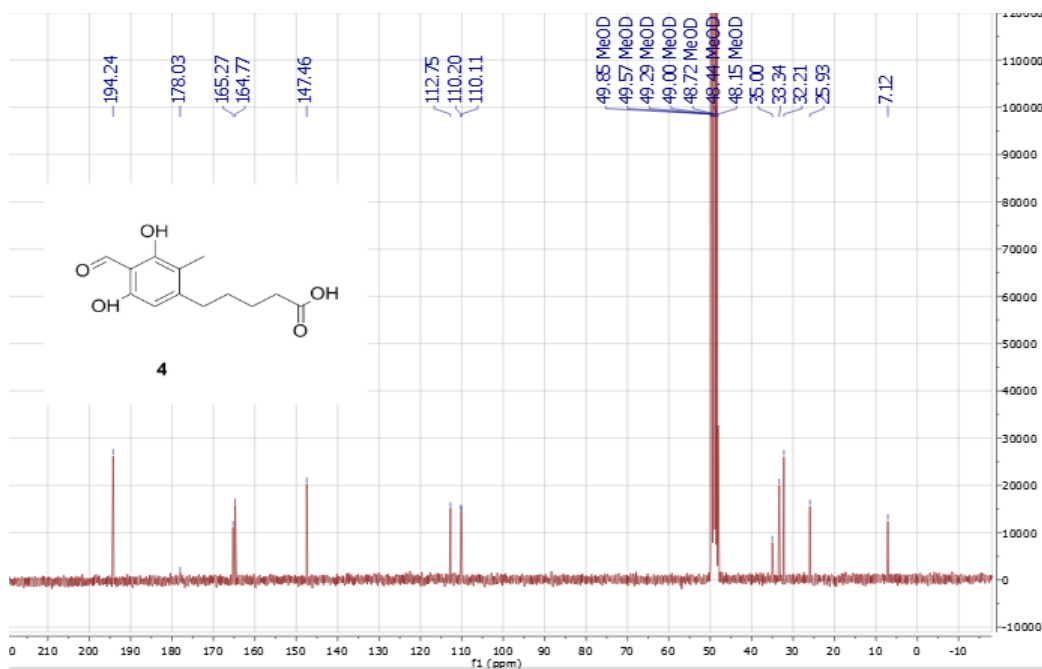
Fig. S26 COSY spectrum of compound **4**
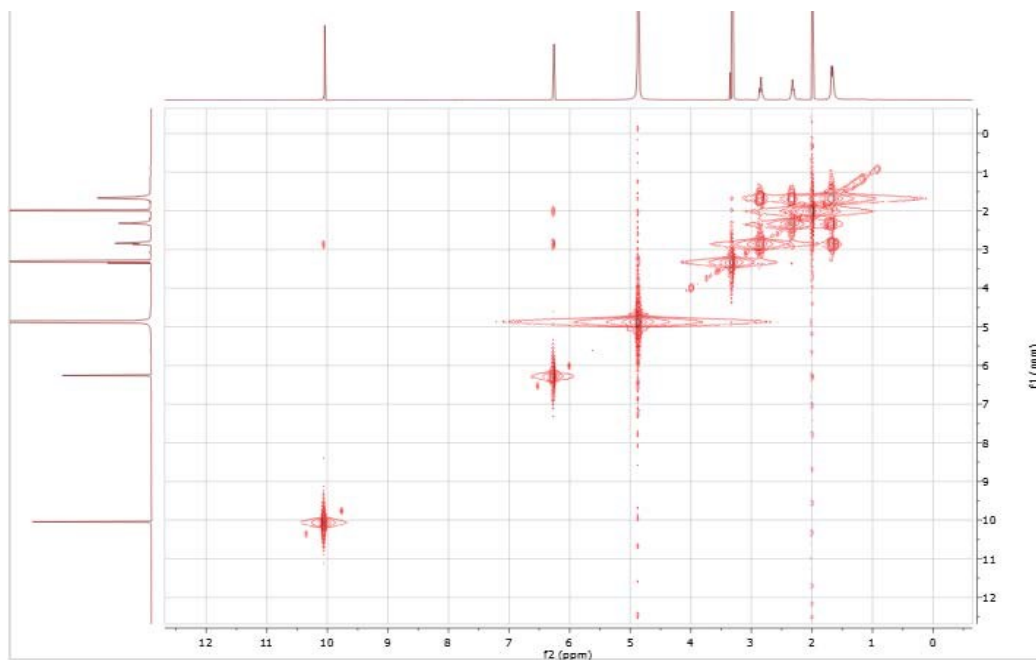
Fig. S27 HSQC spectrum of compound **4**

18
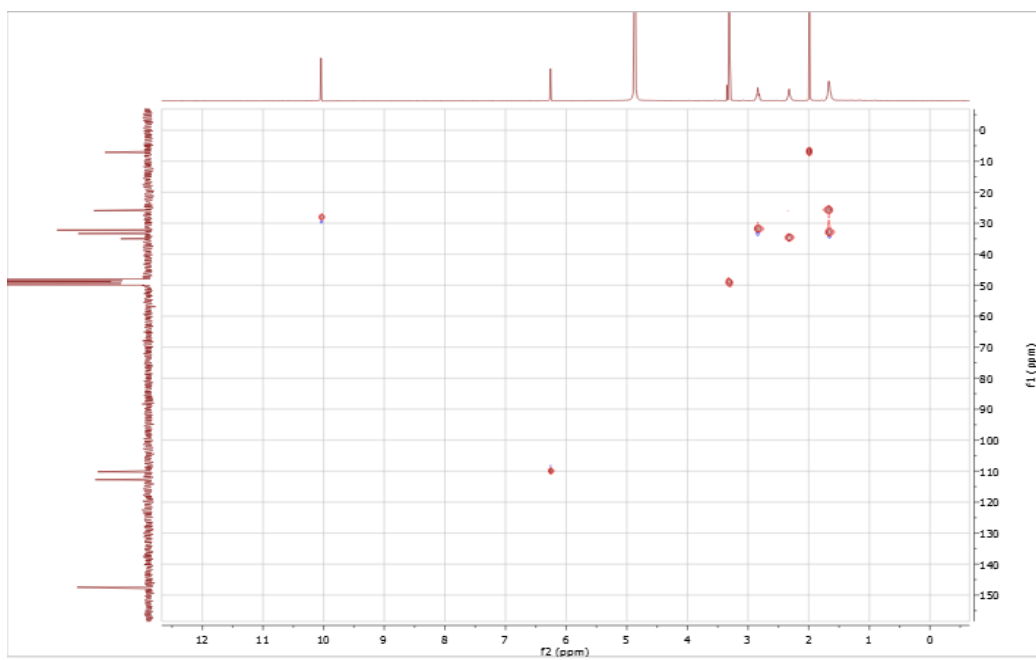
Fig. S28 HMBC spectrum of compound **4**
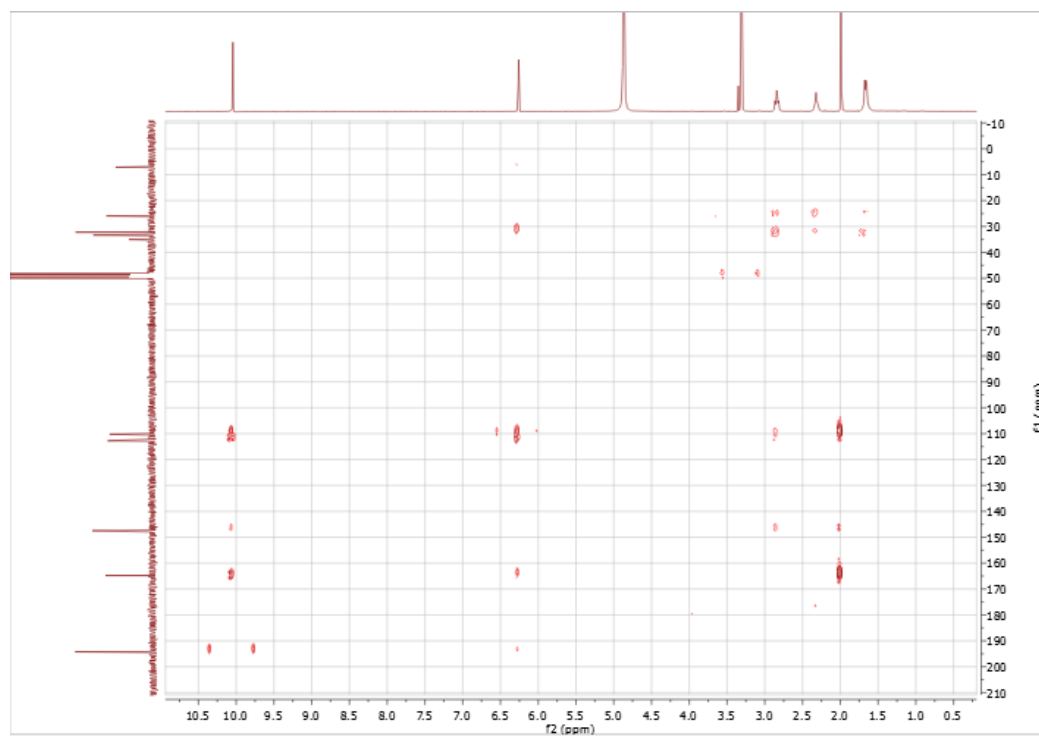
Fig. S29 HRESIMS of compound **4**

Acquisition Parameter

Source Type	ESI	Ion Polarity	Negative	Set Nebulizer	0.3 Bar
Focus	Not active	Set Capillary	2800 V	Set Dry Heater	200 °C
Scan Begin	50 m/z	Set End Plate Offset	-500 V	Set Dry Gas	4.0 l/min
Scan End	1650 m/z	Set Collision Cell RF	700.0 Vpp	Set Divert Valve	Waste

-MS, 2.5-2.7min #152-160

Meas. m/z	#	Ion Formula	m/z	err [ppm]	mSigma	# mSigma	Score	rdb	e⁻ Conf	N-Rule
251.0923	1	C13H15O5	251.0925	0.6	4.2	1	100.00	6.5	even	ok
	2	C14H11N4O	251.0938	5.9	17.3	2	37.97	11.5	even	ok

**Fig. S30** HPLC chromatogram of compound **5**
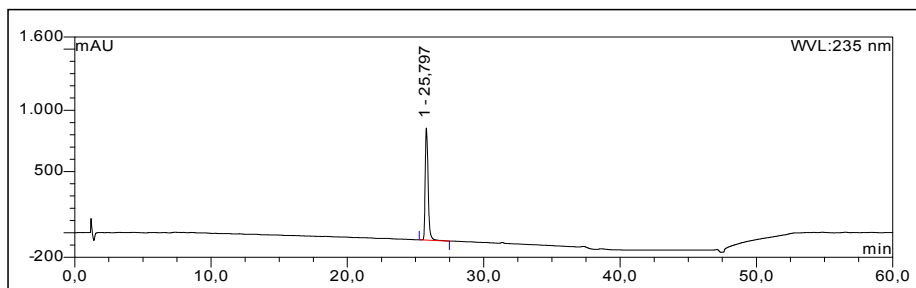
UV absorption of compound **5**
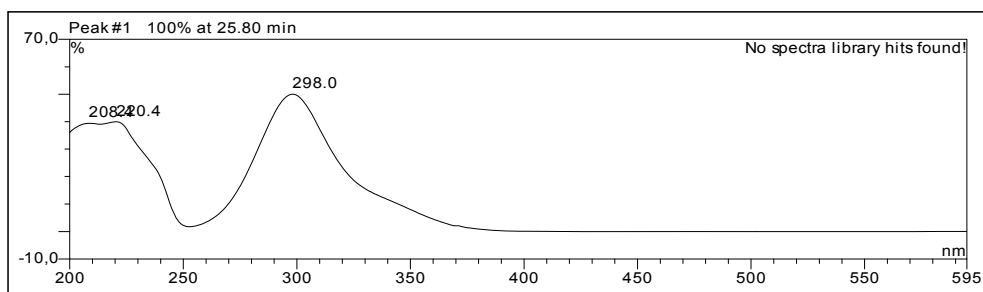
Fig. S31 ^{1}H-NMR (300 MHz, methanol-d_4) spectrum of compound **5**

20

Fig. S32 ^{13}C-NMR (75 MHz, methanol-d_4) spectrum of compound **5**
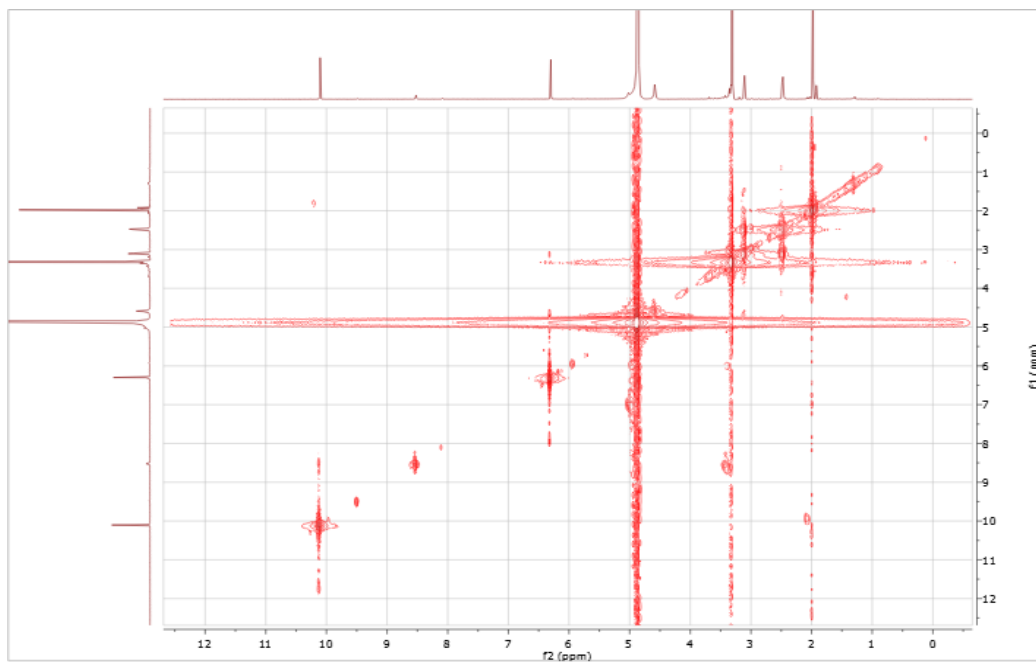

Fig. S33 COSY spectrum of compound **5**

21

Fig. S34 HSQC spectrum of compound **5**
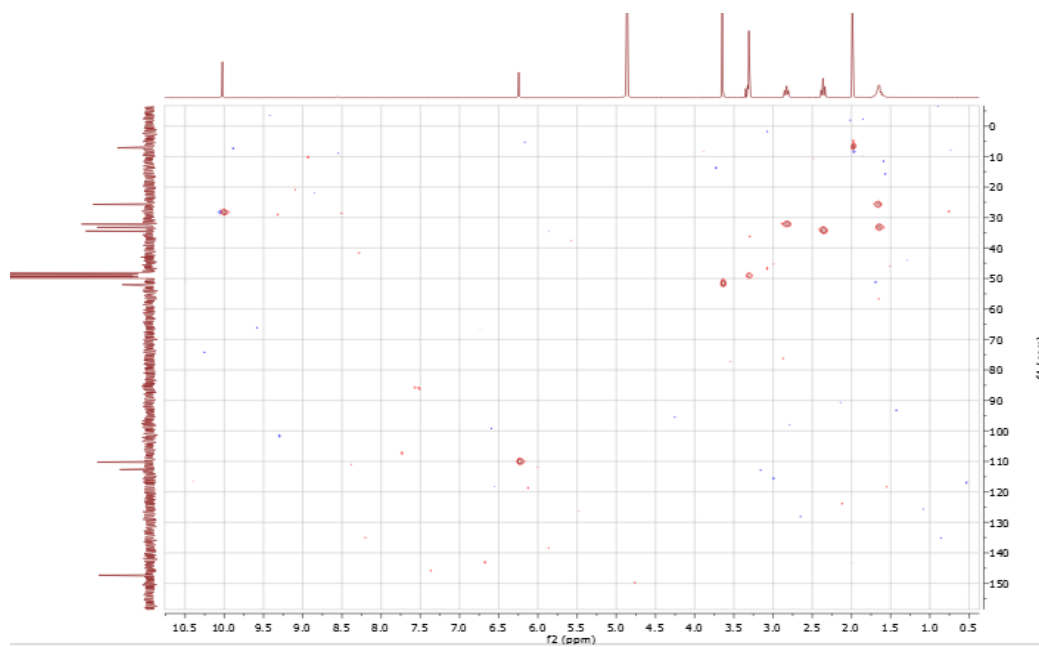
Fig. S35 HMBC spectrum of compound **5**

22
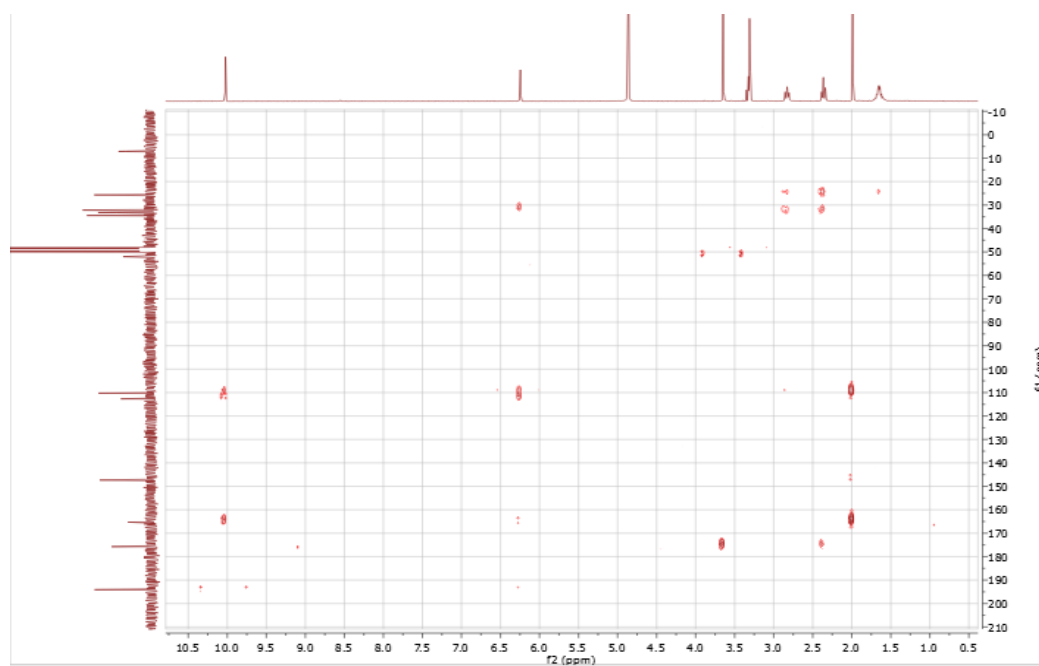
Fig. S36 HRESIMS of compound **5**

Fig. S37 HPLC chromatogram of compound **6**
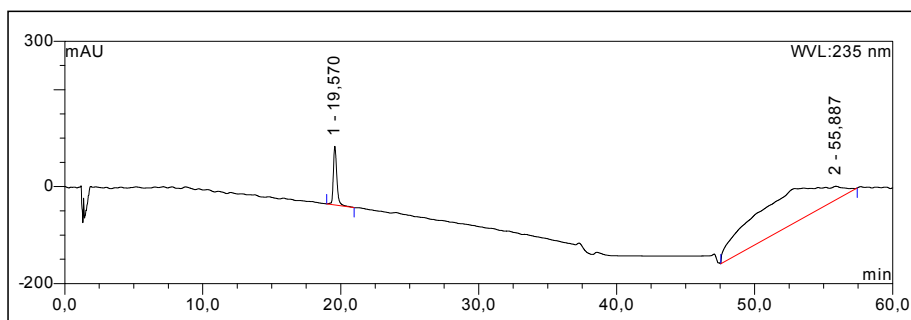
UV absorption of compound **6**
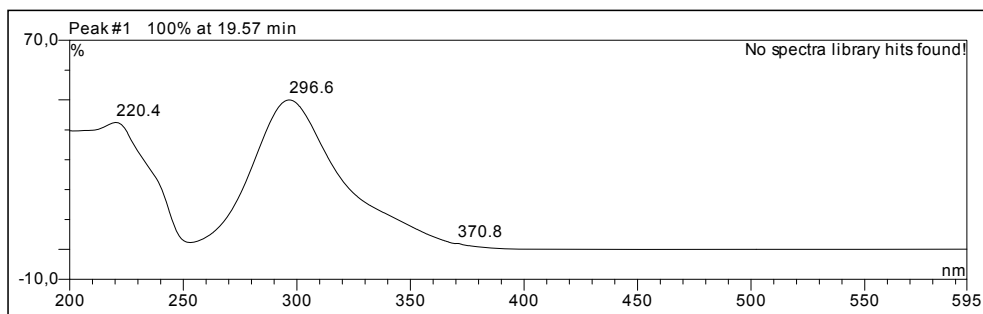
Fig. S38 ^{1}H-NMR (600 MHz, methanol-d_4) spectrum of compound **6**

Fig. S39 ^{13}C-NMR (150 MHz, methanol-d_4) spectrum of compound **6**

24
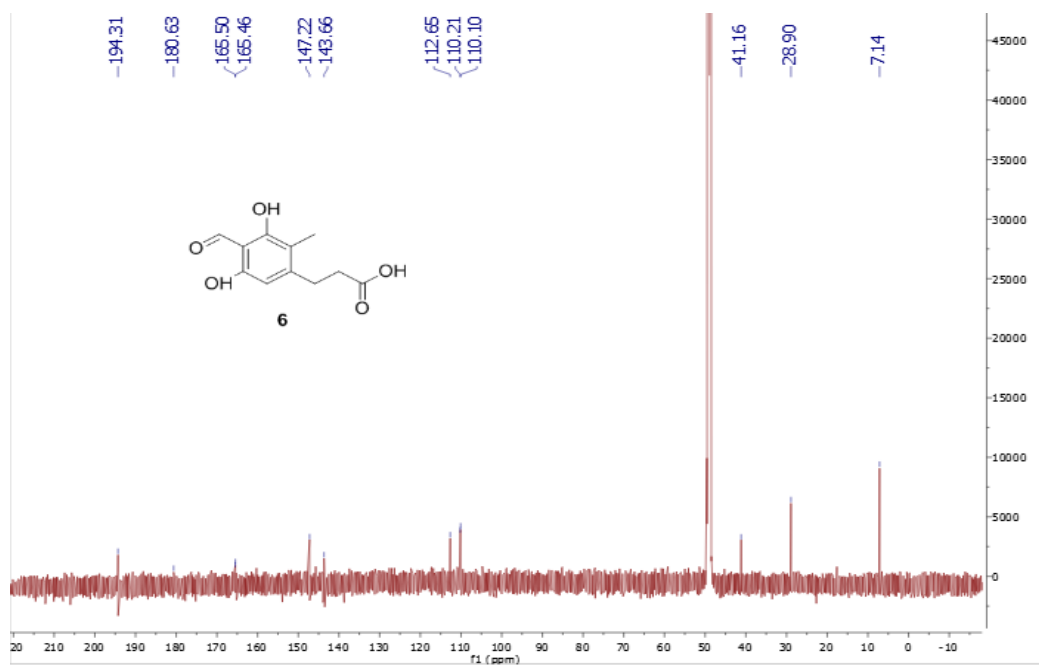
Fig. S40 COSY spectrum of compound **6**

Fig. S41 HSQC spectrum of compound **6**

25
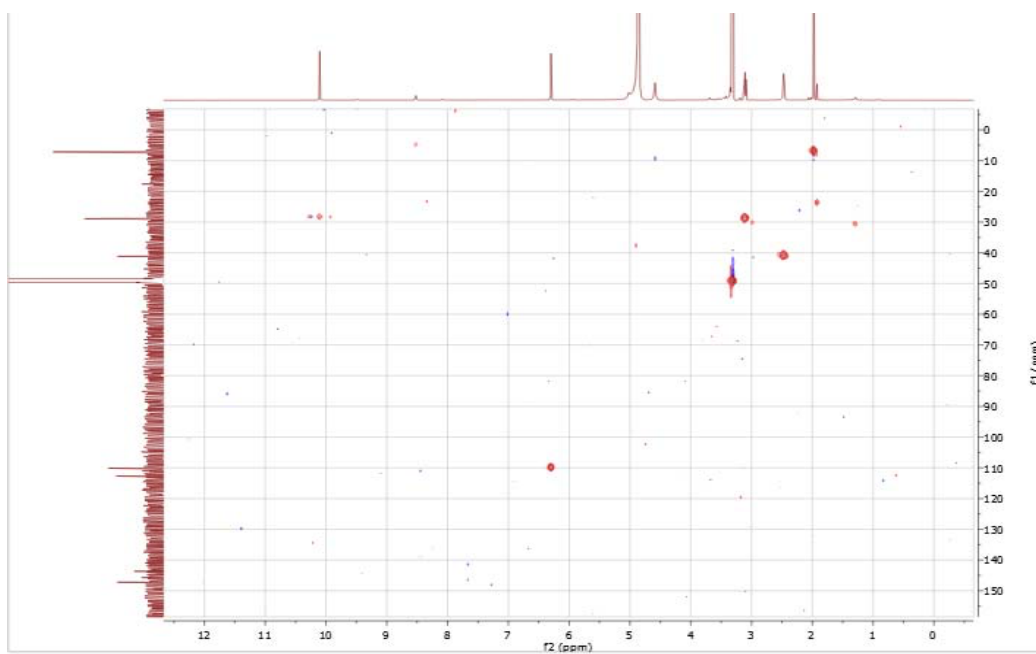
Fig. S42 HMBC spectrum of compound **6**
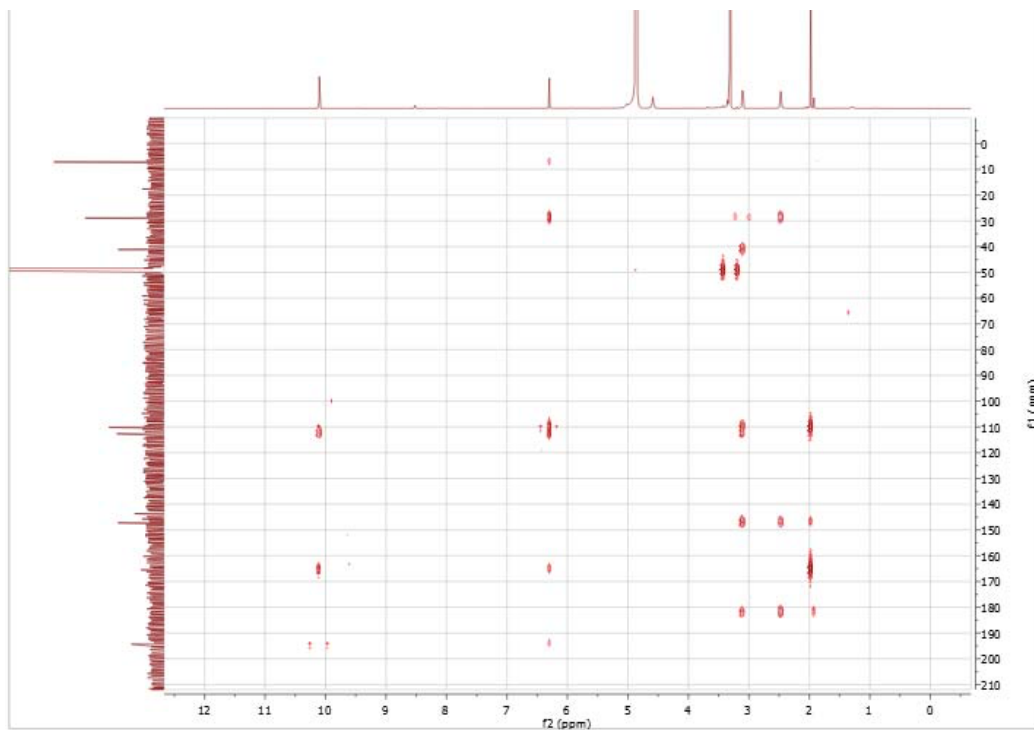
Fig. S43 HRESIMS of compound **6**
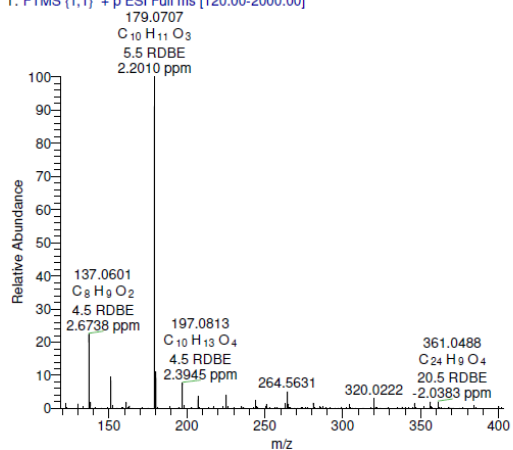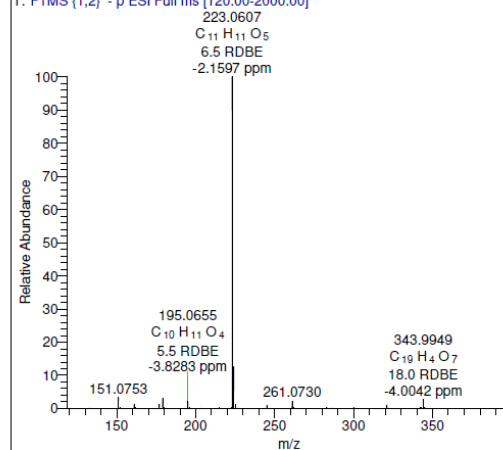
Table S1 Minimum inhibitory concentrations (MIC) of the new compounds **1** and **6**.

Bacterial strains	1	6
	MIC (μM)	MIC (μM)
Staphylococcus aureus (ATCC 29213 and 700699)	50	25 and 50
Enterococcus faecalis (ATCC 29212 and 51299)	100	>100
Enterococcus faecium (ATCC 35667 and 700221)	100	>100
Bacillus subtilis (ATCC 169)	25	not tested
Escherichia coli (ATCC 2469)	100	>100

Fig. S44 The inhibitory zone of compound **1** against *Candida albicans* ATCC 24433 (hyphae form) and *Saccharomyces cerevisiae* as evaluated by the disc diffusion method.
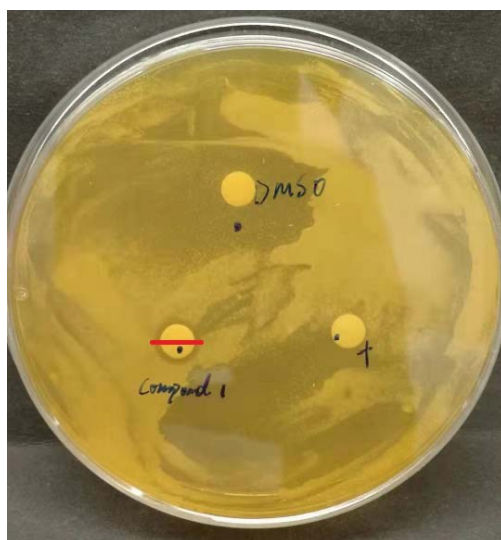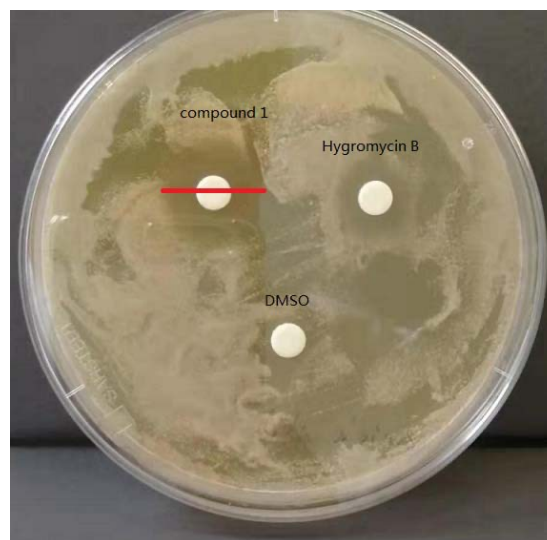
Candida albicans ATCC 24433 (hyphae form)	*Saccharomyces cerevisiae*
(diameter of 8 mm)	(diameter of 18 mm)

27

Chapter 3 Publication 2

Sesterterpenes and macrolide derivatives from the endophytic fungus *Aplosporella javeedii*

Published in: "Fitoterapia"

Impact factor: 2.527

Contribution: First authorship, contributed to 70% of this publication. The first author conducted most of the laboratory work including extraction, isolation, acetylation experiments, literature research, and manuscript preparation.

Reprinted by permission from "**Ying Gao**, Fabian Stuhldreier, Laura Schmitt, Sebastian Wesselborg, Lin Wang, Werner E. G. Müller, Rainer Kalscheuer, Zhiyong Guo, Kun Zou, Zhen Liu, Peter Proksch (2020) Sesterterpenes and macrolide derivatives from the endophytic fungus *Aplosporella javeedii*." *Fitoterapia*, **146**, 104652. Copyright © 2020 Elsevier B.V.

Sesterterpenes and macrolide derivatives from the endophytic fungus *Aplosporella javeedii*

Ying Gao[a], Fabian Stuhldreier[b], Laura Schmitt[b], Sebastian Wesselborg[b], Lin Wang[a], Werner E.G. Müller[c], Rainer Kalscheuer[a], Zhiyong Guo[d], Kun Zou[d], Zhen Liu[a,*], Peter Proksch[a,d,*]

[a] *Institute of Pharmaceutical Biology and Biotechnology, Heinrich Heine University Düsseldorf, Universitätsstrasse 1, 40225 Düsseldorf, Germany*
[b] *Institute of Molecular Medicine I, Medical Faculty, Heinrich Heine University Düsseldorf, Universitätsstrasse 1, 40225 Düsseldorf, Germany*
[c] *Institute of Physiological Chemistry, Universitätsmedizin der Johannes Gutenberg-Universität Mainz, 55128 Mainz, Germany*
[d] *Hubei Key Laboratory of Natural Products Research and Development, College of Biological and Pharmaceutical Sciences, China Three Gorges University, Yichang 443002, China*

ABSTRACT

Five sesterterpenes (1–5) including two new compounds (1 and 2), as well as a new (6) and a known macrolide (7) were isolated from the endophytic fungus *Aplosporella javeedii*. The structures of the new compounds were elucidated by analysis of their 1D and 2D NMR and HRMS data as well as by comparison with the literature. Compound 4 and its acetyl derivatives 4a, 4b, 4c which were prepared by acetylation of 4 exhibited moderate cytotoxicity against the mouse lymphoma cell line L5178Y with IC_{50} values ranging from 6.2 to 12.8 μM, respectively. Moreover, 4a and 4c exhibited also cytotoxicity against human leukemia (Jurkat J16) and lymphoma (Ramos) cell lines. Compound 7 showed strong cytotoxicity against the L5178Y cell line, as well as against human Jurkat J16 and Ramos cells with IC_{50} values of 0.4, 5.8, and 4.4 μM, respectively. Mechanistic studies indicated that 7 induces apoptotic cell death. In addition, compounds 3, 4 and 7 showed low antibacterial activities against *Mycobacterium tuberculosis* H37Rv and compound 6 against *Staphylococcus aureus*, respectively, with MICs of 100 μM. Preliminary structure-activity relationships are discussed.

1. Introduction

Endophytic fungi are an important source of new natural products with some of them showing pronounced biological activities and even exhibiting new modes of action [1–5]. Recent examples from our group include the mitochondrial toxin phomoxanthone A that disturbs the inner mitochondrial membrane within seconds and shows strong anticancer activity [6,7], as well as the unusual chlorinated flavonoid chlorflavonin that shows strong antimycobacterial activity [8]. In the search for new natural products from fungal endophytes ecologically unique and less investigated habitats such as Mangrove swamps [9] or newly discovered fungal species that have not been analyzed previously with regard to their secondary constituents are of special importance. During our ongoing studies on bioactive natural products from endophytic fungi [10–13], we isolated the endophyte *Aplosporella javeedii* from stem tissue of *Orychophragmus violaceus* (L.) O. E. Schul (Brassicaceae) collected in Beijing. This fungus was first described in 2013 [14], and has up to now hardly been studied with regard to its chemical constituents. A first investigation of this fungus yielded a series of new antifungal polyketide derivatives with some of them showing pronounced activity against *Candida albicans* [15]. In continuation of our study on *A. javeedii*, we report now five sesterterpenes (1–5) including two new compounds (1 and 2) as well as a new (6) and a known macrolide derivative (7) and their antibacterial and cytotoxic activities (Fig. 1).

2. Results and discussion

Compound 1 was isolated as colorless oil. The molecular formula of 1 was established as $C_{25}H_{40}O_4$ based on the HRESIMS data, indicating six degrees of unsaturation. The ^{13}C NMR spectrum of 1 displayed the presence of 25 carbons including one ketone carbonyl (δ_C 212.0, C-18), six olefinic carbons, three oxygenated carbons, three aliphatic methines, six methylenes, five methyls, and one aliphatic quaternary carbon, accounting for four degrees of unsaturation. Thus, compound 1 was suggested to be bicyclic. The ^1H and ^{13}C NMR data of 1 (Table 1)
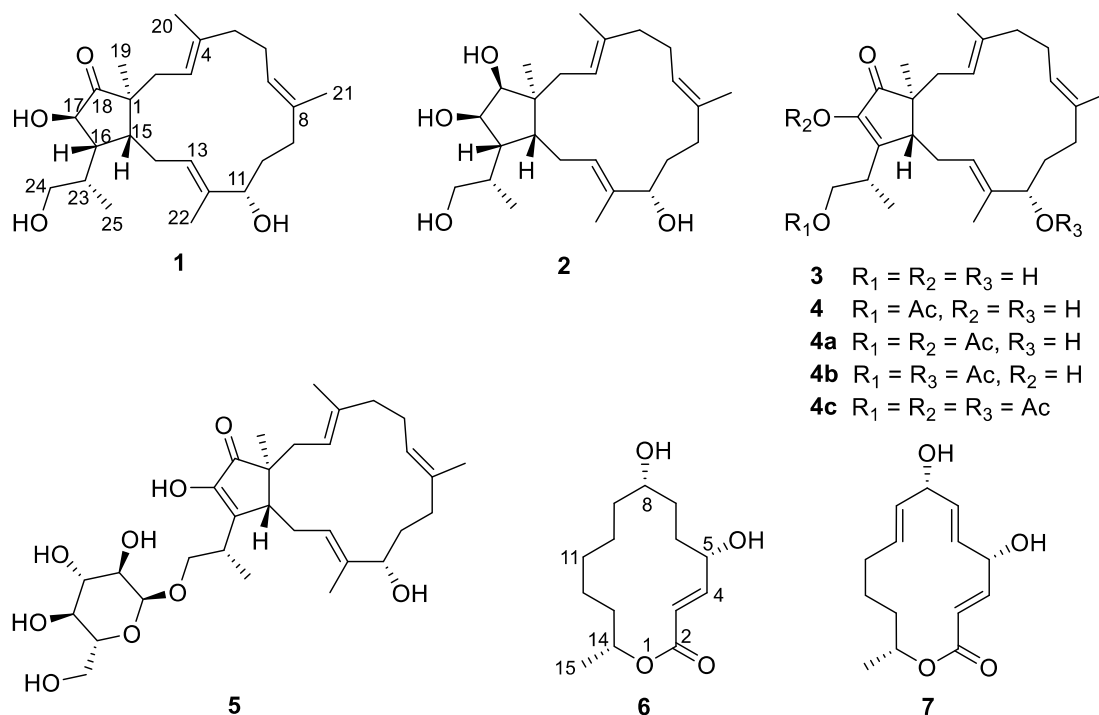
Fig. 1. Structures of isolated compounds from *A. javeedii*.

Table 1
^{1}H and ^{13}C NMR Data for compounds **1** and **2**.

| Position	**1**[a]		**2**[a]	
	δ_C, type	δ_H (*J* in Hz)	δ_C, type[b]	δ_H (*J* in Hz)
1	52.3, C		48.9, C	
2	37.0, CH$_2$	2.14, m, 2.08, m	33.8, CH$_2$	2.30, dd (13.9, 9.0), 1.99, m
3	122.5, CH	5.25, t (7.8)	124.8, CH	5.26, t (8.1)
4	138.8, C		136.4, C	
5	41.1, CH$_2$	2.16, m, 2.11, m	40.8, CH$_2$	2.13, m, 2.07, m
6	24.7, CH$_2$	2.22, m	24.8, CH$_2$	2.16, m
7	125.3, CH	5.19, m	126.1, CH	5.16, m
8	133.9, C		133.4, C	
9	36.0, CH$_2$	2.06, m, 1.82, m	36.1, CH$_2$	2.01, m, 1.84, m
10	31.2, CH$_2$	1.77, m, 1.62, m	31.1, CH$_2$	1.79, m, 1.59, m
11	77.5, CH	3.90, dd (9.9, 4.4)	77.6, CH	3.84, dd (10.7, 3.9)
12	136.5, C		134.4, C	
13	132.1, CH	5.18, m	132.9, CH	5.13, m
14	25.3, CH$_2$	2.25, m, 2.14, m	24.9, CH$_2$	2.04, m, 1.93, m
15	43.0, CH	2.29, m	44.8, CH	1.96, m
16	46.7, CH	2.06, m	50.3, CH	2.06, m
17	77.6, CH	4.07, d (13.1)	74.2, CH	3.87, dd (8.0, 6.7)
18	212.0, C		80.7, CH	3.59, d (6.8)
19	19.0, CH$_3$	1.01, s	21.8, CH$_3$	1.04, s
20	15.9, CH$_3$	1.66, s	15.8, CH$_3$	1.64, s
21	15.6, CH$_3$	1.64, s	15.0, CH$_3$	1.62, s
22	10.8, CH$_3$	1.57, s	10.8, CH$_3$	1.56, s
23	37.3, CH	2.00, m	36.6, CH	1.81, m
24	67.3, CH$_2$	3.61, dd (10.5,4.4), 3.41, dd (10.5,6.6)	67.6, CH$_2$	3.56, dd (10.5, 3.9) 3.23, dd (10.5, 7.5)
25	15.7, CH$_3$	1.20, d (6.7)	15.9, CH$_3$	1.14, d (6.6)

[a] Recorded at 600 MHz (^{1}H) and 150 MHz (^{13}C) in CD$_3$OD.
[b] Data extracted from HSQC and HMBC spectra.
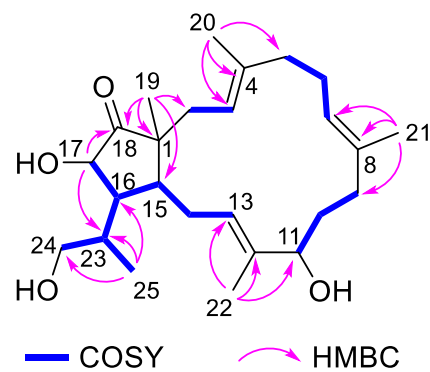
Fig. 2. Key COSY and HMBC correlations for compound **1**.

were similar to those of the co-isolated known bicyclic sesterterpene, (−)-terpestacin (**3**) [16,17]. Compound **1** differed from **3**, however, by the presence of two additional protons at δ_H 4.07 (H-17) and 2.06 (H-16). The observed COSY correlations between H-17/H-16, H-16/H-15 (δ_H 2.29), along with the HMBC correlations from H-17 to C-18 and C-23 (δ_C 37.3), and from Me-25 to C-16 (δ_C 46.7), C-23, and C-24 (δ_C 67.3), indicated the disappearance of the double bond at C-16/C-17 of **3** in compound **1** (Fig. 2). Detailed analysis of the 2D NMR spectra of **1** revealed that the remaining substructure of **1** was identical to that of **3**. Thus, compound **1** was identified as a 16,17-dihydro-(−)-terpestacin derivative, for which the trivial name terpestacin B is proposed. The three double bonds in **1** were *E*-configured as evident from the NOE correlations between H-3 (δ_H 5.25)/H-5b (δ_H 2.11), Me-20 (δ_H 1.66)/H-2b (δ_H 2.08), H-7 (δ_H 5.19)/H-9b (δ_H 1.82), Me-21 (δ_H 1.64)/H-6 (δ_H 2.22), H-13 (δ_H 5.18)/H-11 (δ_H 3.90), and Me-22 (δ_H 1.57)/H-14b (δ_H 2.14). The large coupling constant (13.2 Hz) between H-17 and H-16 indicated their *trans* orientation. The ROESY correlations between H-17/H-14b, H-14b/Me-22, Me-22/Me-19, Me-19/H-14b suggested that
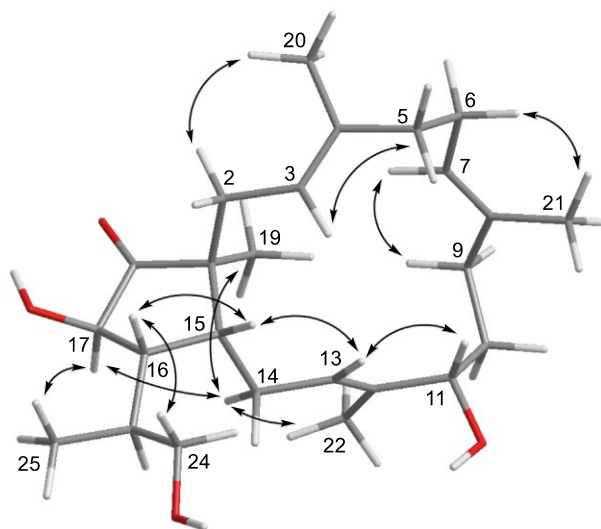
Fig. 3. Key ROESY correlations for compound **1**.

Table 2
^{1}H and ^{13}C NMR Data for compound **6**.[a]

position	δ_C, type	δ_H (J in Hz)
2	168.7, C	
3	121.4, CH	6.03, dd (15.8, 1.5)
4	152.7, CH	6.93, dd (15.8, 5.4)
5	71.0, CH	4.48, m
6	31.9, CH$_2$	1.89, ddt (14.7, 9.5, 2.7), 1.81, dddd (14.7, 8.2, 6.0, 2.5)
7	31.1, CH$_2$	1.69, m, 1.30, m
8	70.1, CH	3.45, m
9	35.5, CH$_2$	1.45, m, 1.32, m
10	25.1, CH$_2$	1.49, m, 1.32, m
11	27.0, CH$_2$	1.25, m
12	24.4, CH$_2$	1.56, m, 1.23, m
13	35.2, CH$_2$	1.66, m
14	71.9, CH	5.00, dqd (8.2, 6.3, 4.6)
15	20.7, CH$_3$	1.28, d (6.3)

[a] Recorded at 600 MHz (^{1}H) and 150 MHz (^{13}C) in CD$_3$OD.

these substituents were on the same face of the ring, whereas the ROESY relationship between H-16/H-15, H-15/H-13, H-13/H-11 indicated that these protons were on the opposite side of the ring (Fig. 3). Thus, the relative configuration of compound **1** was assigned as 1S*, 11S*, 15R*, 16R*, 17R*, 23S*. Considering the close biogenetic relationship between **1** and **3**, the absolute configuration of **1** may be tentatively assigned as 1S, 11S, 15R, 23S which is identical to that of **3** for which the absolute configuration had been earlier confirmed by X-ray crystallographic analysis [18] and total enantioselective synthesis [19–22].

On the basis of the HRESIMS data, the molecular formula of compound **2** was determined as C$_{25}$H$_{42}$O$_4$, containing two additional protons when compared to **1**. The NMR data (Table 1) of **2** were similar to those of **1** except for the replacement of the ketone moiety by an additional oxygenated methine (δ_C 80.7 and δ_H 3.59, CH-18) in **2**. The location of this additional methine at C-18 was confirmed by the COSY correlations between H-18/H-17 (δ_H 3.87), H-17/H-16 (δ_H 2.06), H-16/H-23 (δ_H 1.81), and H-23/Me-25 (δ_H 1.14) in addition to the HMBC correlations from H-18 to C-2 (δ_C 33.8), C-15 (δ_C 44.8), C-16 (δ_C 50.3) and C-19 (δ_C 21.8). The remaining substructure of **2** was determined to be identical to that of **1** by analysis the 2D NMR data of **2**. Thus, the structure of compound **2** was elucidated as shown, for which the trivial name terpestacin C is proposed. In the ROESY spectrum of **2**, H-18 exhibited correlations to H-17 and Me-19 (δ_H 1.04), indicating that those protons have the same orientation. Based on the similar NOE correlations and the biogenetic relationship to the known compound **3**, the relative configuration of **2** was assigned as 1S*, 11S*, 15R*, 16R*, 17R*, 18S*, 23S*. Based on the close biogenetic relationship of both compounds the relative configuration of **2** probably matches its absolute configuration like in the case of **1**.

The molecular formula of compound **6** was established as C$_{14}$H$_{24}$O$_4$ by HRESIMS, indicating three degrees of unsaturation. The ^{13}C NMR spectra of **6** exhibited one ester carbonyl carbon at δ_C 168.7 (C-2), two olefinic carbons at δ_C 152.7 (C-4) and 121.4 (C-3), three oxygenated carbons at δ_C 71.9 (C-14), 71.0 (C-5), and 70.1 (C-8), and one methyl group at δ_C 20.7 (C-15) in addition to seven aliphatic methylenes (Table 2). Detailed analysis of the 2D NMR spectra indicated that **6** was similar to the co-isolated known compound mutolide (**7**) [23,24] as well as to the previously reported macrolide, pestalotioprolide C [10]. This was further confirmed by the COSY correlations between H-3/H-4, H-4/H-5, H-5/H$_2$-6, H$_2$-6/H$_2$-7, H$_2$-7/H$_2$-8, H-8/H$_2$-9, H$_2$-10/H$_2$-11, H$_2$-12/H$_2$-13, H$_2$-13/H-14, H-14/Me-15, along with key HMBC

correlations from H-8 to C-10, from H$_2$-13 to C-11, and from H-3, H-4, and H-14 to C-2. Thus, compound **6** was identified as 6,7,9,10-tetrahydromutolide. The large coupling constant (15.8 Hz) between H-3 and H-4 indicated E configuration for the double bond. The relative configuration at C-5, 8, and 14 of **6** cannot be directly deduced from the ROESY spectrum due to the flexibility of the macrocyclic ring and overlapping signals in the ^{1}H NMR spectrum. The absolute configuration of mutolide (**7**) had been determined as 5S, 8S, and 14R by X-ray analysis [23]. 6,7,9,10-Tetrahydromutolide (**6**) is suggested to share the same configuration at C-5, 8, and 14 as **7** due to their close biogenetic relationship.

The remaining compounds were identified as the known sesterterpenes, fusaproliferin (**4**) [25,26] and 24-α-D-glucosyl-(−)-terpestacin (**5**) [27]. All sesterterpenes (**1–5**) isolated in this study exhibited the same skeleton. Terpestacin (**3**) had been first isolated from *Arthrinium* sp. [16] and showed anti-HIV [16], anti-angiogenic [28], anti-cancer [29,30], as well as anti-fungal [25] activities. Fusaproliferin (**4**) is an acetic acid ester of terpestacin and is known for its phytotoxic [31] and anti-cancer activity [32].

All isolated compounds (**1–7**) were tested for their antibacterial activities against *Mycobacterium tuberculosis* H37Rv, *Staphylococcus aureus* ATCC 29213 and *Acinetobacter baumannii* BAA1605. Compounds **3**, **4** and **7** showed low antibacterial activities against *M. tuberculosis* and compound **6** against *S. aureus*, respectively, with MICs of 100 μM. All other compounds were not active in these assays. All isolated compounds were also tested for their cytotoxicity against the mouse lymphoma cell line L5178Y as well as against human leukemia (Jurkat J16) and lymphoma (Ramos) cell lines (Table 3). Fusaproliferin (**4**)

Table 3
Cytotoxicity (IC$_{50}$, μM) of isolated and semisynthetically derived compounds against L5178Y, Ramos and Jurkat J16 cell lines.

Compound	L5178Y[a] 72 h	Ramos[b] 24 h	Ramos 72 h	Jurkat J16[b] 24 h	Jurkat J16 72 h
1	-[c]	> 20	> 20	16.5	16.5
2	-	14.8	19.4	> 20	> 20
3	-	-	-	-	-
4	10.8	12.1	10.4	> 20	13.4
4a	6.2	15.3	12.6	18.2	13.2
4b	12.8	> 20	4.8	> 20	10.5
4c	11.0	12.0	4.6	18.1	15.9
5	-	-	-	-	-
6	-	-	-	-	-
7	0.4	4.4	0.8	5.8	1.4

[a] Kahalalide F (IC$_{50}$ = 4.3 μM) was used as positive control.
[b] Staurosporine (STS, IC$_{50}$ = 2.5 μM) was used as positive control.
[c] Not active.

3

exhibited cytotoxicity with an IC$_{50}$ value of 10.8 μM against the L5178Y cell line after 72 h of incubation, whereas (−)-terpestacin (**3**) was inactive in comparison. The presence of an acetyl function in fusaproliferin (**4**) thus increases the cytotoxicity compared to the hydroxyl analogue **3**. Based on this result the diacetyl derivatives **4a** and **4b** and the triacetyl derivative **4c** of fusaproliferin (**4**) were prepared by acetylation of **4**. Compounds **4a**, **4b**, **4c** exhibited IC$_{50}$ values of 6.2, 12.8, and 11.0 μM against the L5178Y cell line after 72 h of incubation, respectively. Whereas **4b** and **4c** were almost equipotent to the parent compound fusaproliferin (**4**), acetylation of the hydroxy group at C-17 increased the cytotoxicity of **4a** compared to **4** against the L5178Y cell line. In the human lymphoma (Ramos) cell line, compounds **2**, **4**, **4a**, and **4c** exhibited IC$_{50}$ values of 14.8, 12.1, 15.3, and 12.0 μM after 24 h of incubation, respectively, whereas compounds **1**, **4a**, and **4c** showed cytotoxicity against the human leukemia (Jurkat J16) cell line with IC$_{50}$ values of 16.5, 18.2, and 18.1 μM after 24 h of incubation, respectively. Thus, **4a** and **4c** showed cytotoxicity against both human cell lines, whereas **4b** was inactive (IC$_{50}$ > 20 μM) against both cell lines in comparison.

The macrolide mutolide (**7**) displayed strong cytotoxicity against the L5178Y cell line with an IC$_{50}$ value of 0.4 μM after 72 h of incubation, which was ten times lower than that of the positive control kahalalide F (IC$_{50}$ 4.3 μM), whereas compound **6** was inactive in comparison. The absence of double bonds at $\Delta^{6,7}$ and $\Delta^{9,10}$ in the 14-membered ring of **6** apparently leads to a complete loss of cytotoxicity compared to **7**. Mutolide (**7**) showed also significant cytotoxicity against the human leukemia (Jurkat J16) and lymphoma (Ramos) cell lines. After 24 h incubation, the IC$_{50}$ values of mutolide (**7**) against Jurkat J16 and Ramos cells were 5.8 and 4.4 μM, respectively whereas after 72 h of incubation these values dropped to 1.4 and 0.8 μM respectively. Mutolide (**7**) has been reported as an anti-inflammatory compound which exerts its anti-inflammatory effect via NF-κB inhibition [24]. The compound, however, showed also pro-apoptotic activity in this study. Apoptosis is the process of programmed cell death which leads to the elimination of damaged cells. Dysregulation of apoptosis is a significant factor in many human diseases such as cancer [33,34]. In order to evaluate the pro-apoptotic mechanism of mutolide (**7**), we performed an immunoblot analysis for the cleavage of the caspase-substrate poly (ADP-ribose) polymerase-1 (PARP-1) [11]. Caspases are cysteine-dependent aspartate-directed proteases and act as central executioners of the apoptotic machinery. During apoptosis PARP1 is cleaved upon activation of effector caspases such as caspase-3 that comprises a point of convergence of extrinsic and intrinsic apoptosis pathways [34]. In the Western blot experiment in the Ramos cell line, treatment of cells with 10 μM mutolide (**7**) for 2–8 h lead to an explicit cleavage of PARP-1, indicating the activation of caspase-3 and induction of apoptosis (Fig. 4). Furthermore, processing of the fluorogenic caspase-3 substrate Ac-DEVD-AMC was detected, which can identify and quantify caspase-3 activity in apoptotic cells. After treatment with mutolide (**7**) at concentrations up to 10 μM cleavage of Ac-DEVD-AMC was observed within a few hours, which is an additional proof for
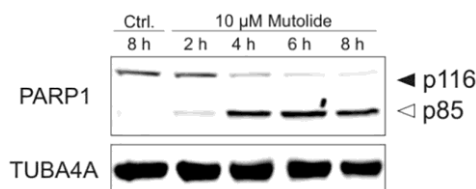

Fig. 4. Mutolide (**7**) induces apoptosis in Ramos cell line (Burkitt's lymphoma B lymphocytes). After incubation for 2–8 h, cleavage of PARP was determined by Western blot analysis. Solid arrowheads indicate the uncleaved form of PARP, open arrowheads indicate the cleaved form. The expression of TUBA4A was determined as protein loading control. Negative control (Ctrl.) was 0.1% DMSO.
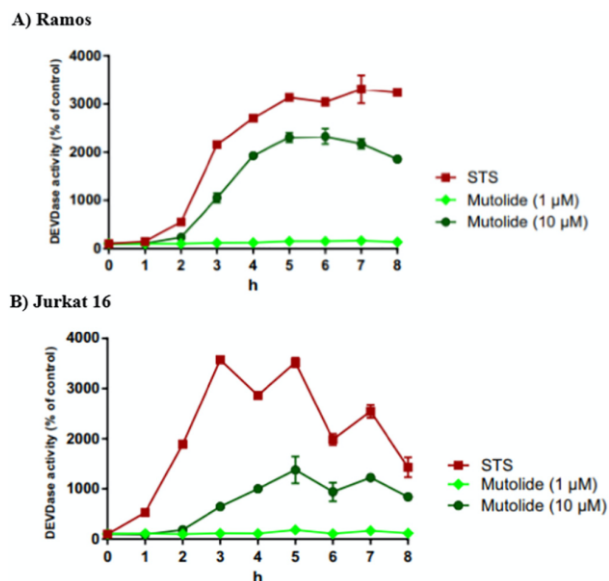

Fig. 5. The kinetics of caspase-3 activation in (A) Ramos cells (Burkitt's lymphoma B lymphocytes) and (B) Jurkat J16 cells (acute T cell leukemia cells) after treatment with indicated concentrations of mutolide (**7**). Caspase-3 activity was measured by the rate of cleavage of Ac-DEVD-AMC. Cells treated with staurosporine (STS, IC$_{50}$ = 2.5 μM) were used as positive control. Cells treated with 0.1% DMSO were used as negative control and set to 0. Data shown are the mean ± SD from a representative experiment performed in triplicate.

mutolide (**7**)-induced apoptosis (Fig. 5). Mutolide (**7**) is thus of interest for further studies on anticancer activity.

3. Experimental section

3.1. General experimental procedures

Optical rotations were measured using a Perkin-Elmer-241 MC polarimeter. ^{1}H, ^{13}C and 2D NMR spectra were recorded at 25 °C in CD$_3$OD on a Bruker ARX 600 NMR spectrometer. Chemical shifts were referenced to the solvent residual peaks. Mass spectra (ESI) were measured on a Finnigan LCQ Deca XP Thermoquest mass spectrometer (Bremen, Germany). HRESIMS data were recorded with a UHR-QTOF maxis 4G (Bruker Daltonics) mass spectrometer. HPLC analysis was performed with a Dionex UltiMate-3400SD system with a LPG-3400SD pump and a photodiode array detector (DAD 3000RS), using the routine detection channels at 235, 254, 280 and 340 nm. The analytical HPLC column (125 × 4 mm) was prefilled with Eurosphere-10 C$_{18}$ (Knauer, Germany). Semi-preparative HPLC was carried out on a Merck Hitachi HPLC system (UV detector L7400; pump L7100; Eurosphere-100 C$_{18}$, 300 × 8 mm, Knauer, Germany). TLC plates precoated with silica gel F$_{254}$ (Merck, Germany) were used for analysis of fractions under 254 and 366 nm or after spraying the plates with anisaldehyde reagent followed by heating. Merck MN silica gel 60 M (0.04–0.063 mm) or Sephadex LH-20 were used for column chromatography. Distilled or spectral grade solvents were used for column chromatography and spectroscopic measurements, respectively.

3.2. Fungal material and identification

The endophytic fungus was isolated from fresh, healthy stem tissue of *Orychophragmus violaceus* (L.) O. E. Schul (*Brassicaceae*), which was collected in April 2018 in Beijing, P.R. China. The isolation of the fungal strain was achieved according to a standard procedure as described before [35]. It was identified as *Aplosporella javeedii* according

to DNA amplification and sequencing of the ITS region with the Gen-Bank accession number MN720704. The fungal strain (ID code ZGB-B) is kept in the Institute of Pharmaceutical Biology and Biotechnology, Heinrich-Heine University, Duesseldorf, Germany.

3.3. Cultivation, extraction and isolation

The fungus was cultivated in ten 1 L Erlenmeyer flasks on solid rice medium (100 g rice and 110 mL demineralized water). After auto-claving at 121 °C for 20 min and cooling down to room temperature, the fungal strain was added. After growing for around 20 days, the fungal cultures were extracted with 800 mL EtOAc each which resulted in a brown extract (10.5 g). Silica gel vacuum liquid column chromatography (VLC) was used for the separation of the crude extract. Using solvents of increasing polarity (n-hexane, EtOAc, CH_2Cl_2, and MeOH), 12 fractions (V1 to V12) were obtained in total. Fraction V4 (1.1 g) was separated on a silica gel column with a n-hexane-EtOAc gradient (20:1 to 0:100), affording ten subfractions. Subfraction V4-S4 (165.5 mg) was purified by semi-preparative HPLC using MeOH-H_2O (70:30 to 95:5) to give 4 (56.6 mg). Fraction V5 (235.9 mg) was subjected to a Sephadex LH-20 column using CH_2Cl_2-MeOH (1:1) as eluent to obtain seven subfractions. Subfraction V5-S2 (48.8 mg) was purified by semi-preparative HPLC using MeOH-H_2O (70:30 to 93:7) to give 3 (8.7 mg). Fraction V6 (261.4 mg) was separated on a Sephadex LH-20 column using CH_2Cl_2-MeOH (1:1) as eluent to obtain six subfractions. Subfraction V6-S3 (88.6 mg) was purified by semi-preparative HPLC using MeOH-H_2O (30:70 to 55:45) to give 1 (1.8 mg), 6 (3.0 mg), and 7 (2.5 mg). Fractions V7 (206.4 mg) and V8 (100.2 mg) were combined and applied to a Sephadex LH-20 column with CH_2Cl_2-MeOH (1:1) as eluent, followed by purification using semi-preparative HPLC with MeOH-H_2O (40:60) as mobile phase to give 2 (3.7 mg). Fraction V9 (1.0 g) was separated on a Sephadex LH-20 column using CH_2Cl_2-MeOH (1:1) to give six subfractions. Subfraction V9-S3 (102.8 mg) was subjected to a silica gel column with a CH_2Cl_2-MeOH gradient (20:1 to 0:100), followed by purification using semi-preparative HPLC with MeOH-H_2O (75:25) as mobile phase to afford 5 (2.0 mg).

Terpestacin B (1): Colorless oil; $[\alpha]_D^{20}$ − 68 (c 0.2, MeOH); UV (MeOH) λ_{max} 201 nm; ^{1}H and ^{13}C NMR data, see Table 1; HRESIMS [M + Na]$^+$ m/z 427.2821 (calcd for $C_{25}H_{40}O_4Na$ 427.2819).

Terpestacin C (2): Colorless oil; $[\alpha]_D^{20}$ − 537 (c 0.2, MeOH); UV (MeOH) λ_{max} 201 nm; ^{1}H and ^{13}C NMR data, see Table 1; HRESIMS [M + Na]$^+$ m/z 429.2982 (calcd for $C_{25}H_{42}O_4Na$ 429.2975).

6,7,9,10-Tetrahydromutolide (6): Colorless powder; $[\alpha]_D^{20}$ − 29 (c 0.2, MeOH); UV (MeOH) λ_{max} 212 nm; ^{1}H and ^{13}C NMR data, see Table 2; HRESIMS [M + Na]$^+$ m/z 279.1570 (calcd for $C_{14}H_{24}O_4Na$ 279.1567).

3.4. Acylation of compound 4

To compound 4 (14.7 mg) was added acetic anhydride (1 mL) followed by stirring overnight at room temperature. Then the mixture was washed with nanopure water (1 mL). The organic layer was evaporated under vacuum and gave a colorless oil. The resulting oil was separated by semi-preparative HPLC using MeCN-H_2O (50:50 to 85:15) to give 4 (0.7 mg, residual), 4a (3.1 mg), 4b (1.5 mg), and 4c (4.7 mg). The structures of the semisynthetic compounds 4a, 4b and 4c were elucidated by interpretation of their NMR and MS spectra and by comparison with the spectra of the parent compound 4.

Compound 4a: Colorless oil; $[\alpha]_D^{20}$ − 17 (c 0.2, MeOH); UV (MeOH) λ_{max} 202 and 236 nm; ESIMS [M-H_2O + H]$^+$ m/z 469.3, [2 M + Na]$^+$ m/z 995.5; ^{1}H NMR (600 MHz, CD$_3$OD) δ 5.39 (m, 1H), 5.32 (dd, J = 10.4, 5.0 Hz, 1H), 5.17 (m, 1H), 4.20 (dd, J = 10.8, 6.4 Hz, 1H), 4.17 (dd, J = 10.8, 8.1 Hz, 1H), 3.99 (dd, J = 9.7, 4.1 Hz, 1H), 2.99 (m, 1H), 2.92 (dd, J = 11.0, 2.4 Hz, 1H), 2.48 (m, 1H), 2.35–2.28 (m, 3H), 2.25 (s, 3H), 2.17–2.04 (m, 4H), 2.00 (s, 3H), 1.86–1.75 (m, 3H), 1.65 (s, 6H), 1.58 (s, 3H), 1.27 (d, J = 7.1 Hz, 3H),

1.02 (s, 3H).

Compound 4b: Colorless oil; $[\alpha]_D^{20}$ − 35 (c 0.2, MeOH); UV (MeOH) λ_{max} 201 and 263 nm; ESIMS [M + Na]$^+$ m/z 509.5; ^{1}H NMR (600 MHz, CD$_3$OD) δ 5.53 (m, 1H), 5.33 (dd, J = 10.5, 5.0 Hz, 1H), 5.23–5.20 (m, 1H), 5.19 (dd, J = 10.3, 3.8 Hz, 1H), 4.30 (dd, J = 10.4, 8.1 Hz, 1H), 4.25 (dd, J = 10.4, 6.7 Hz, 1H), 2.80 (m, 1H), 2.73 (dd, J = 11.3, 2.3 Hz, 1H), 2.42 (m, 1H), 2.37–2.29 (m, 3H), 2.17–2.07 (m, 3H), 2.00 (s, 3H), 1.99 (s, 3H), 1.95 (ddd, J = 18.0, 11.4, 7.7 Hz, 1H), 1.86–1.82 (m, 1H), 1.78–1.75 (m, 1H), 1.70 (dd, J = 13.7, 4.8 Hz, 1H), 1.66 (s, 3H), 1.65 (s, 3H), 1.59 (s, 3H), 1.29 (d, J = 7.1 Hz, 3H), 0.96 (s, 3H).

Compound 4c: Colorless oil; $[\alpha]_D^{20}$ − 41 (c 0.2, MeOH); UV (MeOH) λ_{max} 205 and 236 nm; ESIMS [M + Na]$^+$ m/z 551.5; ^{1}H NMR (600 MHz, CD$_3$OD) δ 5.53 (m, 1H), 5.34 (dd, J = 10.3, 5.4 Hz, 1H), 5.21 (m, 1H), 5.19 (dd, J = 10.2, 4.0 Hz, 1H), 4.20 (dd, J = 10.8, 6.3 Hz, 1H), 4.15 (dd, J = 10.8, 8.2 Hz, 1H), 2.98 (m, 1H), 2.93 (dd, J = 11.0, 2.5 Hz, 1H), 2.47 (m, 1H), 2.37–2.28 (m, 3H), 2.25 (s, 3H), 2.19–2.06 (m, 4H), 2.00 (s, 3H), 1.99 (s, 3H), 1.88–1.82 (m, 2H), 1.79–1.76 (m, 1H), 1.67 (s, 3H), 1.66 (s, 3H), 1.61 (s, 3H), 1.25 (d, J = 7.1 Hz, 3H), 1.01 (s, 3H).

3.5. Cytotoxicity and apoptosis assays

The cytotoxicity against the L5178Y mouse lymphoma cell line (European Collection of Authenticated Cell Cultures, Catalogue No. 87111908) was tested using the MTT method as described previously [36]. Kahalalide F was used as positive control (IC$_{50}$ 4.3 μM) and media with 0.1% DMSO were used as negative control. The cytotoxicity against adult lymphoblastic leukemia T cells (Jurkat J16, No. ACC-282) and Burkitt's lymphoma B cells (Ramos, No. ACC-603) was tested as described previously [11]. The protein kinase inhibitor staurosporine (STS, #S5921) was used as positive control for apoptosis, while media with 0.1% DMSO were used as negative control. Activation of caspase-3 as a hallmark of apoptosis was determined as described earlier. Briefly, fluorescence of the pro-fluorescent caspase-3 substrate Ac-DEVD-AMC (Biomol, #ABD-13402) was measured via microplate spectrophotometer and served as an indirect measure of apoptotic cell death [37]. All experiments were carried out in triplicate.

3.6. Antibacterial assay

The antibacterial assay was performed with the broth microdilution method following the recommendation of the Clinical and Laboratory Standards Institute (CLSI) [38]. The antibacterial activity was evaluated by calculating the MIC against a panel of Gram positive and negative bacterial strains including Mycobacterium tuberculosis H37Rv, Staphylococcus aureus ATCC 29213, and Acinetobacter baumannii BAA1605. MICs of 50–100 μM are considered to reflect a weak activity, whereas MIC > 100 μM is considered inactive.

Acknowledgments

Appendix A. Supplementary data

Supplementary data to this article can be found online at https://doi.org/10.1016/j.fitote.2020.104652.

5

References

[1] A.H. Aly, A. Debbab, P. Proksch, Fungal endophytes: unique plant inhabitants with great promises, Appl. Microbiol. Biotechnol. 90 (2011) 1829–1845.

[2] A.H. Aly, A. Debbab, J. Kjer, P. Proksch, Fungal endophytes from higher plants: a prolific source of phytochemicals and other bioactive natural products, Fungal Divers. 41 (2010) 1–16.

[3] F. Uzma, C.D. Mohan, A. Hashem, et al., Endophytic fungi—alternative sources of cytotoxic compounds: a review, Front. Pharmacol. 9 (2018) 309.

[4] S. Gouda, G. Das, S.K. Sen, H.S. Shin, J.K. Patra, Endophytes: a treasure house of bioactive compounds of medicinal importance, Front. Microbiol. 7 (2016) 1538.

[5] A.H. Aly, A. Debbab, P. Proksch, Fungal endophytes—secret producers of bioactive plant metabolites, Die Pharmazie 68 (2013) 499–505.

[6] P. Böhler, F. Stuhldreier, R. Anand, et al., The mycotoxin phomoxanthone a disturbs the form and function of the inner mitochondrial membrane, Cell Death Dis. 9 (2018) 286.

[7] C. Wang, L. Engelke, D. Bickel, et al., The tetrahydroxanthone-dimer phomoxanthone a is a strong inducer of apoptosis in cisplatin-resistant solid cancer cells, Bioorg. Med. Chem. 27 (2019) 115044.

[8] N. Rehberg, H.S. Akone, T.R. Ioerger, et al., Chlorflavonin targets acetohydroxyacid synthase catalytic subunit IlvB1 for synergistic killing of *Mycobacterium tuberculosis*, ACS Infect. Dis. 4 (2018) 123–134.

[9] E. Ancheeva, G. Daletos, P. Proksch, Lead compounds from mangrove-associated microorganisms, Mar. Drugs. 16 (2018) 319.

[10] S. Liu, H. Dai, G. Makhloufi, et al., Cytotoxic 14-membered macrolides from a mangrove-derived endophytic fungus, *Pestalotiopsis microspora*, J. Nat. Prod. 79 (2016) 2332–2340.

[11] H. Harwoko, G. Daletos, F. Stuhldreier, et al., Dithiodiketopiperazine derivatives from endophytic fungi *Trichoderma harzianum* and *Epicoccum nigrum*, Nat. Prod. Res. (2019) 1–9.

[12] S. Liu, Y. Zhao, C. Heering, et al., Sesquiterpenoids from the endophytic fungus *Rhinocladiella similis*, J. Nat. Prod. 82 (2019) 1055–1062.

[13] Y. Liu, F. Stuhldreier, et al., Daldinone derivatives from the mangrove-derived endophytic fungus *Annulohypoxylon* sp, RSC Adv. 7 (2017) 5381–5393.

[14] F. Jami, B. Slippers, M.J. Wingfield, M. Gryzenhout, *Botryosphaeriaceae* species overlap on four unrelated, native south African hosts, Fungal Biol. 118 (2014) 168–179.

[15] Y. Gao, et al., Antifungal polyketide derivatives from the endophytic fungus Aplosporella javeedii, Bioorg. Med. Chem. 28 (2020) 115456.

[16] M. Oka, S. Iimura, O. Tenmyo, et al., Terpestacin, a new syncytium formation inhibitor from *Arthrinium* sp, J. Antibiot. 46 (1993) 367–373.

[17] S. Iimura, M. Oka, Y. Narita, et al., Terpestacin, a novel syncytium formation inhibitor, isolated from *Arthrinium* species, Tetrahedron Lett. 34 (1993) 493–496.

[18] M. Oka, S. Iimura, Y. Narita, et al., Stereochemistry and biosynthesis of terpestacin, a new syncytium formation inhibitor, J. Organomet. Chem. 58 (1993) 1875–1881.

[19] J. Chan, T.F. Jamison, Enantioselective synthesis of (−)-terpestacin and structural revision of siccanol using catalytic stereoselective fragment couplings and macrocyclizations, J. Am. Chem. Soc. 126 (2004) 10682–10691.

[20] G.O. Berger, M.A. Tius, Terpestacin core sructure: control of stereochemistry, Org. Lett. 7 (2005) 5011–5013.

[21] G.O. Berger, M.A. Tius, Total synthesis of (±)-terpestacin and (±)-11-*epi*-terpestacin, J. Organomet. Chem. 72 (2007) 6473–6480.

[22] A.G. Myers, M. Siu, F. Ren, Enantioselective synthesis of (−)-terpestacin and (−)-fusaproliferin: clarification of optical rotational measurements and absolute configurational assignments establishes a homochiral structural series, J. Am. Chem. Soc. 124 (2002) 4230–4232.

[23] H.B. Bode, M. Walker, A. Zeeck, Structure and biosynthesis of mutolide, a novel macrolide from a UV mutant of the fungus F-24′707, Eur. J. Org. Chem. (8) (2000) 1451–1456.

[24] M. Shah, S.K. Deshmukh, S.A. Verekar, et al., Anti-inflammatory properties of mutolide isolated from the fungus *Lepidosphaeria* species (PM0651419), SpringerPlus. 4 (2015) 706.

[25] A. Cimmino, S. Sarrocco, M. Masi, et al., Fusaproliferin, terpestacin and their derivatives display variable allelopathic activity against some ascomycetous fungi, Chem. Biodivers. 13 (2016) 1593–1600.

[26] A. Santini, A. Ritieni, V. Fogliano, et al., Structure and absolute stereochemistry of fusaproliferin, a toxic metabolite from *Fusarium proliferatum*, J. Nat. Prod. 59 (1996) 109–112.

[27] D.L. Guo, M. Zhao, S.J. Xiao, et al., Two new diketopiperazines and a new glucosyl sesterterpene from *Alternaria alternata*, an endophytic fungi from *Ceratostigma griffithii*, Phytochem. Lett. 14 (2015) 260–264.

[28] H.J. Jung, H.B. Lee, C.J. Kim, et al., Anti-angiogenic activity of terpestacin, a bicyclo sesterterpene from *Embellisia chlangdospora*, J. Antibiot. 56 (2003) 492–496.

[29] H.J. Jung, J.S. Shim, J. Lee, et al., Terpestacin inhibits tumor angiogenesis by targeting UQCRB of mitochondrial complex III and suppressing hypoxia-induced reactive oxygen species production and cellular oxygen sensing, J. Biol. Chem. 285 (2010) 11584−11595.

[30] K.C. Park, S.H. Choi, Effects of endostatin and a new drug terpestacin against human neuroblastoma xenograft and cell lines, Pediatr. Surg. Int. 29 (2013) 1327–1340.

[31] A. Santini, G. Meca, S. Uhlig, et al., Fusaproliferin, beauvericin and enniatins: occurrence in food-a review, World Mycotoxin J. 5 (2012) 71–81.

[32] N. Hoque, C.M. Hasan, M.S. Rana, et al., Fusaproliferin, a fungal phytotoxin shows rapid and potent cytotoxicity against pancreatic cancer cell lines, Molecules. 23 (2018) 3288.

[33] S. Elmore, Apoptosis: a review of programmed cell death, Toxicol. Pathol. 35 (2007) 495–516.

[34] R.S. Wong, Apoptosis in cancer: from pathogenesis to treatment, J. Exp. Clin. Cancer Res. 30 (2011) 87.

[35] A. Debbab, A.H. Aly, et al., Bioactive metabolites from the endophytic fungus *Stemphylium globuliferum* isolated from *Mentha pulegium*, J. Nat. Prod. 72 (2009) 626–631.

[36] M. Ashour, R.A. Edrada, R. Ebel, et al., Kahalalide derivatives from the Indian sacoglossan mollusk *Elysia grandifolia*, J. Nat. Prod. 69 (2006) 1547–1553.

[37] J. Manns, M. Daubrawa, S. Driessen, et al., Triggering of a Novel Intrinsic Apoptosis Pathway by the Kinase Inhibitor Staurosporine: Activation of Caspase-9 in the Absence of Apaf-1, 25 (2011), pp. 3250–3261.

[38] CLSI, Methods for Dilution Antimicrobial Susceptibility Tests for Bacteria that Grow Aerobically. 11th Ed. CLSI Standard M07, Clinical and Laboratory Standards Institute, Wayne, PA, 2018.

Support information

Sesterterpenes and macrolide derivatives from the endophytic fungus

Aplosporella javeedii

Ying Gao,[a] Fabian Stuhldreier,[b] Laura Schmitt,[b] Sebastian Wesselborg,[b] Lin Wang,[a] Werner E. G. Müller,[c] Rainer Kalscheuer,[a] Zhiyong Guo,[d] Kun Zou,[d] Zhen Liu,*[a] and Peter Proksch*[a,d]

[a]Institute of Pharmaceutical Biology and Biotechnology, Heinrich Heine University Düsseldorf, Universitätsstrasse 1, 40225 Düsseldorf, Germany.

[b]Institute of Molecular Medicine I, Medical Faculty, Heinrich Heine University Düsseldorf, Universitätsstrasse 1, 40225 Düsseldorf, Germany.

[c]Institute of Physiological Chemistry, Universitätsmedizin der Johannes Gutenberg-Universität Mainz, 55128 Mainz, Germany.

[d]Hubei Key Laboratory of Natural Products Research and Development, College of Biological and Pharmaceutical Sciences, China Three Gorges University, Yichang 443002, China.

*Corresponding authors. E-mail address: zhenfeizi0@sina.com (Z. Liu); proksch@uni-duesseldorf (P. Proksch).

1

Content

Fig. S1 HPLC chromatogram of compound **1**

UV absorption of compound **1**

Fig. S2 ¹H-NMR (600 MHz, methanol-*d₄*) spectrum of compound **1**

Fig. S3 ¹³C-NMR (150 MHz, methanol-*d₄*) spectrum of compound **1**

4
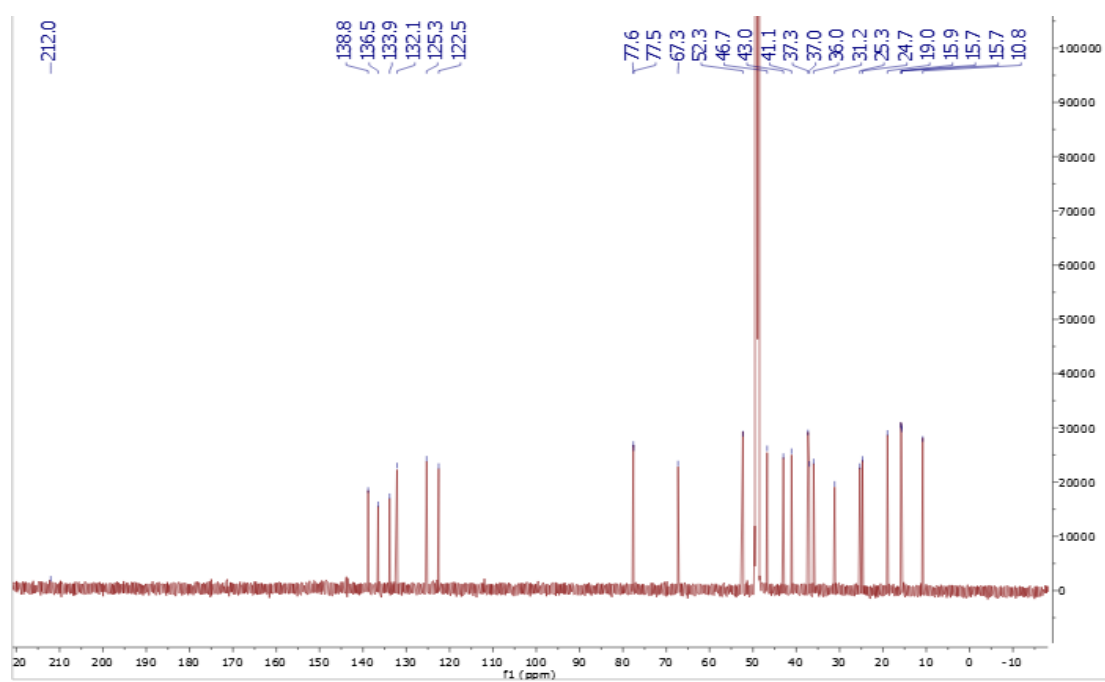
Fig. S4 COSY spectrum of compound **1**
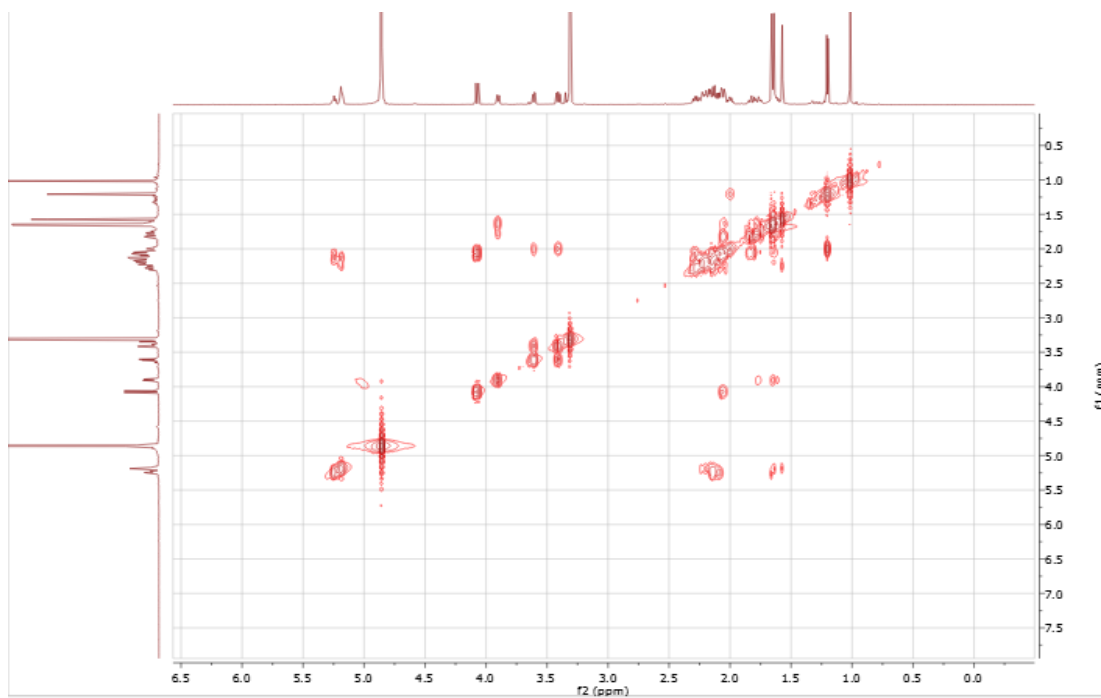
Fig. S5 HSQC spectrum of compound **1**

5
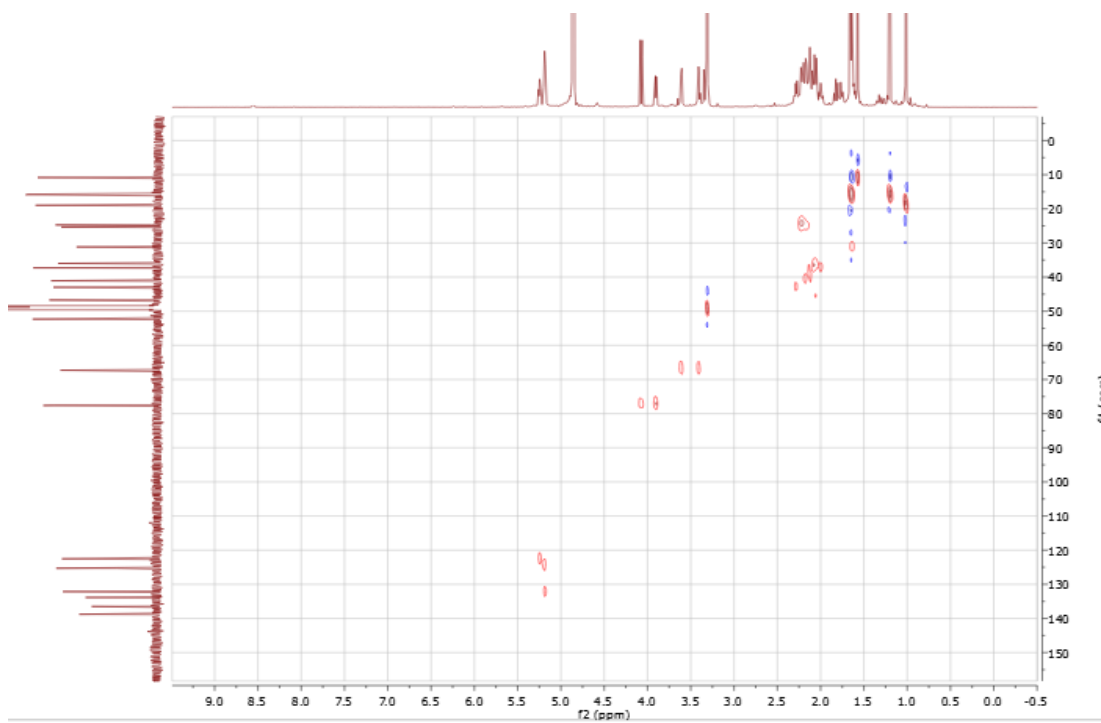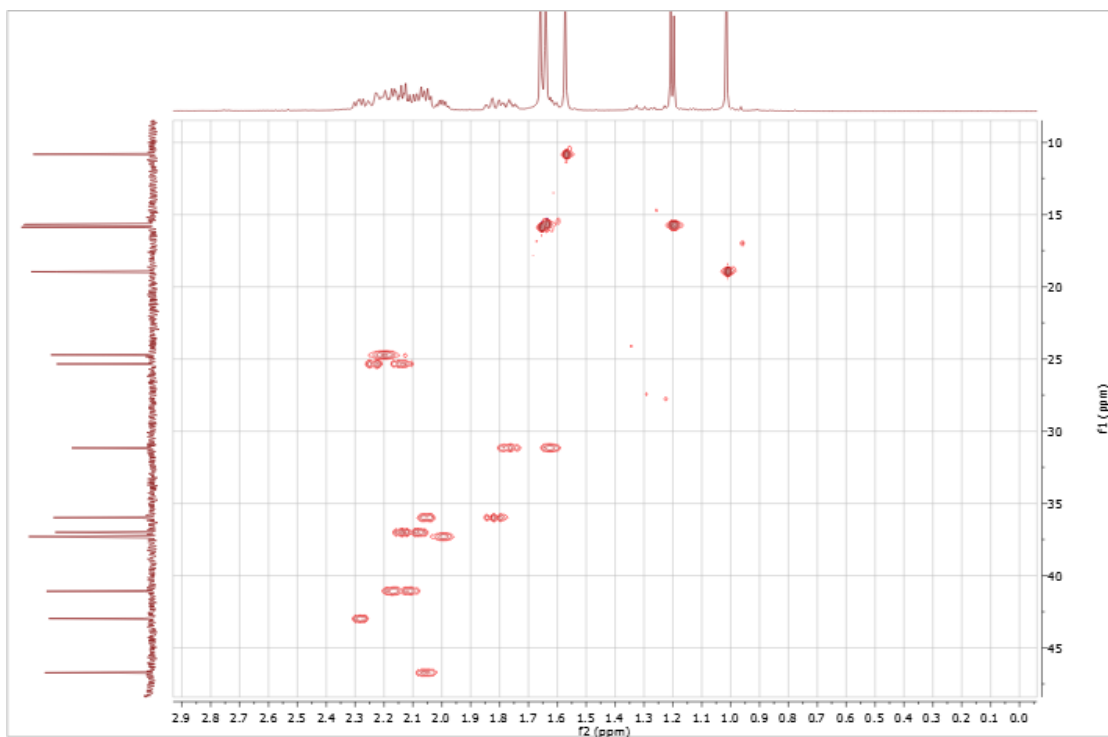
Fig. S6 HMBC spectrum of compound **1**
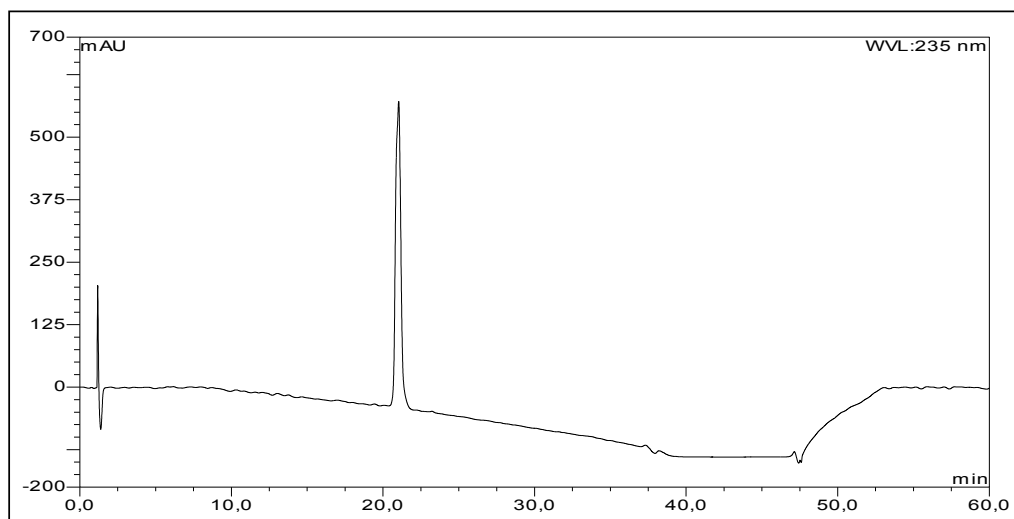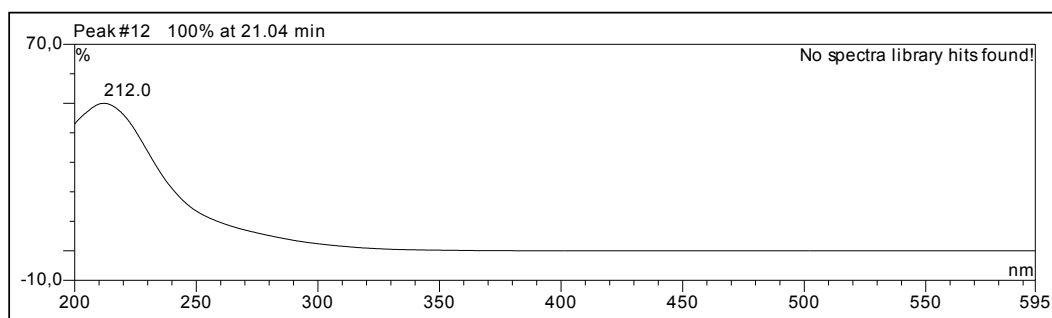

6
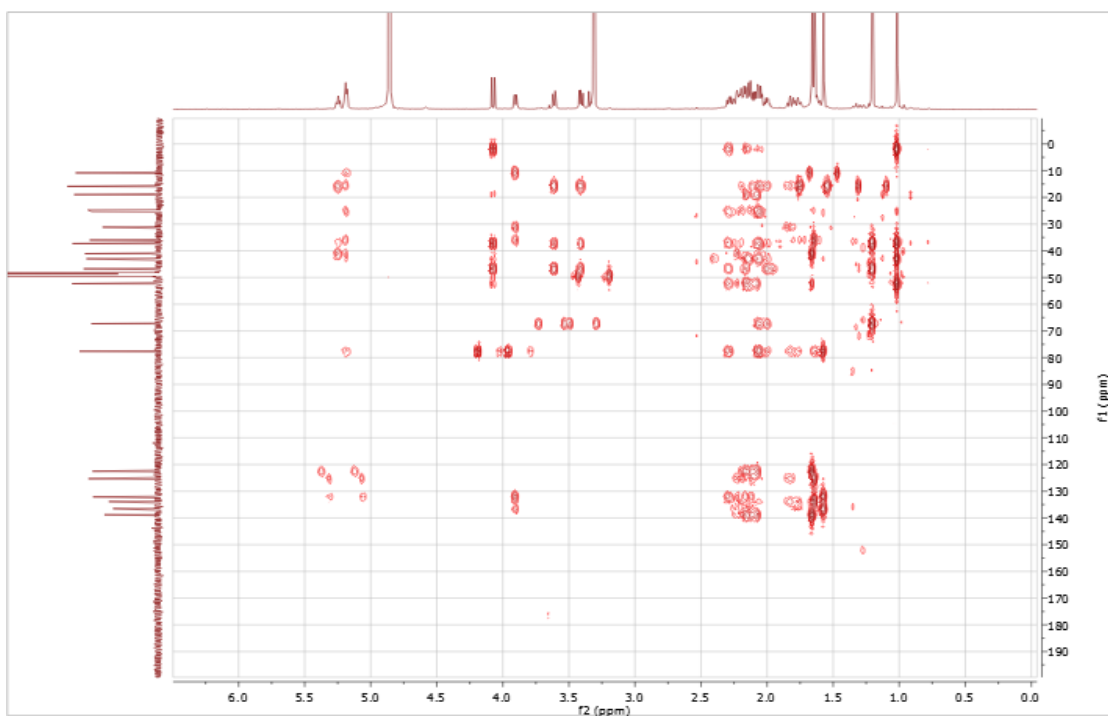
Fig. S7 ROESY spectrum of compound **1**
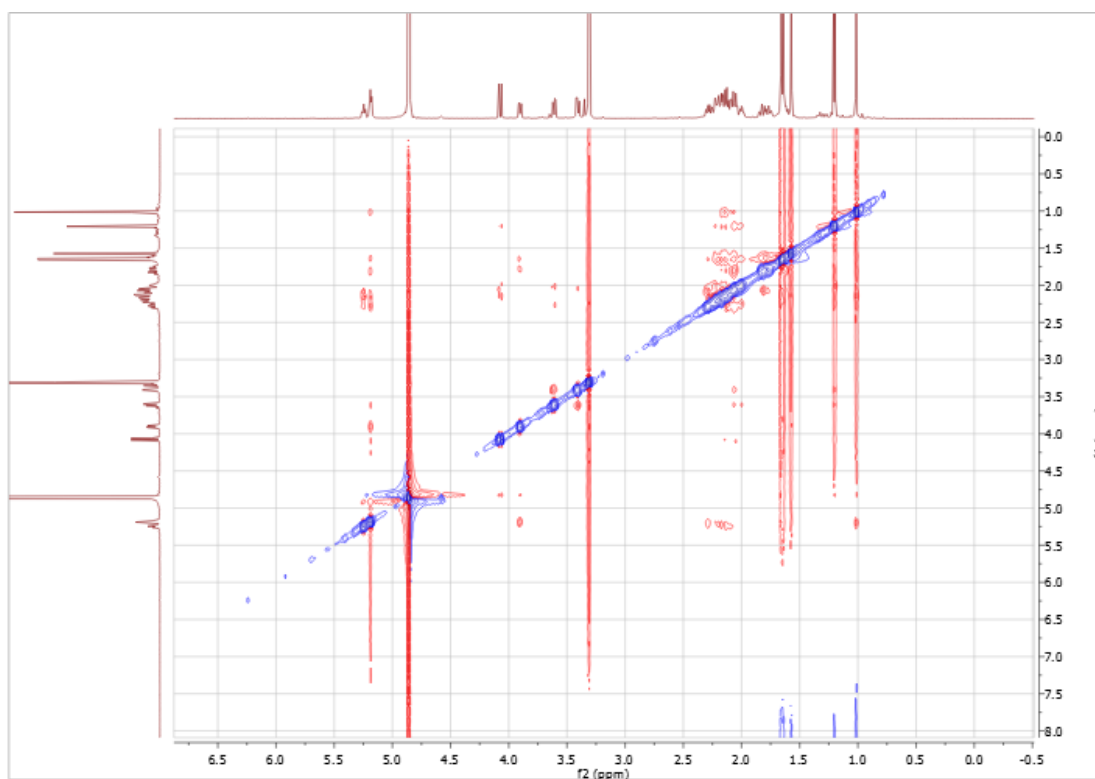
Fig. S8 HRESIMS of compound **1**

Acquisition Parameter

Source Type	ESI	Ion Polarity	Positive	Set Nebulizer	0.3 Bar
Focus	Not active	Set Capillary	4000 V	Set Dry Heater	180 °C
Scan Begin	50 m/z	Set End Plate Offset	-500 V	Set Dry Gas	4.0 l/min
Scan End	1500 m/z	Set Collision Cell RF	600.0 Vpp	Set Divert Valve	Source
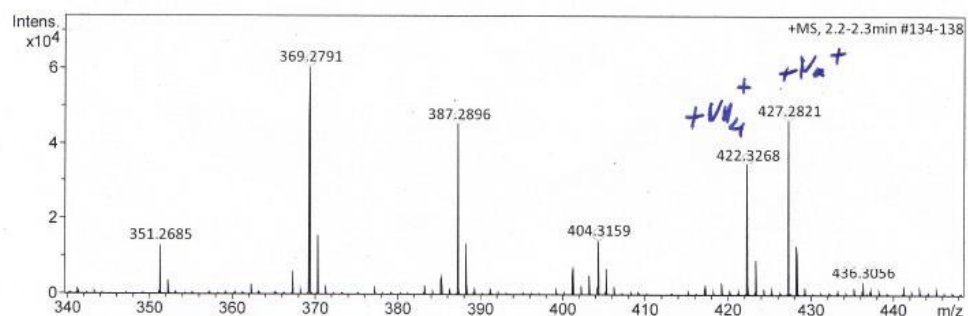
| Meas. m/z	#	Ion Formula	m/z	err [ppm]	mSigma	# mSigma	Score	rdb	e⁻ Conf	N-Rule
369.2791	1	C25H37O2	369.2788	-0.7	10.8	1	100.00	7.5	even	ok
387.2896	1	C25H39O3	387.2894	-0.7	13.1	1	100.00	6.5	even	ok
404.3159	1	C25H42NO3	404.3159	-0.0	n.a.	1	100.00	5.5	even	ok
422.3268	1	C25H44NO4	422.3265	-0.6	5.6	1	100.00	4.5	even	ok
427.2821	1	C25H40NaO4	427.2819	-0.5	2.2	1	100.00	5.5	even	ok

7

Fig. S9 HPLC chromatogram of compound **2**

UV absorption of compound **2**

8
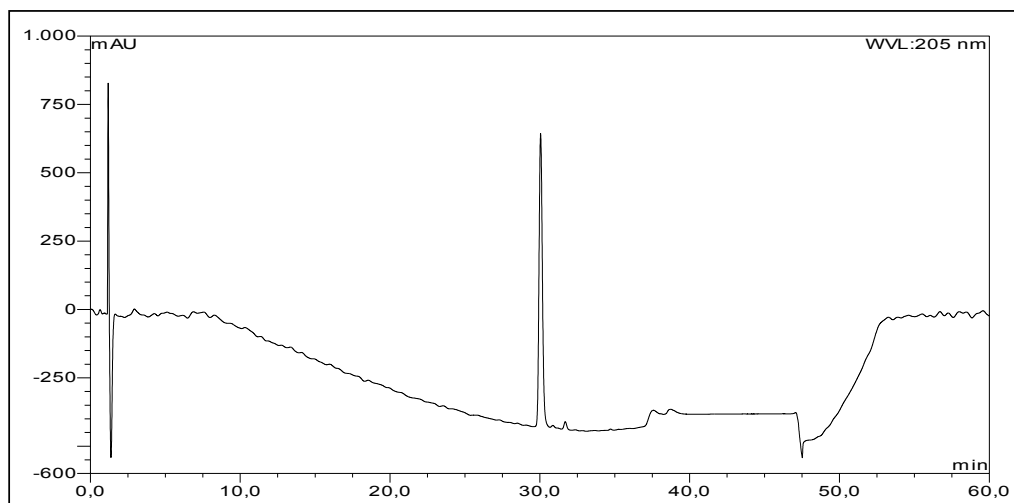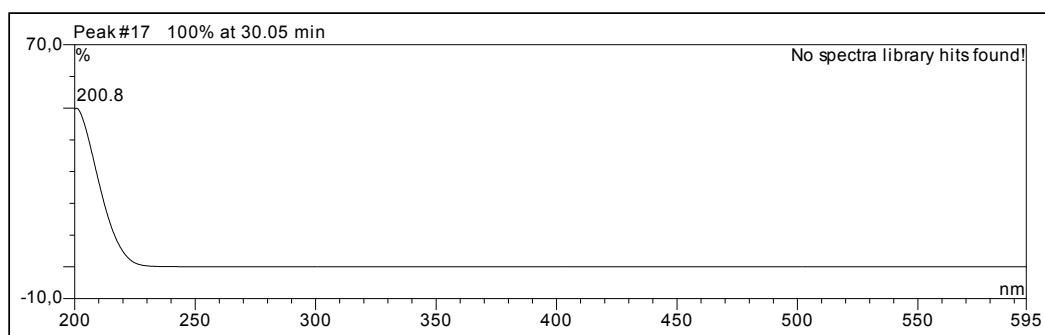
Fig. S10 ^{1}H-NMR (600 MHz, methanol-d_4) spectrum of compound **2**
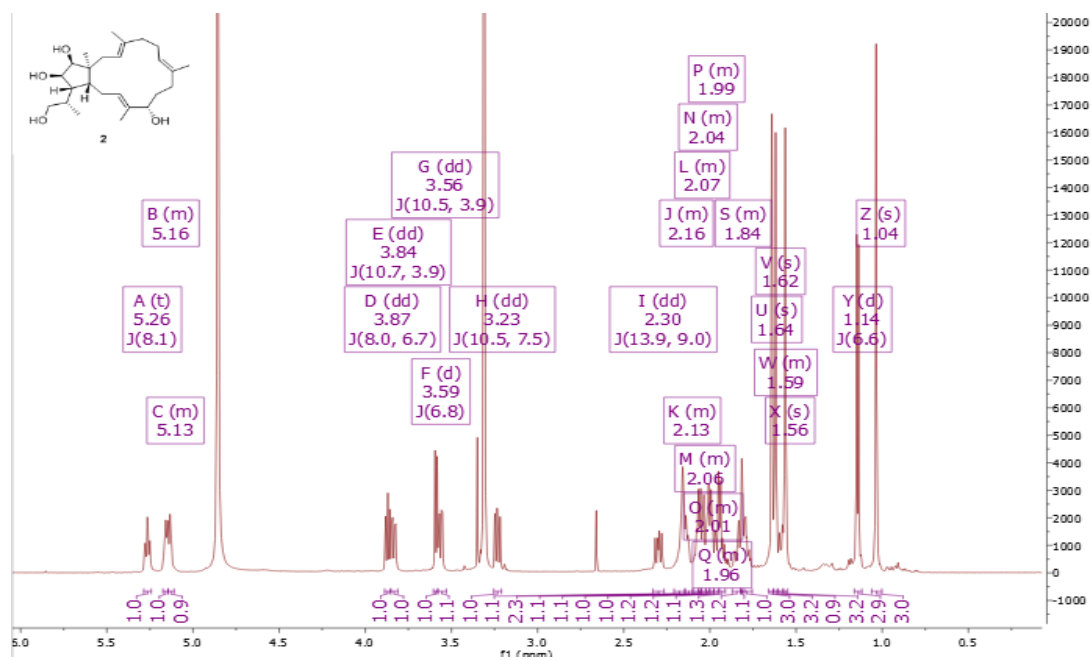
Fig. S11 COSY spectrum of compound **2**

Fig. S12 HSQC spectrum of compound **2**
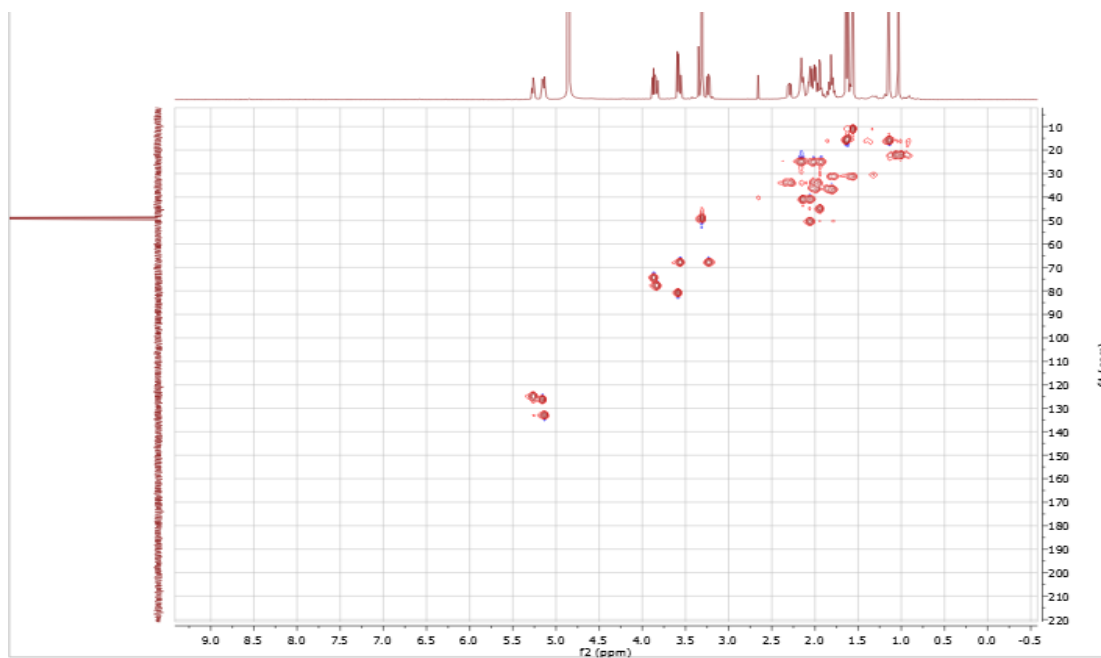
Fig. S13 HMBC spectrum of compound **2**

10
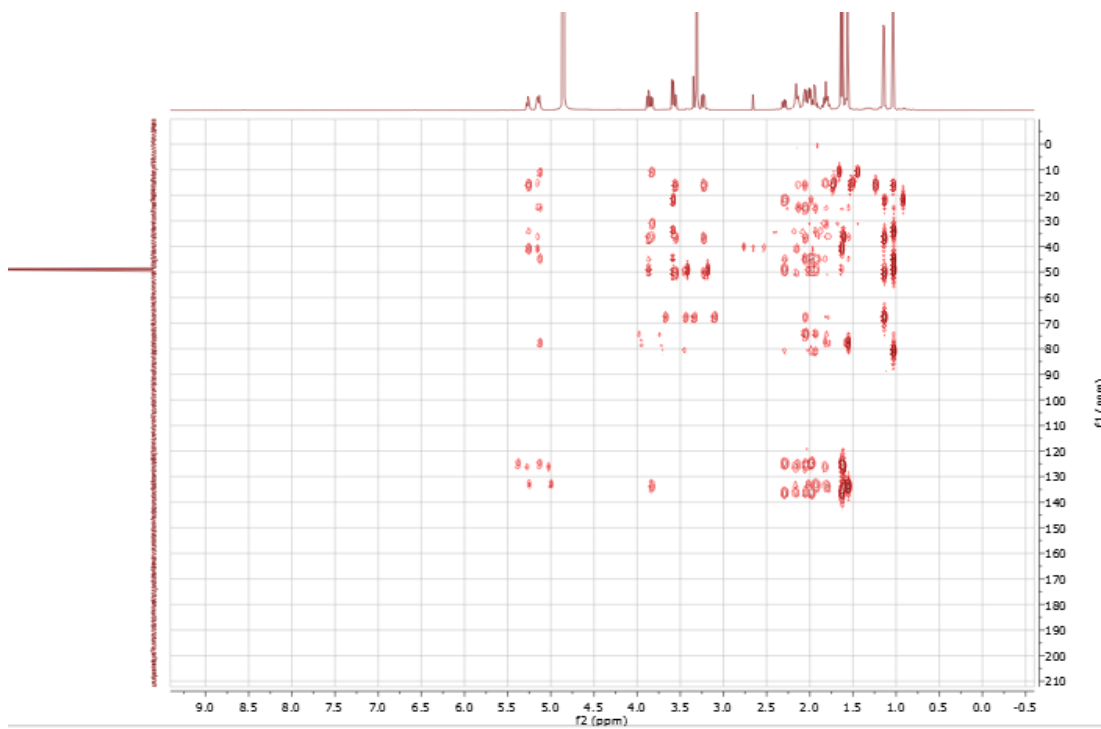
Fig. S14 ROESY spectrum of compound **2**

Fig. S15 HRESIMS of compound **2**

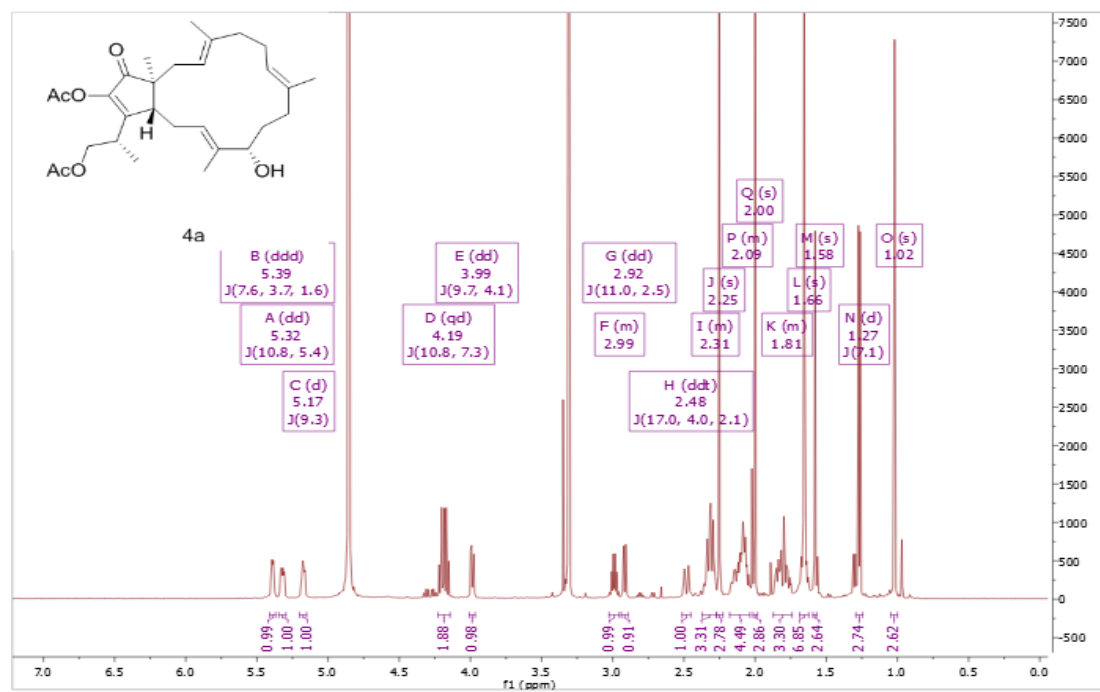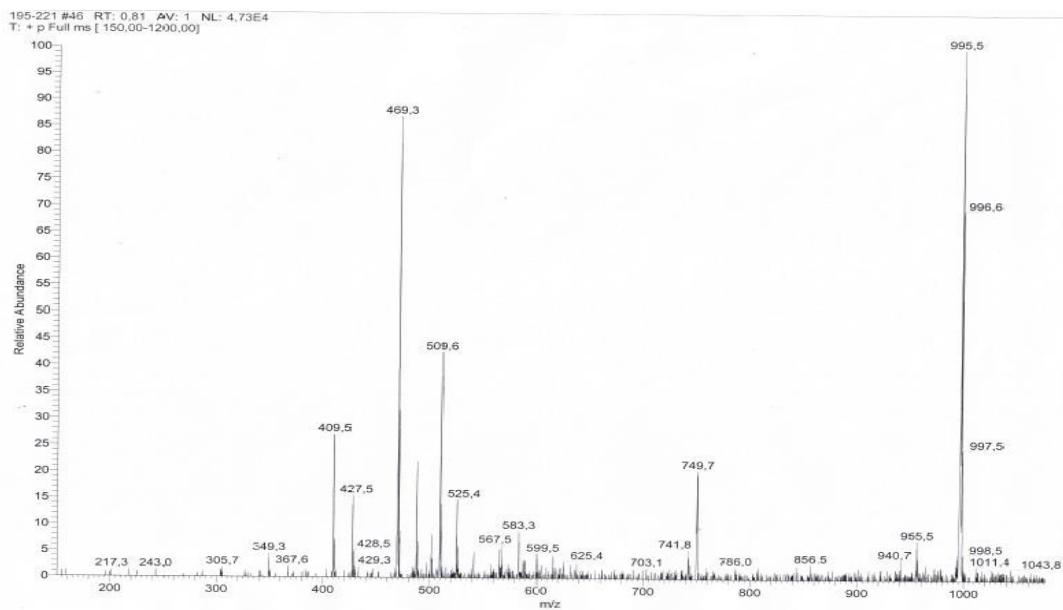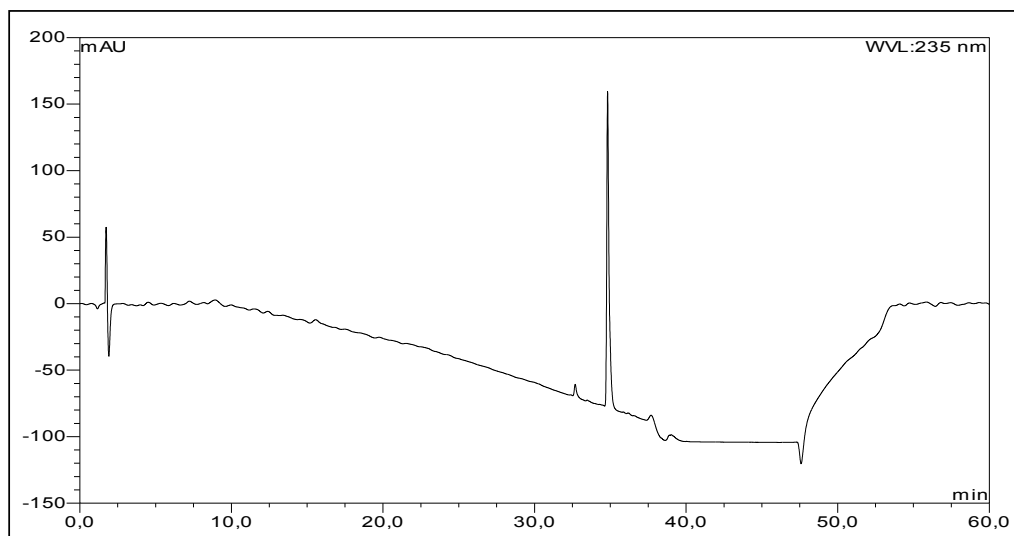**Fig. S16** HPLC chromatogram of compound **6**

UV absorption of compound **6**

Fig. S17 ^{1}H-NMR (600 MHz, methanol-d_4) spectrum of compound **6**
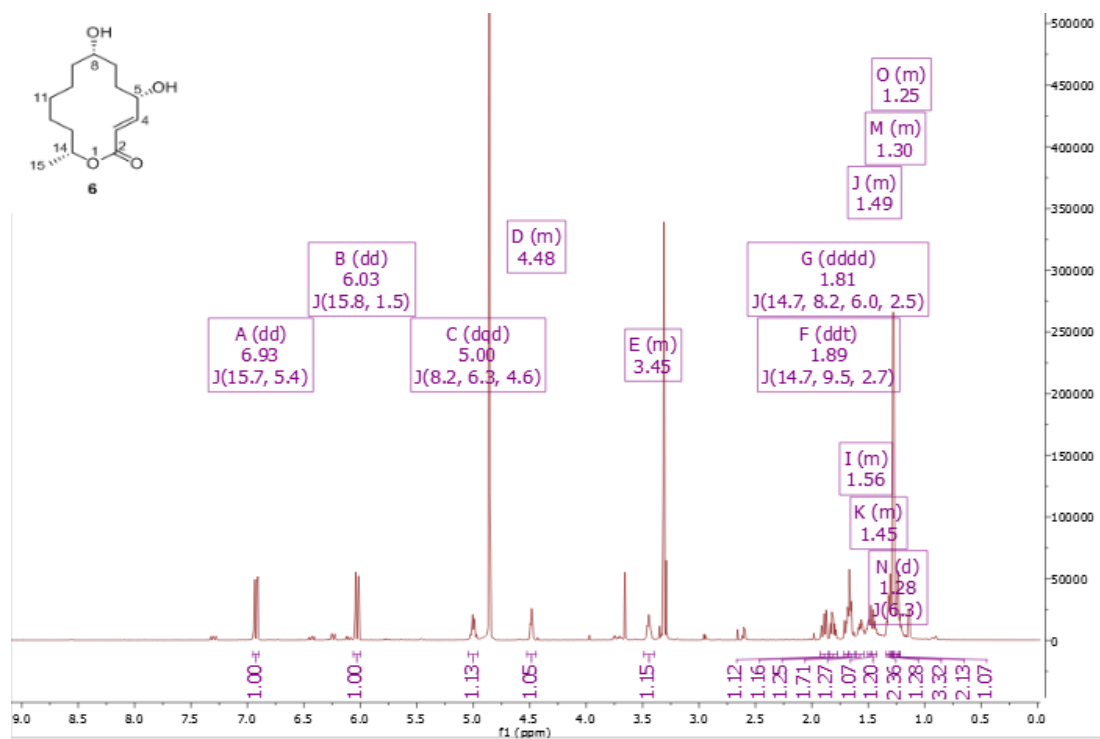
Fig. S18 ^{13}C-NMR (150 MHz, methanol-d_4) spectrum of compound **6**

13
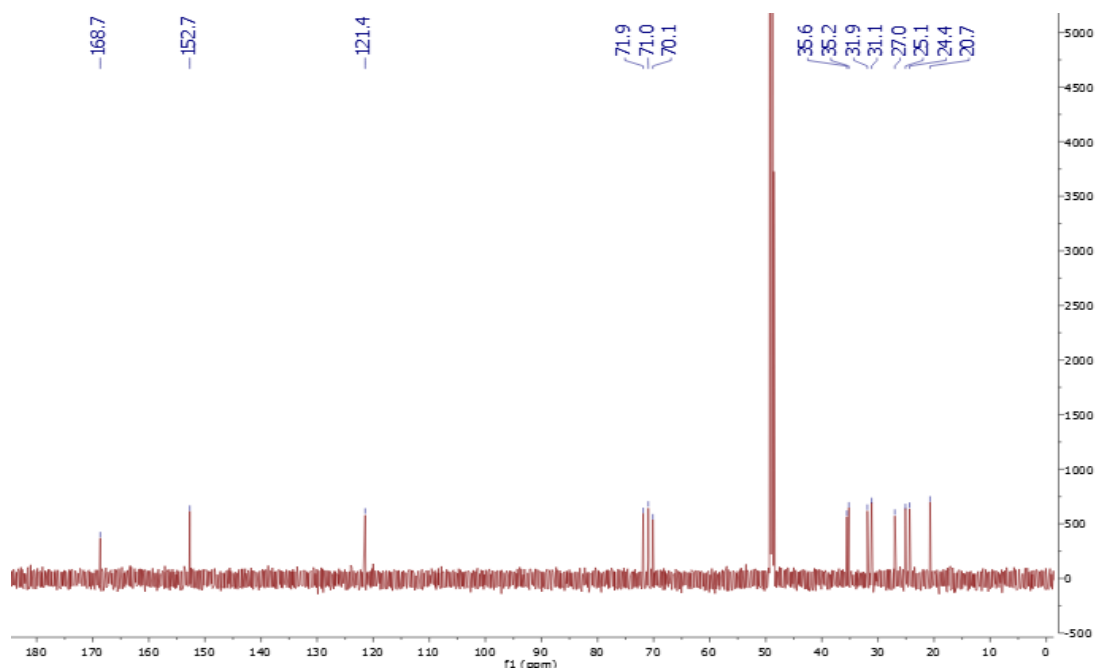
Fig. S19 COSY spectrum of compound **6**

Fig. S20 HSQC spectrum of compound **6**

14
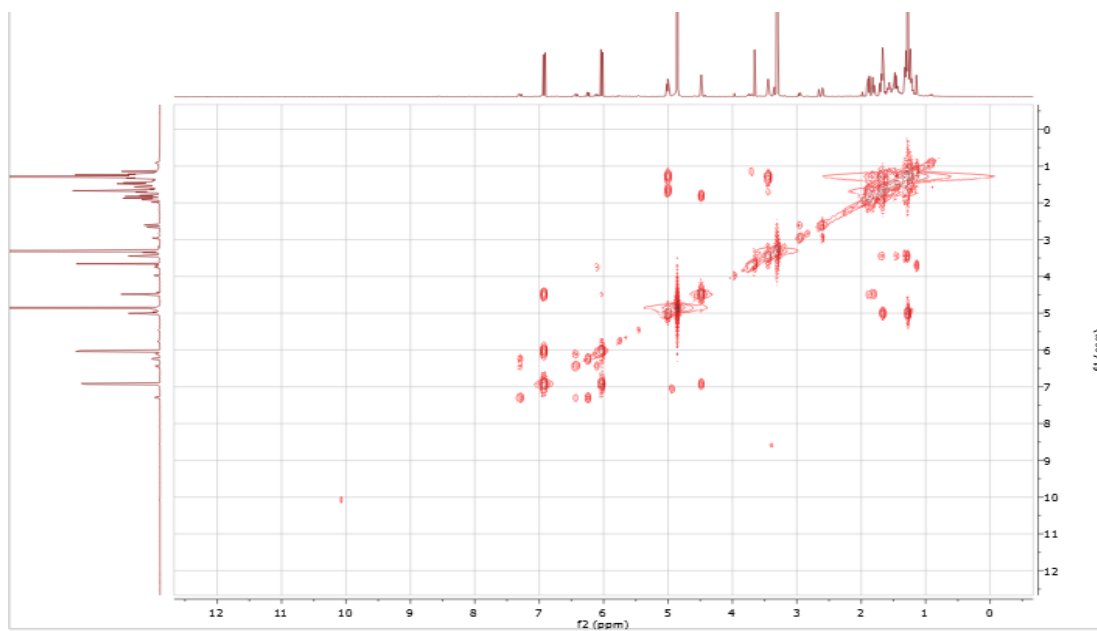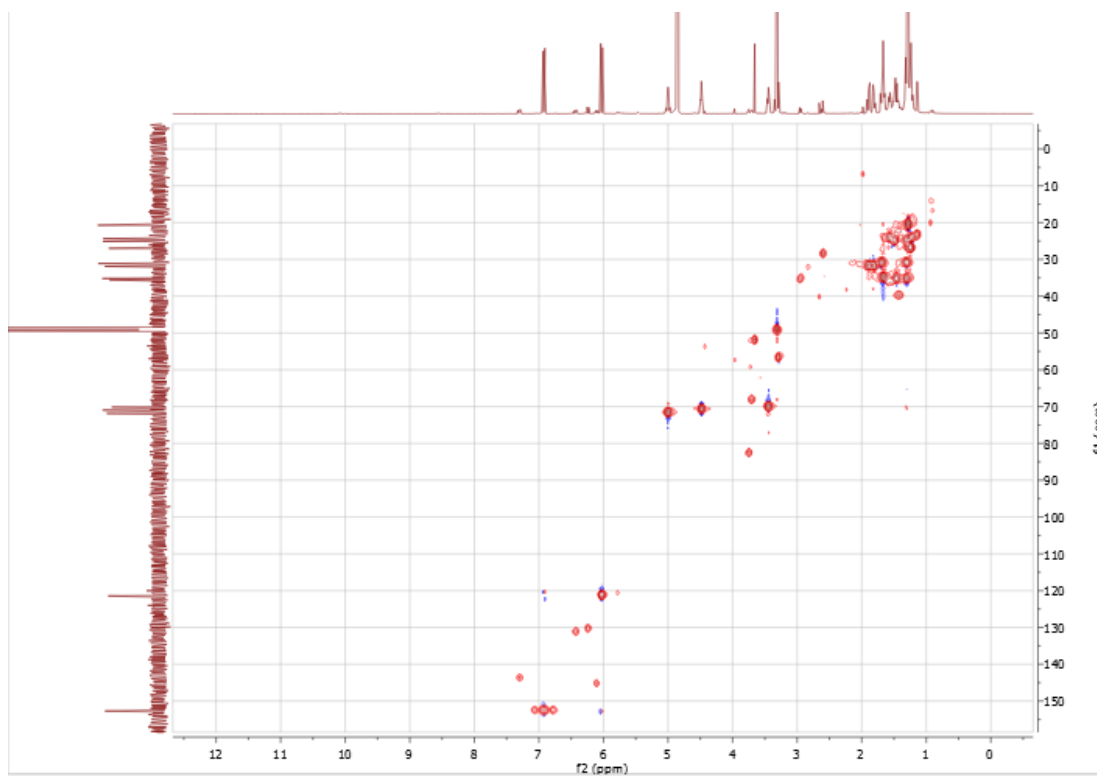
Fig. S21 HMBC spectrum of compound **6**
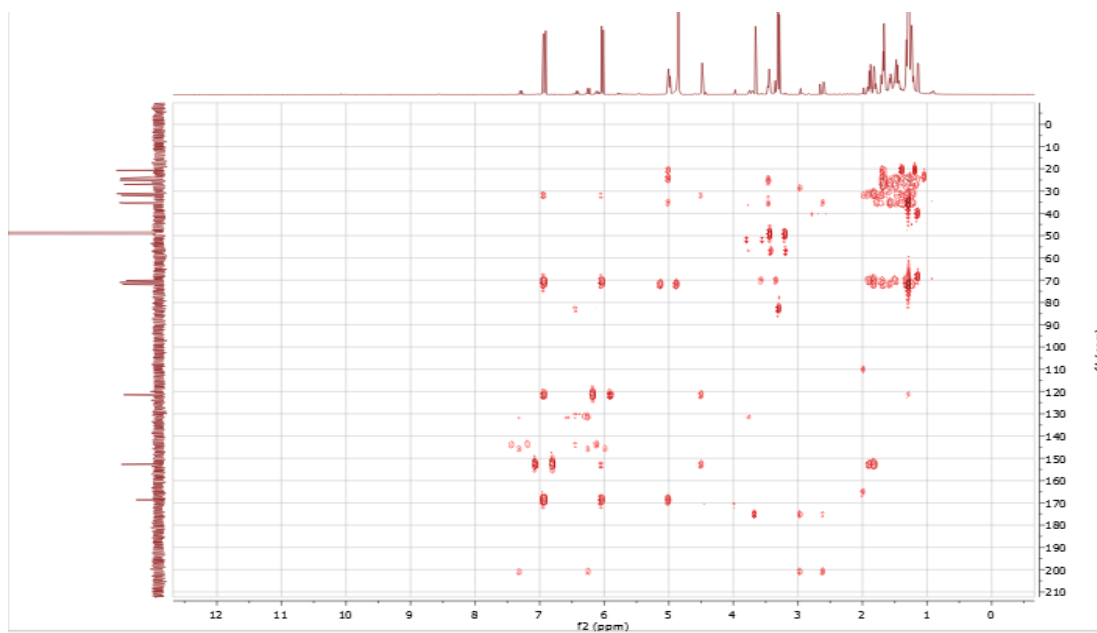
Fig. S22 ROESY spectrum of compound **6**

15
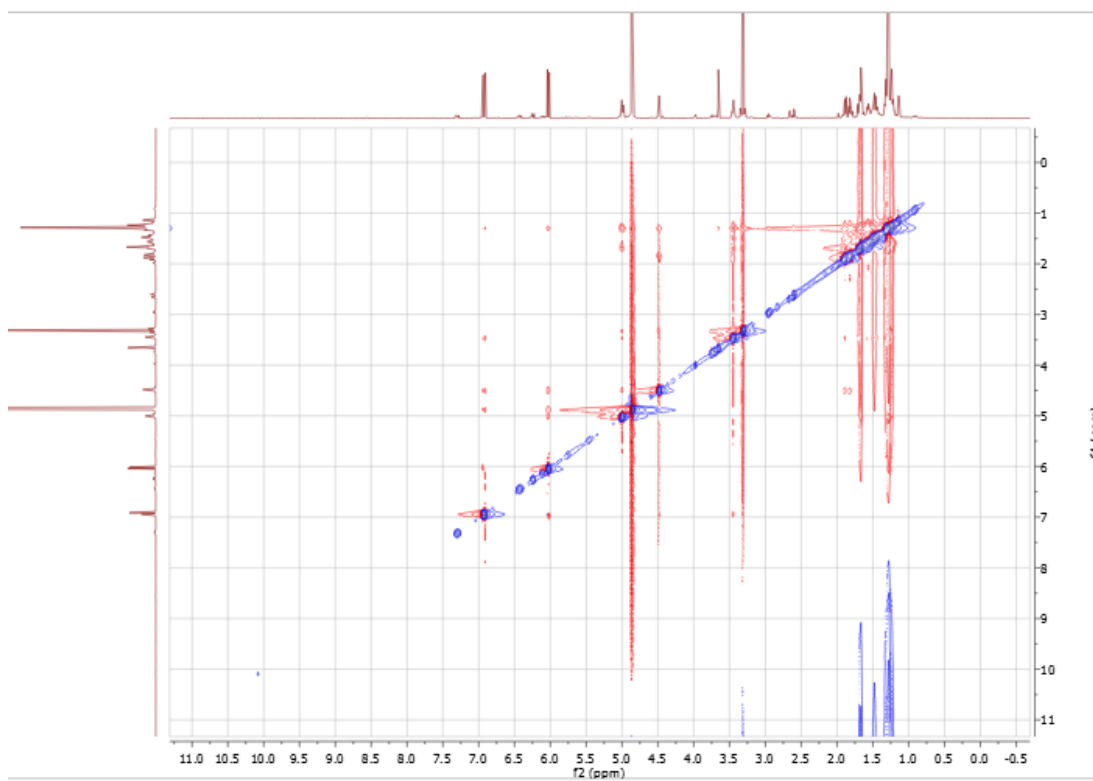
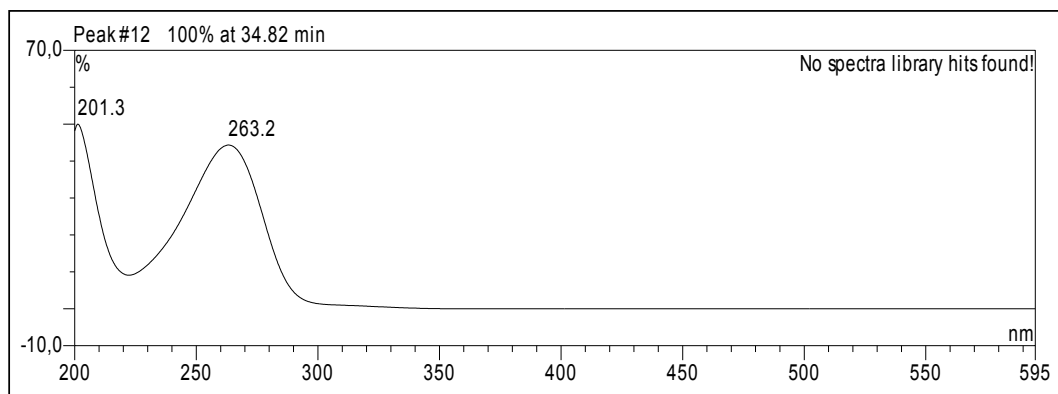**Fig. S23** HRESIMS of compound **6**
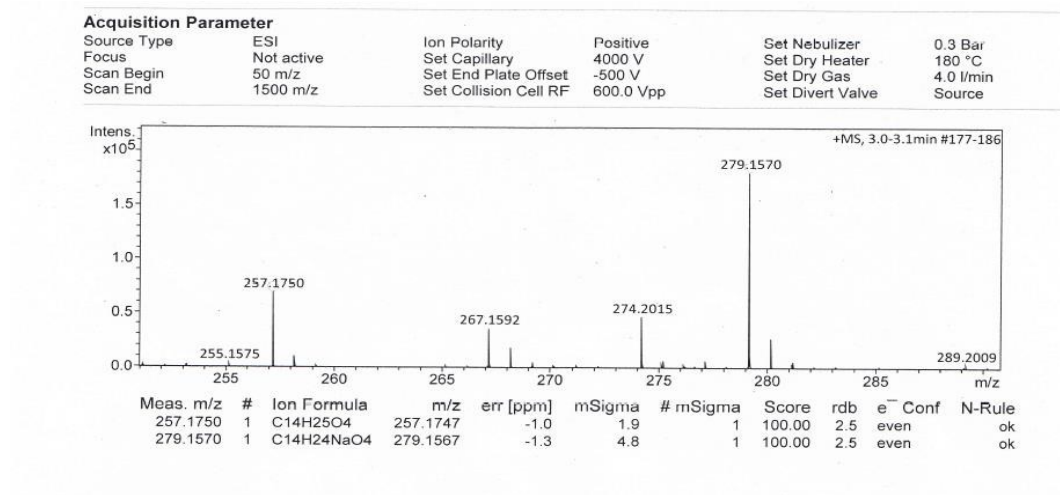
Fig. S24 HPLC chromatogram of compound **4a**
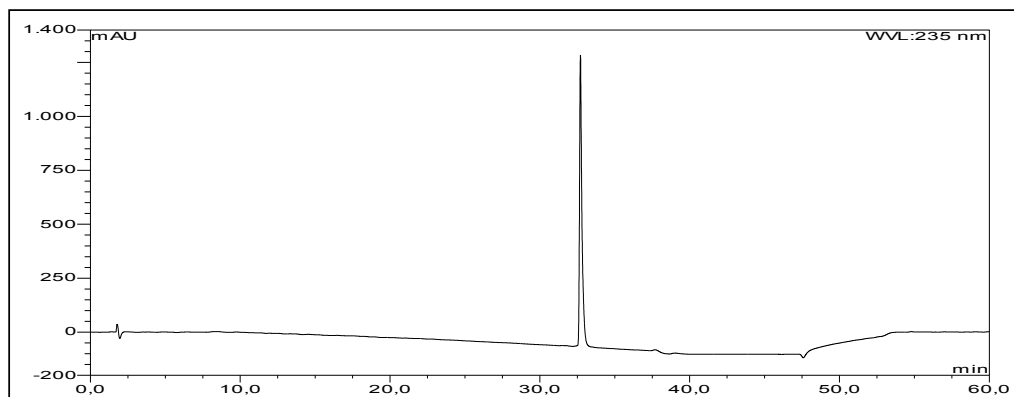
UV absorption of compound **4a**

16
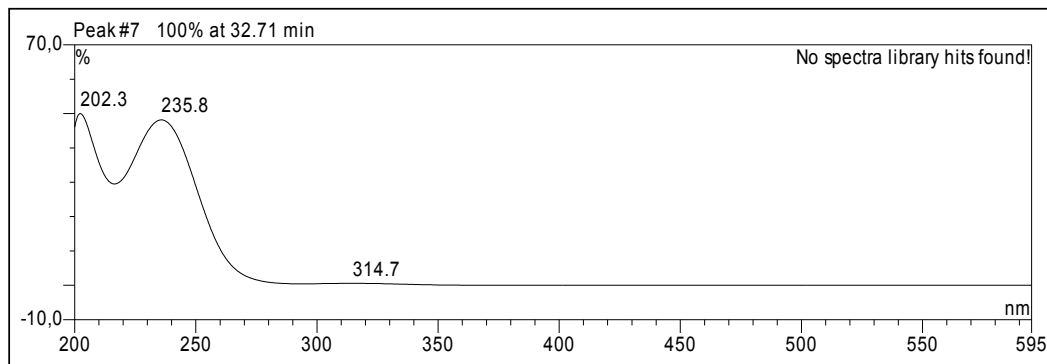
Fig. S25 ¹H-NMR (600 MHz, methanol-*d₄*) spectrum of compound **4a**

Fig. S26 ESIMS of compound **4a**

Fig. S27 HPLC chromatogram of compound **4b**
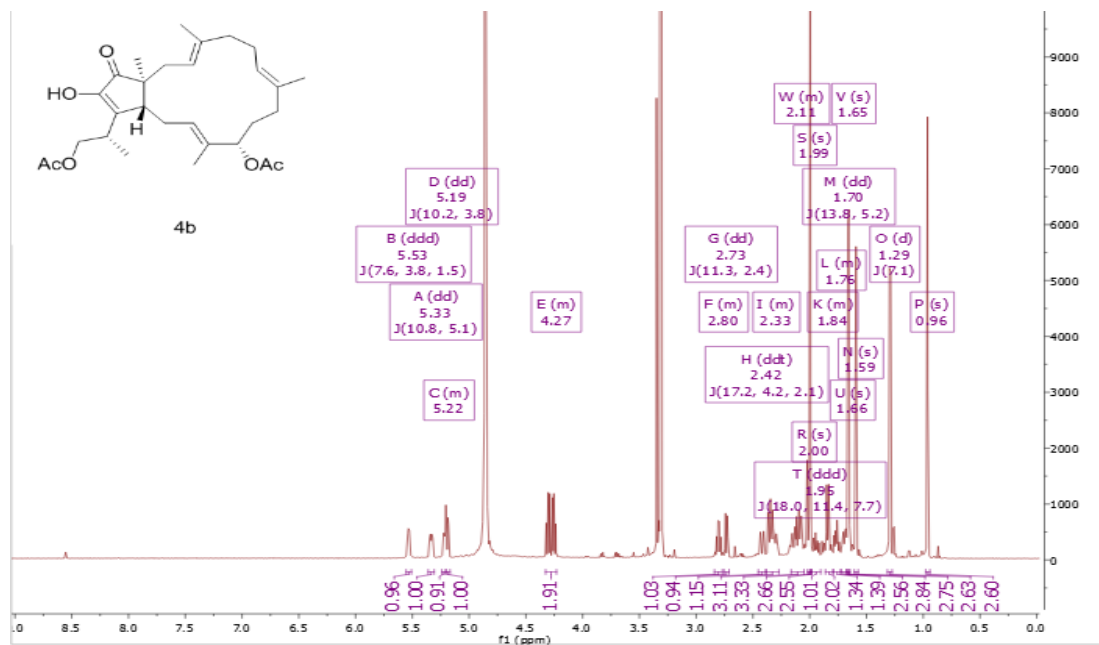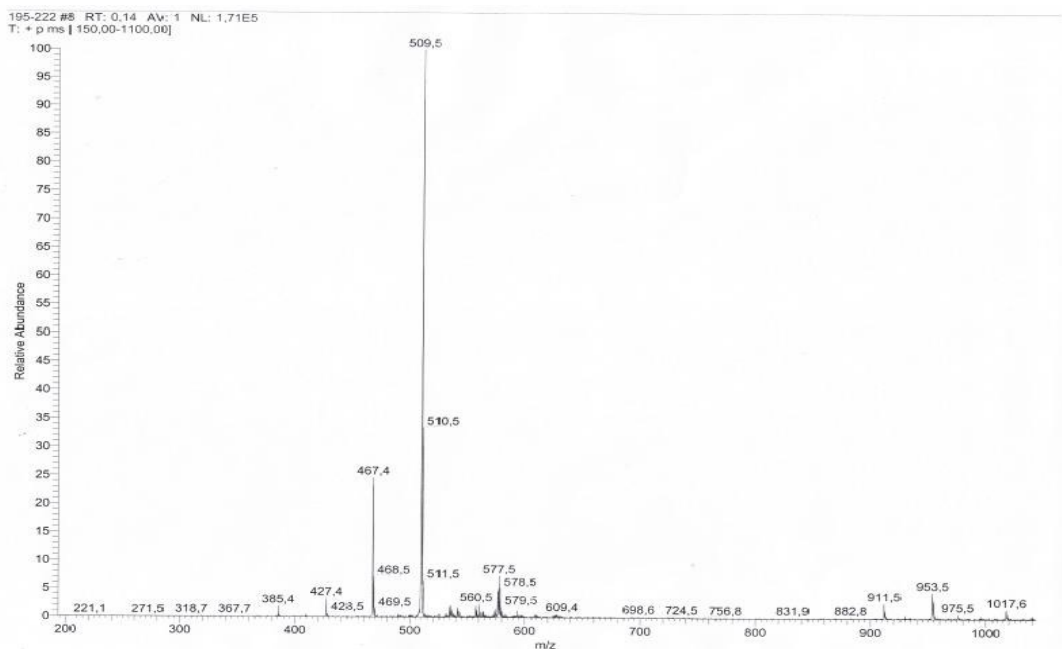

UV absorption of compound **4b**

18

Fig. S28 ^{1}H-NMR (600 MHz, methanol-d_4) spectrum of compound **4b**

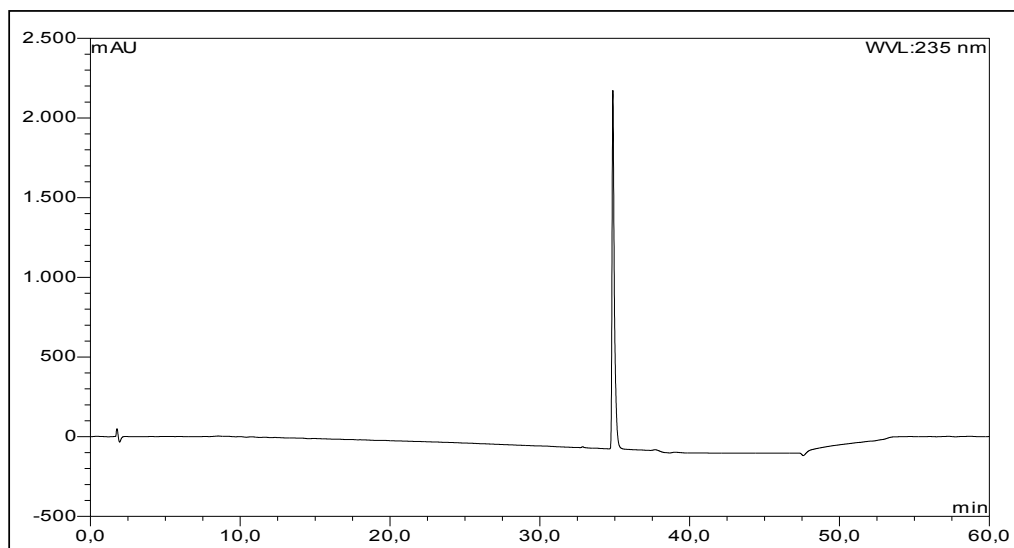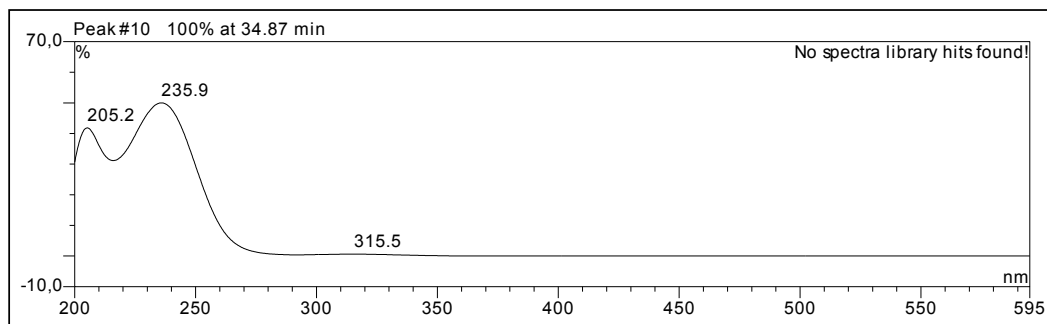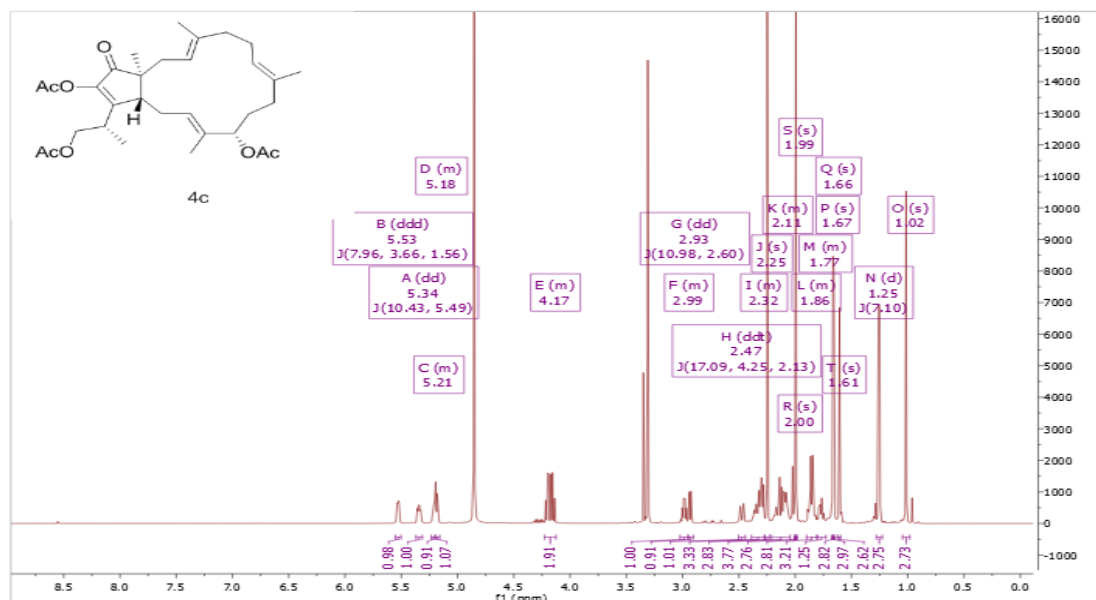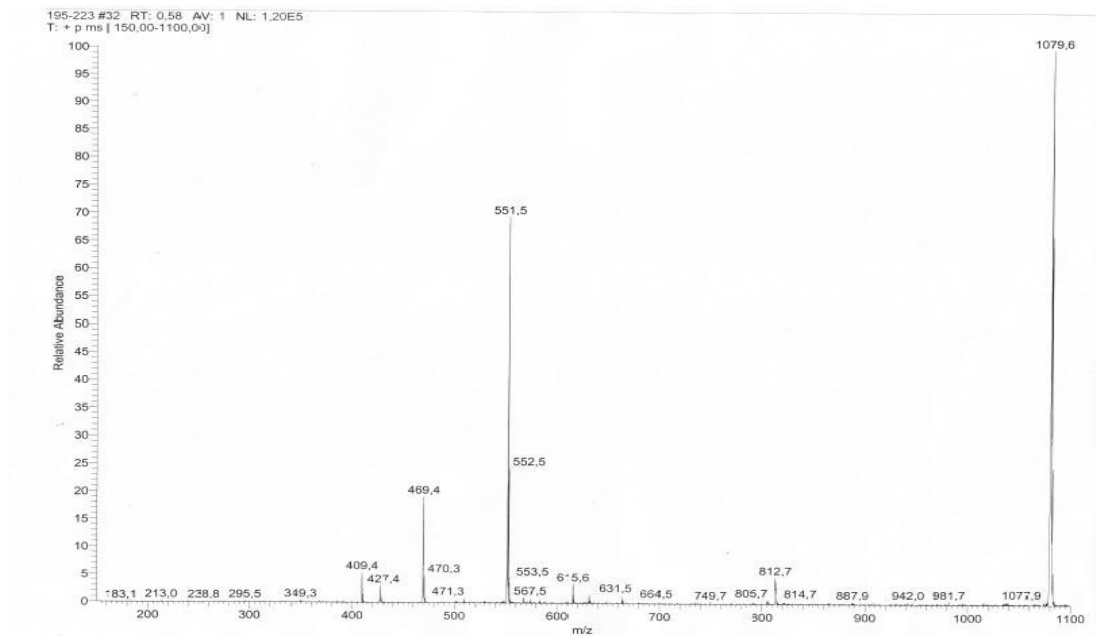**Fig. S29** ESIMS of compound **4b**

19

Fig. S30 HPLC chromatogram of compound **4c**

UV absorption of compound **4c**

20

Fig. S31 ^{1}H-NMR (600 MHz, methanol-d_4) spectrum of compound **4c**

Fig. S32 ESIMS of compound **4c**

21

Chapter 4 Publication 3

Induction of new lactam derivatives from the endophytic fungus *Aplosporella javeedii* through an OSMAC approach

Published in: "Frontiers in Microbiology"

Impact factor: 4.235

Contribution: First authorship, contributed to 70% of this publication. The first author conducted most of the laboratory work including the application of OSMAC approach, extraction, isolation, structure elucidation, literature research, and manuscript preparation.

frontiers
in Microbiology

Induction of New Lactam Derivatives From the Endophytic Fungus *Aplosporella javeedii* Through an OSMAC Approach

Ying Gao[1], Fabian Stuhldreier[2], Laura Schmitt[2], Sebastian Wesselborg[2], Zhiyong Guo[3], Kun Zou[3], Attila Mándi[4], Tibor Kurtán[4], Zhen Liu[1*] and Peter Proksch[1,3*]

[1] Institute of Pharmaceutical Biology and Biotechnology, Heinrich Heine University Düsseldorf, Düsseldorf, Germany, [2] Institute of Molecular Medicine I, Medical Faculty, Heinrich Heine University Düsseldorf, Düsseldorf, Germany, [3] Hubei Key Laboratory of Natural Products Research and Development, College of Biological and Pharmaceutical Sciences, China Three Gorges University, Yichang, China, [4] Department of Organic Chemistry, University of Debrecen, Debrecen, Hungary

Fermentation of the endophytic fungus *Aplosporella javeedii* on solid rice medium in presence of either 3.5% $NaNO_3$ or 3.5% monosodium glutamate caused a significant change of the fungal metabolite pattern compared to fungal controls grown only on rice. Chemical investigation of the former fungal extracts yielded 11 new lactam derivatives, aplosporellins A–K (**2–12**), in addition to the known compound, pramanicin A (**1**). All of these compounds were not detected when the fungus was grown on rice medium without these activators thereby indicating the power of this OSMAC approach. The structures of the new compounds were elucidated by one- and two- dimensional NMR spectroscopy, DFT-NMR calculations and by mass spectrometry as well as by comparison with the literature whereas the absolute configuration of the lactam core was determined by TDDFT-ECD and OR calculations. Pramanicin A (**1**) showed strong cytotoxicity against human lymphoma (Ramos) and leukemia (Jurkat J16) cells with IC_{50} values of 4.7 and 4.4 µM, respectively. Mechanistic studies indicated that **1** activates caspase-3 and induces apoptotic cell death.

Keywords: *Aplosporella javeedii*, lactam derivatives, OSMAC approach, DFT-NMR, TDDFT-ECD, OR calculations, apoptosis

INTRODUCTION

Endophytic fungi have been proven to be important sources for bioprospecting for new pharmaceutical lead compounds (Frank et al., 2015; Ancheeva et al., 2018; Bohler et al., 2018; Rehberg et al., 2018). However, conventional screening of endophytes that had been cultivated under standard laboratory conditions often fails to reveal the full biosynthetic potential of fungi and leads to re-isolation of already known metabolites. Strategies to activate silent biosynthetic gene clusters that are not expressed using conventional fermentation methods include co-cultivation of fungi with bacteria or the so called OSMAC (One Strain Many Compounds) approach (Daletos et al., 2017). The OSMAC approach makes use of altering cultivation parameters such as medium composition (carbon/nitrogen ratio, salinity, metal ions), physical parameters (temperature, pH, oxygen condition), or addition of enzyme inhibitors/inducers and biosynthetic precursors in order

81

to activate silent biosynthetic gene clusters and to expand the metabolite pattern produced by endophytes (Bode et al., 2002; Pan et al., 2019). Recent successful examples of OSMAC application from our own group include: addition of 2% tryptophan to rice medium which led to the accumulation of a new strongly cytotoxic bismacrolactone by the endophytic fungus *Trichocladium* sp. (Tran-Cong et al., 2019), addition of a mixture of salts (MgSO$_4$, NaNO$_3$, and NaCl) to solid Czapek medium which induced accumulation of nine new secondary metabolites by the endophytic fungus *Bulgaria inquinans* (Ariantari et al., 2019), and the accumulation of new brominated tyrosine-derived alkaloids by the soil fungus *Gymnascella dankaliensis* caused by addition of NaBr to solid rice medium (Wang et al., 2016).

As a part of our ongoing studies on fungal endophytes, we investigated the endophytic fungus *Aplosporella javeedii* derived from *Orychophragmus violaceus* (L.) O. E. Schul (Brassicaceae). *O. violaceus* is used in the Traditional Medicine of China for dissipating swelling and for treating unknown pyrogenic infections (Medicinal Plant Images Database, 2007). Recent studies have found that the plant also shows hepatoprotective effects (Huo et al., 2017). Previous chemical investigations of the fungus *A. javeedii* grown on solid rice medium resulted in the isolation of six new antifungal polyketides, five sesterterpenes including two new compounds, as well as a new macrolide, with some of the metabolites exhibiting cytotoxic and antimicrobial activities (Gao et al., 2020a,b). Due to the pronounced chemical diversity of natural products obtained from this fungus, we have now conducted an OSMAC study which involved the addition of different salts including 3.5% NaBr, 3.5% NaCl, 3.5% NaF, 3.5% KCl, 3.5% NH$_4$Cl, 3.5% (NH$_4$)$_2$SO$_4$, 3.5% C$_5$H$_8$NNaO$_4$·H$_2$O (monosodium glutamate), 3.5% NaNO$_3$, 3.5% Na$_2$HPO$_4$, 3.5% K$_2$HPO$_4$·3H$_2$O, 3.5% KH$_2$PO$_4$, 3.5% FeSO$_4$, 3.5% ZnSO$_4$, or 3.5% MgSO$_4$ to solid rice medium. The selection of most of these salts was based on previous studies which indicated their usefulness for activation of non-transcribed biosynthetic gene clusters (Hammerschmidt et al., 2015; Wang et al., 2016, 2018; Ariantari et al., 2019). The most striking effects with regard to an alteration of the fungal metabolite pattern, however, were detected following addition of either 3.5% NaNO$_3$ or of 3.5% monosodium glutamate to solid rice medium compared to fungal control cultures lacking either of these activators (Figure 1). Chemical investigation of fungal extracts obtained from fermentation of *A. javeedii* in presence of either 3.5% NaNO$_3$ or of 3.5% monosodium glutamate led to the isolation of 11 new lactam derivatives, aplosporellins A–K (2–12), in addition to the known compound, pramanicin A (1) (Figure 2), all of which were not detected when the fungus was grown on rice medium without these activators. Herein we report the structure elucidation of the new metabolites and the pro-apoptotic activity of pramanicin A (1).

MATERIALS AND METHODS

General Experimental Procedures

A Perkin-Elmer-241 MC polarimeter was used to measure optical rotations. ECD spectra were recorded on a J-810 spectropolarimeter. One- and two-dimensional NMR spectra were recorded on a Bruker ARX 600 spectrometer. Mass spectra (ESI) were recorded with a Finnigan LCQ Deca mass spectrometer. A UHR-QTOF maxis 4G mass spectrometer (Bruker Daltonics) was used to record HRESIMS data. A Dionex UltiMate-3400SD system with a LPG-3400SD pump and a photodiode array detector (DAD 3000RS) as well as a separation column (Eurosphere-10 C$_{18}$, 125 × 4 mm, Knauer) were used for HPLC analysis. Detection wave lengths were set at 235, 254, 280, and 340 nm. Semi-preparative HPLC analysis was performed with a Merck Hitachi Chromaster HPLC system (UV detector L7400; pump L7100; column Eurosphere-100 C$_{18}$, 300 × 8 mm, Knauer; flow rate at 5 mL/min). Silica gel 60 M (0.04–0.063 mm, Macherey-Nagel) or Sephadex LH-20 were used for column chromatography. TLC plates precoated with silica gel F$_{254}$ (Merck) were used to monitor isolation fractions. Distilled and spectral grade solvents were used for column chromatography and spectroscopic measurements, respectively.
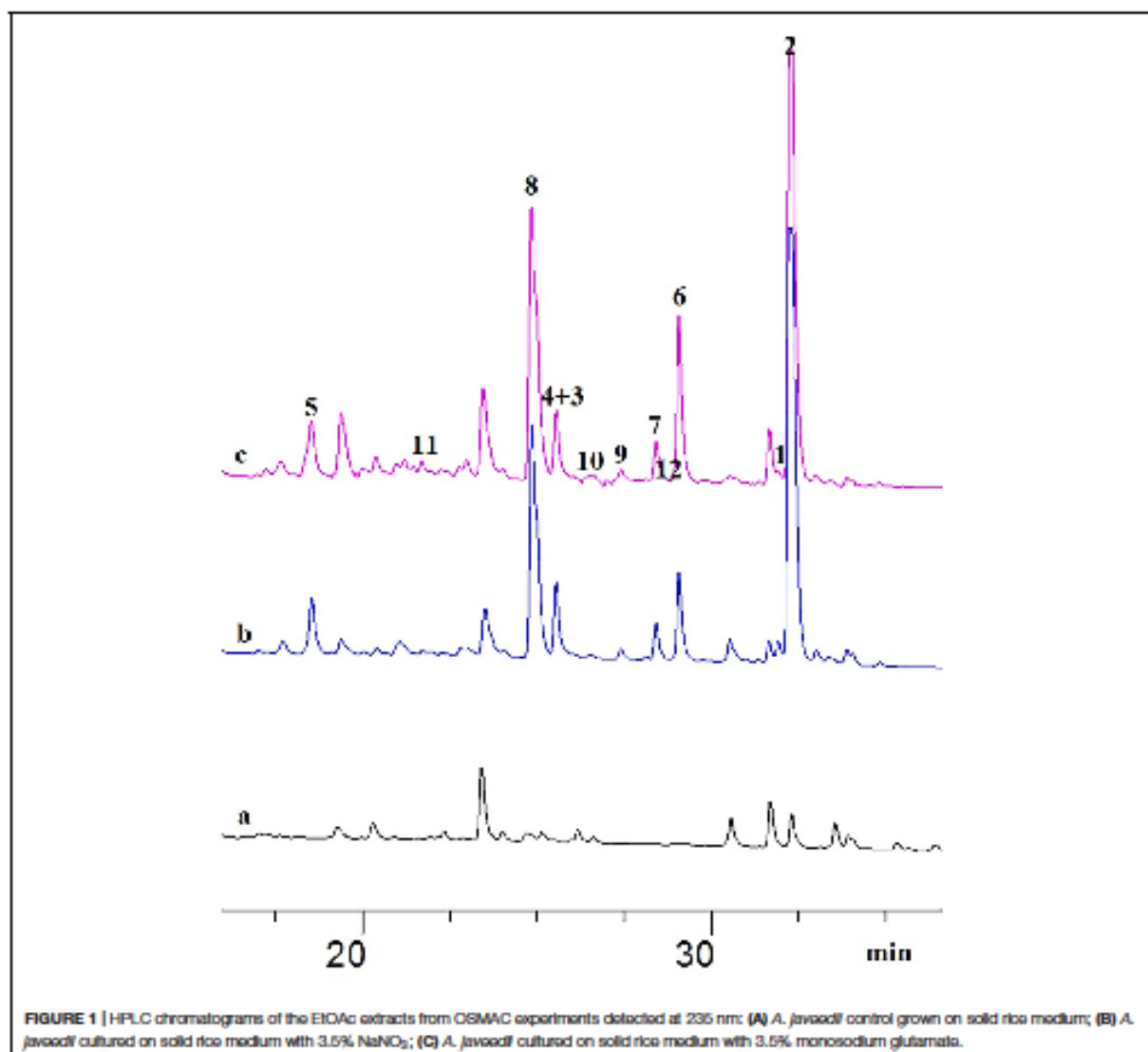
Fungal Material and Fermentation

The fungus *A. javeedii* (ID code ZGB-B) was isolated from fresh, healthy stems of *Orychophragmus violaceus* (L.) O. E. Schul (*Brassicaceae*), collected in April 2018 in Beijing, China. Fungal identification was carried out according to a standard protocol as described previously (Kjer et al., 2010). The GenBank accession number is MN720704. The fungal strain is kept in the Institute of Pharmaceutical Biology and Biotechnology, Heinrich Heine University, Duesseldorf, Germany.

The fungus was cultivated in two 1 L Erlenmeyer flasks, of which each was filled with solid rice medium containing 100 g rice and 110 mL demineralized water. After autoclaving at 121°C for 20 min and cooling down to room temperature, the fungal strain that was preserved on the ager plats for a week was cut into pieces and added in each flask under sterile condition. The fermentation was maintained under static conditions at room temperature until the rice medium was completely overgrown by the fungus which lasted around 20 days (control cultivation). OSMAC cultivations were carried out following the same procedure by growing the fungus on solid rice medium containing 3.5% NaBr, 3.5% NaCl, 3.5% NaF, 3.5% KCl, 3.5% NH$_4$Cl, 3.5% (NH$_4$)$_2$SO$_4$, 3.5% C$_5$H$_8$NNaO$_4$·H$_2$O (monosodium glutamate), 3.5% NaNO$_3$, 3.5% Na$_2$HPO$_4$, 3.5% K$_2$HPO$_4$·3H$_2$O, 3.5% KH$_2$PO$_4$, 3.5% FeSO$_4$, 3.5% ZnSO$_4$, or 3.5% MgSO$_4$. Two flasks were used for each experiment and each flask contained 100 g rice, 110 mL demineralized water and 3.5 g salts. The usefulness of 3.5% salts in the OSMAC approach has been proved by previous experiments with other fungi (Hammerschmidt et al., 2015; Wang et al., 2016, 2018). Based on the chromatographic profiles obtained from the extractions of these fermentations, fungal cultivations with striking changes of metabolite patterns were selected for further investigation.

Extraction and Isolation

The fungal culture grown on solid rice medium with addition of 3.5% NaNO$_3$ or 3.5% monosodium glutamate was extracted with 800 mL EtOAc followed by evaporation to dryness to afford the crude extract. The obtained brown extracts from the 3.5%

FIGURE 1 | HPLC chromatograms of the EtOAc extracts from OSMAC experiments detected at 235 nm: **(A)** *A. javeedii* control grown on solid rice medium; **(B)** *A. javeedii* cultured on solid rice medium with 3.5% NaNO₃; **(C)** *A. javeedii* cultured on solid rice medium with 3.5% monosodium glutamate.

NaNO₃ and 3.5% monosodium glutamate cultures were 2.3 and 2.8 g, respectively. The two crude extracts were subjected to a silica gel vacuum liquid chromatography (VLC) column, and eluted with 100% n-hexane, n-hexane-EtOAc (9:1), n-hexane-EtOAc (1:1), 100% EtOAc, CH₂Cl₂-MeOH (1:1), and 100% MeOH, respectively, which resulted in 6 fractions (V1 to V6) for each extract.

From the 3.5% NaNO₃ culture extract, fraction V5 (0.55 g) was subjected to a Sephadex LH-20 column using 100% MeOH as eluent to give five subfractions (V5-S1 to V5-S5). Subfraction V5-S2 was then submitted to a RP-18 (40–63 μm) vacuum liquid chromatography column and eluted with 5–100% aqueous MeOH to yield 7 subfractions (V5-S2-RP1 to V5-S2-RP7). Subfraction V5-S2-RP4 was purified by semi-preparative HPLC using a mixture of MeCN and H₂O (10:90) containing 0.1%

HCOOH to give **4** (4.5 mg), **8** (8.2 mg), and **11** (4.3 mg). Subfraction V5-S2-RP5 was purified by semi-preparative HPLC using a gradient of MeCN and H₂O (15:85 to 50:50) containing 0.1% HCOOH to give **2** (23.5 mg), **3** (5.1 mg), **6** (6.0 mg), and **7** (5.9 mg).

From the 3.5% monosodium glutamate culture extract, fraction V4 (0.45 g) was subjected to a Sephadex LH-20 column using CH₂Cl₂-MeOH (1:1) as eluent to obtain three subfractions (V4-S1 to V4-S3). Subfraction V4-S2 was then submitted to RP-18 (40–63 μm) vacuum liquid chromatography column and eluted with 10–100% aqueous MeOH to yield 10 subfractions (V4-S2-RP1 to V4-S2-RP10). Subfraction V4-S2-RP5 was purified by semi-preparative HPLC using MeOH-0.1% HCOOH in H₂O (50:50 to 72:28) to give **10** (2.3 mg). Subfraction V4-S2-RP7 was purified by semi-preparative HPLC

83

FIGURE 2 | Structures of compounds isolated from *A. javeedii*.
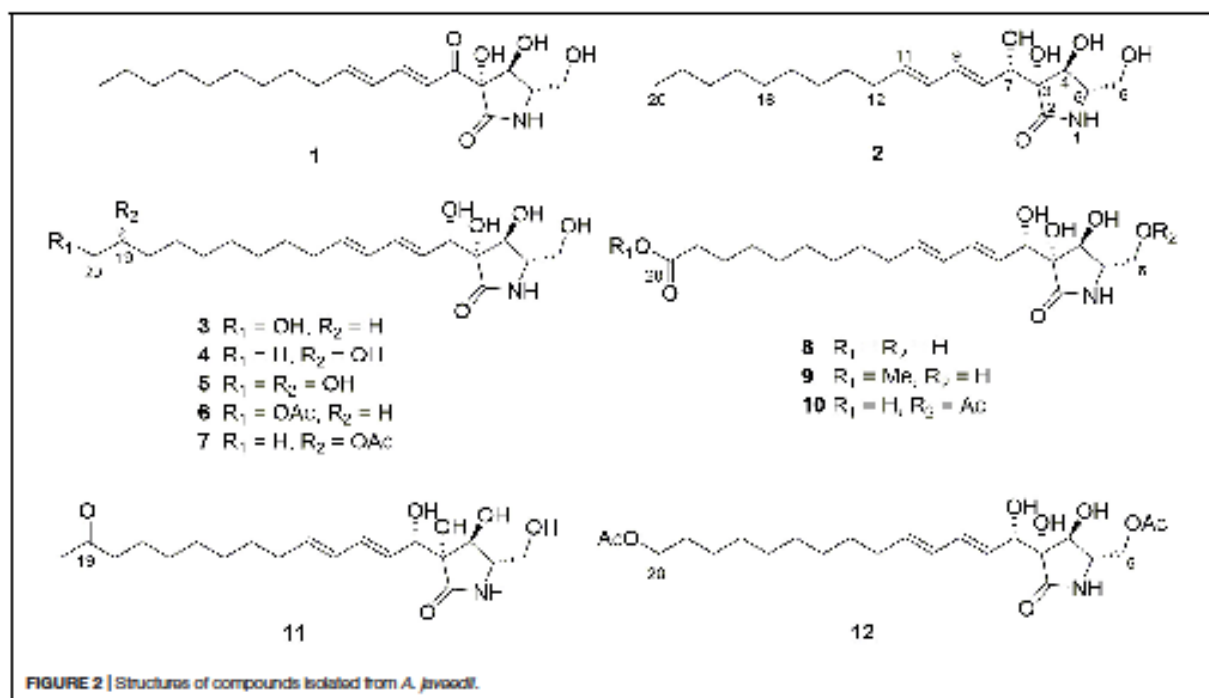
using MeOH-0.1% HCOOH in H_2O (65:35 to 86:14) to give 1 (25 mg) and 12 (1.4 mg). Fraction V5 (0.68 g) was subjected to a Sephadex LH-20 column using 100% MeOH as eluent to obtain eight subfractions (V5-S1 to V5-S8). Subfraction V5-S4 was submitted to a RP-18 (40–63 μm) vacuum liquid chromatography column and eluted with 10–100% aqueous MeOH to yield 10 subfractions (V5-S4-RP1 to V5-S4-RP10). Subfraction V5-S4-RP4 was purified by semi-preparative HPLC using MeOH-0.1% HCOOH in H_2O (50:50 to 70:30) to give 5 (2.5 mg). Subfraction V5-S4-RP6 was purified by semi-preparative HPLC using MeOH-0.1% HCOOH in H_2O (60:40) to give 9 (3.0 mg).

Pramanicin A (1): white solid; $[\alpha]^{20}_D$ -121 (c 0.1, MeOH).

Aplosporellin A (2): Colorless oil; $[\alpha]^{20}_D$ -21 (c 0.1, MeOH); UV (MeOH) λ_{max} 233 nm; ECD λ [nm] (φ): 239 (−1.54), 219 (1.06), 197 (−8.99); ^{1}H and ^{13}C NMR data, see **Table 1**; HRESIMS $[M + Na]^+$ m/z 378.2252 (calcd for $C_{19}H_{33}NNaO_5$ 378.2251) (**Supplementary Figures S1–S13**).

Aplosporellin B (3): Colorless oil; $[\alpha]^{20}_D$ -55 (c 0.1, MeOH); UV (MeOH) λ_{max} 233 nm; ECD λ [nm] (φ): 233 (−7.06), 199 (−8.83); ^{1}H and ^{13}C NMR data, see **Table 1**; HRESIMS $[M + Na]^+$ m/z 394.2197 (calcd for $C_{19}H_{33}NNaO_6$ 394.2200) (**Supplementary Figures S14–S21**).

Aplosporellin C (4): Colorless oil; $[\alpha]^{20}_D$ -26 (c 0.1, MeOH); UV (MeOH) λ_{max} 234 nm; ECD λ [nm] (φ): 233 (−0.98), 197 (−2.03); ^{1}H and ^{13}C NMR data, see **Table 2**; HRESIMS $[M + Na]^+$ m/z 394.2201 (calcd for $C_{19}H_{33}NNaO_6$ 394.2200) (**Supplementary Figures S22–S29**).

Aplosporellin D (5): Colorless oil; $[\alpha]^{20}_D$ -24 (c 0.1, MeOH); UV (MeOH) λ_{max} 234 nm; ^{1}H and ^{13}C NMR data, see **Table 2**;

HRESIMS $[M + Na]^+$ m/z 410.2145 (calcd for $C_{19}H_{33}NNaO_7$ 410.2149) (**Supplementary Figures S30–S37**).

Aplosporellin E (6): Colorless oil; $[\alpha]^{20}_D$ -33 (c 0.1, MeOH); UV (MeOH) λ_{max} 233 nm; ^{1}H and ^{13}C NMR data, see **Table 2**; HRESIMS $[M + Na]^+$ m/z 436.2307 (calcd for $C_{21}H_{35}NNaO_7$ 436.2306) (**Supplementary Figures S38–S45**).

Aplosporellin F (7): Colorless oil; $[\alpha]^{20}_D$ -36 (c 0.1, MeOH); UV (MeOH) λ_{max} 234 nm; ^{1}H and ^{13}C NMR data, see **Table 3**; HRESIMS $[M + Na]^+$ m/z 436.2304 (calcd for $C_{21}H_{35}NNaO_7$ 436.2306) (**Supplementary Figures S46–S53**).

Aplosporellin G (8): Colorless oil; $[\alpha]^{20}_D$ -57 (c 0.1, MeOH); UV (MeOH) λ_{max} 233 nm; ECD λ [nm] (φ): 234 (−2.59), 197 (−7.64); ^{1}H and ^{13}C NMR data, see **Table 3**; HRESIMS $[M + Na]^+$ m/z 408.1990 (calcd for $C_{19}H_{31}NNaO_7$ 408.1993) (**Supplementary Figures S54–S61**).

Aplosporellin H (9): Colorless oil; $[\alpha]^{20}_D$ -26 (c 0.1, MeOH); UV (MeOH) λ_{max} 232 nm; ^{1}H and ^{13}C NMR data, see **Table 3**; HRESIMS $[M + Na]^+$ m/z 422.2150 (calcd for $C_{20}H_{33}NNaO_7$ 422.2149) (**Supplementary Figures S62–S69**).

Aplosporellin I (10): Colorless oil; $[\alpha]^{20}_D$ -31 (c 0.1, MeOH); UV (MeOH) λ_{max} 233 nm; ^{1}H and ^{13}C NMR data, see **Table 4**; HRESIMS $[M + Na]^+$ m/z 450.2102 (calcd for $C_{21}H_{33}NNaO_8$ 450.2098) (**Supplementary Figures S70–S76**).

Aplosporellin J (11): Colorless oil; $[\alpha]^{20}_D$ -7 (c 0.1, MeOH); UV (MeOH) λ_{max} 234 nm; ^{1}H and ^{13}C NMR data, see **Table 4**; HRESIMS $[M + Na]^+$ m/z 392.2048 (calcd for $C_{19}H_{31}NNaO_6$ 392.2044) (**Supplementary Figures S77–S84**).

Aplosporellin K (12): Colorless oil; $[\alpha]^{20}_D$ -17 (c 0.1, MeOH); UV (MeOH) λ_{max} 232 nm; ^{1}H and ^{13}C NMR data, see **Table 4**;

HRESIMS [M + Na]+ m/z 478.2410 (calcd for $C_{23}H_{37}NNaO_8$ 478.2411) (Supplementary Figures S85–S91).

Cytotoxicity and Apoptosis Assays

Cytotoxicity against adult Burkitt's lymphoma B cells (Ramos, No. ACC-603) and lymphoblastic leukemia T cells (Jurkat J16, No. ACC-282) was tested as described previously (Harwoko et al., 2019). In the apoptosis assays, the protein kinase inhibitor staurosporine (STS, 2.5 μM, #S5921, Sigma-Aldrich) was used as positive control, and standard growth medium supplemented with 0.1% DMSO was used as negative control. Determination of cell viability, western blot analysis and measurement of caspase-3 activity were performed as described previously (Manns et al., 2011; Liu et al., 2017). All experiments were carried out in triplicate.

Computational Methods

Mixed torsional/low-mode conformational searches were carried out by means of the Macromodel 10.8.011 software using the MMFF with an implicit solvent model for CHCl₃ applying a 21 kJ mol⁻¹ energy window (MacroModel, 2015). Geometry reoptimizations of the resultant conformers [B3LYP/6-31 + G(d,p) level in vacuo, ωB97X/TZVP with PCM solvent model for MeCN and MeOH], DFT-NMR, TDDFT-ECD and SOR calculations were performed with Gaussian 09 (Frisch et al.,

2013). For NMR calculations the mPW1PW91/6-311 + G(2d,p) level while for the ECD and SOR calculations the B3LYP/TZVP, BH&HLYP/TZVP, CAM-B3LYP/TZVP and PBE0/TZVP levels were applied with the same or no solvent model as in the preceding DFT optimization level. ECD spectra were generated as the sum of Gaussians with 4200 and 3000 cm⁻¹ half-height widths, using dipole-velocity-computed rotational strengths (Stephens and Harada, 2010). Computed NMR shift data were corrected with I = −185.6277 and S = −1.0175 (Pierens, 2014). Boltzmann distributions were estimated from the B3LYP and the ωB97X energies. The MOLEKEL program was used for visualization of the results (Varetto, 2009).

RESULTS

Chemical Identification of the Isolated Compounds

Compound 2 was obtained as a colorless oil, with UV absorption at λ_{max} 233 nm. Its molecular formula was established as $C_{19}H_{33}NO_5$ on the basis of HRESIMS data, accounting for four degrees of unsaturation. The NMR spectra of 2 (Table 1) were recorded in methanol-d_4 as well as in DMSO-d_6. The latter solvent revealed the exchangeable protons of one NH proton

TABLE 1 | ¹H and ¹³C NMR data of compounds **2 and 3**.

No.	2[a] δ_C, type	2[a] δ_H (J in Hz)	2[b] δ_C, type	2[b] δ_H (J in Hz)	3[b] δ_C, type	3[b] δ_H (J in Hz)
1	NH	7.69, br s				
2	174.4, C		177.3, C		177.4, C	
3	78.8, C		80.8, C		80.8, C	
4	76.1, CH	3.89, t (5.9)	77.9, CH	4.12, d (6.6)	78.0, CH	4.12, d (6.5)
5	59.5, CH	3.16, ddd (5.9, 5.5, 3.5)	61.2, CH	3.38, ddd (6.6, 5.8, 3.2)	61.2, CH	3.38, ddd (6.5, 5.8, 3.3)
6	61.6, CH₂	3.54, ddd (11.1, 5.0, 3.5) 3.30, ddd (11.1, 5.5, 5.0)	62.9, CH₂	3.76, dd (11.6, 3.2) 3.52, dd (11.6, 5.8)	62.9, CH₂	3.76, dd (11.6, 3.3) 3.52, dd (11.6, 5.8)
7	73.0, CH	4.22, dd (6.5, 5.9)	74.5, CH	4.43, d (7.1)	74.5, CH	4.43, d (7.0)
8	130.8, CH	5.82, dd (15.4, 6.5)	129.6, CH	5.83, dd (15.4, 7.1)	129.6, CH	5.82, dd (15.4, 7.0)
9	131.0, CH	6.14, dd (15.4, 10.6)	134.6, CH	6.32, dd (15.4, 10.4)	134.6, CH	6.32, dd (15.4, 10.5)
10	130.2, CH	6.00, dd (15.1, 10.6)	131.2, CH	6.07, dd (15.0, 10.4)	131.2, CH	6.07, dd (15.0, 10.5)
11	133.6, CH	5.62, dt (15.1, 7.3)	136.3, CH	5.70, dt (15.0, 7.3)	136.3, CH	5.70, dt (15.0, 7.3)
12	32.0, CH₂	2.04, q (7.3)	33.7, CH₂	2.08, q (7.3)	33.6, CH₂	2.08, q (7.3)
13	28.8, CH₂	1.34, m	30.5, CH₂	1.39, m	30.4, CH₂	1.39, m
14	29.0, CH₂	1.24, m	30.7, CH₂	1.29, m	30.7, CH₂	1.31, m
15	28.9, CH₂	1.24, m	30.6, CH₂	1.29, m	30.6, CH₂	1.31, m
16	28.7, CH₂	1.24, m	30.5, CH₂	1.29, m	30.5, CH₂	1.31, m
17	28.6, CH₂	1.24, m	30.3, CH₂	1.29, m	30.3, CH₂	1.31, m
18	31.3, CH₂	1.23, m	33.1, CH₂	1.28, m	26.9, CH₂	1.35, m
19	22.1, CH₂	1.25, m	23.7, CH₂	1.31, m	33.7, CH₂	1.52, m
20	13.9, CH₃	0.85, t (6.9)	14.4, CH₃	0.90, t (7.0)	63.0, CH₂	3.54, t (6.7)
3-OH		5.03, s				
4-OH		5.47, d (5.9)				
6-OH		4.74, t (5.0)				
7-OH		4.75, d (5.9)				

[a]Recorded at 600 (¹H) and 150 MHz (¹³C) in DMSO-d_6. [b]Recorded at 600 (¹H) and 150 MHz (¹³C) in CD₃OD.

Lactam Derivatives From *Apiosporella javeedii*

TABLE 2 | ¹H and ¹³C NMR data of compounds 4–6.

No.	4 δ$_C$, type	4 δ$_H$ (J in Hz)	5 δ$_C$, type	5 δ$_H$ (J in Hz)	6 δ$_C$, type	6 δ$_H$ (J in Hz)
2	177.3, C		177.4, C		177.4, C	
3	80.8, C		80.8, C		80.8, C	
4	77.9, CH	4.12, d (6.5)	78.0, CH	4.12, d (6.5)	78.0, CH	4.12, d (6.5)
5	61.2, CH	3.38, ddd (6.5, 5.8, 3.2)	61.2, CH	3.38, ddd (6.5, 5.8, 3.3)	61.2, CH	3.38, ddd (6.5, 5.8, 3.2)
6	62.9, CH$_2$	3.76, dd (11.5, 3.2) 3.52, dd (11.5, 5.8)	63.0, CH$_2$	3.76, dd (11.6, 3.3) 3.52, dd (11.6, 5.8)	63.0, CH$_2$	3.76, dd (11.5, 3.2) 3.52, dd (11.5, 5.8)
7	74.5, CH	4.43, d (7.1)	74.6, CH	4.43, d (7.1)	74.5, CH	4.43, d (7.0)
8	129.6, CH	5.82, dd (15.3, 7.1)	129.6, CH	5.82, dd (15.3, 7.1)	129.7, CH	5.82, dd (15.3, 7.0)
9	134.6, CH	6.32, dd (15.3, 10.5)	134.6, CH	6.32, dd (15.3, 10.5)	134.6, CH	6.32, dd (15.3, 10.5)
10	131.2, CH	6.07, dd (15.0, 10.5)	131.2, CH	6.07, dd (15.0, 10.5)	131.2, CH	6.07, dd (15.0, 10.5)
11	136.3, CH	5.70, dt (15.0, 7.3)	136.3, CH	5.70, dt (15.0, 7.3)	136.3, CH	5.70, dt (15.0, 7.3)
12	33.7, CH$_2$	2.08, q (7.3)	33.7, CH$_2$	2.09, q (7.3)	33.7, CH$_2$	2.08, q (7.3)
13	30.4, CH$_2$	1.39, m	30.4, CH$_2$	1.40, m	30.3, CH$_2$	1.39, m
14	30.7, CH$_2$	1.31, m	30.8, CH$_2$	1.33, m	30.6, CH$_2$	1.31, m
15	30.6, CH$_2$	1.31, m	30.5, CH$_2$	1.33, m	30.5, CH$_2$	1.31, m
16	30.2, CH$_2$	1.31, m	30.2, CH$_2$	1.33, m	30.4, CH$_2$	1.31, m
17	26.9, CH$_2$	1.40, m 1.33, m	26.7, CH$_2$	1.48, m 1.34, m	30.2, CH$_2$	1.31, m
18	40.2, CH$_2$	1.44, m 1.40, m	34.4, CH$_2$	1.49, m 1.36, m	27.0, CH$_2$	1.35, m
19	68.6, CH	3.70, m	73.3, CH	3.56, m	29.7, CH$_2$	1.62, m
20	23.5, CH$_3$	1.14, d (6.2)	67.4, CH$_2$	3.46, dd (11.2, 4.5) 3.41, dd (11.2, 6.5)	65.7, CH$_2$	4.05, t (6.7)
20-OAc					20.8, CH$_3$ 173.1, C	2.02, s

ᵃRecorded at 600 (¹H) and 150 MHz (¹³C) in CD$_3$OD.

TABLE 3 | ¹H and ¹³C NMR data of compounds 7–9.

No.	7 δ$_C$, type	7 δ$_H$ (J in Hz)	8 δ$_C$, type	8 δ$_H$ (J in Hz)	9 δ$_C$, type	9 δ$_H$ (J in Hz)
2	177.3, C		177.3, C		177.3, C	
3	80.8, C		80.9, C		80.8, C	
4	77.9, CH	4.12, d (6.5)	77.9, CH	4.12, d (6.5)	78.0, CH	4.12, d (6.5)
5	61.2, CH	3.38, ddd (6.5, 5.8, 3.2)	61.1, CH	3.39, ddd (6.6, 5.8, 3.2)	61.2, CH	3.38, ddd (6.6, 5.8, 3.3)
6	62.9, CH$_2$	3.76, dd (11.5, 3.2) 3.52, dd (11.5, 5.8)	62.9, CH$_2$	3.76, dd (11.6, 3.2) 3.52, dd (11.6, 5.8)	63.0, CH$_2$	3.76, dd (11.5, 3.3) 3.52, dd (11.5, 5.8)
7	74.5, CH	4.43, d (7.1)	74.5, CH	4.44, d (7.1)	74.6, CH	4.43, d (7.0)
8	129.6, CH	5.83, dd (15.3, 7.1)	129.5, CH	5.82, dd (15.3, 7.1)	129.7, CH	5.82, dd (15.4, 7.0)
9	134.6, CH	6.32, dd (15.3, 10.5)	134.6, CH	6.32, dd (15.3, 10.5)	134.6, CH	6.32, dd (15.4, 10.6)
10	131.2, CH	6.07, dd (15.1, 10.5)	131.2, CH	6.07, dd (15.0, 10.5)	131.2, CH	6.07, dd (15.0, 10.6)
11	136.3, CH	5.70, dt (15.1, 7.3)	136.3, CH	5.70, dt (15.0, 7.3)	136.3, CH	5.70, dt (15.0, 7.3)
12	33.6, CH$_2$	2.08, q (7.3)	33.6, CH$_2$	2.08, q (7.3)	33.7, CH$_2$	2.08, q (7.3)
13	30.4, CH$_2$	1.39, m	30.3, CH$_2$	1.39, m	30.3, CH$_2$	1.39, m
14	30.5, CH$_2$	1.31, m	30.4, CH$_2$	1.32, m	30.5, CH$_2$	1.31, m
15	30.5, CH$_2$	1.31, m	30.3, CH$_2$	1.32, m	30.4, CH$_2$	1.31, m
16	30.2, CH$_2$	1.31, m	30.2, CH$_2$	1.32, m	30.2, CH$_2$	1.31, m
17	26.5, CH$_2$	1.31, m	30.1, CH$_2$	1.32, m	30.1, CH$_2$	1.31, m
18	36.9, CH$_2$	1.58, m 1.50, m	26.2, CH$_2$	1.59, m	26.0, CH$_2$	1.60, m
19	72.4, CH	4.86, m	35.2, CH$_2$	2.27, t (7.4)	34.8, CH$_2$	2.31, t (7.4)
20	20.2, CH$_3$	1.20, d (6.2)	178.1, C		176.1, C	
19-OAc	21.2, CH$_3$ 172.7, C	2.00, s				
20-OMe					52.0, CH$_3$	3.65, s

ᵃRecorded at 600 (¹H) and 150 MHz (¹³C) in CD$_3$OD.

86

at δ_H 7.69 (NH-1) as well as four OH protons at δ_H 5.47 (4-OH), 5.03 (3-OH), 4.75 (7-OH), and 4.74 (6-OH). The ^{13}C NMR spectrum of 2 displayed one carbonyl group at δ_C 174.4 (C-2), and four olefinic carbons at δ_C 133.6 (C-11), 131.0 (C-9), 130.8 (C-8), and 130.2 (C-10), accounting for three degrees of unsaturation. The presence of a γ-lactam ring was confirmed by the COSY correlations between 4-OH/H-4 (δ_H 3.89)/H-5 (δ_H 3.16)/H$_2$-6 (δ_H 3.54 and 3.30)/6-OH and the HMBC correlations from NH-1 to C-3, C-4, and C-5, from 3-OH to C-2, C-3 and C-4, from 4-OH to C-3, and from H-5 to C-2 (**Figure 3**). The COSY correlations between H-8 (δ_H 5.82)/H-9 (δ_H 6.14)/H-10 (δ_H 6.00)/H-11 (δ_H 5.62)/H$_2$-12 (δ_H 2.04)/H$_2$-13 (δ_H 1.34)/H$_2$-14 (δ_H 1.24), and between Me-20 (δ_H 0.85)/H$_2$-19 (δ_H 1.24) together with the HMBC correlations from Me-20 to C-19 (δ_C 22.1) and C-18 (δ_C 31.3) and the observation of characteristic aliphatic methylenes at 29.0, 28.9, 28.7, 28.6, and δ_H 1.24 (CH$_2$-14, 15, 16, and 17), established the presence of a trideca-1,3-diene subunit

in 2. In addition, the COSY correlations between H-8/H-7 (δ_H 4.22)/7-OH along with the HMBC correlations from H-7 to C-2, C-3, and C-4, and from 3-OH to C-7 indicated the trideca-1,3-diene side chain to be connected to the γ-lactam moiety via the oxygenated carbon at C-7. Therefore, the planar structure of 2 was elucidated, which was similar to that of the co-isolated known compound, pramanicin A (1) (Schwartz et al., 1994; Harrison et al., 2000). The major difference between both compounds was the presence of an additional hydroxy group in 2 instead of the ketone group in 1 at position C-7. The trivial name aplosporellin A is proposed for 2.

The large values of $J_{8,9}$ (15.4 Hz) and $J_{10,11}$ (15.1 Hz) supported the *E* configuration for the double bonds at C-8/C-9 and C-10/C-11 in 2. The relative configuration of the γ-lactam ring was deduced through the ROESY spectrum and by comparison with pramanicin A (1) (Harrison et al., 2000), virgaricins A and B (Ishii et al., 2012, 2015). The NOE

TABLE 4 | ^{1}H and ^{13}C NMR data of compounds 10–12.

No.	10[a]		11[a]		12[a]	
	δ_C[b], type	δ_H (*J* in Hz)	δ_C, type	δ_H (*J* in Hz)	δ_C[b], type	δ_H (*J* in Hz)
2	177.3, C		177.3, C		177.4, C	
3	80.5, C		80.8, C		80.6, C	
4	78.1, CH	4.10, d (6.8)	77.9, CH	4.12, d (6.5)	78.1, CH	4.10, d (6.7)
5	58.2, CH	3.55, ddd (6.8, 6.2, 3.3)	61.2, CH	3.38, ddd (6.5, 5.8, 3.2)	58.3, CH	3.55, ddd (6.7, 6.2, 3.4)
6	65.0, CH$_2$	4.30, dd (11.6, 3.3) 4.05, dd (11.6, 6.2)	63.0, CH$_2$	3.76, dd (11.6, 3.2) 3.52, dd (11.6, 5.8)	65.0, CH$_2$	4.30, dd (11.7, 3.4) 4.04, dd (11.7, 6.2)
7	74.5, CH	4.42, d (7.0)	74.5, CH	4.43, d (7.1)	74.6, CH	4.42, d (7.1)
8	129.4, CH	5.82, dd (15.3, 7.0)	129.7, CH	5.82, dd (15.3, 7.1)	129.4, CH	5.82, dd (15.4, 7.1)
9	134.5, CH	6.32, dd (15.3, 10.5)	134.5, CH	6.32, dd (15.3, 10.5)	134.5, CH	6.32, dd (15.4, 10.6)
10	131.2, CH	6.07, dd (15.1, 10.5)	131.2, CH	6.07, dd (15.0, 10.5)	131.2, CH	6.07, dd (15.0, 10.6)
11	136.3, CH	5.70, dt (15.1, 7.3)	136.3, CH	5.70, dt (15.0, 7.3)	136.3, CH	5.71, dt (15.0, 7.3)
12	33.6, CH$_2$	2.08, q (7.3)	33.6, CH$_2$	2.08, q (7.3)	33.6, CH$_2$	2.08, q (7.3)
13	30.2, CH$_2$	1.39, m	30.2, CH$_2$	1.39, m	30.3, CH$_2$	1.40, m
14	30.4, CH$_2$	1.32, m	30.3, CH$_2$	1.31, m	30.6, CH$_2$	1.31, m
15	30.3, CH$_2$	1.32, m	30.2, CH$_2$	1.31, m	30.5, CH$_2$	1.31, m
16	30.2, CH$_2$	1.32, m	30.1, CH$_2$	1.31, m	30.4, CH$_2$	1.31, m
17	30.1, CH$_2$	1.32, m	24.8, CH$_2$	1.54, m	30.2, CH$_2$	1.31, m
18	26.7, CH$_2$	1.59, m	44.3, CH$_2$	2.47, t (7.3)	27.0, CH$_2$	1.35, m
19	36.6, CH$_2$	2.22, t (7.4)	212.3, C		29.6, CH$_2$	1.62, m
20	179.8, C		29.8, CH$_3$	2.13, s	65.7, CH$_2$	4.05, t (6.7)
6-OAc	20.5, CH$_3$ 172.5, C	2.07, s			20.5, CH$_3$ 172.4, C	2.07, s
20-OAc					20.8, CH$_3$ 173.0, C	2.02, s

[a]Recorded at 600 (^{1}H) and 150 MHz (^{13}C) in CD$_3$OD.[b]Data extracted from HSQC and HMBC spectra.

FIGURE 3 | COSY and key HMBC correlations of compound 2.
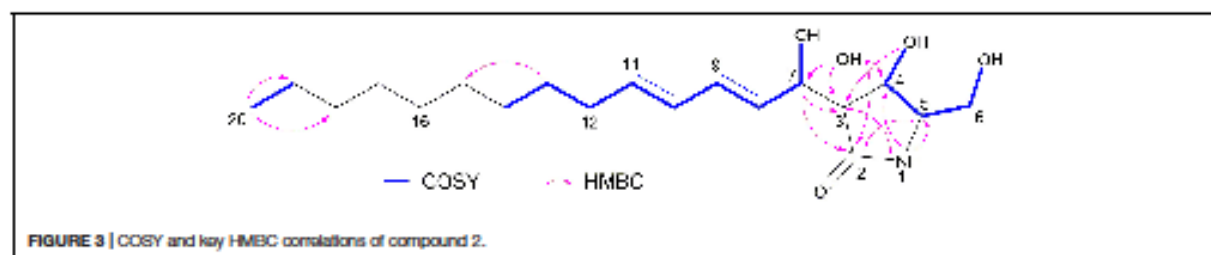
correlations between 3-OH/H-4, H-4/H$_2$-6 indicated that 3-OH, H-4 and H$_2$-6 were located on the same side of the ring. In contrast, the NOE correlations between H-7/4-OH, 4-OH/H-5, indicated that 4-OH and H-5 were located on the opposite side compared to 3-OH, H-4 and H$_2$-6. On the basis of these findings, the relative stereochemistry of **2** in the γ-lactam moiety was assigned to be identical to that of pramanicin A (**1**).

Pramanicin A (**1**) was reported together with pramanicin from the fungus *Stagonospora* sp. (Schwartz et al., 1994), the latter contained an epoxide group at C-10/C-11 instead of a double bond. The absolute configuration of pramanicin A (**1**) was deduced by comparison to pramanicin through biogenetic considerations (Duspara et al., 1998; Harrison et al., 1998, 2000; Chen and Harrison, 2004) and by total synthesis (Cow et al., 1997; Barrett et al., 1999a,b; Tan et al., 2014, 2015, 2017), which confirmed that the compound has (3*S*,4*S*,5*S*) configuration. The large absolute value of the specific optical rotation (SOR) of **1** allowed testing the TDDFT-SOR method (Polavarapu, 2002; Mándi and Kurtán, 2019) and the ωB97X functional (Chai and Head-Gordon, 2008; Bremond et al., 2016), which was also applied for the TDDFT-ECD calculations of **2**. Merck Molecular Force Field (MMFF) conformational searches of **1** and the epimers of **2** resulted in a large number of conformers [c.a. 18 thousand by generating 100 thousand structures for (3*R*,4*S*,5*S*,7*S*)-**2**] and the searches were not complete, since many conformers were found only a few times (Mándi et al., 2015). Thus, model compounds were utilized for the calculations, in which the C-3 side-chain was truncated at the C-12 position (**Figure 4**).

The MMFF conformational search of (3*S*,4*S*,5*S*)-**1mod** resulted in 79 conformers in a 21 kJ/mol energy window, which were re-optimized at the ωB97X/TZVP PCM/MeOH level yielding 16 low-energy conformers over 1% Boltzmann-distribution (**Supplementary Figure S92**). SOR values were computed at four levels (B3LYP/TZVP, BH&HLYP/TZVP, CAM-B3LYP/TZVP and PBE0/TZVP all with the PCM solvent model for MeOH) and nice agreements were found with the experimental SOR value (computed SOR values in the range from −91 to −115 compared to the −121 experimental value) (**Supplementary Table S1**).

The absolute configuration of the γ-lactam ring of compound **2** is assumed to be identical to that of **1** based on biogenetic considerations whereas that of the OH group in the side chain at C-7 could not be elucidated. In order to solve this problem, DFT-NMR calculations were performed on the epimeric model compounds (3*R*,4*S*,5*S*,7*R*)-**2mod** and (3*R*,4*S*,5*S*,7*S*)-**2mod** (Lodewyk et al., 2012; Kicsák et al., 2018; Mándi and

Kurtán, 2019). B3LYP/6-31 + G(d,p) re-optimization of the initial 169 and 205 conformers resulted in 8 and 15 low-energy conformers over 1% Boltzmann population, respectively (**Supplementary Figures S93, S94**). The ^{13}C NMR chemical shift data of (3*R*,4*S*,5*S*,7*S*)-**2mod** computed at the mPW1PW91/6-311 + G(2d,p) level reproduced much better the experimental values than those of the other epimer (**Supplementary Table S2**). Mean absolute error (MAE) values were 1.70 vs. 2.17 favoring the (3*R*,4*S*,5*S*,7*S*) epimer. The signal of the terminal C-12 was neglected, since it has an abnormal shift in the computations due to the truncation. Computed and the experimental ^{13}C NMR chemical shift data in the vicinity of the C-7 chirality center also clearly showed superior agreement for the (3*R*,4*S*,5*S*,7*S*) epimer. DP4 + statistical analysis was utilized for the comparison of the experimental and calculated ^{13}C NMR data resulting in 97.31% confidence for the (3*R*,4*S*,5*S*,7*S*) epimer (Smith and Goodman, 2010; Grimblat et al., 2015; Li et al., 2020). Although the experimental SOR value of **2** is small, the SOR calculations performed the same way as for **1mod** were in agreement with the results of the NMR calculation suggesting also (3*R*,4*S*,5*S*,7*S*) absolute configuration. The (3*R*,4*S*,5*S*,7*R*) epimer of **2mod** gave computed SOR values ranging from +4 to +7 while the (3*R*,4*S*,5*S*,7*S*) one in the range from −18 to −23 reproducing better the −21 experimental value of **2** (**Supplementary Tables S3, S4**). For the TDDFT-ECD method, the same MMFF conformers of (3*R*,4*S*,5*S*,7*R*)-**2mod** and (3*R*,4*S*,5*S*,7*S*)-**2mod** were re-optimized at the ωB97X/TZVP PCM/MeCN level and ECD calculations were performed at various levels. Although both epimers gave rather diverse computed ECD spectra for the individual conformers and Boltzmann populations were small, the average ECD spectra of the (3*R*,4*S*,5*S*,7*S*) epimer were found to be similar to the experimental one (**Figure 5**) in line with the NMR and the SOR calculations. Consequently, the absolute configuration of **2** could be elucidated as (3*R*,4*S*,5*S*,7*S*).

The molecular formula of compound **3** was assigned as C$_{19}$H$_{33}$NO$_6$ based on its HRESIMS data, containing an additional oxygen atom when compared to **2**. The NMR data of **3** (**Table 1**) were similar to those of **2**, except for the presence of an oxygenated methylene group resonating at δ$_C$ 63.0 and δ$_H$ 3.54 (t) (CH$_2$-20) and the absence of the terminal methyl group in the side chain. The COSY correlation between H$_2$-20/H$_2$-19 (δ$_H$ 1.52)/H$_2$-18 (δ$_H$ 1.35) together with the HMBC correlations from H$_2$-20 to C-18 (δ$_C$ 26.9) and C-19 (δ$_C$ 33.7) indicated the attachment of a hydroxy group at C-20 in the side chain of **3**. Detailed analysis of its 2D NMR spectra revealed that the remaining substructure of **3** was identical to that of **2**. The absolute configuration of **3** was identical to that of **2** based on their similar ROESY correlations and ECD data.

Aplosporellin C (**4**) exhibited the same molecular formula as **3** as determined by HRESIMS data. The ^{1}H and ^{13}C NMR data of **4** (**Table 2**) were likewise similar to those of **3**, yet showed the signal of a doublet methyl group at δ$_C$ 23.5 and δ$_H$ 1.14 (Me-20) in the side chain and the presence of an oxygenated methine at δ$_C$ 68.6 and δ$_H$ 3.70 (CH-19). The COSY correlations between Me-20/H-19, and between H-19/H$_2$-18 (δ$_H$ 1.44 and 1.40) together with the HMBC correlations from Me-20 to C-19 and C-18 (δ$_C$ 40.2) indicated the presence of a hydroxy group at C-19 in **4**
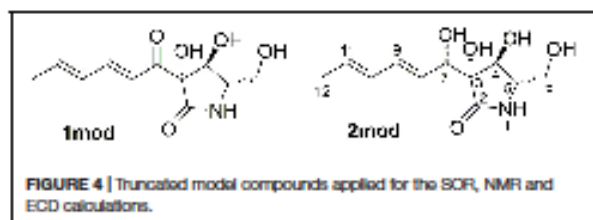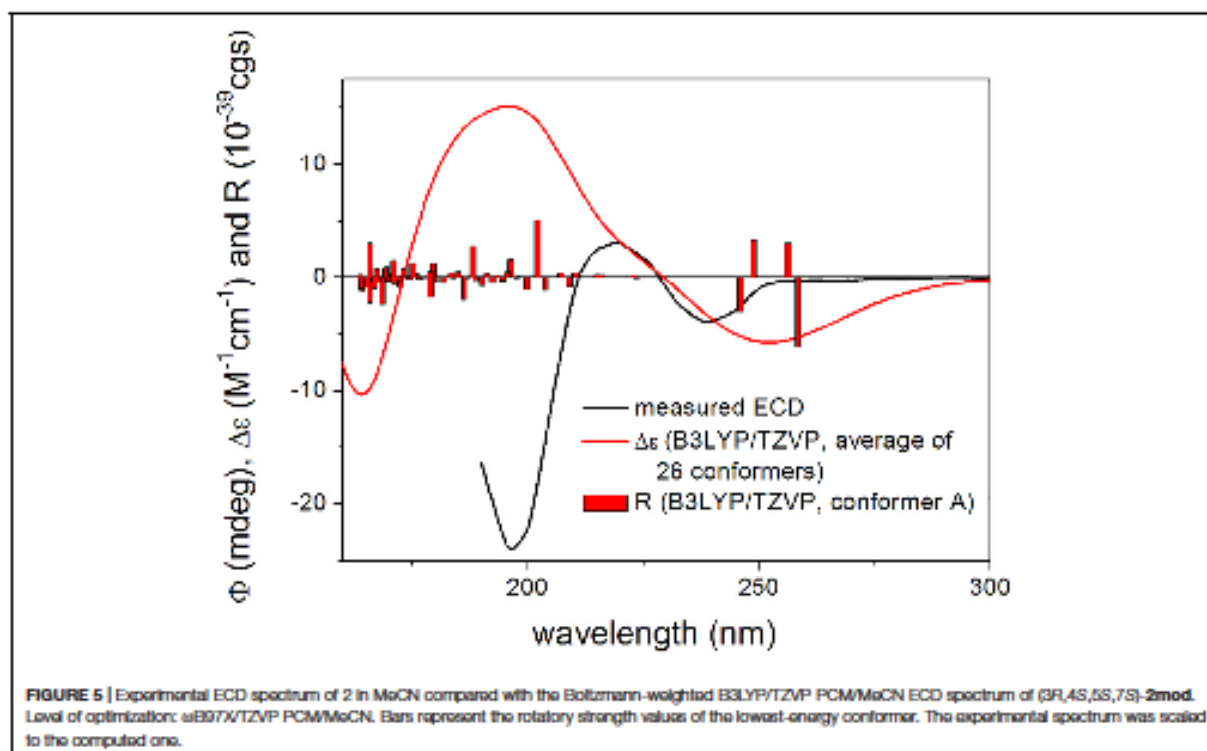

FIGURE 4 | Truncated model compounds applied for the SOR, NMR and ECD calculations.

FIGURE 5 | Experimental ECD spectrum of 2 in MeCN compared with the Boltzmann-weighted B3LYP/TZVP PCM/MeCN ECD spectrum of (3R,4S,5S,7S)-**2mod**. Level of optimization: ωB97X/TZVP PCM/MeCN. Bars represent the rotatory strength values of the lowest-energy conformer. The experimental spectrum was scaled to the computed one.

instead of C-20 as in 3. The remaining substructure of 4 was identical to that of 2 as confirmed by detailed interpretation of the 2D NMR spectra of 4. Due to the limited amount, the absolute configuration at C-19 of 4 could not be determined by converting the compound to its Mosher ester.

Compound 5 had the molecular formula $C_{19}H_{33}NO_7$ as determined by HRESIMS data, containing one additional oxygen atom when compared to 3 and 4. Detailed analysis of the 2D NMR of 5 (**Table 2**) revealed that it was similar to 3 except for the presence of one additional oxygenated methine at δ_C 73.3 and δ_H 3.56 (CH-19). The signal of the terminal oxygenated methylene at C-20 appeared as two dd peaks in the ^{1}H NMR spectrum of 5 instead of a triplet peak of 3. This suggested that the additional hydroxy group of 5 was located at C-19, which was further confirmed by the COSY correlations between H_2-20/H-19/H_2-18 together with the HMBC correlations from H_2-20 to C-19 and C-18. Thus, compound 5 was elucidated as 19,20-dihydroxy derivative of 2.

Aplosporellin E (6) was found to have the molecular formula $C_{21}H_{35}NO_7$ on the basis of HRESIMS data, requiring five degrees of unsaturation. Comparison of the NMR data (**Table 2**) indicated compound 6 to be closely related to compound 3 except for the presence of an additional methyl group (δ_H 2.02 and δ_C 20.8) and an additional carbonyl carbon (δ_C 173.1). The HMBC correlations from protons of the additional methyl and H_2-20 (δ_H 4.05) to the additional carbonyl carbon indicated the attachment of an additional acetoxy group at C-20 in 6 when compared to 3.

The molecular formula of compound 7 was the same as 6 as deduced from HRESIMS. The ^{1}H and ^{13}C NMR data of 7 (**Table 3**) were very similar to those of 6, except for the appearance of a terminal methyl group at δ_H 1.20 (Me-20) which was split into a doublet peak in the ^{1}H NMR spectrum of 7. Detailed analysis of the HSQC and HMBC spectra revealed an oxygenated methine at δ_C 72.4 and δ_H 4.86 (CH-19). The COSY correlations between Me-20/H-19/H_2-18 (δ_H 1.58 and 1.50) together with the HMBC correlations from H-19 and the methyl group at δ_H 2.00 (3H, s) to the carbonyl carbon at δ_C 172.7 indicated the presence of an acetoxy group at C-19. Thus, compound 7 was elucidated as 19-O-acetyl derivative of compound 4.

Compound 8 exhibited the molecular formula $C_{19}H_{31}NO_7$ as determined by the HRESIMS data. Its ^{1}H and ^{13}C NMR data (**Table 3**) were similar to those of 2 except for that signals of the terminal methyl group in the side chain was replaced with a carbonyl group at δ_C 178.1 (C-20). The HMBC correlations from H_2-18 (δ_H 1.59) and H_2-19 (δ_H 2.27, t) to C-20, together with the COSY correlations between H_2-18/H_2-19 indicated a terminal carboxylic acid group in the side chain. The remaining substructure of 8 was identical to that of 2 as confirmed by detailed analysis of the 2D NMR spectra of 8.

The HRESIMS data of 9 gave the molecular formula $C_{20}H_{33}NO_7$. From the 2D NMR spectra of 9 (**Table 3**) it was evident that compound 9 was the 20-O-methyl derivative of 8 as indicated by the presence of an additional methoxy

group at δ_H 3.65 (3H, s) and δ_C 52.0, together with the HMBC correlations from the methoxy group and H_2-19 (δ_H 2.31, t) to the carbonyl carbon at δ_C 176.1 (C-20).

Aplosporellin I (**10**) exhibited the molecular formula $C_{21}H_{33}NO_8$ as determined by HRESIMS, requiring six degrees of unsaturation. The NMR data of **10** (**Table 4**) were similar to those of **8** except for the presence of a methyl group (δ_H 2.07 and δ_C 20.5) and a carbonyl carbon (δ_C 172.5) in addition to minor differences of the chemical shifts of the protons at the γ-lactam ring moiety. The COSY correlations between H-4 (δ_H 4.10)/H-5 (δ_H 3.55)/H_2-6 (δ_H 4.30 and 4.05) together with the HMBC correlations from H_2-6 and the additional methyl group at δ_H 2.07 to the carbonyl carbon at δ_C 172.5 indicated the attachment of an acetoxy group at C-6. Detailed analysis of the 2D NMR spectra and the ROESY spectra of compound **10** revealed that the remaining substructure and relative configuration were identical to compound **8**. Thus, compound **10** was identified as the 6-O-acetyl derivative of **8**.

The molecular formula of **11** was determined as $C_{19}H_{31}NO_6$ based on HRESIMS data, accounting for five degrees of unsaturation. The NMR data of **11** (**Table 4**) were similar to those of **2** but exhibited the signal of an additional carbonyl group at δ_C 212.3 (C-19). Moreover, the methyl group in the side chain was shifted to down field at δ_C 29.8, δ_H 2.13 (Me-20) and appeared as singlet in the ^{1}H NMR spectrum. The HMBC correlations from Me-20, H_2-18 (δ_H 2.47) and H_2-17 (δ_H 1.54) to C-19 indicated the presence of a ketone group in the side chain at C-19 in **11**. The remaining substructure of **11** was identical to that of **2** as confirmed by detailed analysis of the 2D NMR spectra.

On the basis of the HRESIMS data, the molecular formula of **12** was established as $C_{23}H_{37}NO_8$ with six degrees of unsaturation. The NMR data of **12** (**Table 4**) were similar to those of **6**, except for the presence of an additional methyl group (δ_H 2.07 and δ_C 20.6) and a carbonyl carbon (δ_C 172.4). Moreover, the chemical shifts of the protons of the γ-lactam ring in **12** were more comparable to those of **10** rather than **6**. These findings suggested compound **12** was a 6-O-acetyl derivative of **6**, which was confirmed by the HMBC correlations from H_2-6 (δ_H 4.30

and δ_C 4.04) and the additional methyl group at δ_H 2.07 to the carbonyl carbon at δ_C 172.4.

Bioactivities of the Isolated Compounds

All isolated compounds were tested for their cytotoxicity against human lymphoma (Ramos) and leukemia (Jurkat J16) cell lines. Pramanicin A (**1**) exhibited IC_{50} values of 4.7 and 4.4 μM after 24 h of incubation respectively, whereas after 72 h of incubation these values were 3.9 and 4.9 μM, respectively. Treatment with pramanicin A (**1**) significantly affected cell viability in a dose-dependent manner (**Figure 6**) whereas the remaining compounds showed no cytotoxicity in these two cell lines in the observed concentration ranging up to 30 μM. The ketone group at C-7 of pramanicin A (**1**) which is conjugated to the olefinic function at C-8/C-9 is obviously the key factor responsible for the cytotoxicity against human Ramos and Jurkat J16 cell lines. It was suggested that the α,β-unsaturated ketone functionality in pramanicin A (**1**) could be Michael acceptors that can react with a thiol group of cysteine amino acid of proteins or enzymes, and thus causing cytotoxic activity (Amslinger, 2010; Darsih et al., 2015).

In order to evaluate whether the pronounced cytotoxicity of pramanicin A (**1**) is attributable to the induction of apoptosis, we followed the activation of the effector caspases such as caspase-3 in response to pramanicin A (**1**) treatment. In the Western blot experiment, after 2–8 h treatment of Ramos and Jurkat J16 cell lines with 10 μM pramanicin A (**1**) respectively, an explicit cleavage of PARP1 (poly [ADP-ribose] polymerase 1) was observed (**Figure 7**). Cleavage of PARP1, which is a substrate of caspase-3, serves as a surrogate marker for activation of caspase-3 and therefore indicated that pramanicin A (**1**) is able to induce apoptosis. Moreover, we also measured caspase-3 activity by detecting the profluorogenic caspase-3 substrate Ac-DEVD-AMC. After treatment with 10 μM pramanicin A (**1**) in the two cell lines, cleavage of Ac-DEVD-AMC was observed within a few hours, which was more obvious in Ramos cells than in Jurkat J16 cells (**Figure 8**). These results further proved the activation of caspase-3 and thus induction of apoptosis in Ramos and Jurkat J16 cells by pramanicin A (**1**).

FIGURE 6 | Alamar blue assay of pramanicin A (**1**) in Ramos and Jurkat J16 cells. Each cell line was treated with 0–300 μM pramanicin A (**1**) for 24 or 72 h and after incubation, cell viability was evaluated using Alamar blue assay. Results shown are the mean ± SD from triplicates.

FIGURE 7 | Western blot experiment of pramanicin A (1) in Ramos and Jurkat J16 cells. After incubation for 2–8 h, cleavage of PARP1 was determined. Solid arrowheads indicate the uncleaved form of PARP1, open arrowheads indicate the cleaved form. The expression of TUBA4A was determined as protein loading control. Negative control (Ctrl.) was 0.1% DMSO.

FIGURE 8 | Caspase-3 assay: the kinetics of caspase-3 activation in Ramos and Jurkat J16 cells after treatment with indicated concentrations of pramanicin A (1). Caspase-3 activity was measured by the rate of cleavage of Ac-DEVD-AMC. Cells treated with staurosporine (STS, 2.5 µM) were used as positive control. Cells treated with 0.1% DMSO were used as negative control and set to 100%. Results shown are the mean ± SD from triplicates.

DISCUSSION

In the previous biosynthetic study on pramanicin, which differs from pramanicin A (1) by the presence of an epoxide group at C-10/C-11 instead of the double bond, in the fungus *Stagonospora* sp., Duspara et al. (1998) and Harrison et al. (2000) conducted a feeding experiment using ^{2}H, ^{13}C, ^{15}N, and ^{18}O isotopically labeled precursors. It was concluded that pramanicin originates from one starter molecule acetate and six extender malonates to generate the aliphatic acyl tail, whereas L-serine interacts with one acetate to form the pyrrolidone ring. Acetylation of these two moieties provides 3-acyltetramic acid, followed by a series of oxidation and reduction reactions to form pramanicin (Harrison et al., 2000). Proline or glutamate on the other hand were shown not be precursors of the pyrrolidone moiety (Harrison et al., 1998). In our study, the addition of 3.5% NaNO$_3$ or of 3.5% C$_5$H$_8$NNaO$_4$-H$_2$O to solid rice medium was found to induce the accumulation of pramanicin-like compounds. Thus, a feeding study using labeled glutamate as a potential precursor of compounds 1–12 would be of interest as a follow up study of this investigation.

with addition of either 3.5% NaNO$_3$ or 3.5% monosodium glutamate. All of these compounds were not detected when the fungus was grown on rice medium without these activators. To the best of our knowledge, this study was the first report to regulate secondary metabolites from *A. javeedii* applying an OSMAC approach. The results proved the power of the OSMAC approach on mining new secondary metabolites from endophytic fungi. DFT-NMR, TDDFT-ECD and OR calculations were carried out to determine the absolute configuration. Pramanicin A (1) exhibited strong cytotoxicity against human lymphoma (Ramos) and leukemia (Jurkat J16) cell lines with IC$_{50}$ values of 4.7 and 4.4 µM, respectively. Furthermore, mechanistic studies indicated that pramanicin A (1) activates caspase-3 and induces apoptotic cell death.

DATA AVAILABILITY STATEMENT

The original contributions presented in the study are included in the article/Supplementary Material, further inquiries can be directed to the corresponding authors.

AUTHOR CONTRIBUTIONS

YG sentence contributed to extraction, isolation, and manuscript preparation. FS, LS, and SW carried out the cytotoxicity assay. ZG and KZ contributed to part of structure elucidation. AM and TK performed the DFT-NMR, TDDFT-ECD, and OR

CONCLUSION

In summary, 11 new lactam derivatives, aplosporellins A–K (2–12), together with the known analog, pramanicin A (1), were isolated from fermentation of *A. javeedii* on solid rice medium

SUPPLEMENTARY MATERIAL

The Supplementary Material for this article can be found online at: https://www.frontiersin.org/articles/10.3389/fmicb.2020.600983/full#supplementary-material

REFERENCES

Amslinger, S. (2010). The tunable functionality of α,β-unsaturated carbonyl compounds enables their differential application in biological systems. *ChemMedChem.* 5, 351–356. doi: 10.1002/cmdc.200900499

Ancheeva, E., Daletos, G., and Proksch, P. (2018). Lead compounds from mangrove-associated microorganisms. *Mar. Drugs.* 16:319. doi: 10.3390/md16090319

Ariantari, N. P., Daletos, G., Mándi, A., Kurtán, T., Müller, W. E. G., Lin, W. H., et al. (2019). Expanding the chemical diversity of an endophytic fungus *Bulgaria inquinans*, an ascomycete associated with mistletoe, through an OSMAC approach. *RSC Adv.* 9, 25119–25132. doi: 10.1039/c9ra03678d

Barrett, A. G. M., Head, J., Smith, M. L., Stock, N. S., White, A. J. P., and Williams, D. J. (1999a). Fleming–tamao oxidation and masked hydroxyl functionality: total synthesis of (+)-pramanicin and structural elucidation of the antifungal natural product (−)-pramanicin. *J. Org. Chem.* 64, 6005–6018. doi: 10.1021/jo9905672

Barrett, A. G. M., Head, J., Smith, M. L., and Stock, N. S. (1999b). Total synthesis of (+)-pramanicin and stereochemical elucidation of the natural product. *Chem. Commun.* 1999, 133–134. doi: 10.1039/a807988l

Bode, H. B., Bethe, B., Hofs, R., and Zeeck, A. (2002). Big effects from small changes: possible ways to explore nature's chemical diversity. *Chembiochem* 3, 619–627. doi: 10.1002/1439-7633(20020703)3:7<619::AID-CBIC619>3.0.CO;2-9

Bohler, P., Stuhldreier, F., Anand, R., Kondadi, A. K., Schlütermann, D., Berleth, N., et al. (2018). The mycotoxin phomoxanthone A disturbs the form and function of the inner mitochondrial membrane. *Cell Death Dis.* 9:e286. doi: 10.1038/s41419-018-0312-8

Bremond, E., Savarese, M., Su, N. Q., Perez-Jimenez, A. J., Xu, X., Sancho-Garcia, J. C., et al. (2016). Benchmarking density functionals on structural parameters of small-/medium-sized organic molecules. *J. Chem. Theory. Comput.* 12, 459–465. doi: 10.1021/acs.jctc.5b01144

Chai, J. D., and Head-Gordon, M. (2008). Systematic optimization of long-range corrected hybrid density functionals. *J. Chem. Phys.* 128:084106. doi: 10.1063/1.2834918

Chen, H., and Harrison, P. H. M. (2004). Investigation of the origin of C2 units in biosynthesis of streptolydigin. *Org. Lett.* 6, 4033–4036. doi: 10.1021/ol048317h

Cow, C., Valentini, D., and Harrison, P. (1997). Synthesis of the fatty acid of pramanicin. *Can. J. Chem.* 75, 884–889. doi: 10.1139/v97-106

Daletos, G., Ebrahim, W., Ancheeva, E., El-Neketi, M., Lin, W. H., and Proksch, P. (2017). "Microbial co-culture and OSMAC approach as strategies to induce cryptic fungal biogenetic gene clusters," in *Chemical Biology of Natural Products*, eds D. J. Newman, G. M. Cragg, and P. G. Grothaus (Boca Raton FL: CRC Press), 233–284. doi: 10.1201/9781315117089-9

Darsih, C., Prachyawarakorn, V., Wiyakrutta, S., Mahidol, C., Ruchirawat, S., and Kittakoop, P. (2015). Cytotoxic metabolites from the endophytic fungus *Penicillium chermesinum*: discovery of a cysteine-targeted Michael acceptor as a pharmacophore for fragment-based drug discovery, bioconjugation and click reactions. *RSC Adv.* 5, 70595–70603. doi: 10.1039/C5RA13735G

Duspara, P., Jenkins, S. I., Hughes, D. W., and Harrison, P. H. M. (1998).). The biosynthesis of pramanicin: intact incorporation of serine and absolute configuration of the antibiotic. *Chem. Commun.* 1998, 2643–2644. doi: 10.1039/a807401a

Frank, M., Niemann, H., Bohler, P., Stork, B., Wesselborg, S., Lin, W., et al. (2015). Phomoxanthone A–from mangrove forests to anticancer therapy. *Curr. Med. Chem.* 22, 3523–3532. doi: 10.2174/0929867322666150716115300

Frisch, M. J., Trucks, G. W., Schlegel, H. B., Scuseria, G. E., Robb, M. A., Cheeseman, J. R., et al. (2013). *Gaussian 09, Revision E.01.* Wallingford, CT: Gaussian, Inc.

Gao, Y., Stuhldreier, F., Schmitt, L., Wesselborg, S., Wang, L., Müller, W. E. G., et al. (2020a). Sesterterpenes and macrolide derivatives from the endophytic fungus *Aplosporella javeedii*. *Fitoterapia* 146:104652. doi: 10.1016/j.fitote.2020.104652

Gao, Y., Wang, L., Kalscheuer, R., Liu, Z., and Proksch, P. (2020b). Antifungal polyketide derivatives from the endophytic fungus *Aplosporella javeedii*. *Bioorg. Med. Chem.* 28:115456. doi: 10.1016/j.bmc.2020.115456

Grimblat, N., Zanardi, M. M., and Sarotti, A. M. (2015). Beyond DP4: an improved probability for the stereochemical assignment of isomeric compounds using quantum chemical calculations of NMR shifts. *J. Org. Chem.* 80, 12526–12534. doi: 10.1021/acs.joc.5b02396

Hammerschmidt, L., Aly, A. H., Abdel-Aziz, M., Müller, W. E. G., Lin, W. H., Daletos, G., et al. (2015). Cytotoxic acyl amides from the soil fungus *Gymnascella dankaliensis*. *Bioorg. Med. Chem.* 23, 712–719. doi: 10.1016/j.bmc.2014.12.068

Harrison, P. H. M., Duspara, P. A., Jenkins, S. I., Kassam, S. A., Liscombe, D. K., and Hughes, D. W. (2000). The biosynthesis of pramanicin in *Stagonospora* sp. ATCC 74235: a modified acyltetramic acid. *J. Chem. Soc., Perkin Trans.* 2000, 4390–4402. doi: 10.1039/b006007k

Harrison, P. H. M., Hughes, D. W., and William, R. R. (1998). The biosynthesis of pramanicin: origin of the carbon skeleton. *Chem. Commun.* 1998, 273–274. doi: 10.1039/a706799b

Harwoko, H., Daletos, G., Stuhldreier, F., Lee, J., Wesselborg, S., Feldbrugge, M., et al. (2019). Dithiodiketopiperazine derivatives from endophytic fungi *Trichoderma harzianum* and *Epicoccum nigrum*. *Nat. Prod. Res.* 2019, 1–9. doi: 10.1080/14786419.2019.1627348

Huo, X., Liu, C., Gao, L., Xu, X., Zhu, N., and Cao, L. (2017). Hepatoprotective effect of aqueous extract from the seeds of *Orychophragmus violaceus* against liver injury in mice and HepG2 cells. *Int. J. Mol. Sci.* 18:1197. doi: 10.3390/ijms18061197

Ishii, T., Nonaka, K., Iwatsuki, M., Masuma, R., Ōmura, S., and Shiomi, K. (2012). Virgaricin produced by *Virgaria* sp. FKI-4860. *J. Antibiot.* 65, 139–141. doi: 10.1038/ja.2011.123

Ishii, T., Nonaka, K., Sugawara, A., Iwatsuki, M., Masuma, R., Hirose, T., et al. (2015). Cinatrins D and E, and virgaricin B, three novel compounds produced by a fungus, *Virgaria boninensis* FKI-4958. *J. Antibiot.* 68, 633–637. doi: 10.1038/ja.2015.45

Kicsák, M., Mándi, A., Varga, S., Herczeg, M., Batta, G., Bényei, A., et al. (2018). Tricyclanos: conformationally constrained nucleoside analogues with a new heterotricycle obtained from a d-ribofuranose unit. *Org. Biomol. Chem.* 16, 393–401. doi: 10.1039/c7ob02296d

Kjer, J., Debbab, A., Aly, A. H., and Proksch, P. (2010). Methods for isolation of marine-derived endophytic fungi and their bioactive secondary products. *Nat. Protoc.* 5, 479–490. doi: 10.1038/nprot.2009.233

Li, W. S., Yan, R. J., Yu, Y., Shi, Z., Mándi, A., Shen, L., et al. (2020). Determination of the absolute configuration of super-carbon-chain compounds by a combined chemical, spectroscopic, and computational approach: gibbosols A and B. *Angew. Chem., Int. Ed. Engl.* 59, 13028–13036. doi: 10.1002/anie.202004358

Liu, Y., Stuhldreier, F., Kurtán, T., Mándi, A., Arumugam, S., Lin, W. H., et al. (2017). Daldinone derivatives from the mangrove-derived endophytic fungus *Annulohypoxylon* sp. *RSC Adv.* 7, 5381–5393. doi: 10.1039/c6ra27306h

Lodewyk, M. W., Siebert, M. R., and Tantillo, D. J. (2012). Computational prediction of 1H and 13C chemical shifts: a useful tool for natural product, mechanistic, and synthetic organic chemistry. *Chem. Rev.* 112, 1839–1862. doi: 10.1021/cr200106v

MacroModel (2015). *SchrödingerLLC.* Available online at: https://www.schrodinger.com/MacroModel (accessed June 18, 2020).

Mándi, A., and Kurtán, T. (2019). Applications of OR/ECD/VCD to the structure elucidation of natural products. *Nat. Prod. Rep.* 36, 889–918. doi: 10.1039/c9np00002j

Mándi, A., Mudianta, I. W., Kurtán, T., and Garson, M. J. (2015). Absolute configuration and conformational study of psammaplysins A and B from the balinese marine sponge *Aplysinella strongylata*. *J. Nat. Prod.* 78, 2051–2056. doi: 10.1021/acs.jnatprod.5b00369

Manns, J., Daubrawa, M., Driessen, S., Paasch, F., Hoffmann, N., Loffler, A., et al. (2011). Triggering of a novel intrinsic apoptosis pathway by the kinase inhibitor staurosporine: activation of caspase-9 in the absence of Apaf-1. *FASEB J.* 25, 3250–3261. doi: 10.1096/fj.10-177527

Medicinal Plant Images Database (2007). *School of Chinese Medicine.* Hong Kong: Baptist University.

Pan, R., Bai, X., Chen, J., Zhang, H., and Wang, H. (2019). Exploring structural diversity of microbe secondary metabolites using OSMAC strategy: a literature review. *Front. Microbiol.* 10:294. doi: 10.3389/fmicb.2019.00294

Pierens, G. K. (2014). 1H and 13C NMR scaling factors for the calculation of chemical shifts in commonly used solvents using density functional theory. *J. Comput. Chem.* 35, 1388–1394. doi: 10.1002/jcc.23638

Polavarapu, P. L. (2002). Optical rotation: recent advances in determining the absolute configuration. *Chirality* 14, 768–781. doi: 10.1002/chir.10145

Rehberg, N., Akone, H. S., Ioerger, T. R., Erlenkamp, G., Daletos, G., Gohlke, H., et al. (2018). Chlorflavonin targets acetohydroxyacid synthase catalytic subunit IlvB1 for synergistic killing of *Mycobacterium tuberculosis. ACS Infect. Dis.* 4, 123–134. doi: 10.1021/acsinfecdis.7b00055

Schwartz, R. E., Helms, G. L., Bolessa, E. A., Wilson, K. E., Giacobbe, R. A., Tkacz, J. S., et al. (1994). Pramanicin, a novel antimicrobial agent from a fungal fermentation. *Tetrahedron* 50, 1675–1686. doi: 10.1016/s0040-4020(01)80843-7

Smith, S. G., and Goodman, J. M. (2010). Assigning stereochemistry to single diastereoisomers by GIAO NMR calculation: the DP4 probability. *J. Am. Chem. Soc.* 132, 12946–12959. doi: 10.1021/ja105035r

Stephens, P. J., and Harada, N. (2010). ECD cotton effect approximated by the Gaussian curve and other methods. *Chirality* 22, 229–233. doi: 10.1002/chir.20733

Tan, S. W. B., Chai, C. L. L., and Moloney, M. G. (2014). Synthesis of 3-acyltetramates by side chain manipulation and their antibacterial activity. *Org. Biomol. Chem.* 12, 1711–1716. doi: 10.1039/c4ob00095a

Tan, S. W. B., Chai, C. L. L., and Moloney, M. G. (2017). Mimics of pramanicin derived from pyroglutamic acid and their antibacterial activity. *Org. Biomol. Chem.* 15, 1889–1912. doi: 10.1039/c6ob02828d

Tan, S. W. B., Chai, C. L. L., Moloney, M. G., and Thompson, A. L. (2015). Synthesis of mimics of pramanicin from pyroglutamic acid and their antibacterial activity. *J. Org. Chem.* 80, 2661–2675. doi: 10.1021/jo502810b

Tran-Cong, N. M., Mándi, A., Kurtán, T., Müller, W. E. G., Kalscheuer, R., Lin, W. H., et al. (2019). Induction of cryptic metabolites of the endophytic fungus *Trichocladium* sp. through OSMAC and co-cultivation. *RSC Adv.* 9, 27279–27288. doi: 10.1039/c9ra05469c

Varetto, U. (2009). *MOLEKEL, v. 5.4.* Manno: Swiss National Supercomputing Centre.

Wang, H., Dai, H., Heering, C., Janiak, C., Lin, W., Orfali, R. S., et al. (2016). Targeted solid phase fermentation of the soil dwelling fungus *Gymnascella dankaliensis* yields new brominated tyrosine-derived alkaloids. *RSC Adv.* 6, 81685–81693. doi: 10.1039/c6ra14554j

Wang, H., Eze, P. M., Höfert, S. P., Janiak, C., Hartmann, R., Okoye, F. B. C., et al. (2018). Substituted l-tryptophan-l-phenyllactic acid conjugates produced by an endophytic fungus *Aspergillus aculeatus* using an OSMAC approach. *RSC Adv.* 8, 7863–7872. doi: 10.1039/c8ra00200b

Supplementary Material

Induction of New Lactam Derivatives from the Endophytic Fungus *Aplosporella javeedii* through an OSMAC Approach

Ying Gao,[1] Fabian Stuhldreier,[2] Laura Schmitt,[2] Sebastian Wesselborg,[2] Zhiyong Guo,[3] Kun Zou,[3] Attila Mándi,[4] Tibor Kurtán,[4] Zhen Liu,[1],* and Peter Proksch [1,3],*

[1]*Institute of Pharmaceutical Biology and Biotechnology, Heinrich Heine University Düsseldorf, Düsseldorf, Germany.*

[2]*Institute of Molecular Medicine I, Medical Faculty, Heinrich Heine University Düsseldorf, Düsseldorf, Germany.*

[3]*Hubei Key Laboratory of Natural Products Research and Development, College of Biological and Pharmaceutical Sciences, China Three Gorges University, Yichang, China.*

[4]*Department of Organic Chemistry, University of Debrecen, Debrecen, Hungary.*

***Correspondence:**

Zhen Liu

zhenfeizi0@sina.com

Peter Proksch

proksch@uni-duesseldorf.de

1

Table of Contents

3

4

5

Figure S1. HPLC chromatogram of compound **2**

UV absorption of compound **2**

Figure S2. ^{1}H NMR (600M Hz, DMSO-d_6) spectrum of compound **2**

6
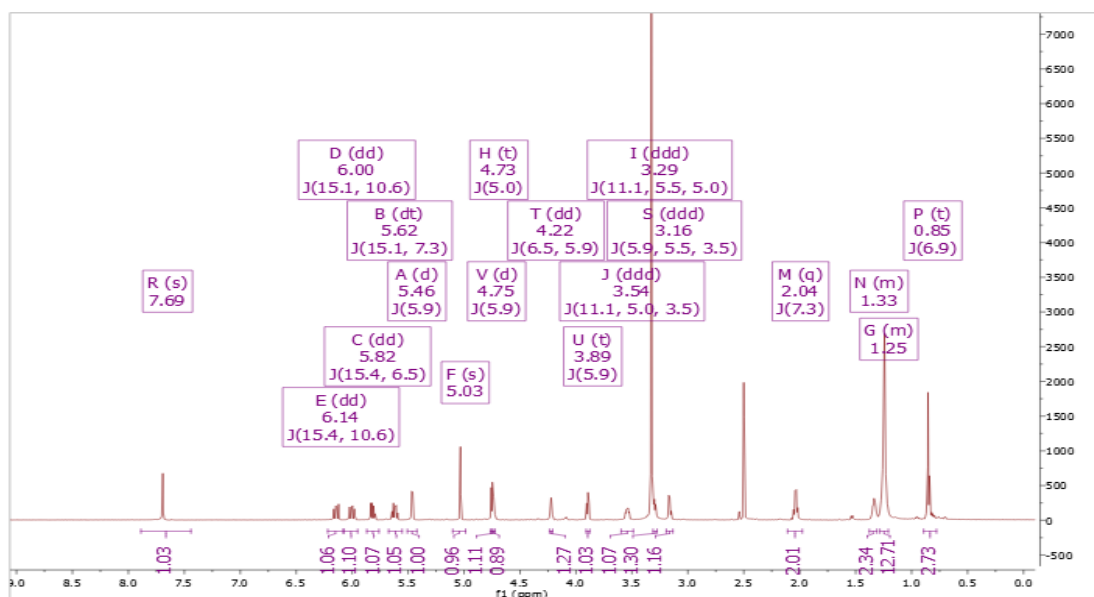
Figure S3. ^{13}C NMR (150M Hz, DMSO-d_6) spectrum of compound **2**
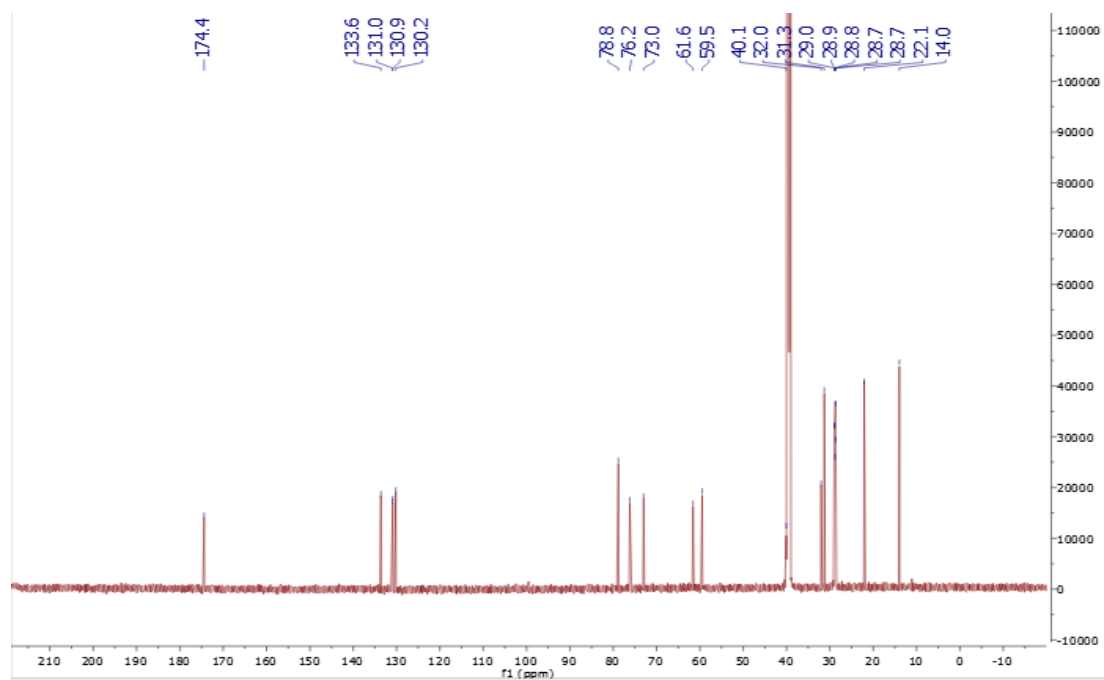
Figure S4. HSQC (DMSO-d_6) spectrum of compound **2**

7
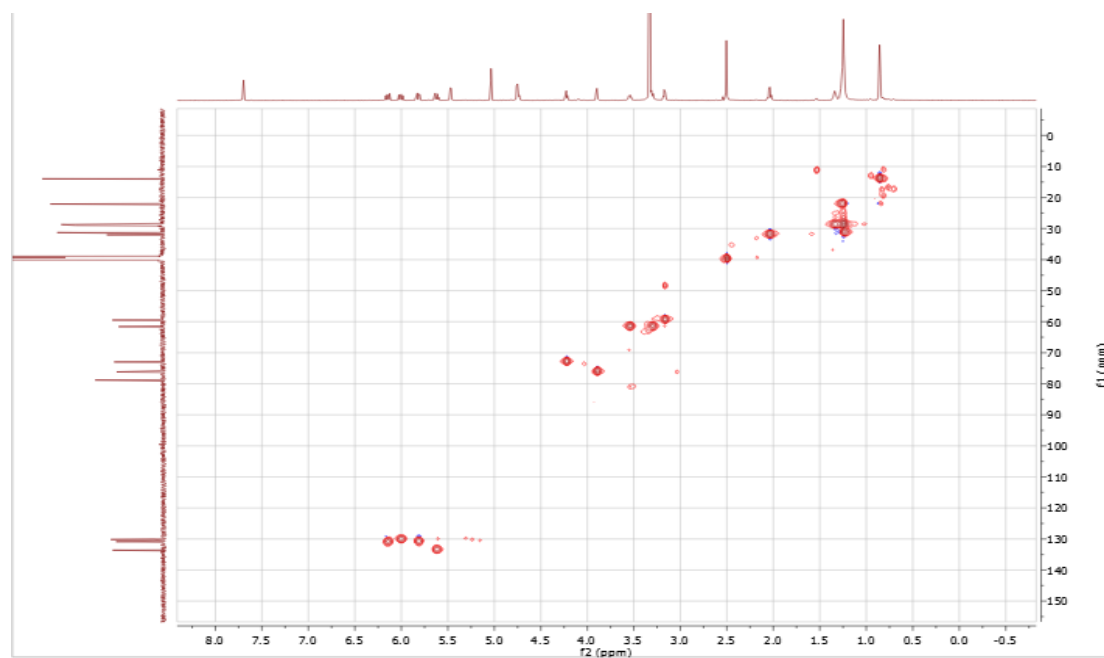
**Figure S5.** COSY (DMSO-d_6) spectrum of compound **2**
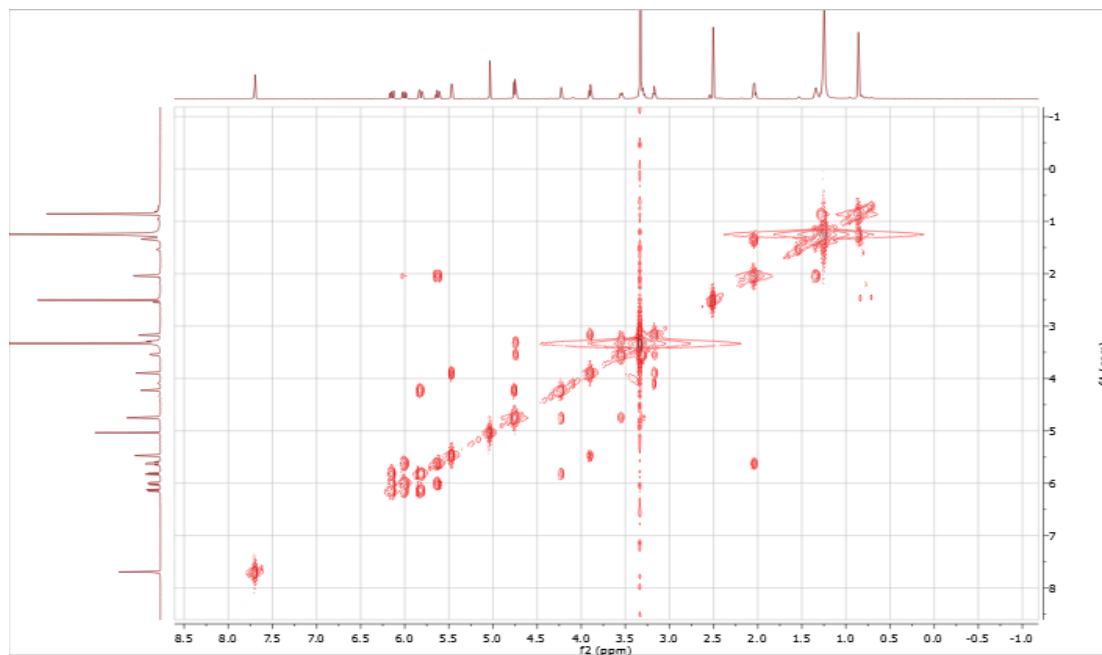
Figure S6. HMBC (DMSO-d_6) spectrum of compound **2**

8
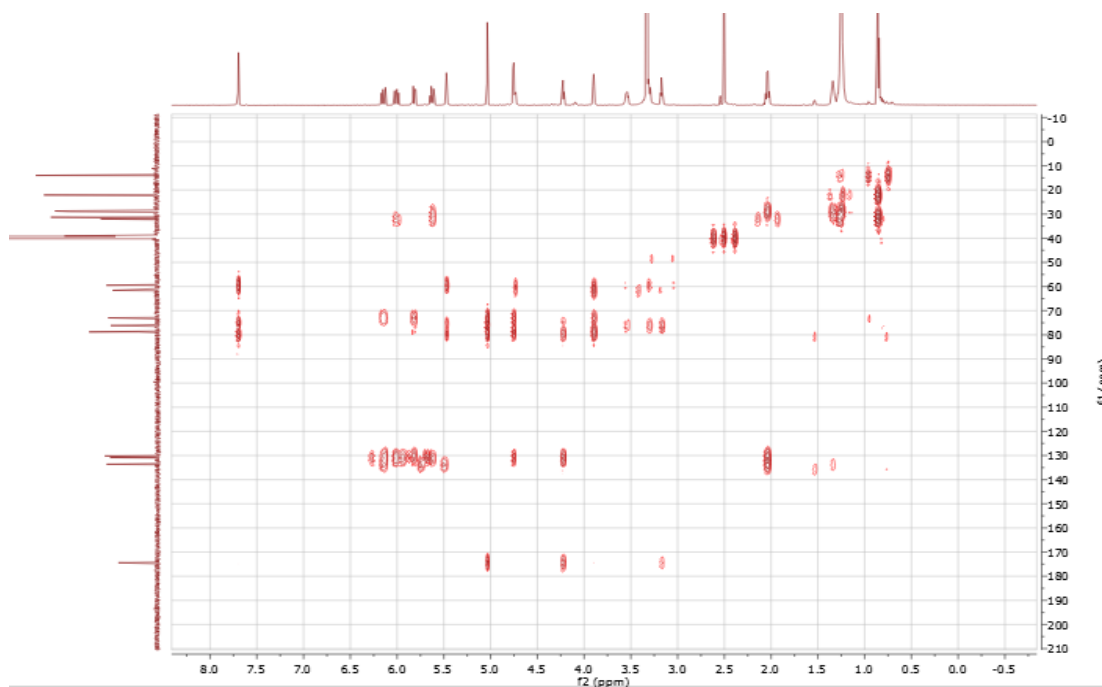
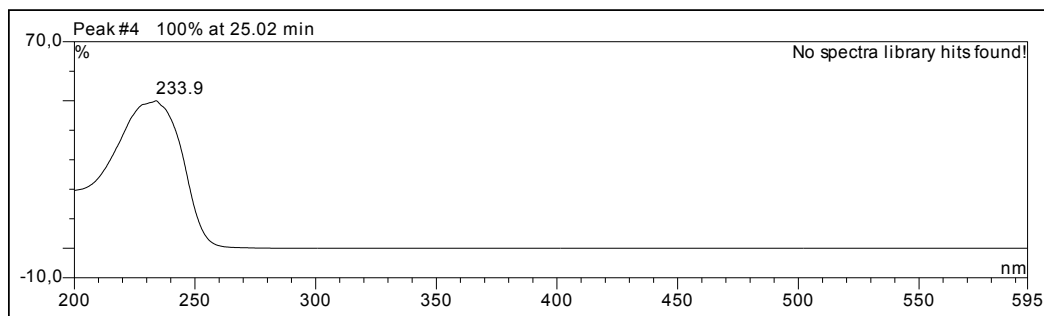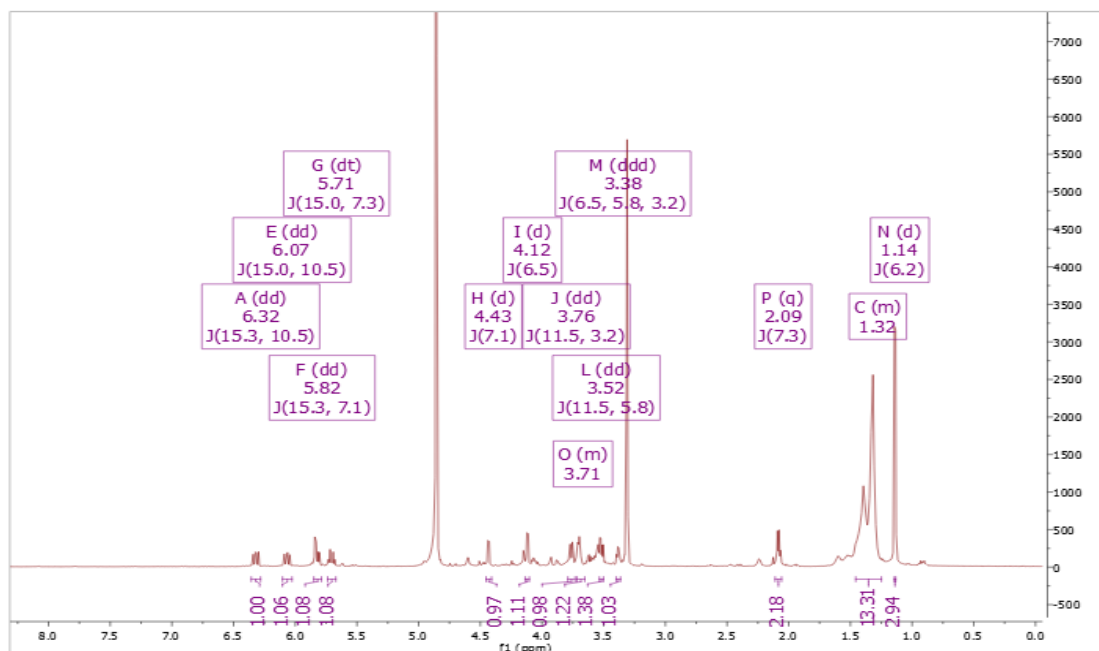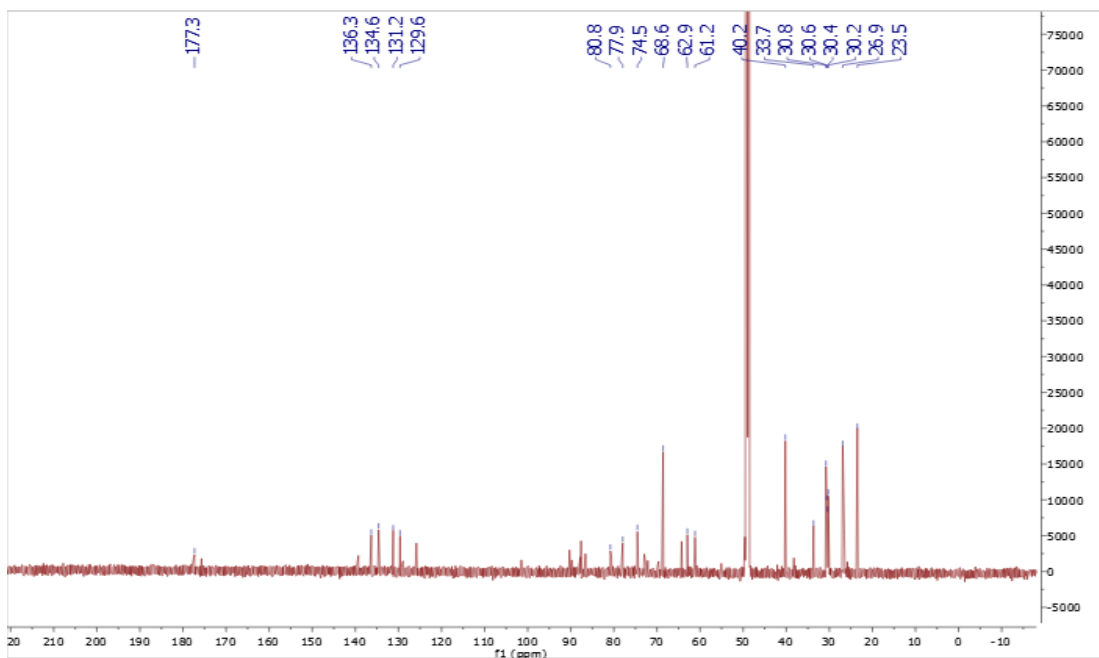**Figure S7.** ROESY (DMSO-d_6) spectrum of compound **2**
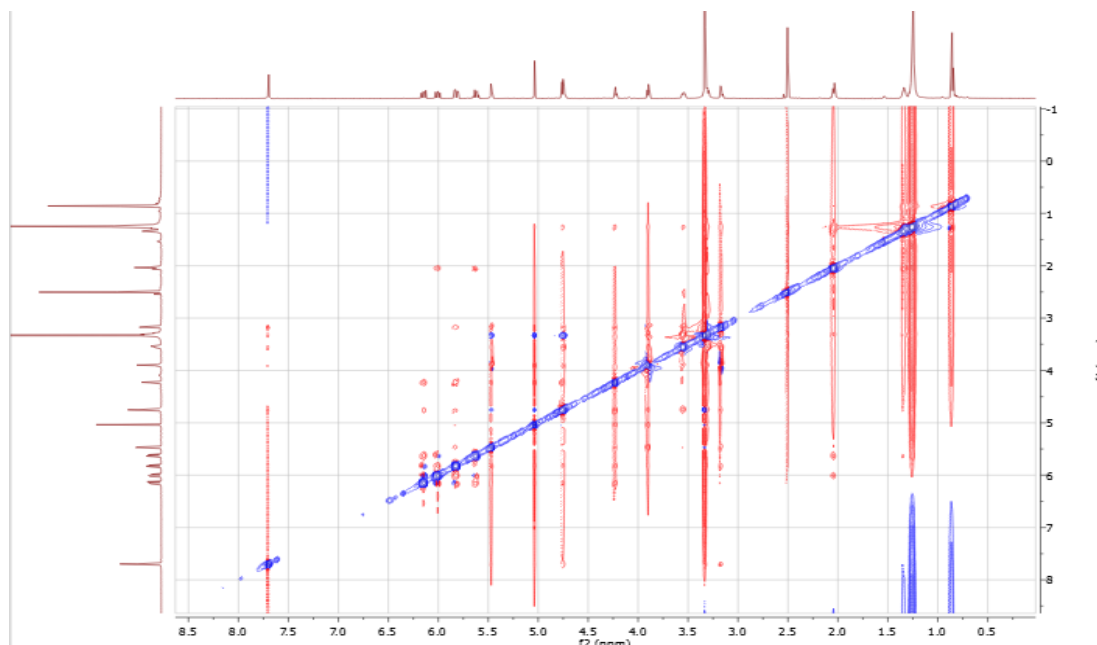
Figure S8. ^{1}H NMR (600M Hz, methanol-d_4) spectrum of compound **2**

9
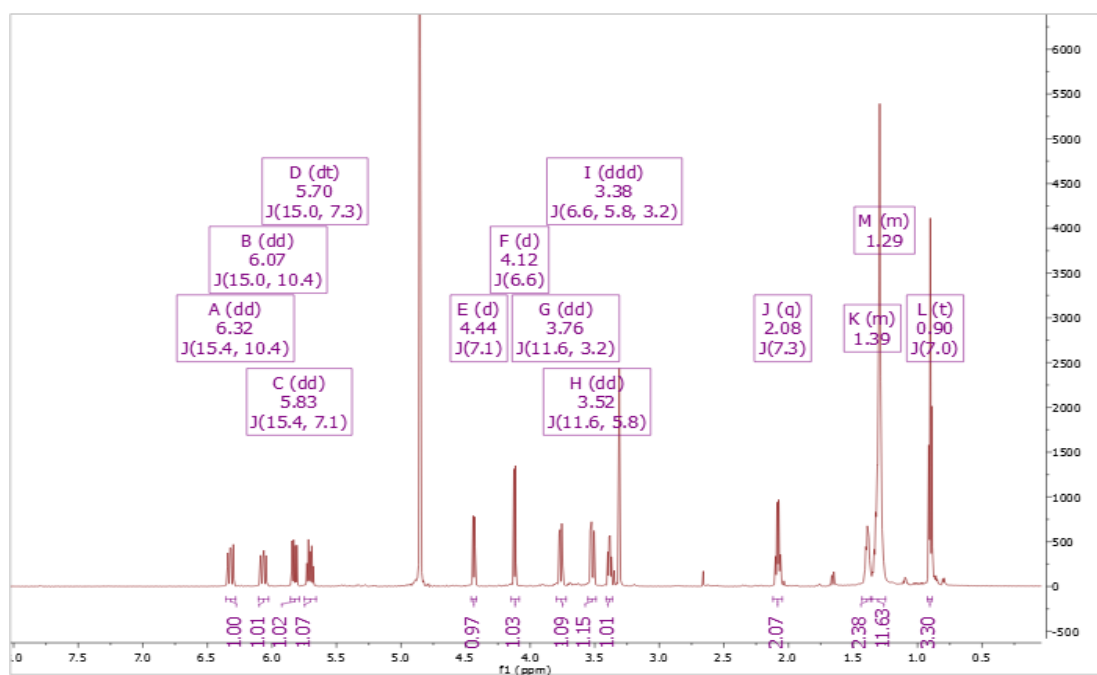
Figure S9. ^{13}C NMR (150M Hz, methanol-d_4) spectrum of compound **2**
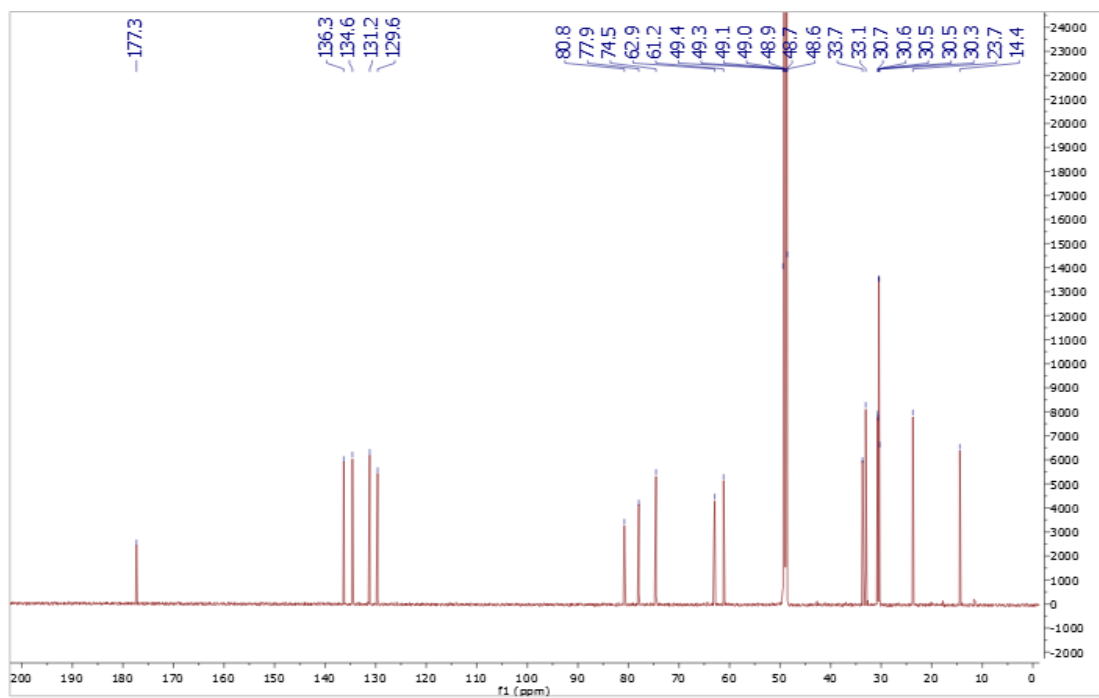
Figure S10. HSQC (methanol-d_4) spectrum of compound **2**

10
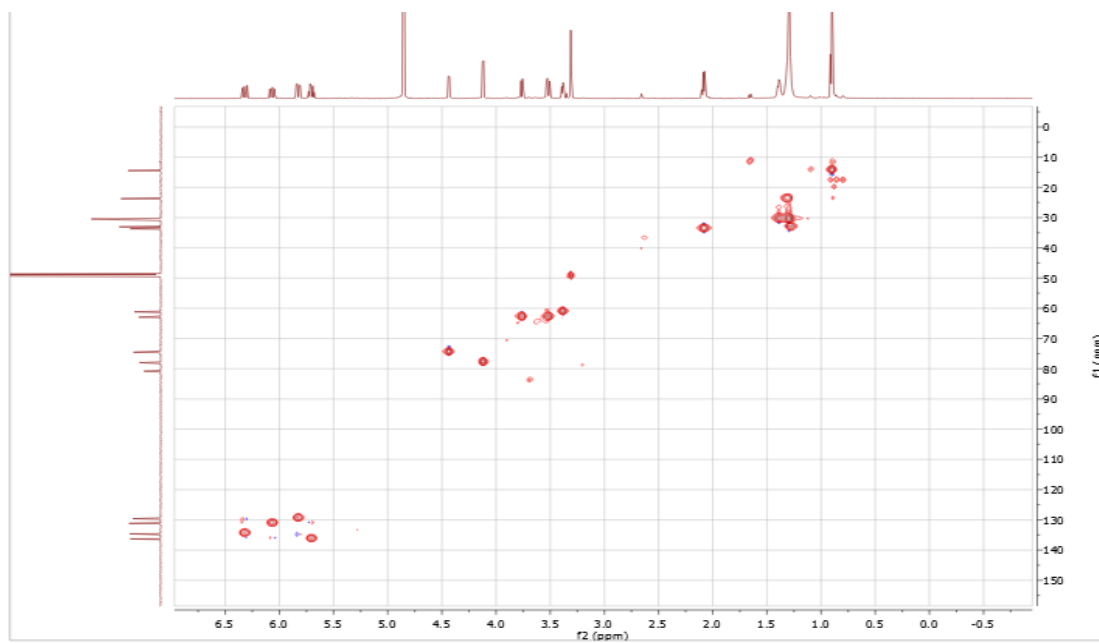
Figure S11. COSY (methanol-d_4) spectrum of compound **2**
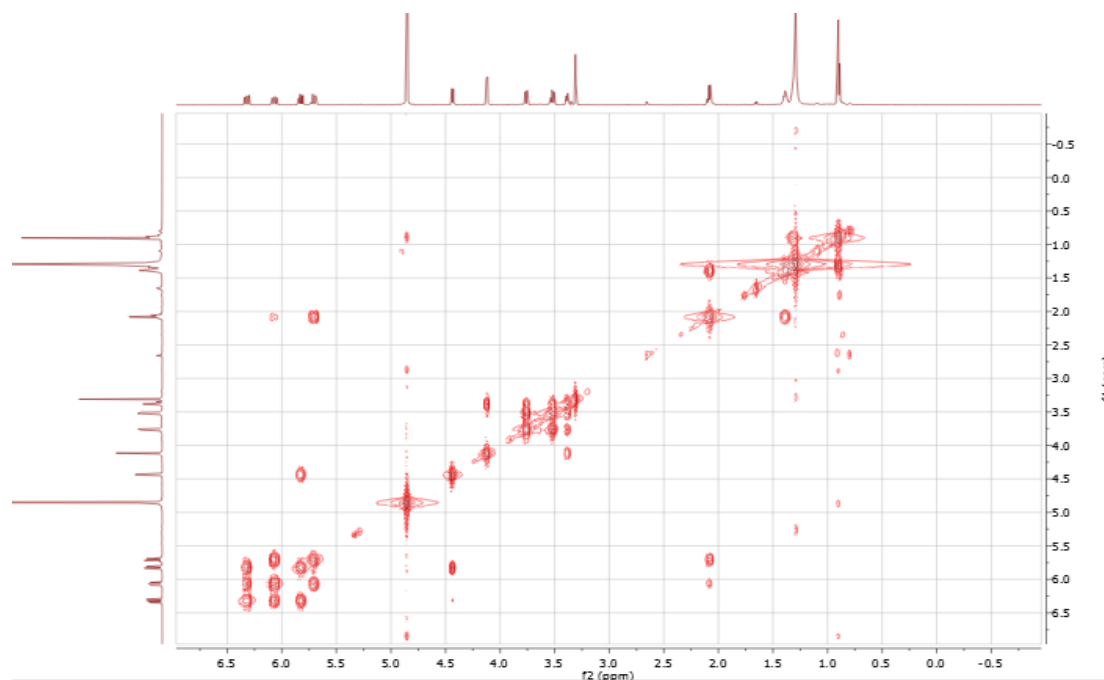
Figure S12. HMBC (methanol-d_4) spectrum of compound **2**

11
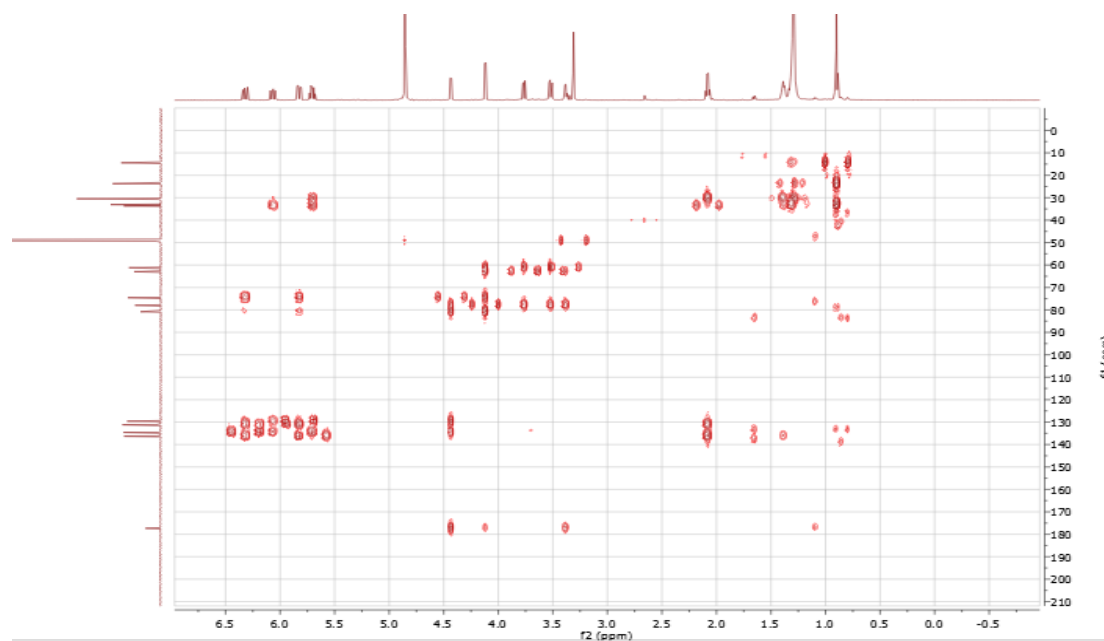
Figure S13. HRESIMS of compound **2**
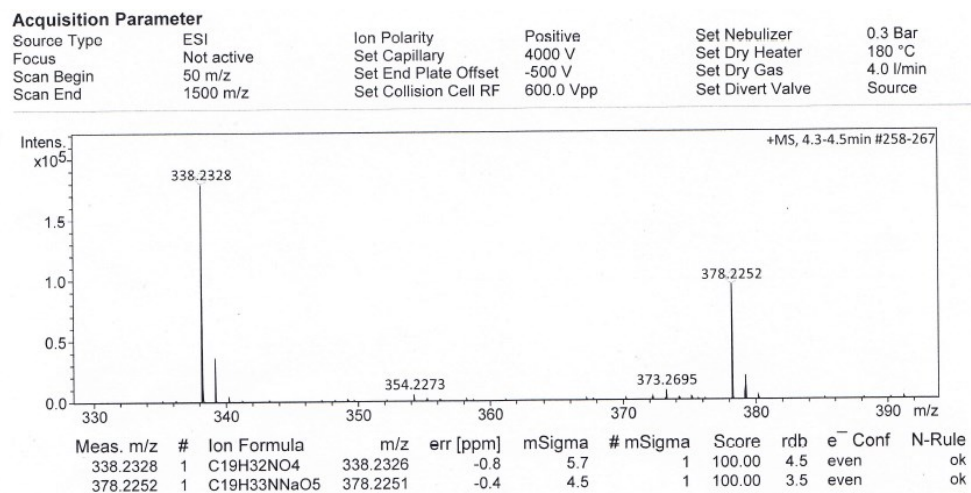
Figure S14. HPLC chromatogram of compound **3**

UV absorption of compound **3**

12
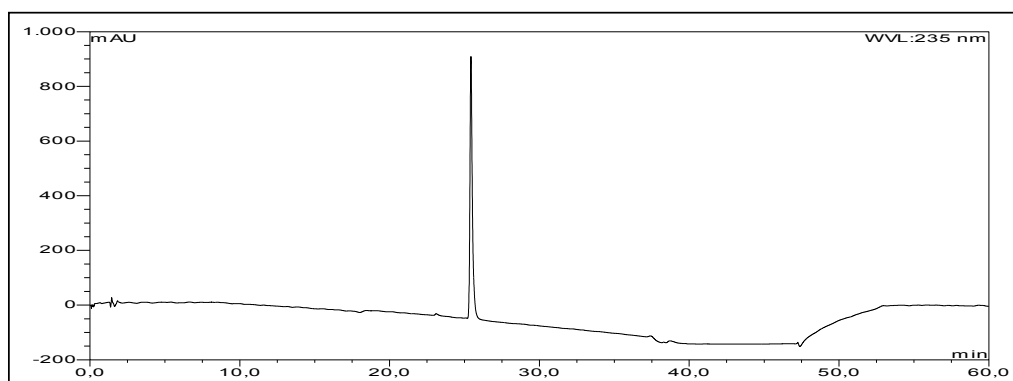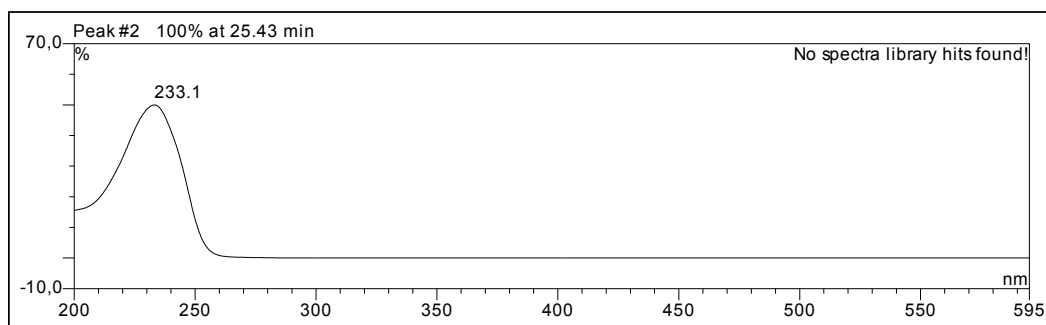
Figure S15. ^{1}H NMR (600M Hz, methanol-d_4) spectrum of compound **3**
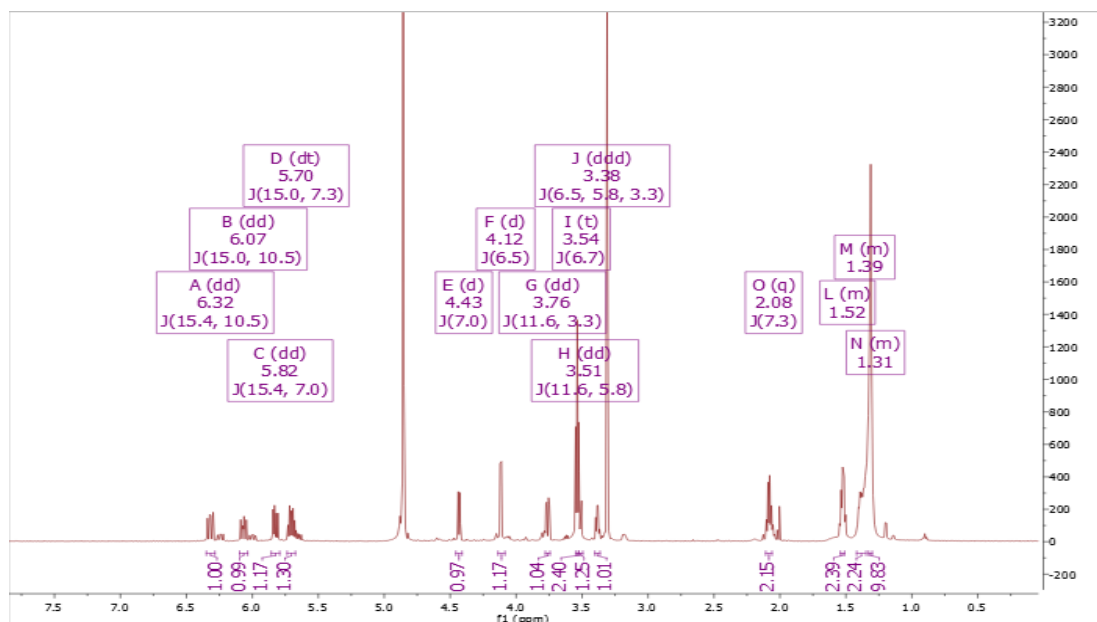
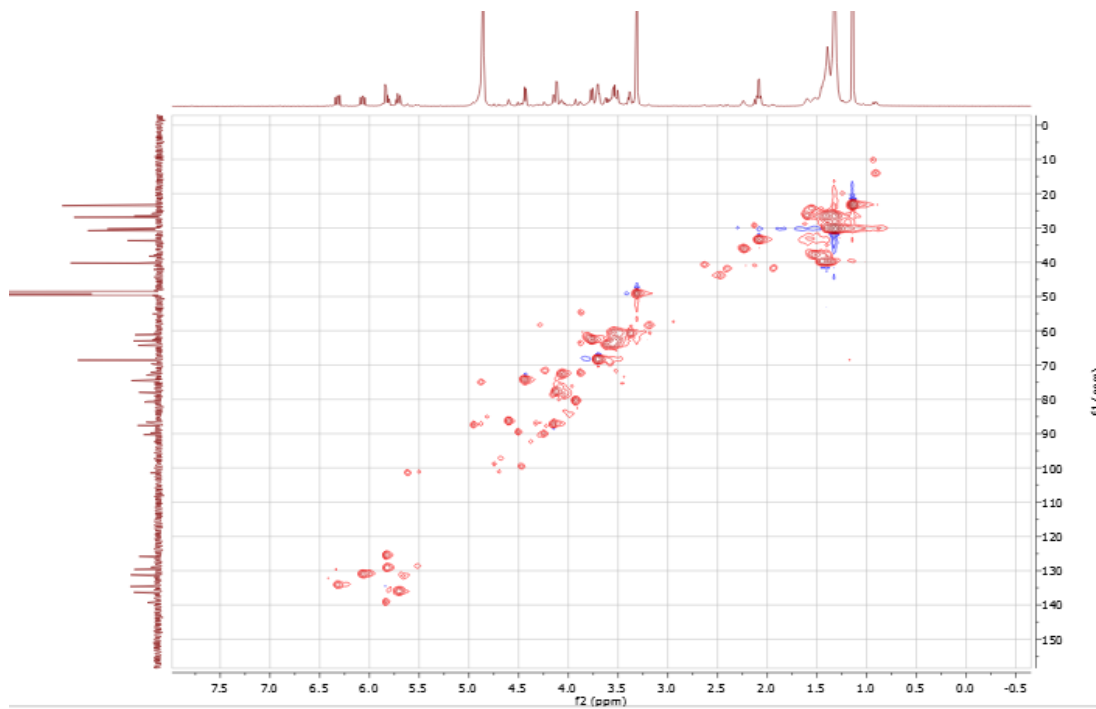**Figure S16.** ^{13}C NMR (150M Hz, methanol-d_4) spectrum of compound **3**

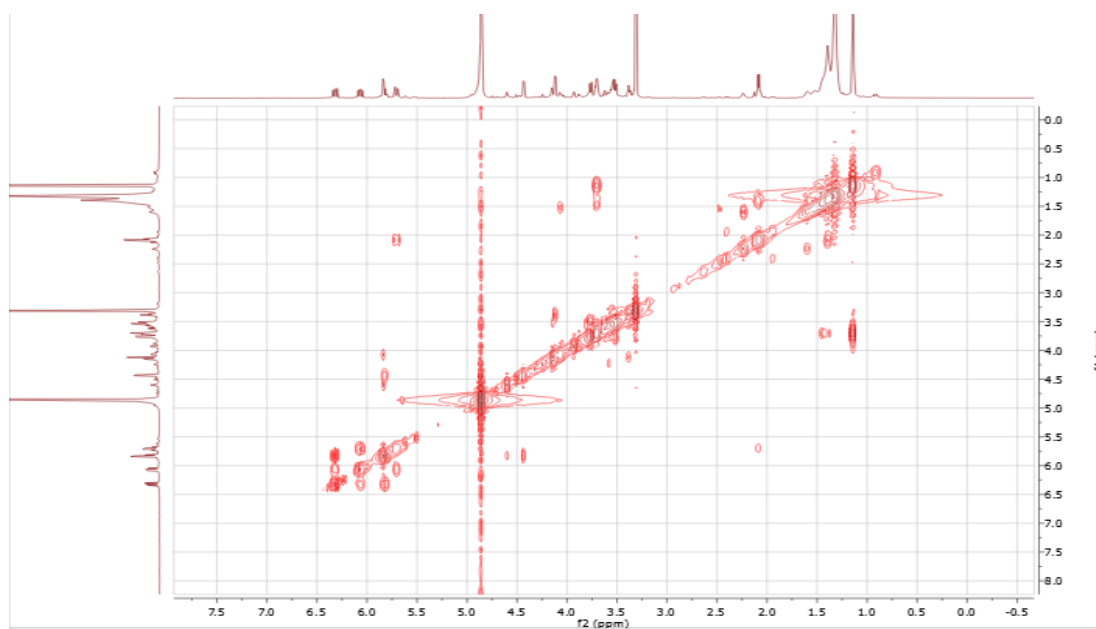13
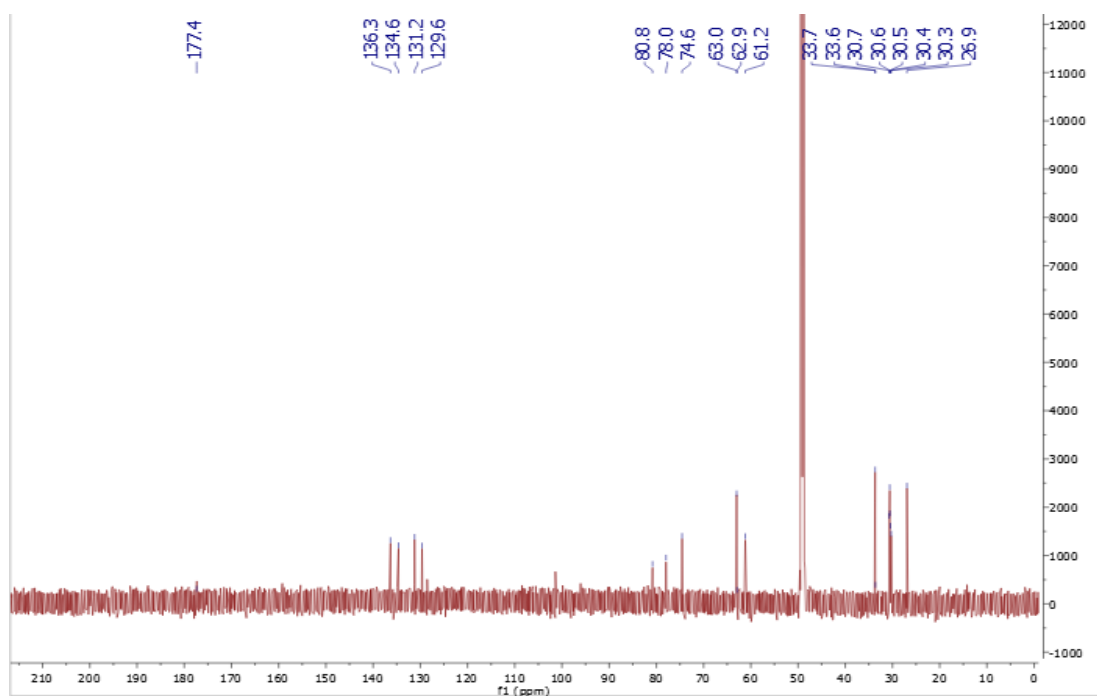
Figure S17. HSQC (methanol-d_4) spectrum of compound **3**
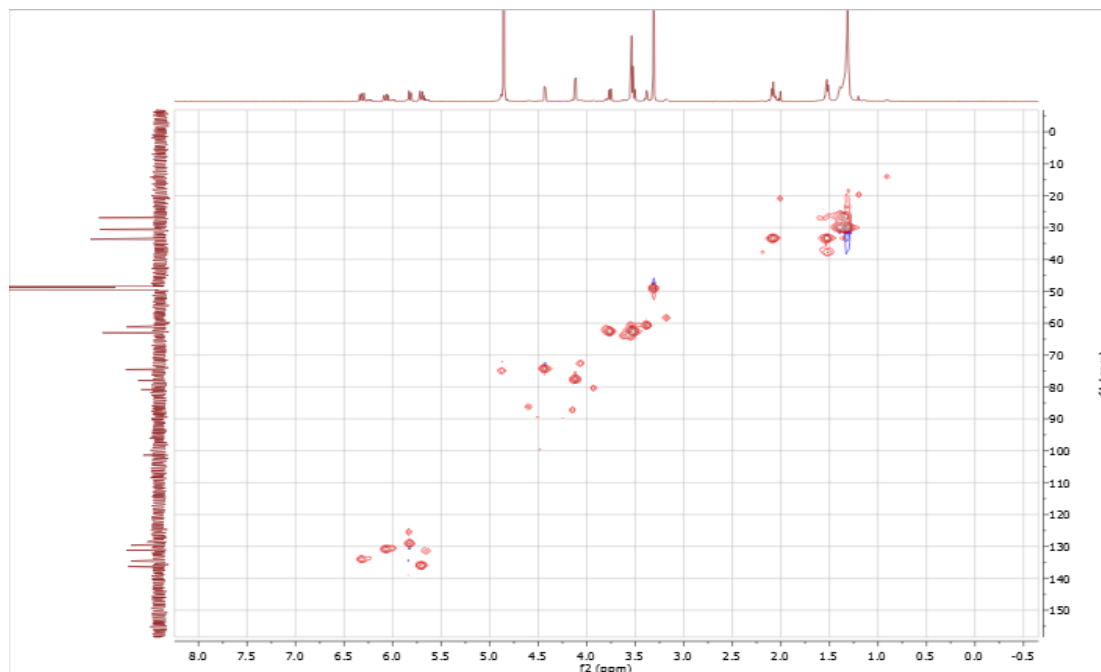
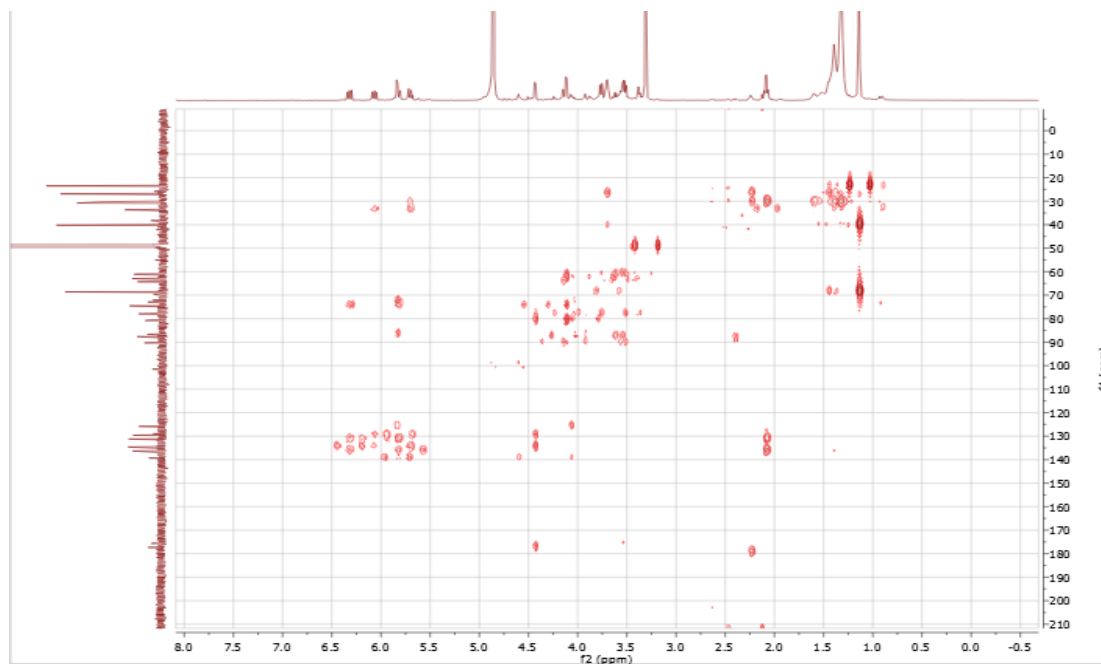**Figure S18.** COSY (methanol-d_4) spectrum of compound **3**

14
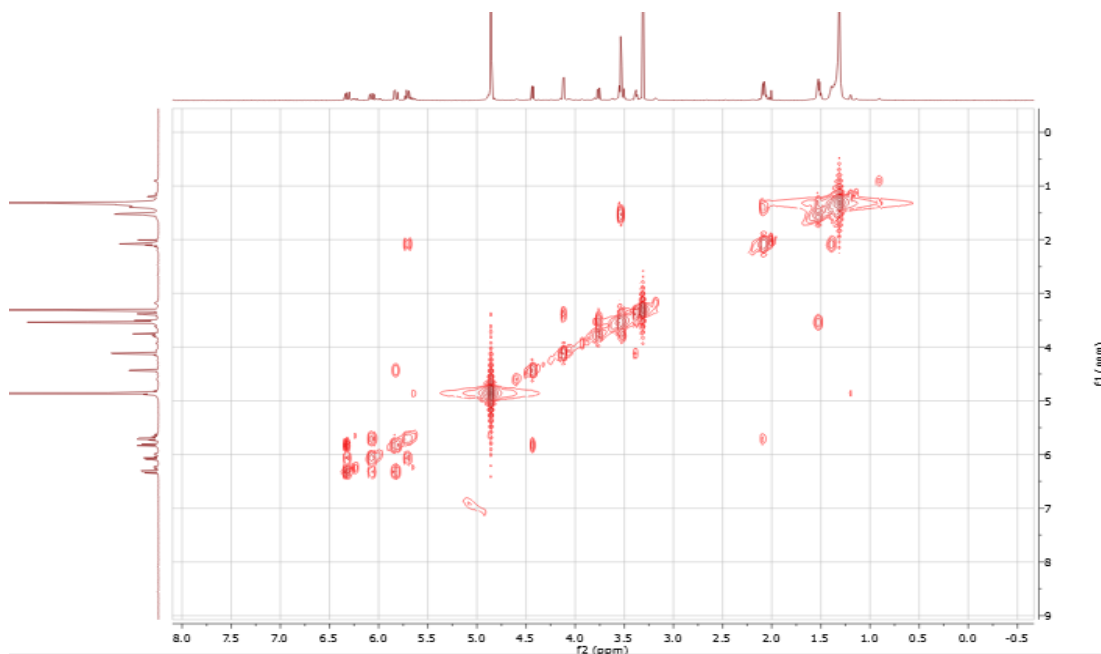
Figure S19. HMBC (methanol-d_4) spectrum of compound **3**
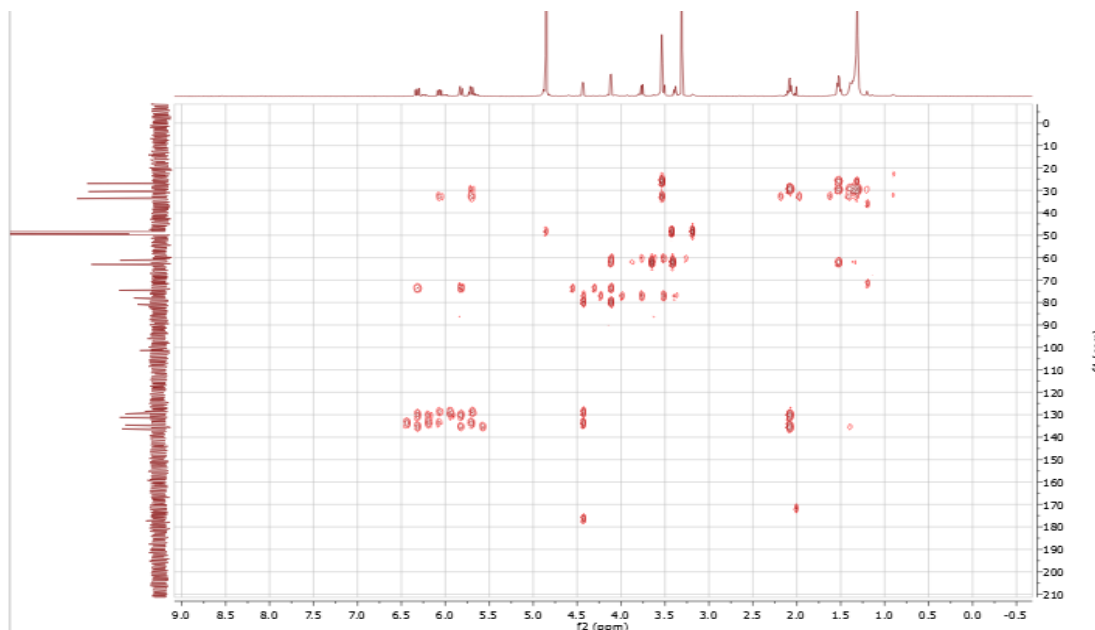
Figure S20. ROESY (methanol-d_4) spectrum of compound **3**

15
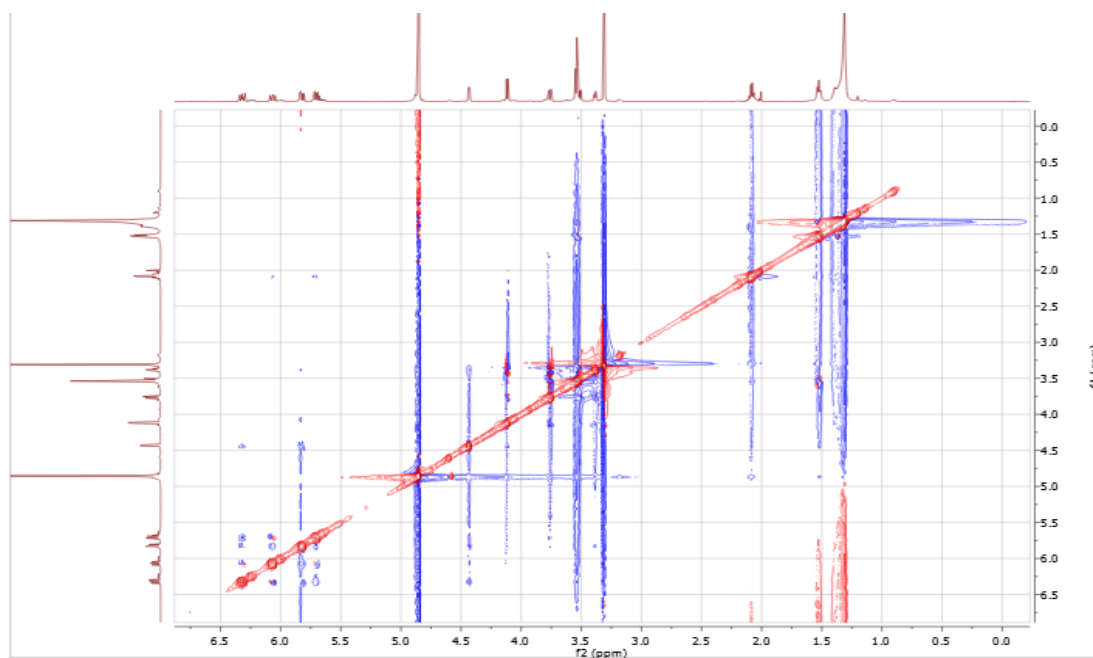
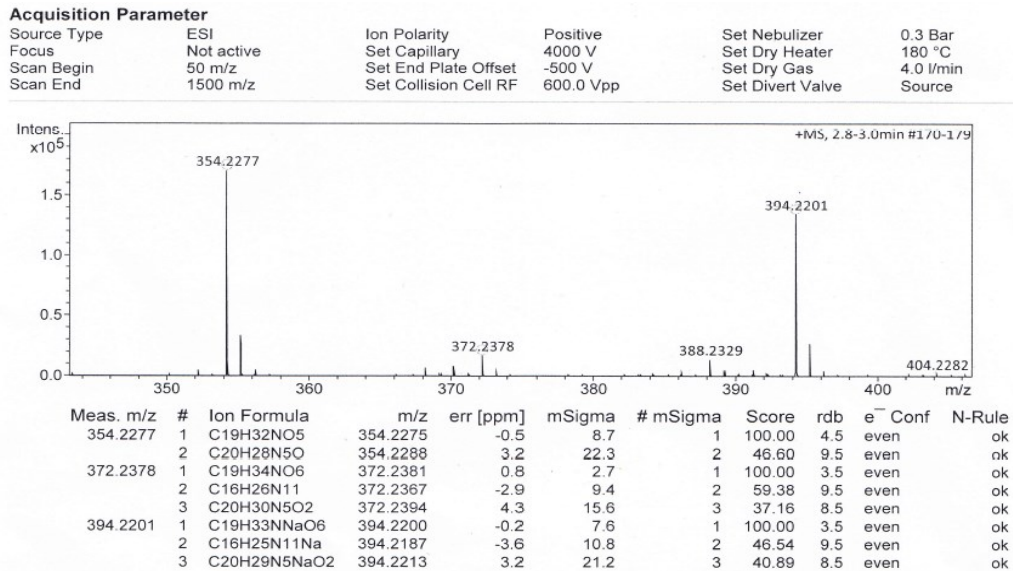**Figure S21.** HRESIMS of compound **3**
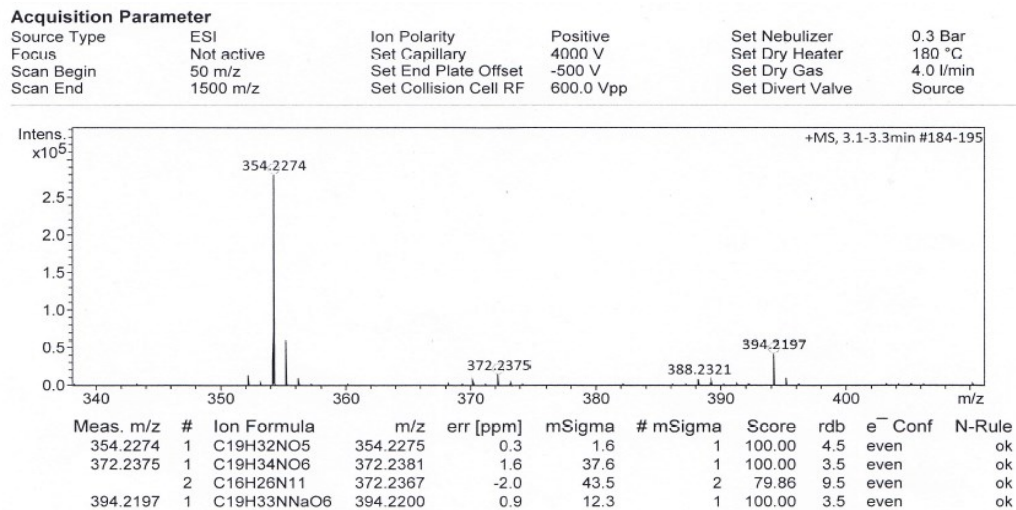
Figure S22. HPLC chromatogram of compound **4**

UV absorption of compound **4**

16
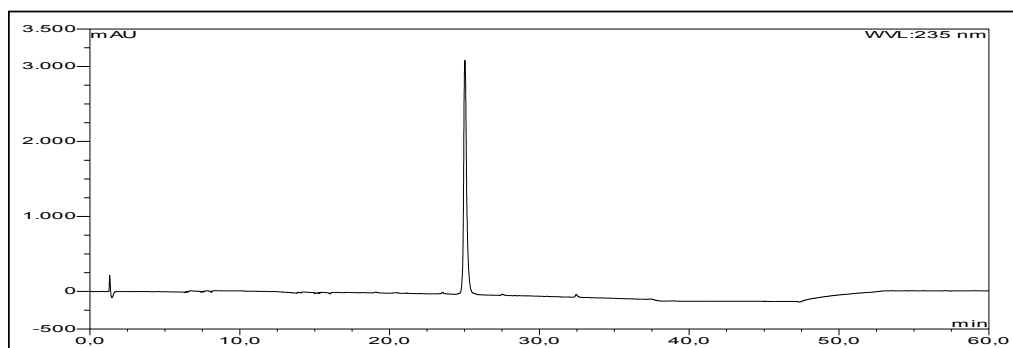
Figure S23. ^{1}H NMR (600M Hz, methanol-d_4) spectrum of compound **4**

Figure S24. ^{13}C NMR (150M Hz, methanol-d_4) spectrum of compound **4**

17

Figure S25. HSQC (methanol-d_4) spectrum of compound **4**

Figure S26. COSY (methanol-d_4) spectrum of compound **4**

18

Figure S27. HMBC (methanol-d_4) spectrum of compound **4**

Figure S28. ROESY (methanol-d_4) spectrum of compound **4**

19
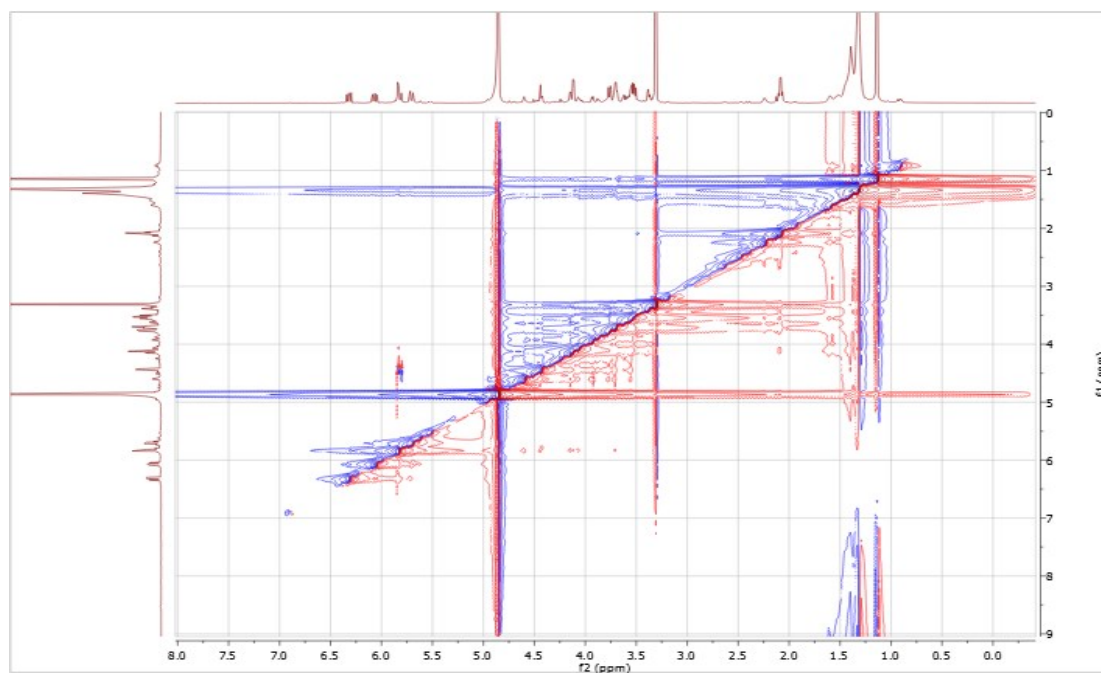
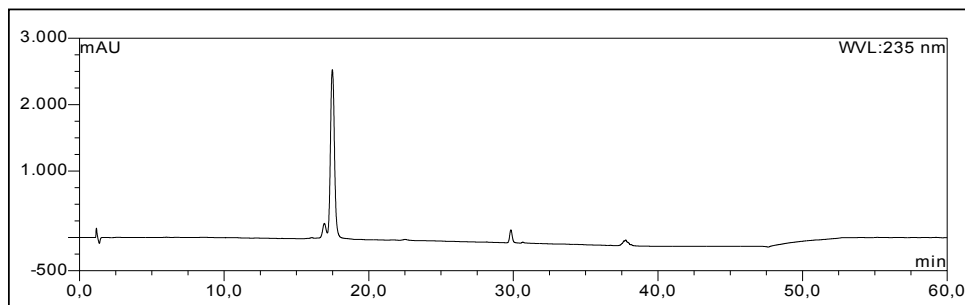**Figure S29.** HRESIMS of compound **4**

Figure S30. HPLC chromatogram of compound **5**
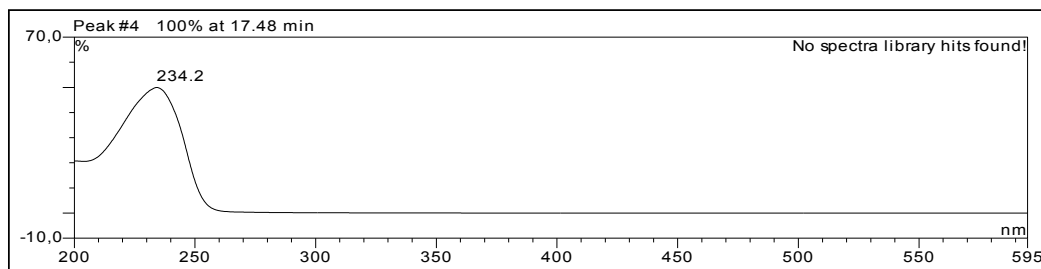

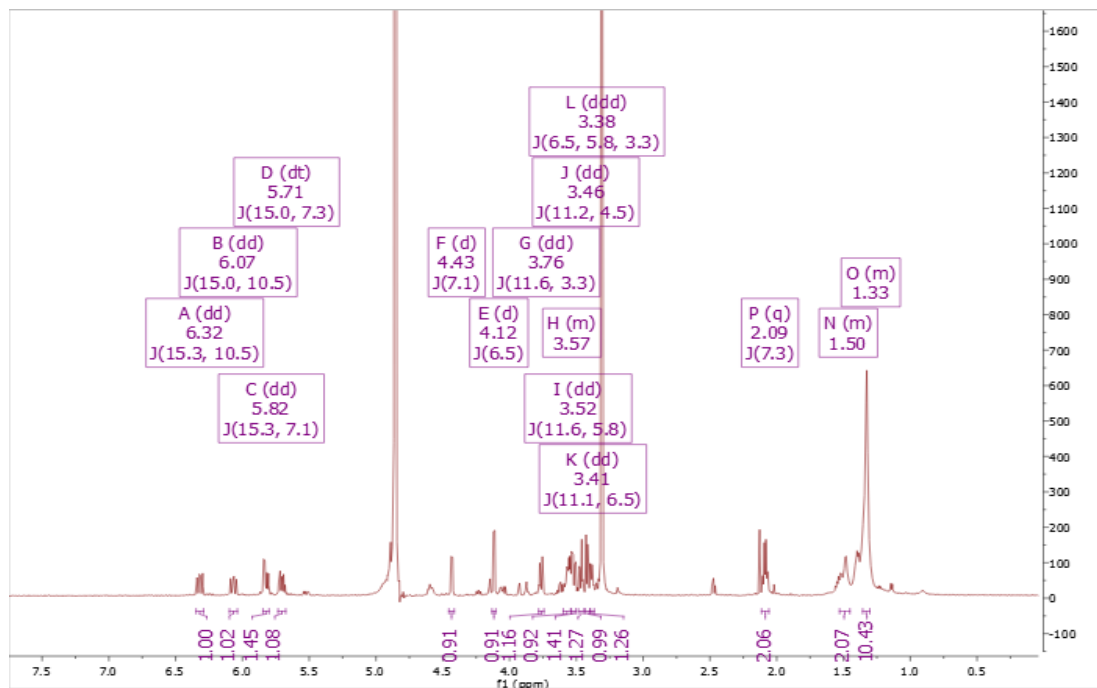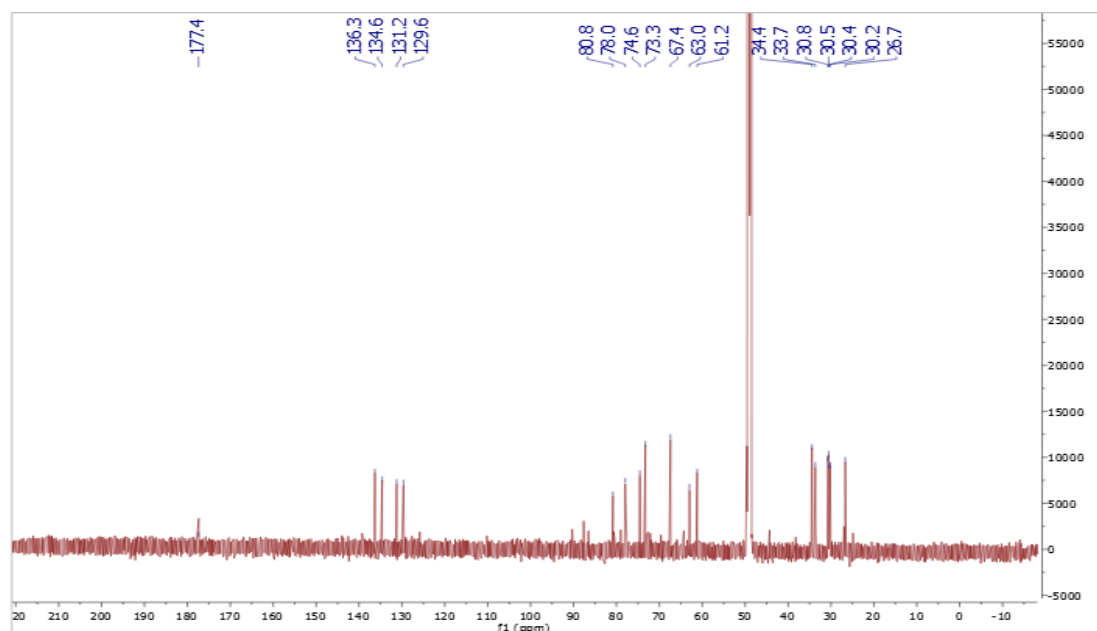UV absorption of compound **5**

20

Figure S31. ^{1}H NMR (600M Hz, methanol-d_4) spectrum of compound **5**

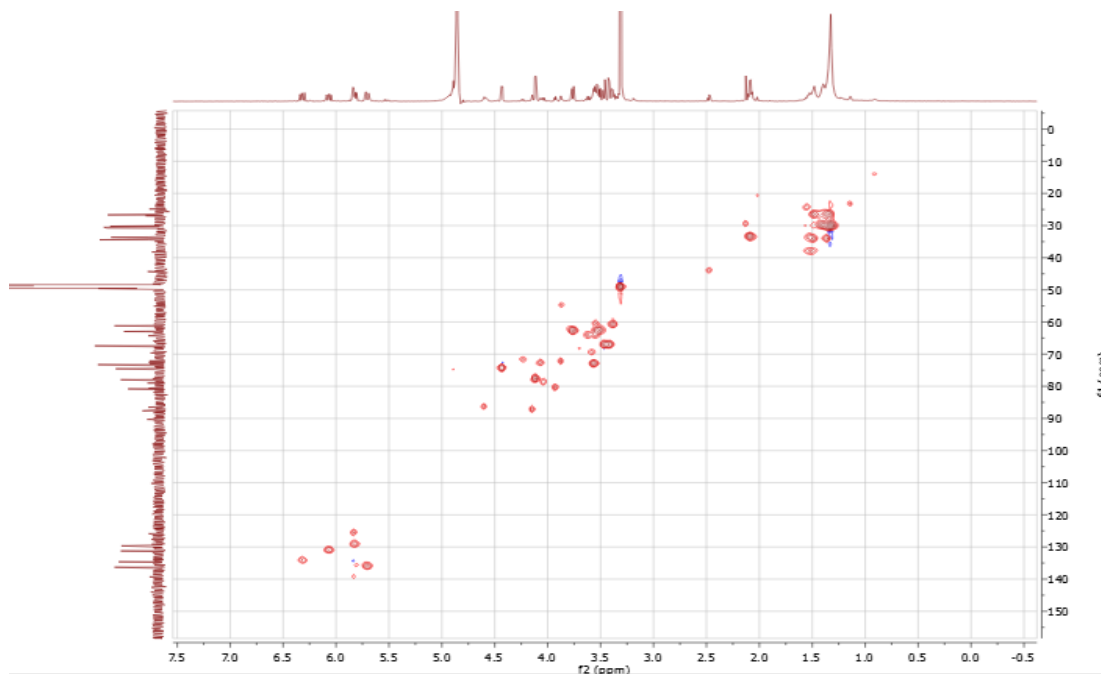**Figure S32.** ^{13}C NMR (150M Hz, methanol-d_4) spectrum of compound **5**
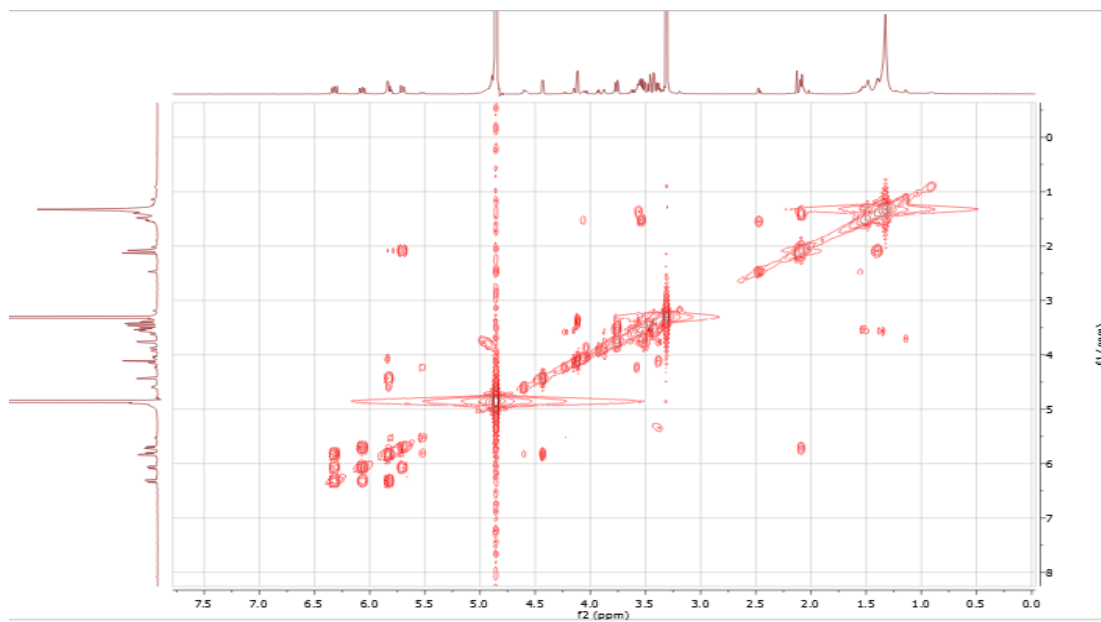

21

Figure S33. HSQC (methanol-*d*₄) spectrum of compound **5**

Figure S34. COSY (methanol-*d*₄) spectrum of compound **5**

22

Figure S35. HMBC (methanol-d_4) spectrum of compound **5**

Figure S36. ROESY (methanol-d_4) spectrum of compound **5**

23

Figure S37. HRESIMS of compound **5**

Figure S38. HPLC chromatogram of compound **6**

UV absorption of compound **6**

Figure S39. ^{1}H NMR (600M Hz, methanol-d_4) spectrum of compound **6**

Figure S40. ^{13}C NMR (150M Hz, methanol-d_4) spectrum of compound **6**

Figure S41. HSQC (methanol-d_4) spectrum of compound **6**

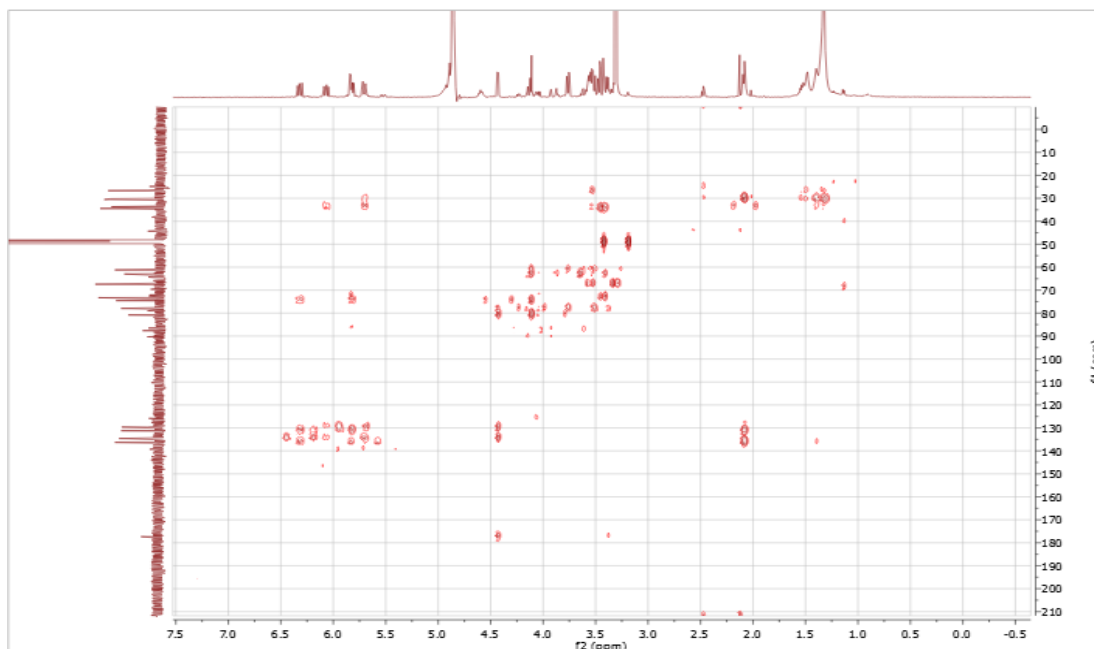**Figure S42.** COSY (methanol-d_4) spectrum of compound **6**
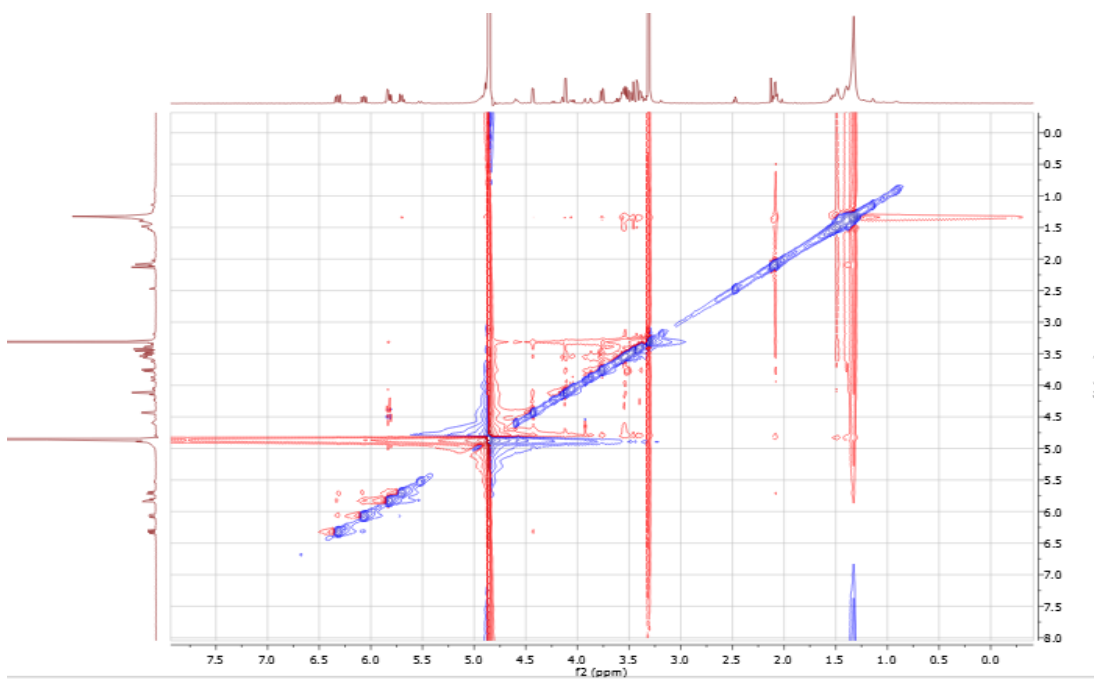

26

Figure S43. HMBC (methanol-d_4) spectrum of compound **6**

Figure S44. ROESY (methanol-d_4) spectrum of compound **6**

27

Figure S45. HRESIMS of compound **6**

Figure S46. HPLC chromatogram of compound **7**

UV absorption of compound **7**

28

Figure S47. ^{1}H NMR (600M Hz, methanol-d_4) spectrum of compound **7**

Figure S48. ^{13}C NMR (150M Hz, methanol-d_4) spectrum of compound **7**

29

Figure S49. HSQC (methanol-d_4) spectrum of compound **7**

Figure S50. COSY (methanol-d_4) spectrum of compound **7**

30
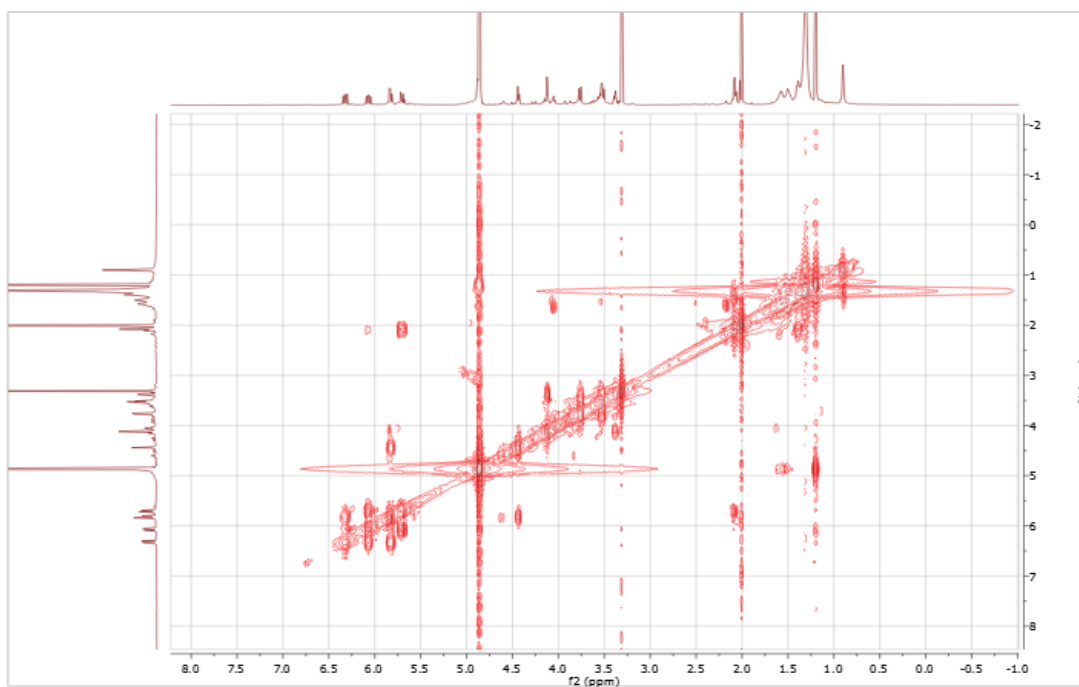
Figure S51. HMBC (methanol-d_4) spectrum of compound **7**
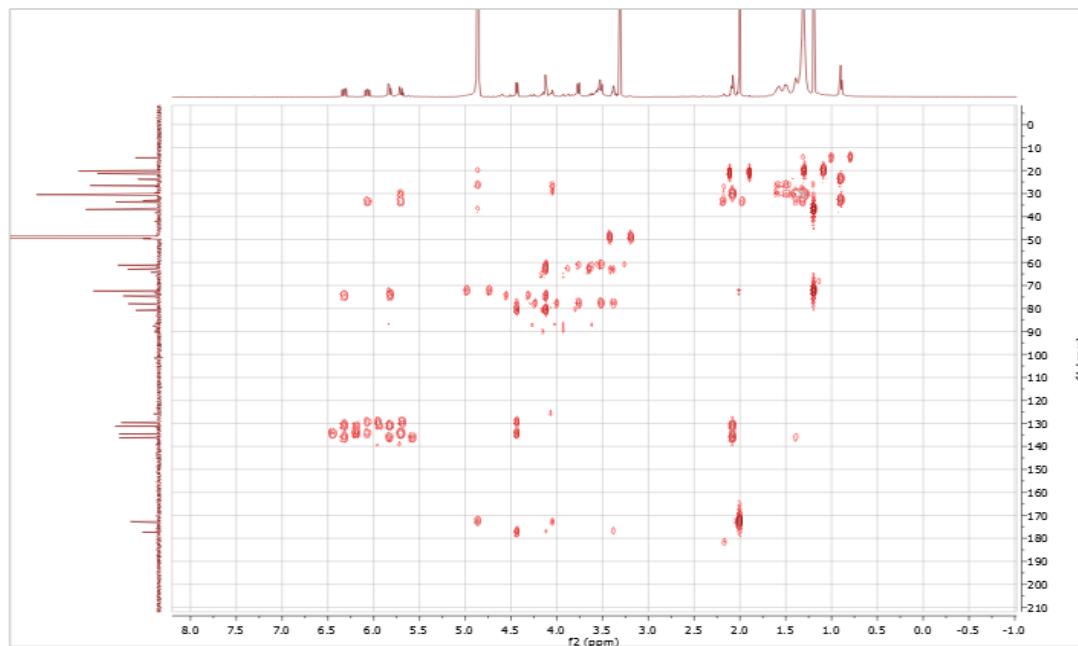
Figure S52. ROESY (methanol-d_4) spectrum of compound **7**
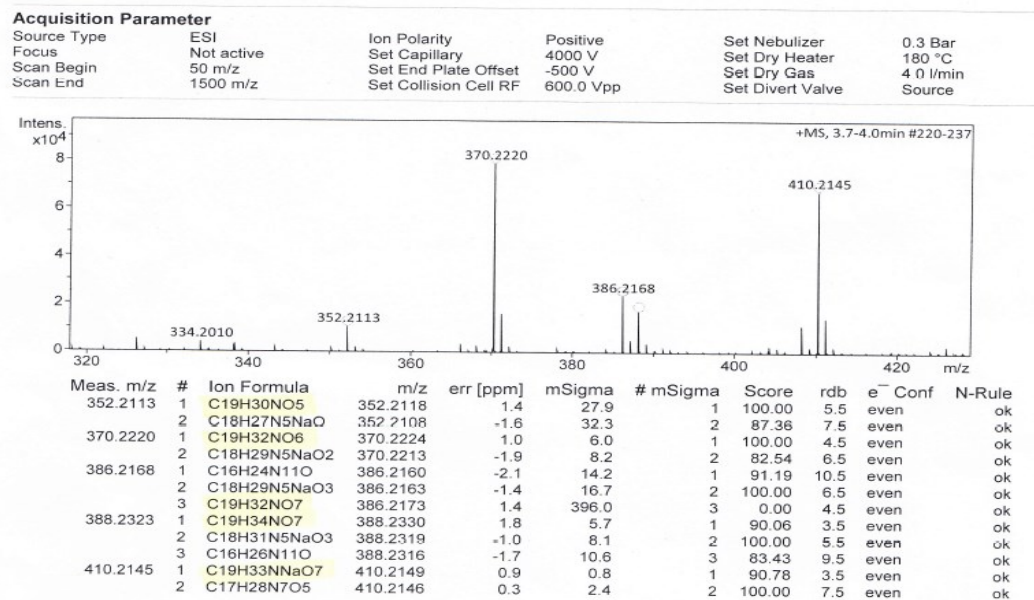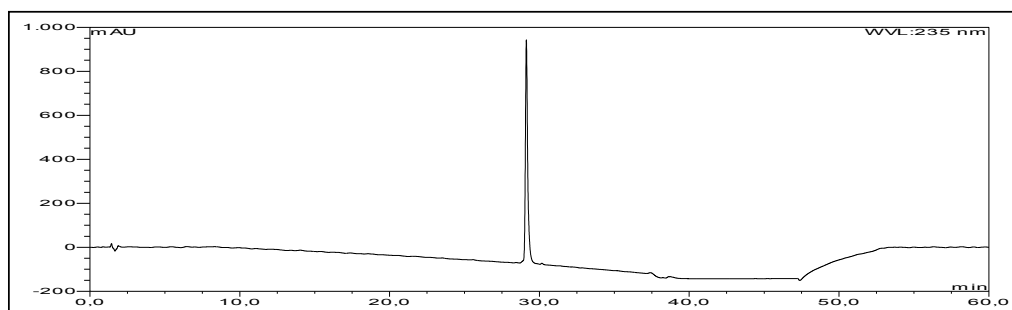

31
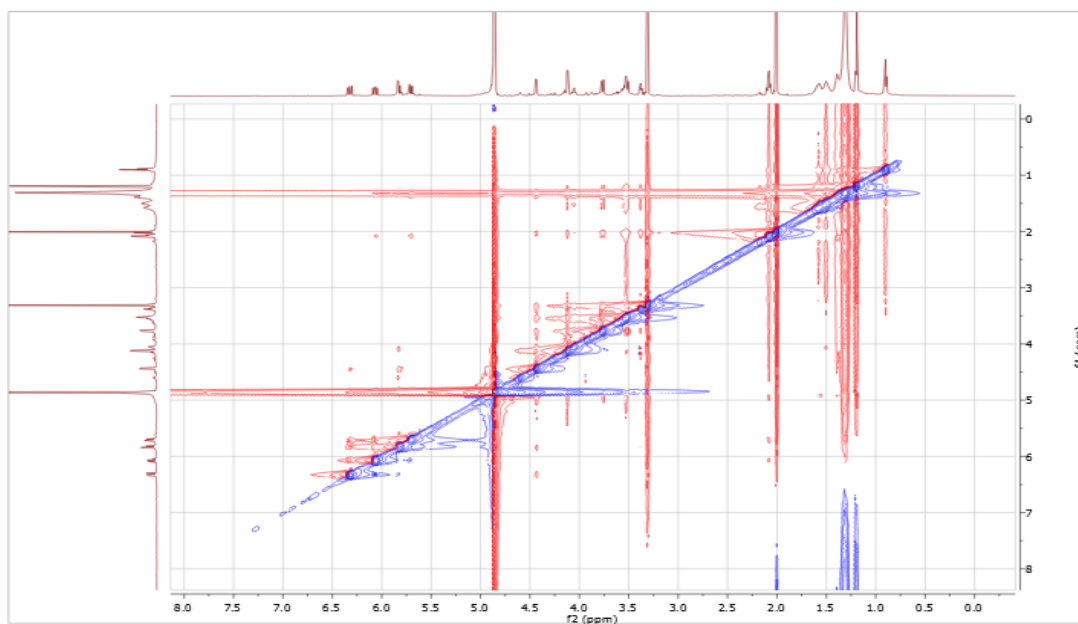
Figure S53. HRESIMS of compound **7**
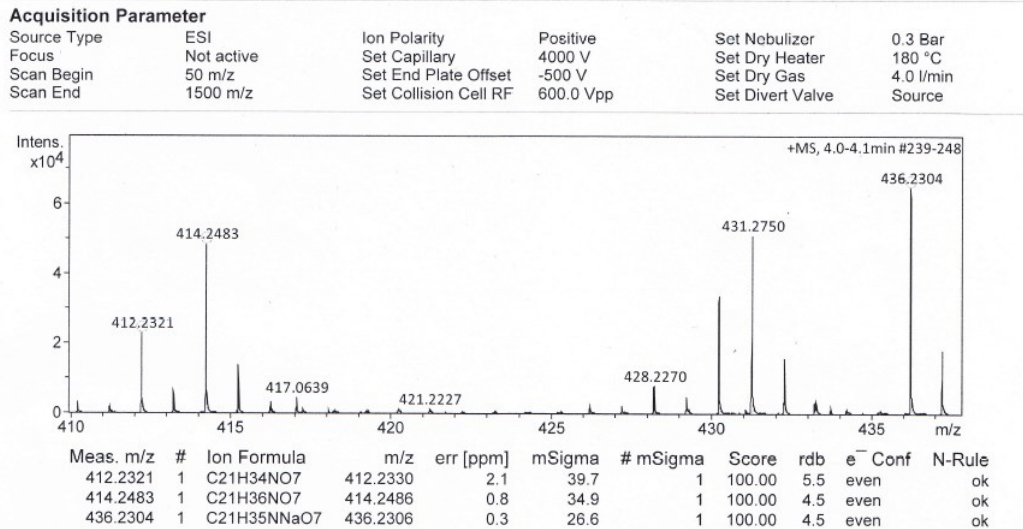
Figure S54. HPLC chromatogram of compound **8**
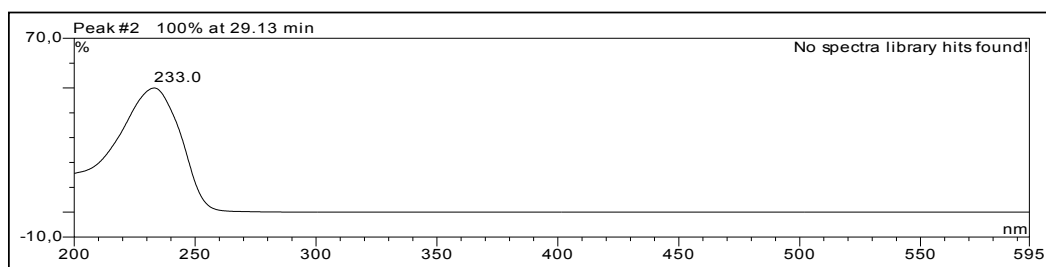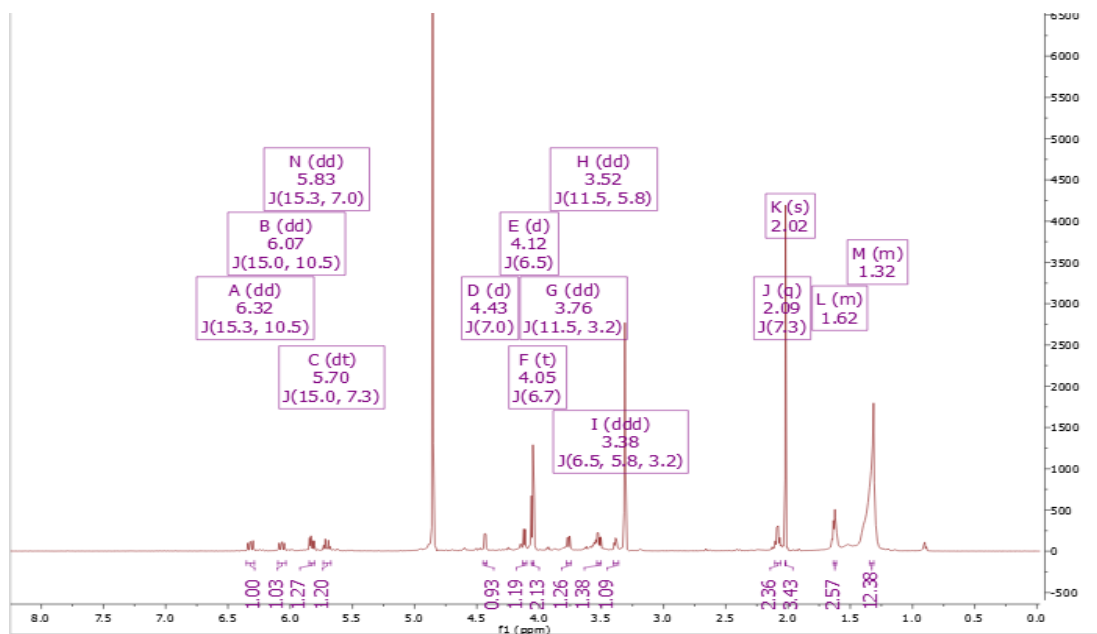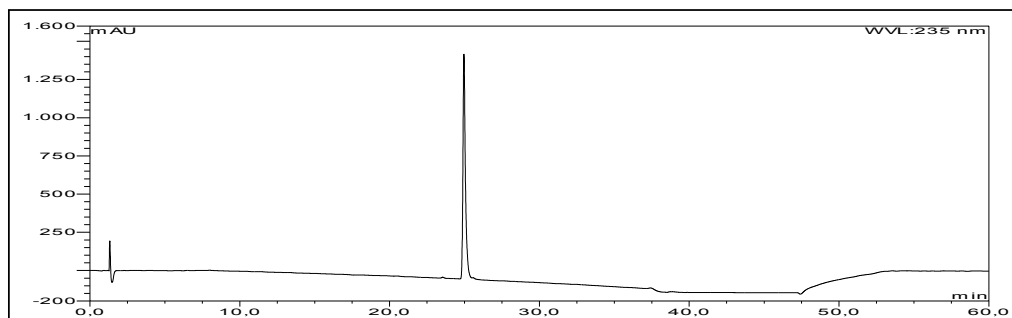

UV absorption of compound **8**
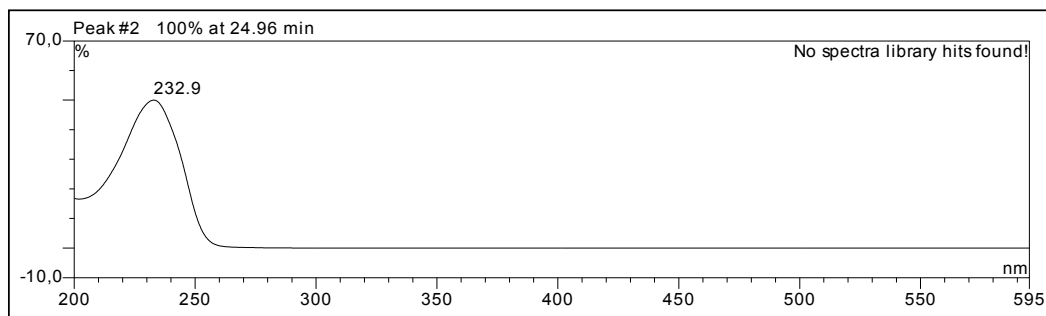
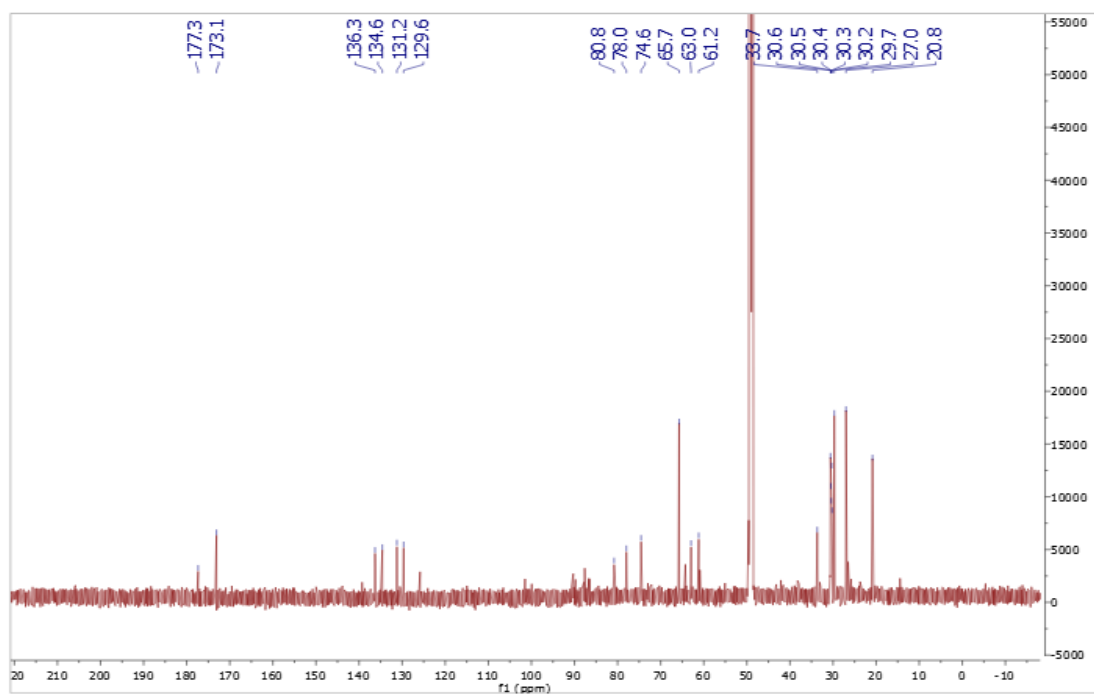**Figure S55.** ^{1}H NMR (600M Hz, methanol-d_4) spectrum of compound **8**
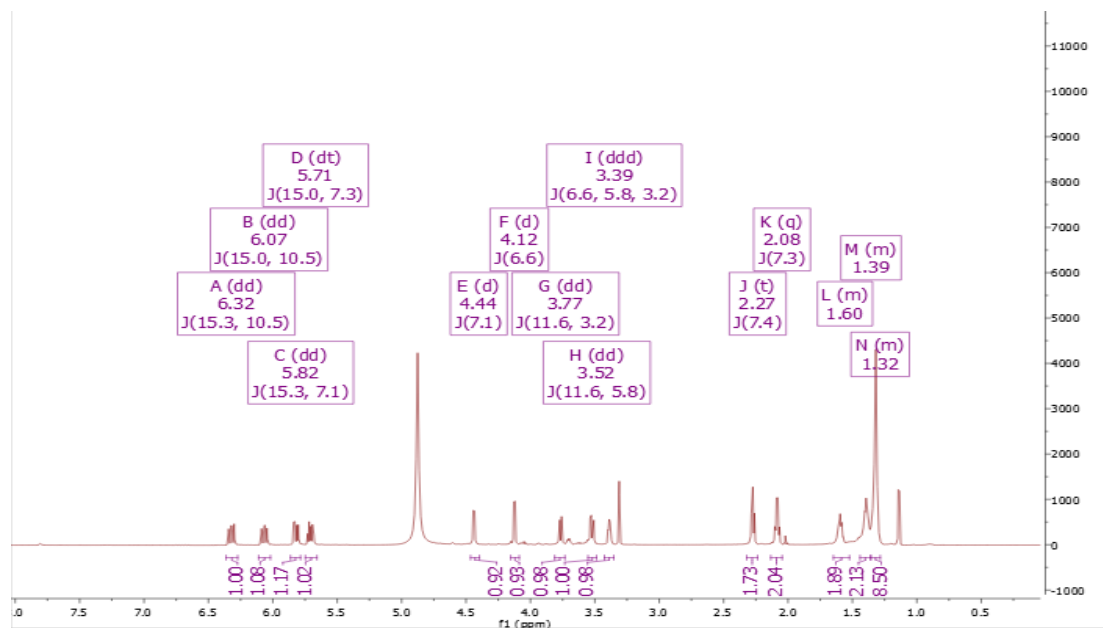
Figure S56. ^{13}C NMR (150M Hz, methanol-d_4) spectrum of compound **8**
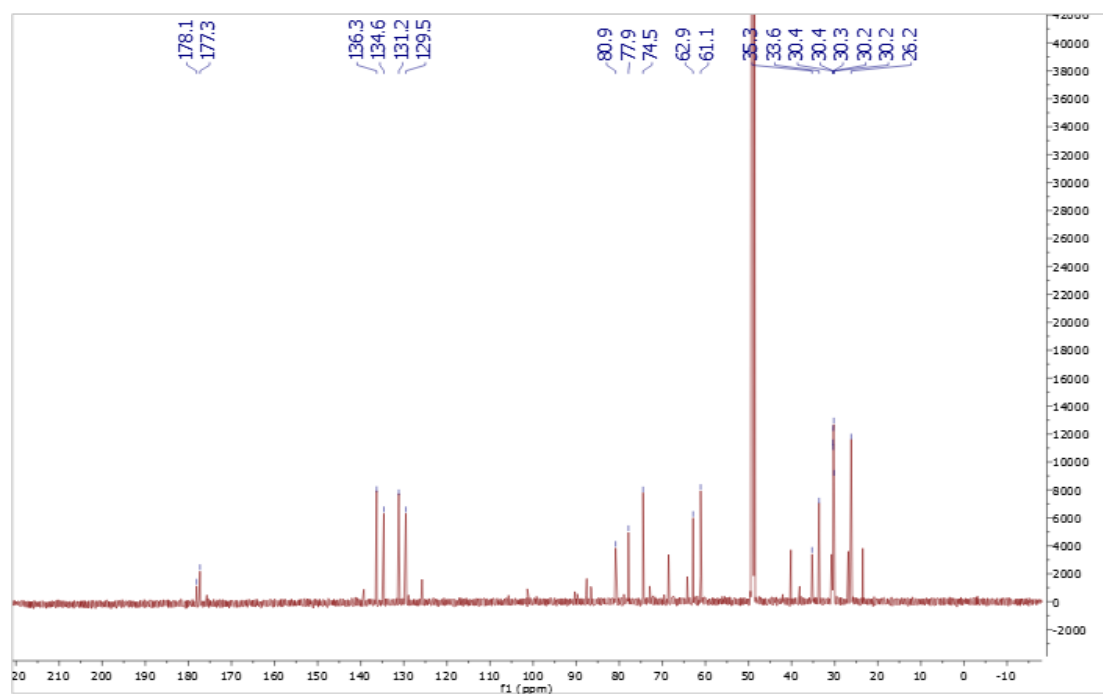
Figure S57. HSQC (methanol-d_4) spectrum of compound **8**
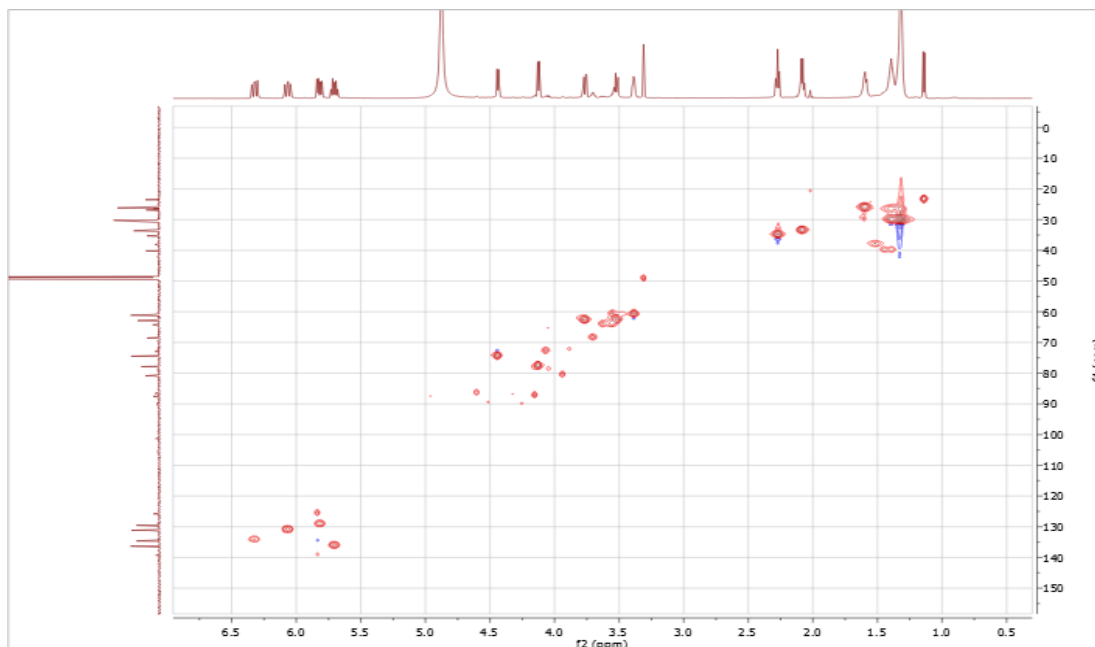
Figure S58. COSY (methanol-d_4) spectrum of compound **8**

34
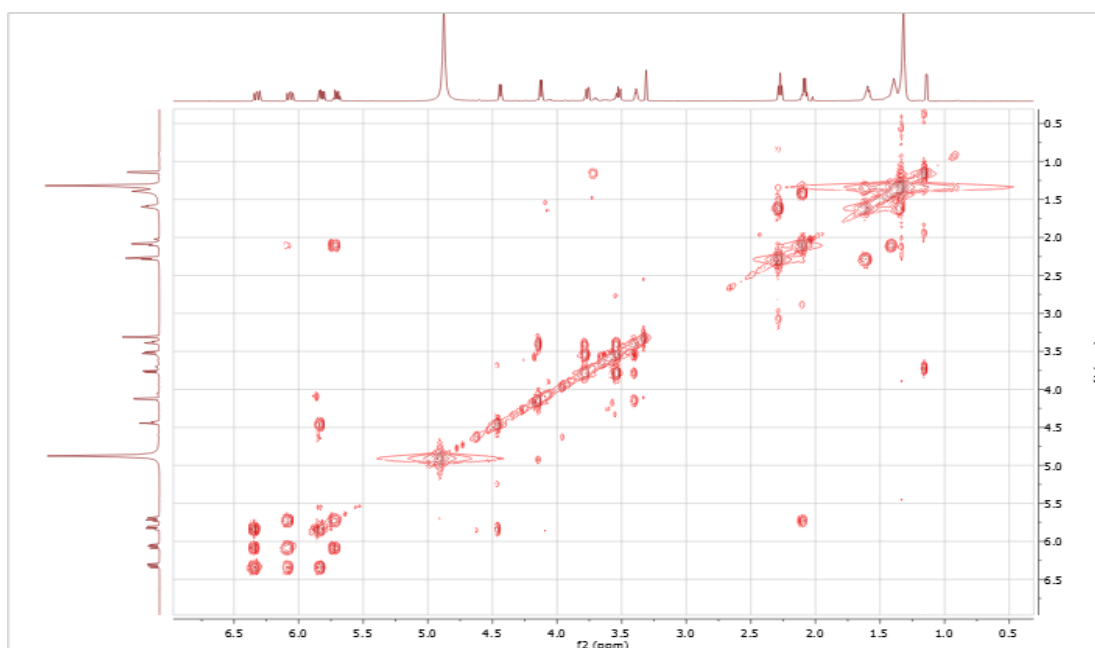
Figure S59. HMBC (methanol-d_4) spectrum of compound **8**
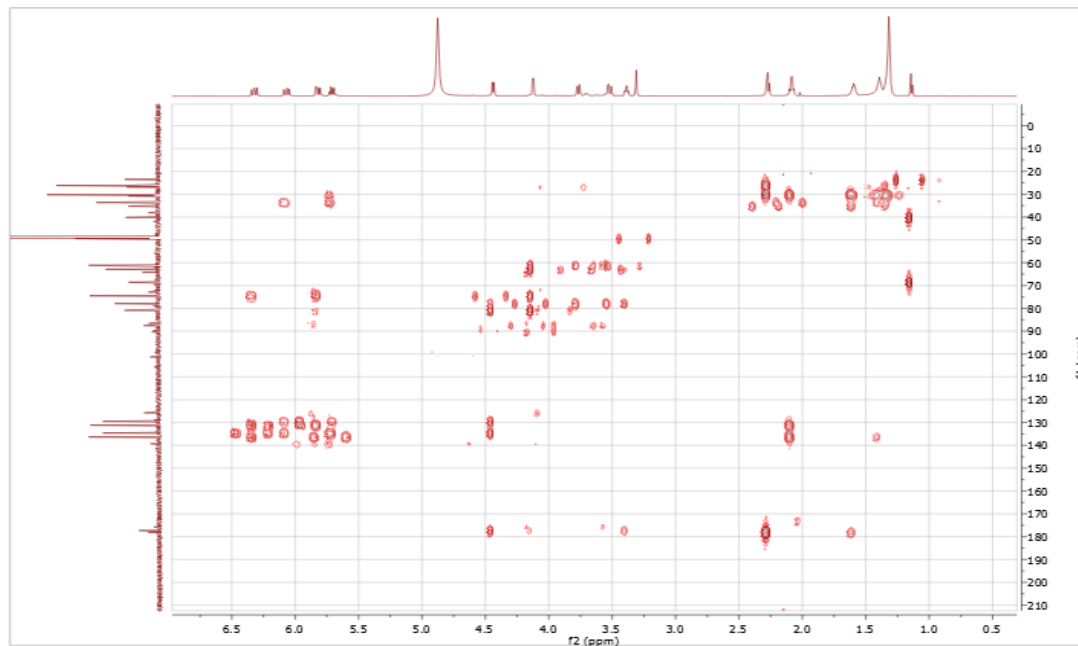
Figure S60. ROESY (methanol-d_4) spectrum of compound **8**

35
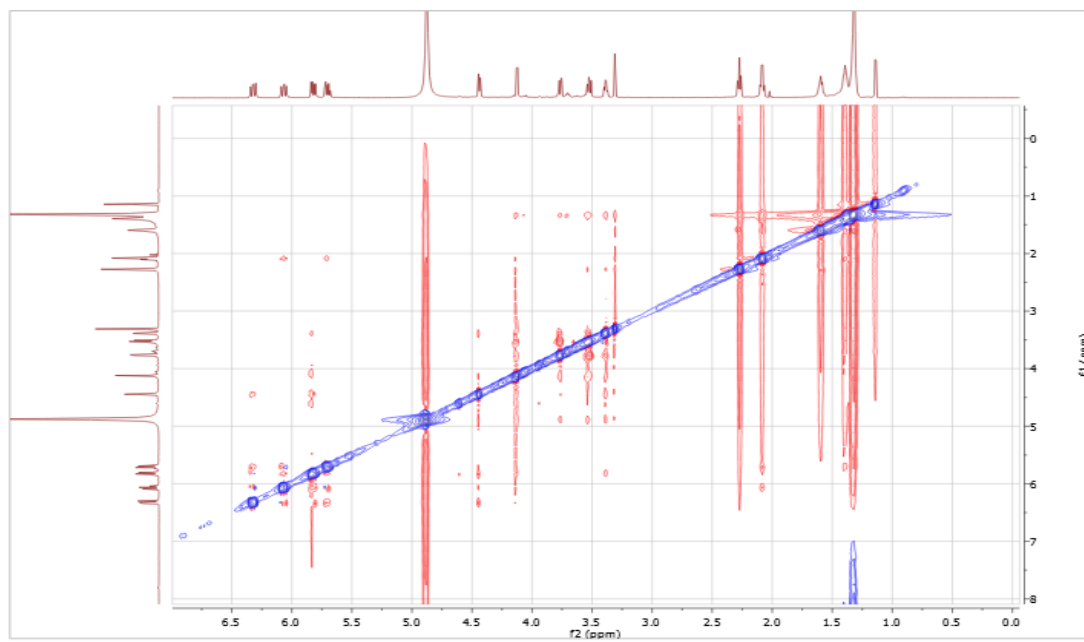
Figure S61. HRESIMS of compound **8**
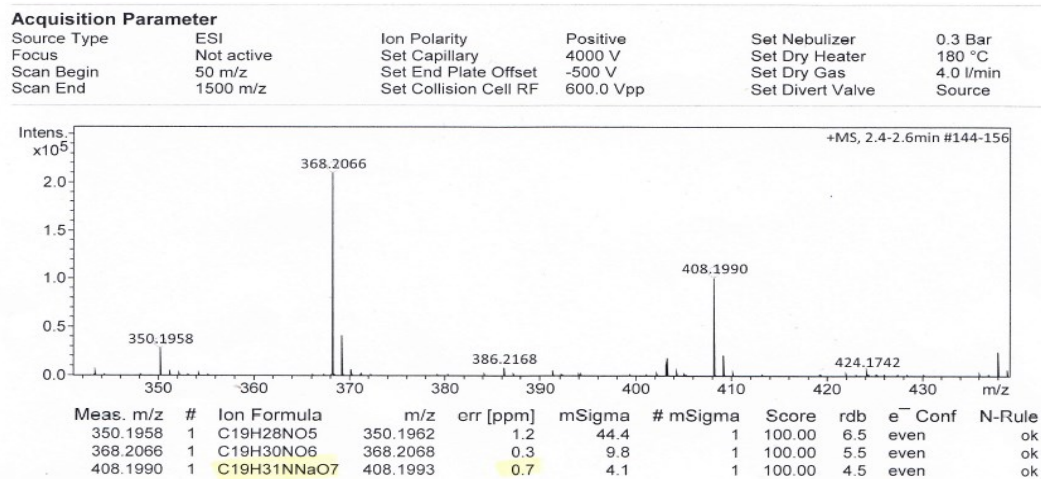
Figure S62. HPLC chromatogram of compound **9**
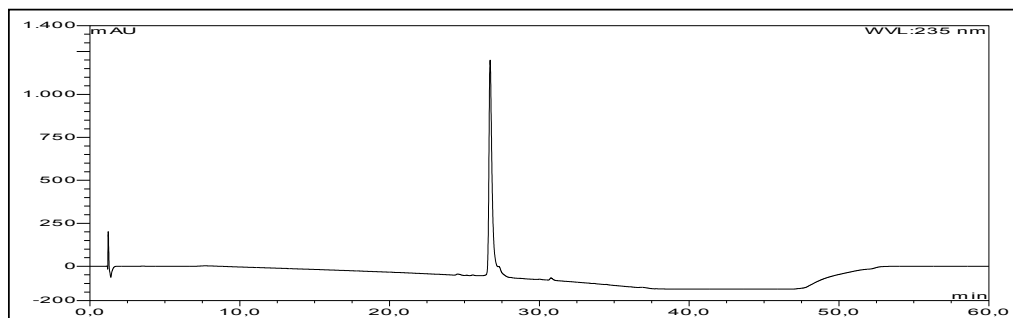
UV absorption of compound **9**
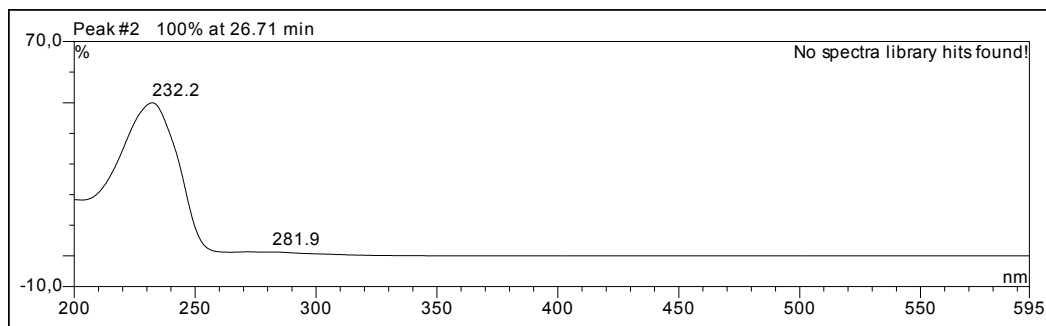
Figure S63. ^{1}H NMR (600M Hz, methanol-d_4) spectrum of compound **9**
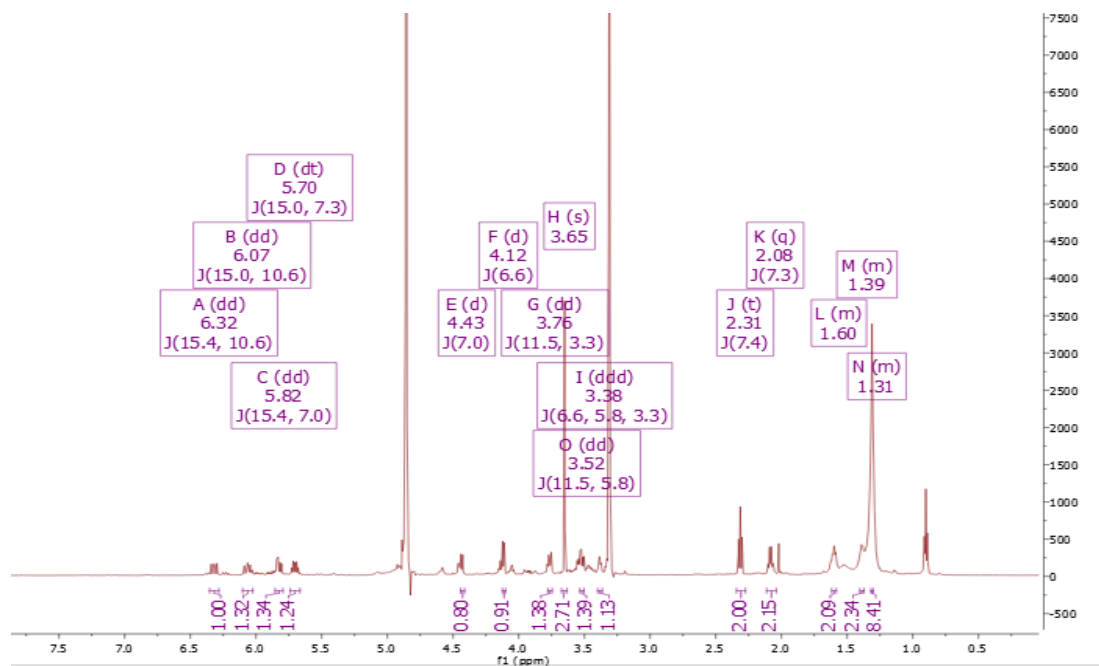
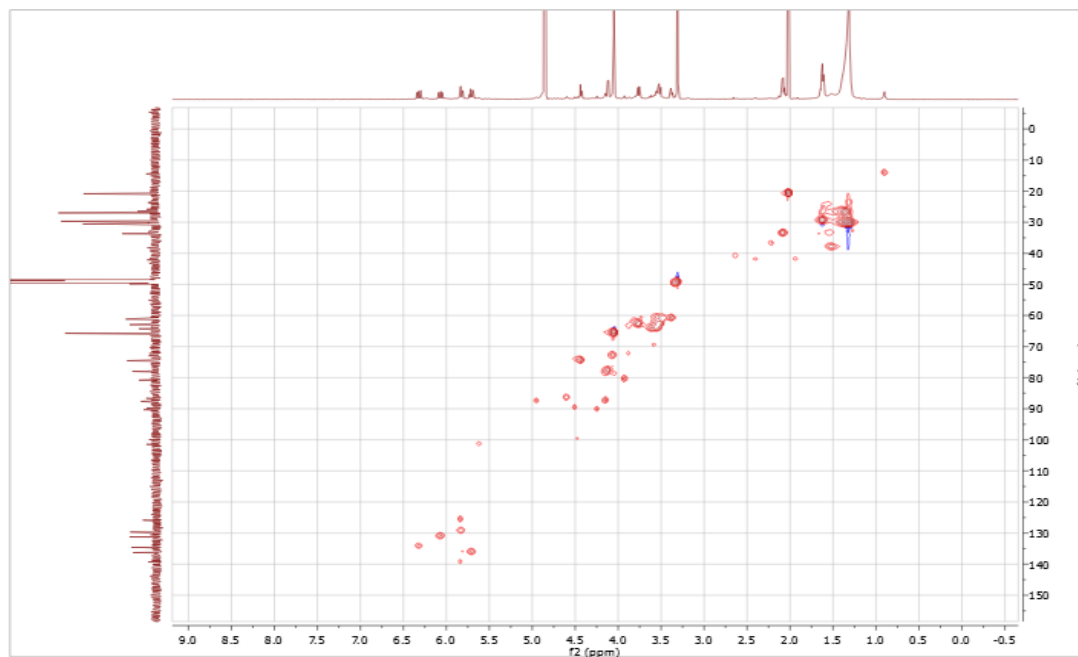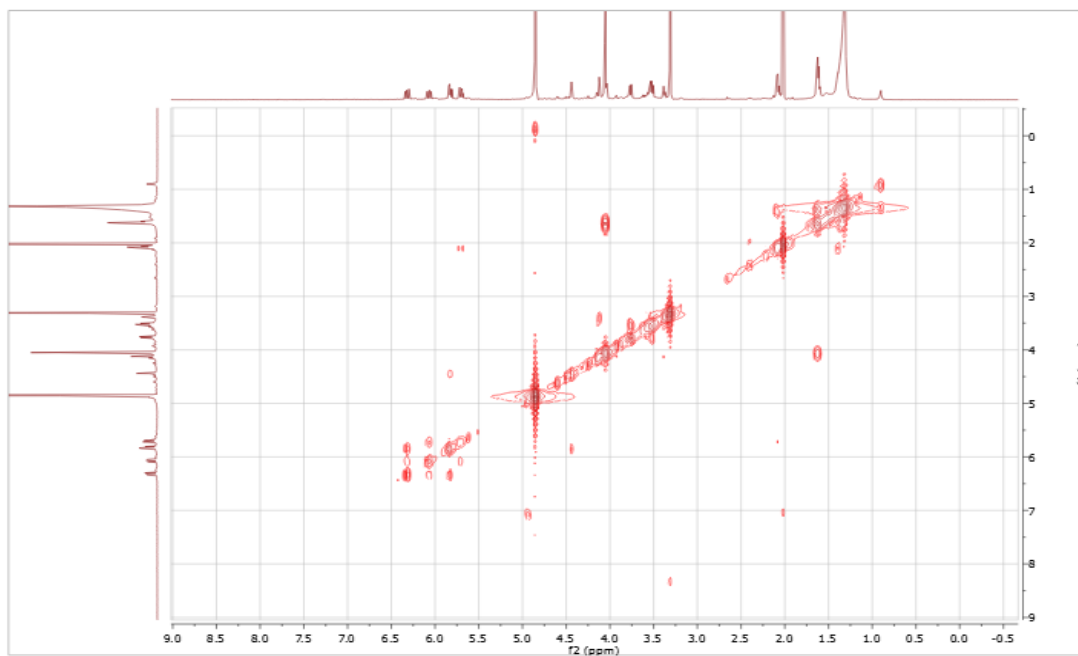**Figure S64.** ^{13}C NMR (150M Hz, methanol-d_4) spectrum of compound **9**

37
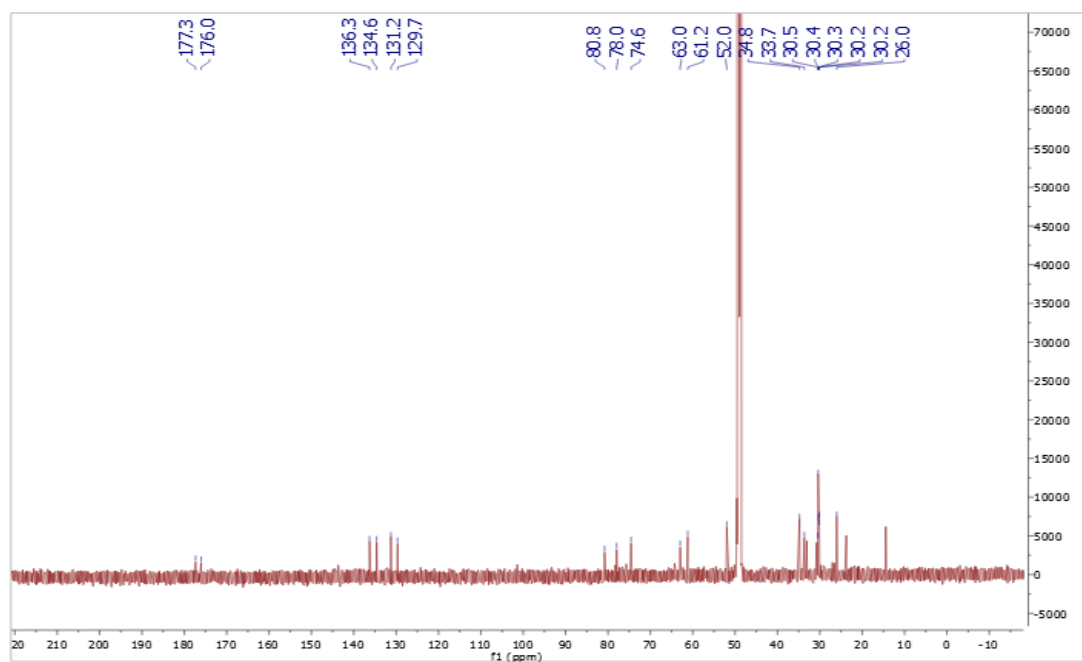
Figure S65. HSQC (methanol-d_4) spectrum of compound **9**
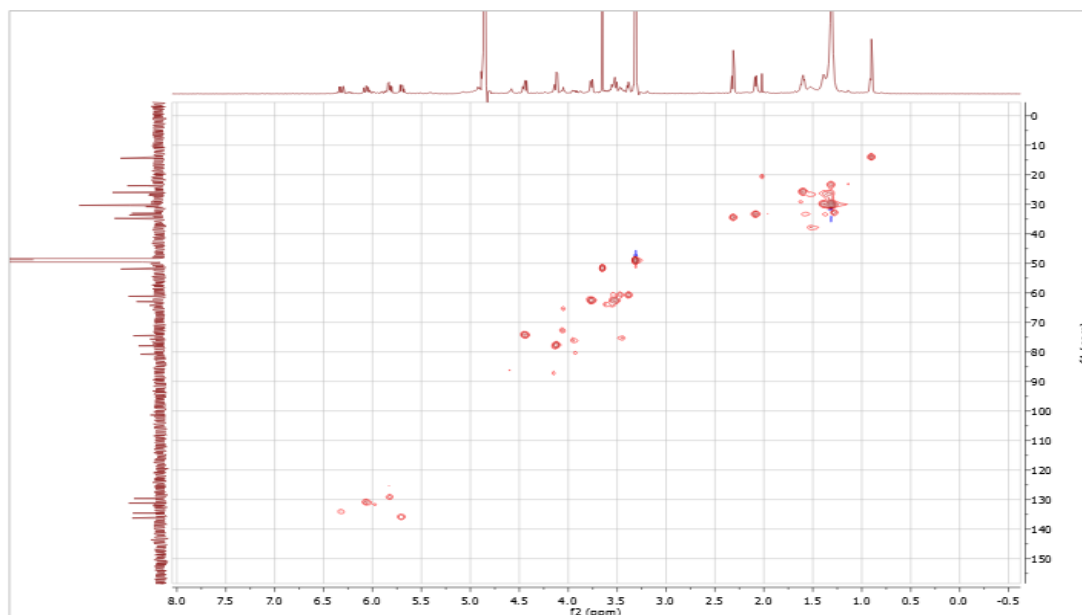
Figure S66. COSY (methanol-d_4) spectrum of compound **9**
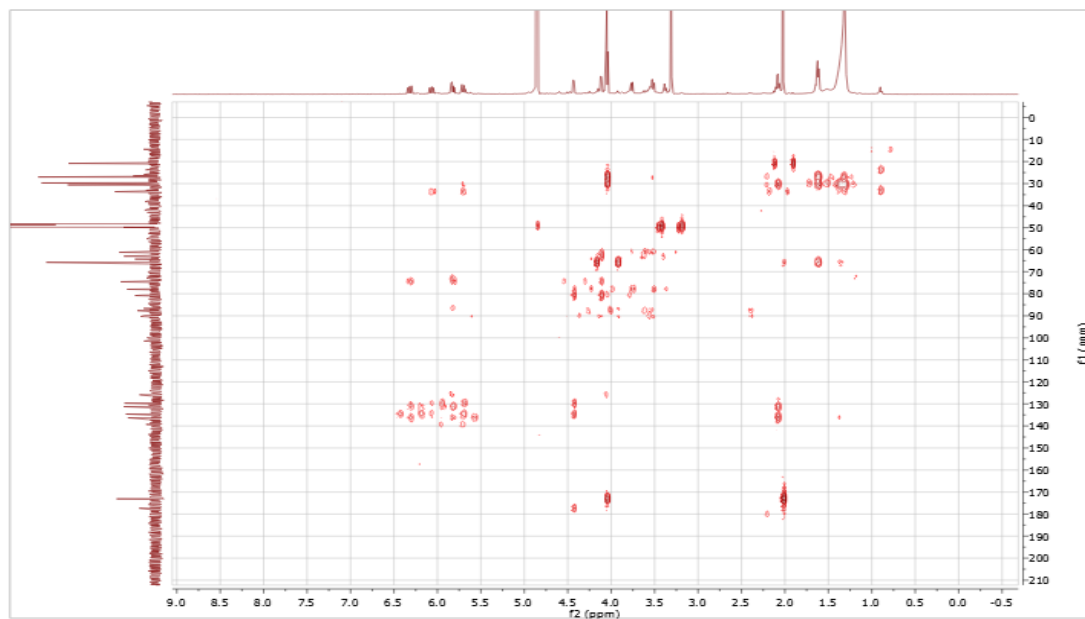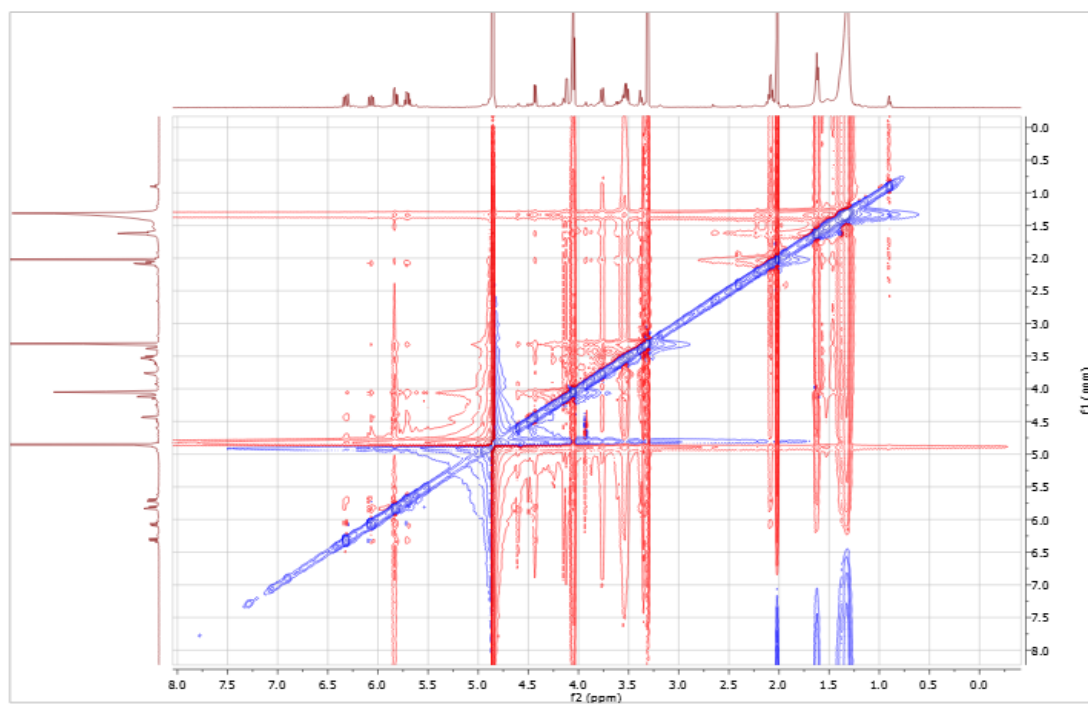

38
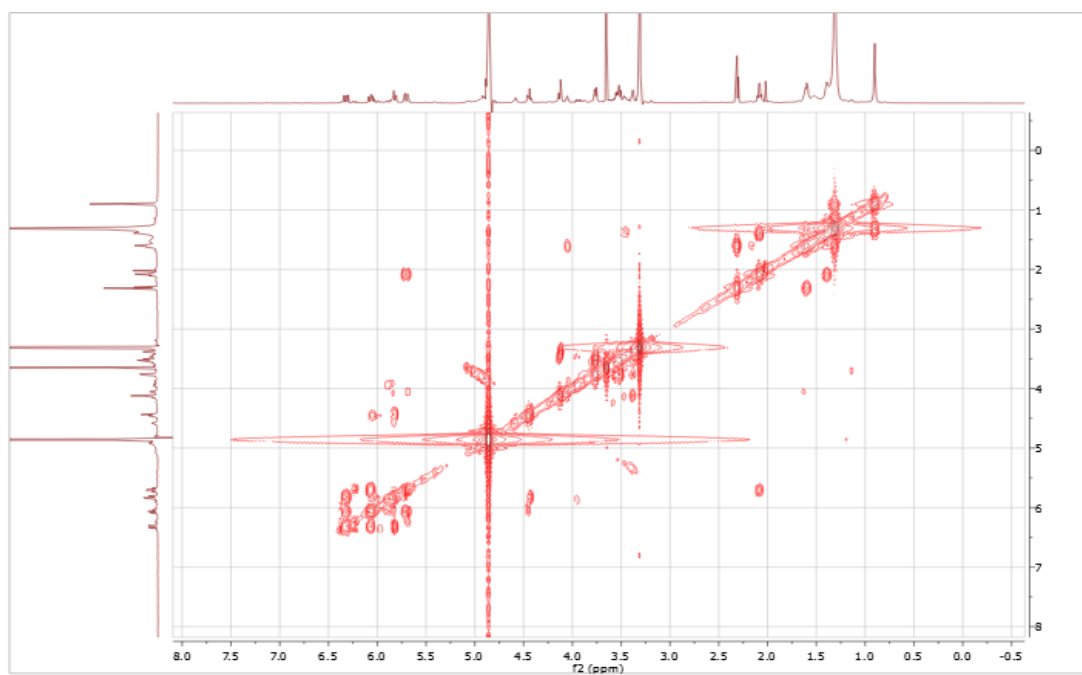
Figure S67. HMBC (methanol-d_4) spectrum of compound **9**
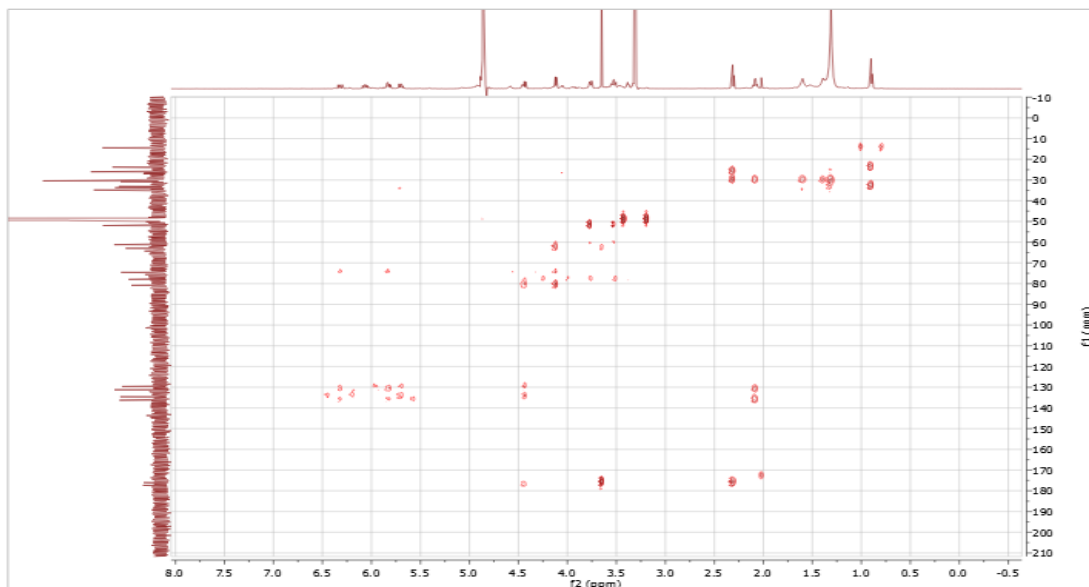
Figure S68. ROESY (methanol-d_4) spectrum of compound **9**

39
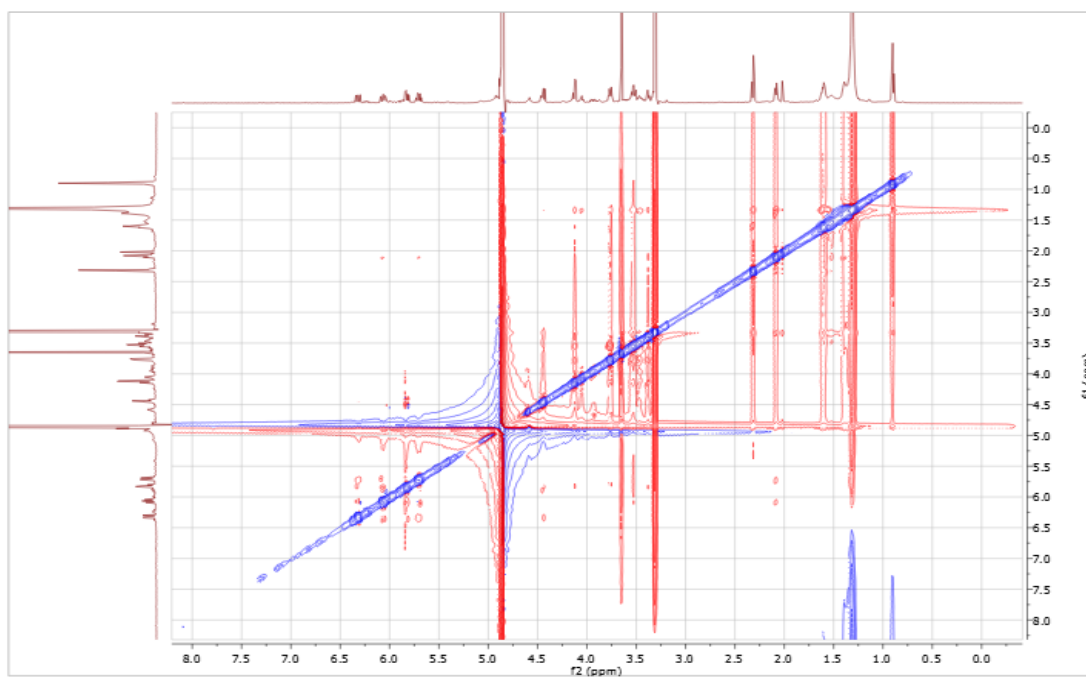
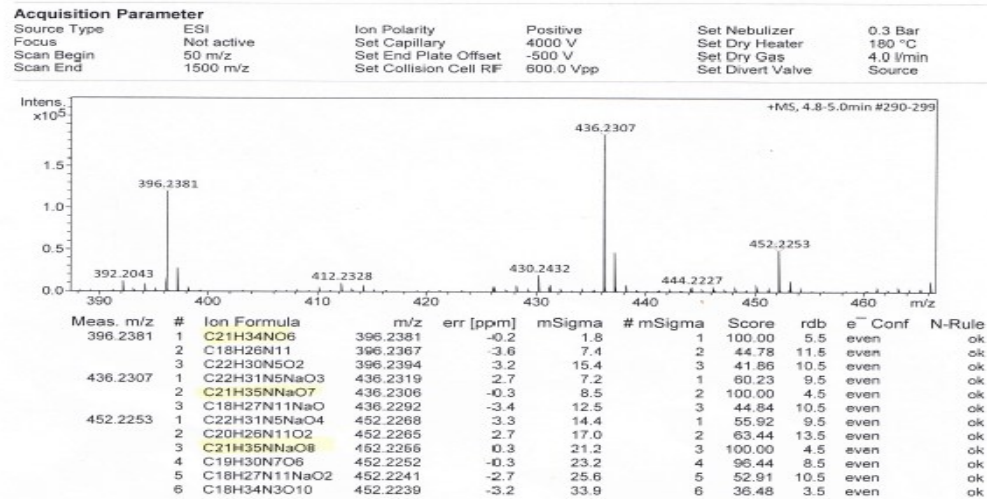**Figure S69.** HRESIMS of compound **9**
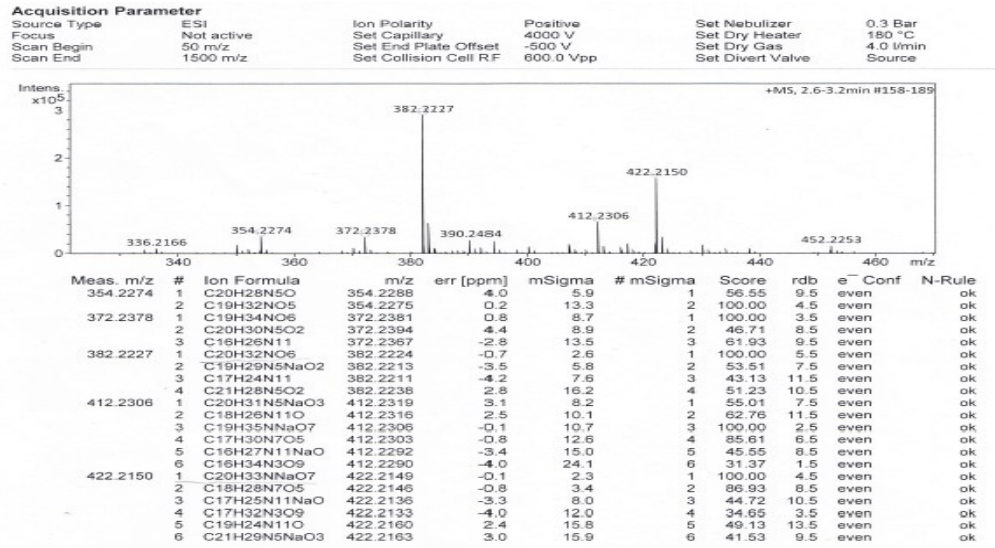
Figure S70. HPLC chromatogram of compound **10**
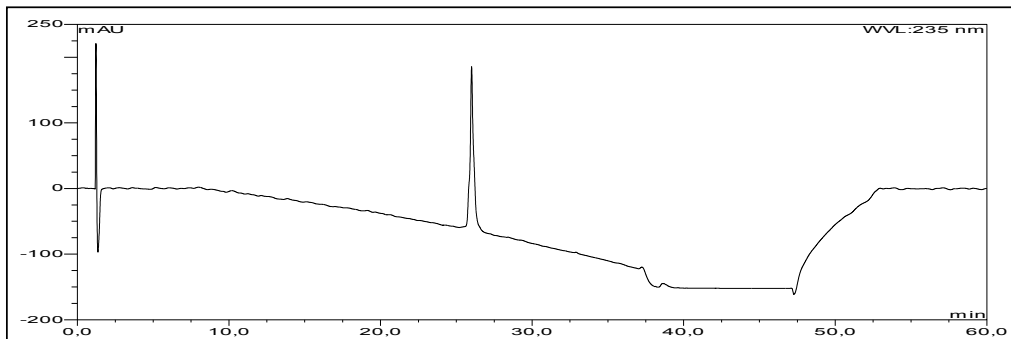
UV absorption of compound **10**

40
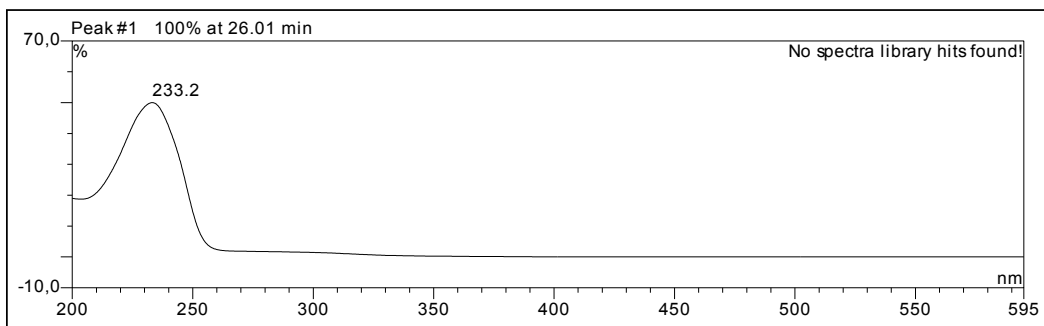
Figure S71. ^{1}H NMR (600M Hz, methanol-d_4) spectrum of compound **10**
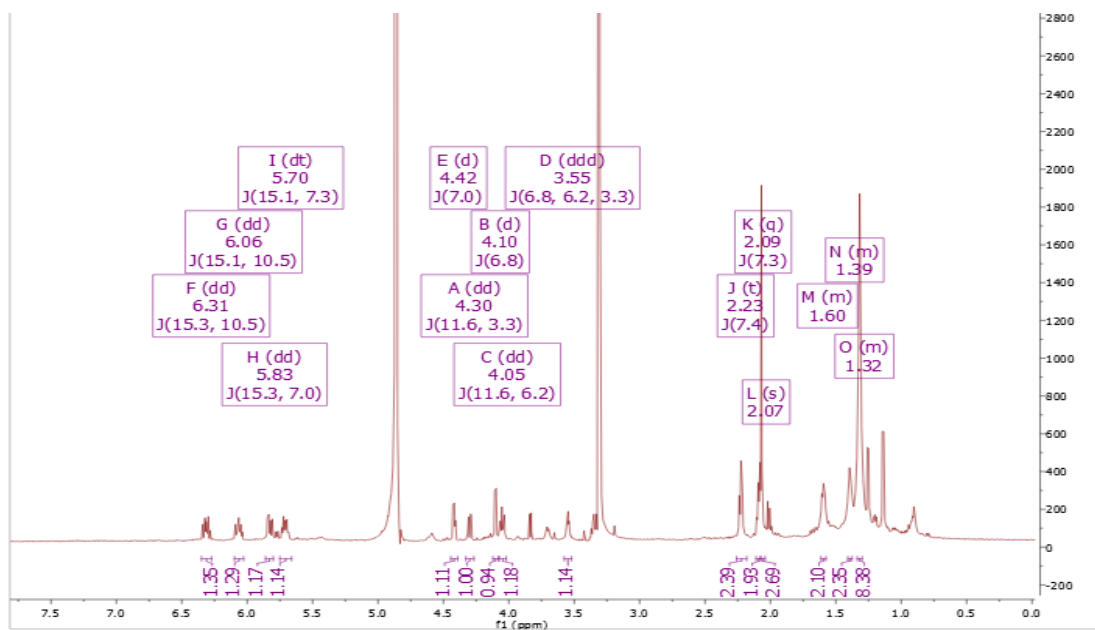
Figure S72. HSQC (methanol-d_4) spectrum of compound **10**

41

Figure S73. COSY (methanol-d_4) spectrum of compound **10**

Figure S74. HMBC (methanol-d_4) spectrum of compound **10**

42

Figure S75. ROESY (methanol-*d*₄) spectrum of compound **10**

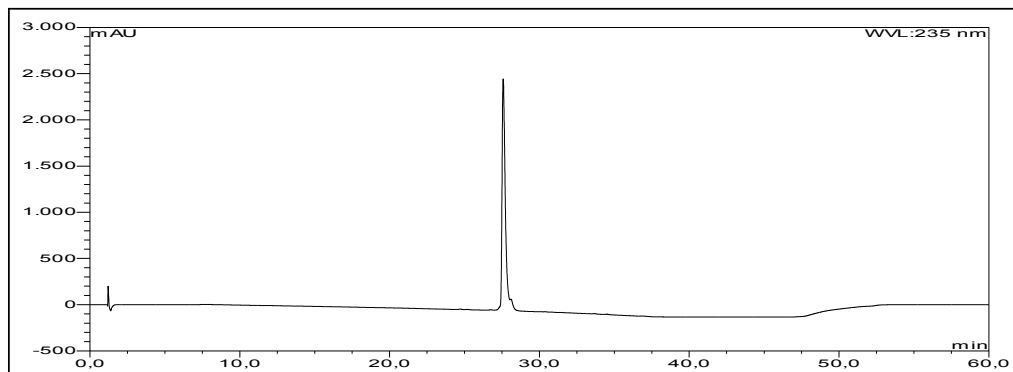**Figure S76.** HRESIMS of compound **10**

43

Figure S77. HPLC chromatogram of compound **11**
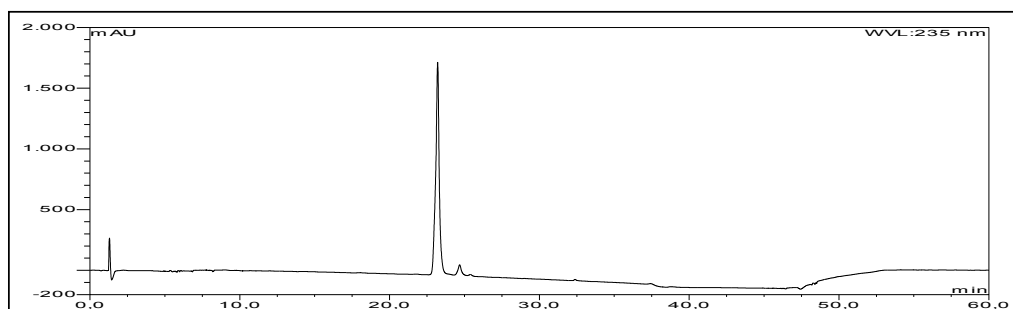
UV absorption of compound **11**
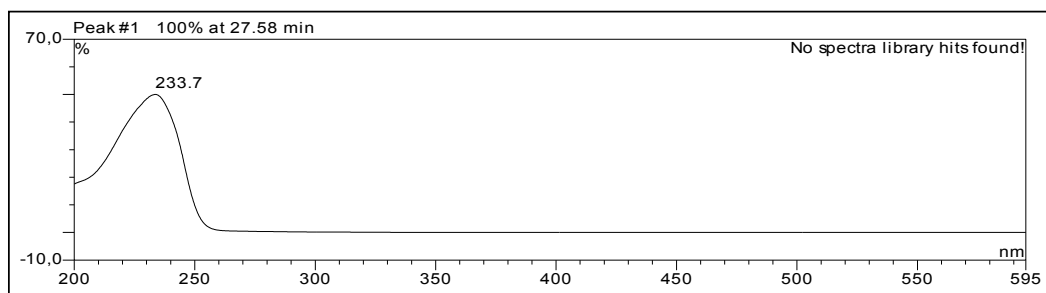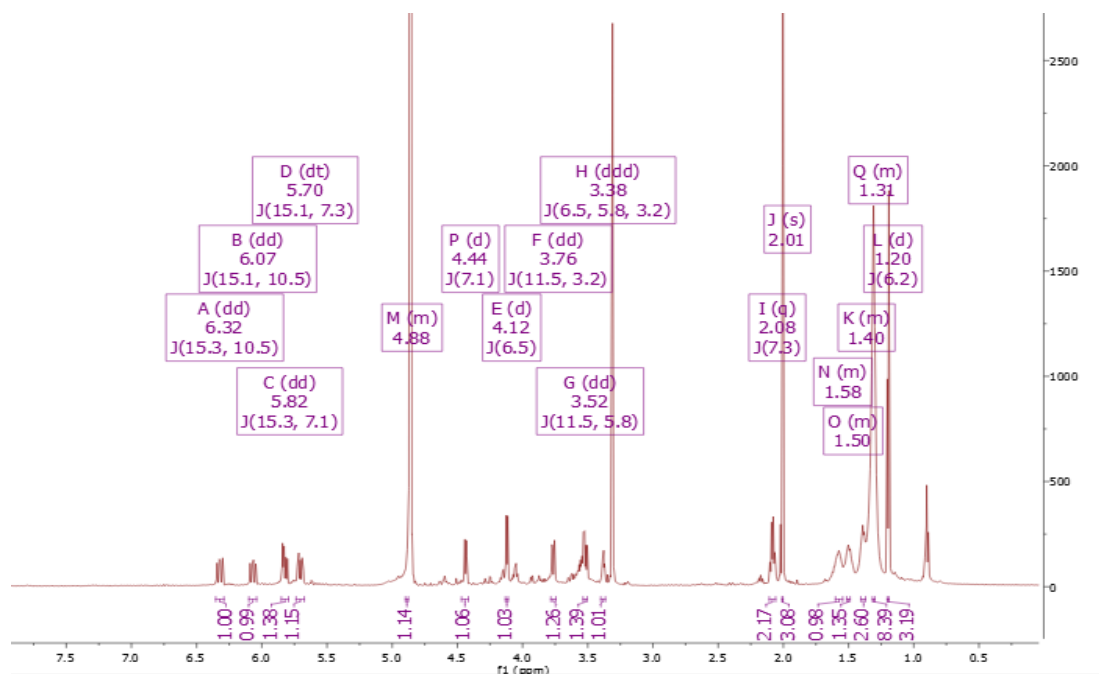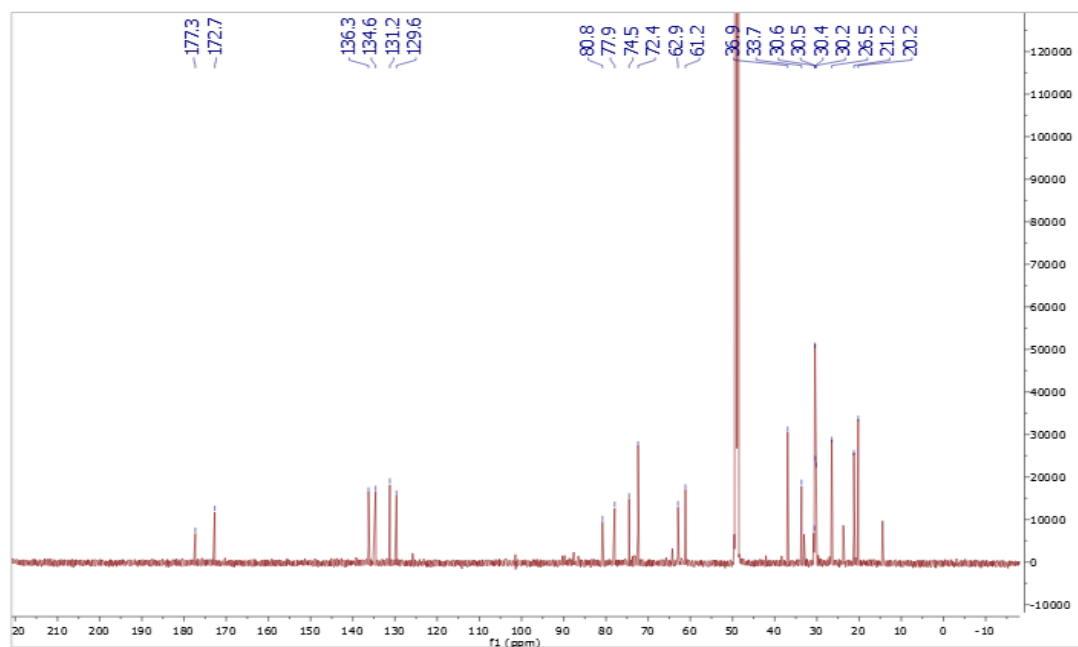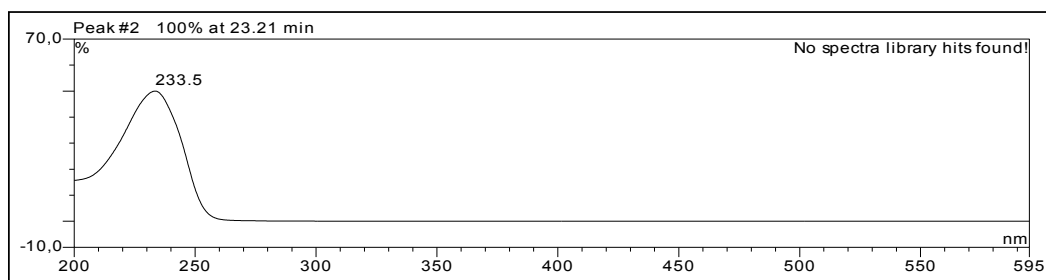

Figure S78. ^{1}H NMR (600M Hz, methanol-d_4) spectrum of compound **11**

44
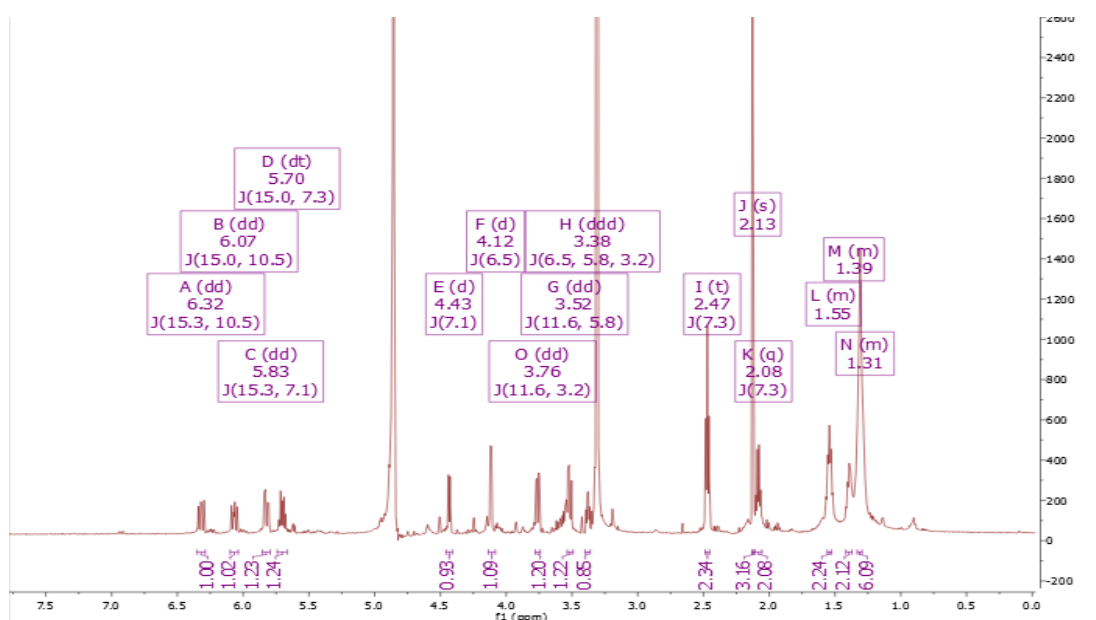
Figure S79. ^{13}C NMR (150M Hz, methanol-d_4) spectrum of compound **11**
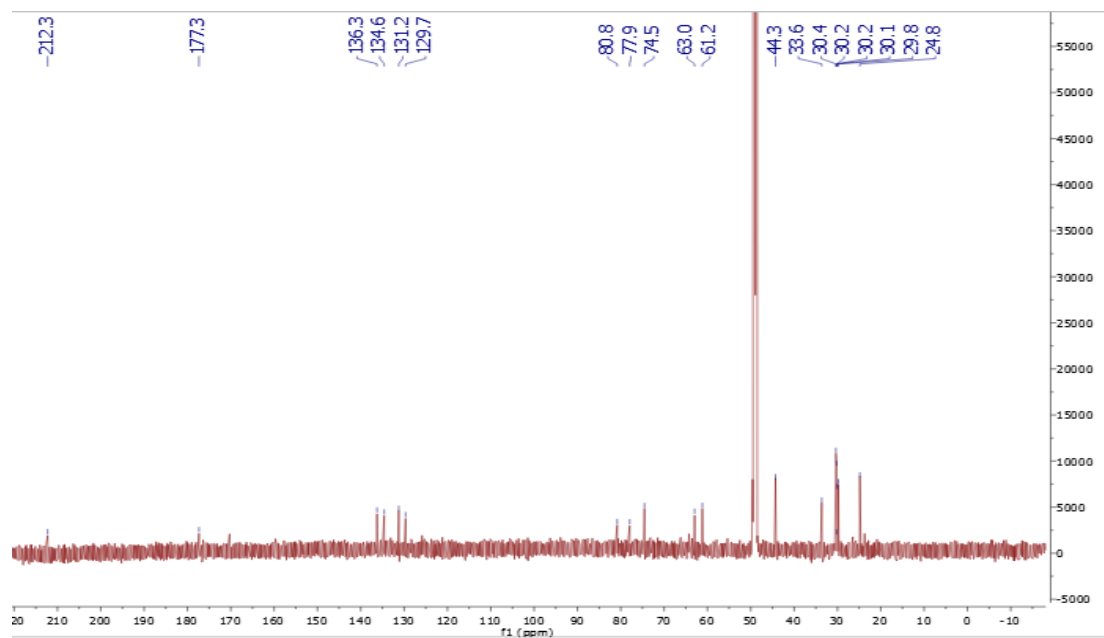
Figure S80. HSQC (methanol-d_4) spectrum of compound **11**

45
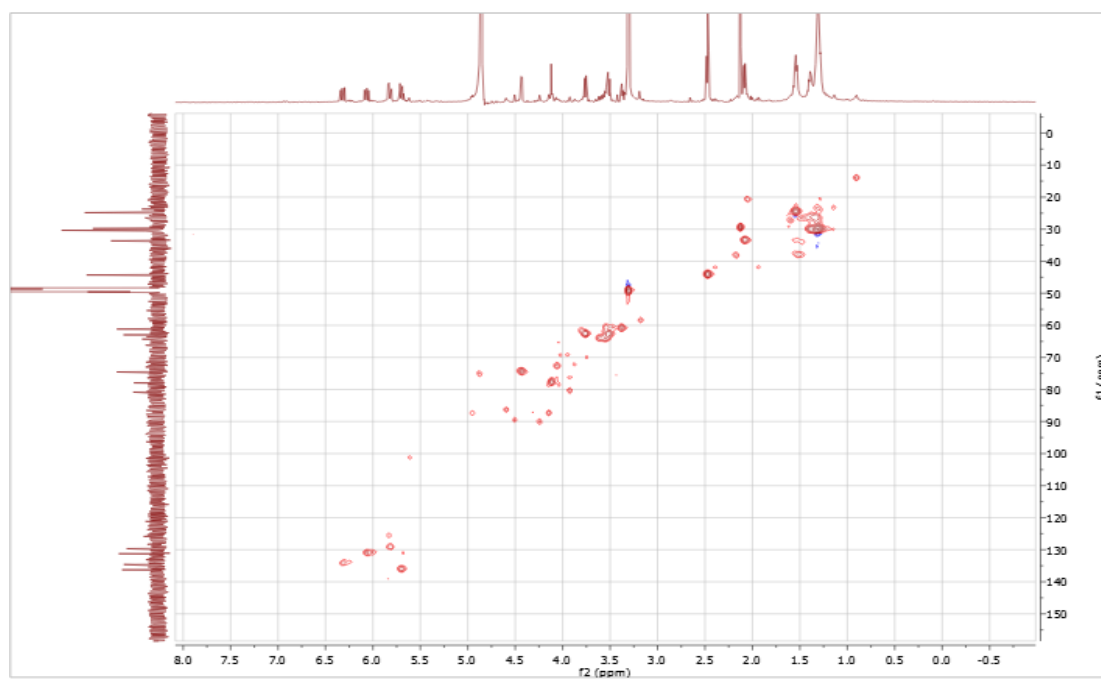
Figure S81. COSY (methanol-d_4) spectrum of compound **11**
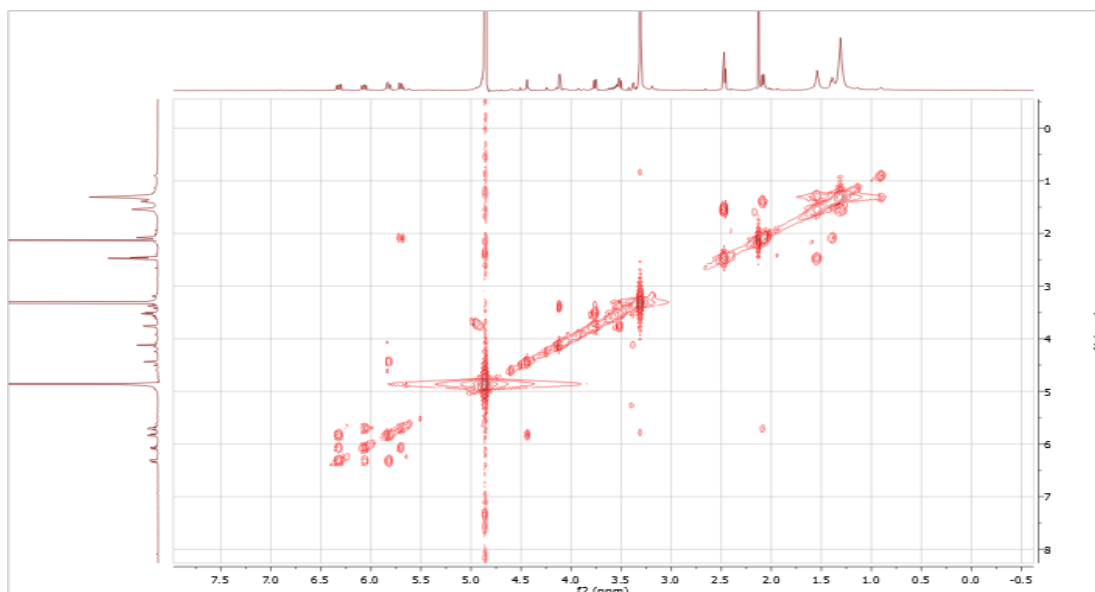
Figure S82. HMBC (methanol-d_4) spectrum of compound **11**

46
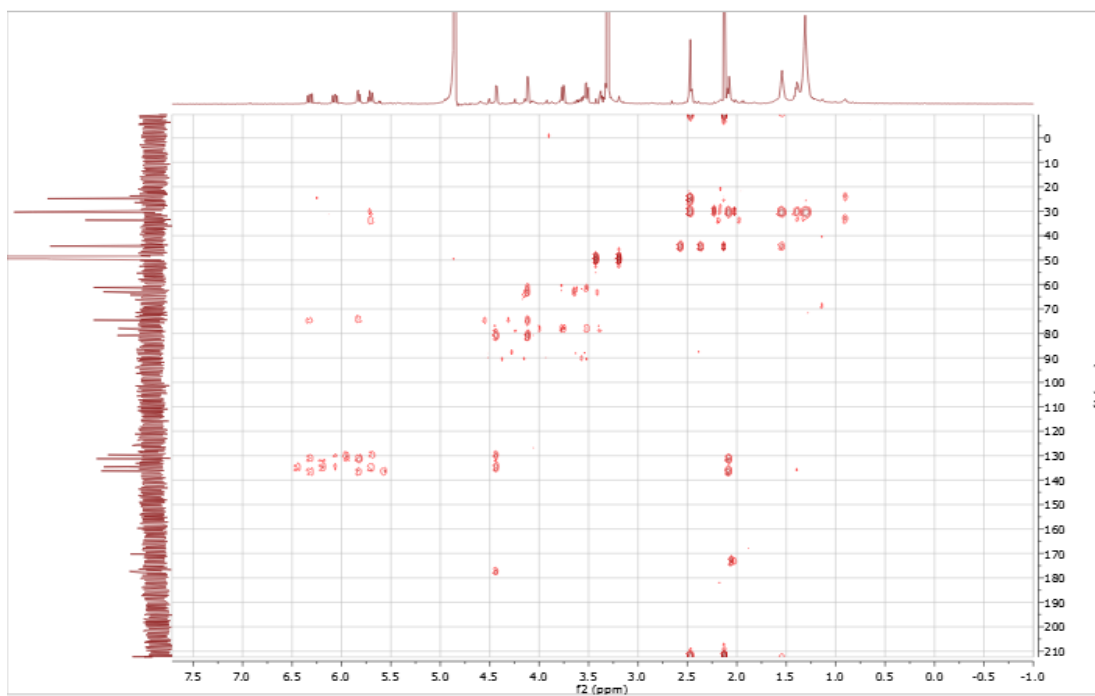
Figure S83. ROESY (methanol-d_4) spectrum of compound **11**
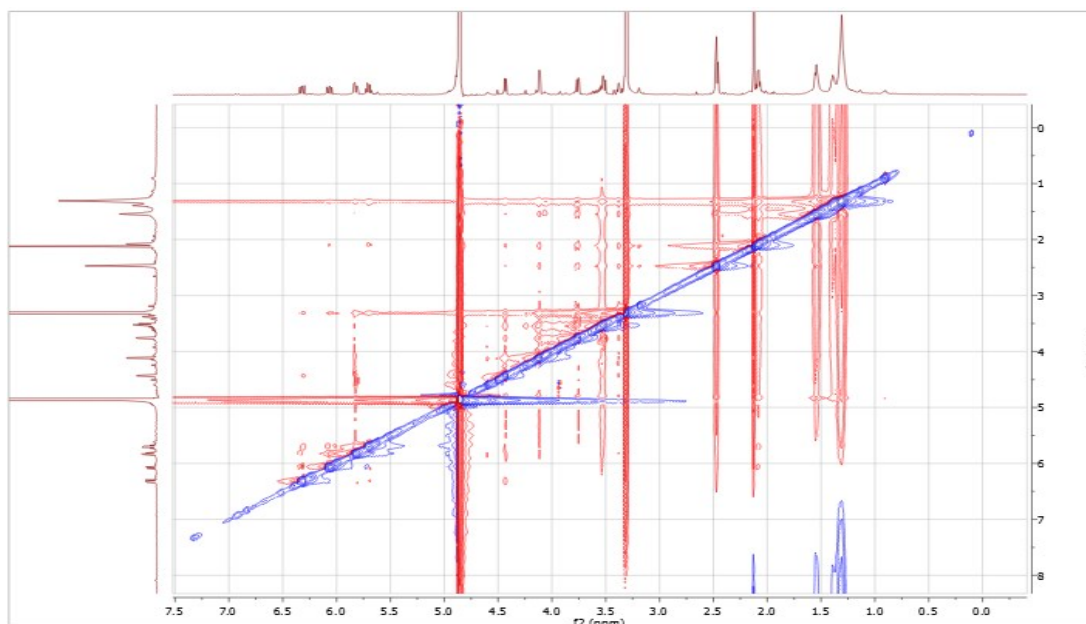
Figure S84. HRESIMS of compound **11**
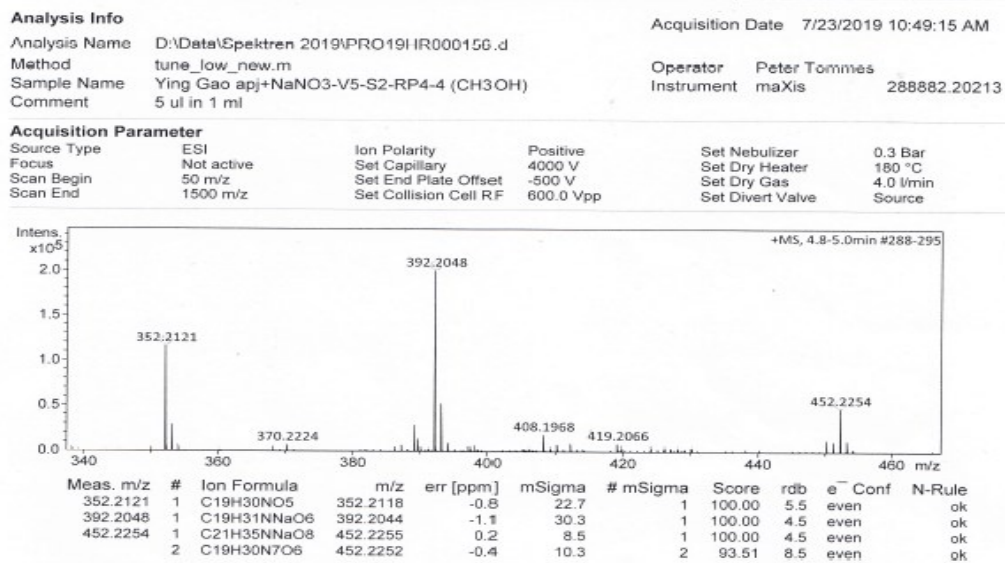
Figure S85. HPLC chromatogram of compound **12**
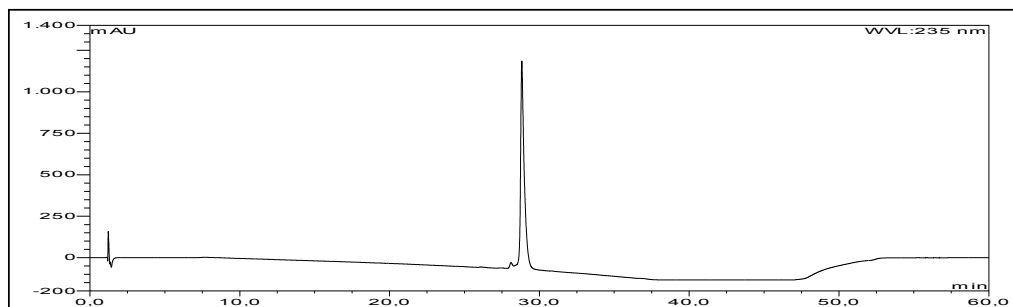
UV absorption of compound **12**
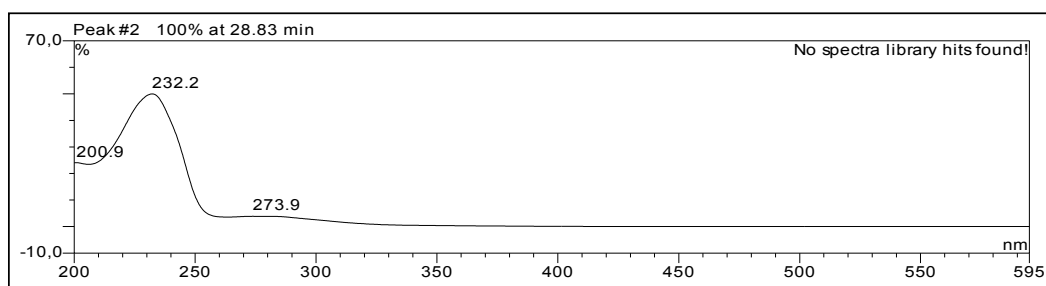
Figure S86. ¹H NMR (600M Hz, methanol-d_4) spectrum of compound **12**
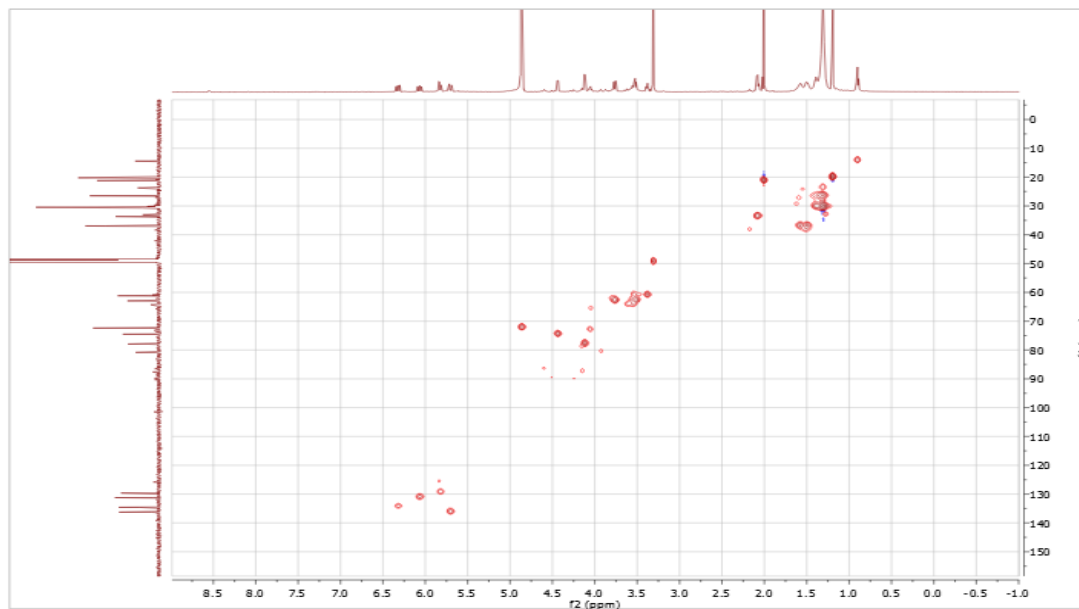

48
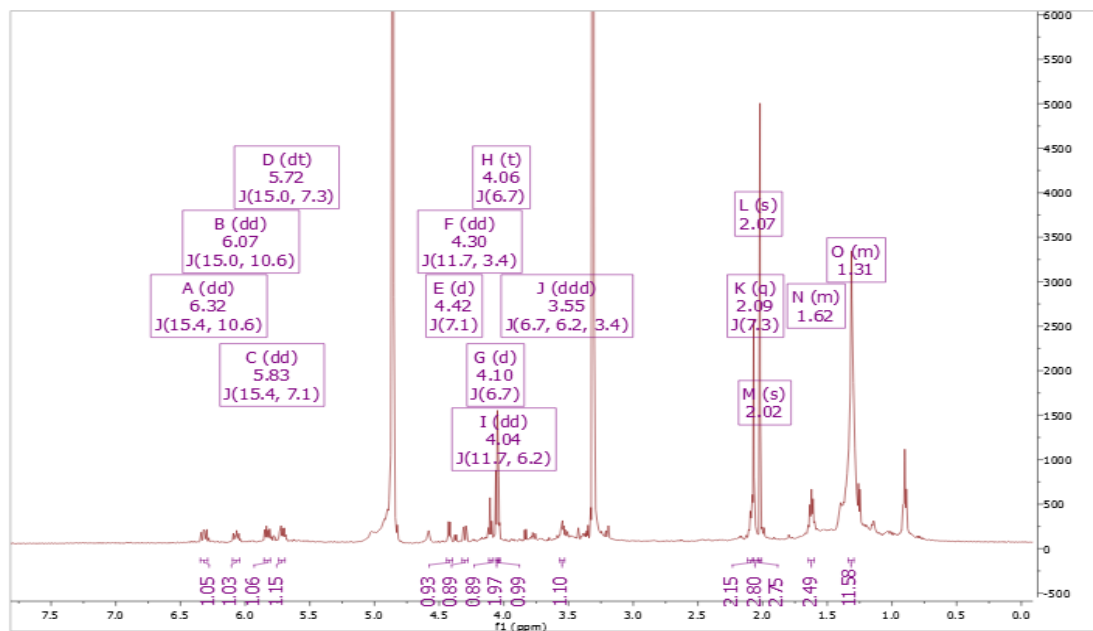
Figure S87. HSQC (methanol-d_4) spectrum of compound **12**
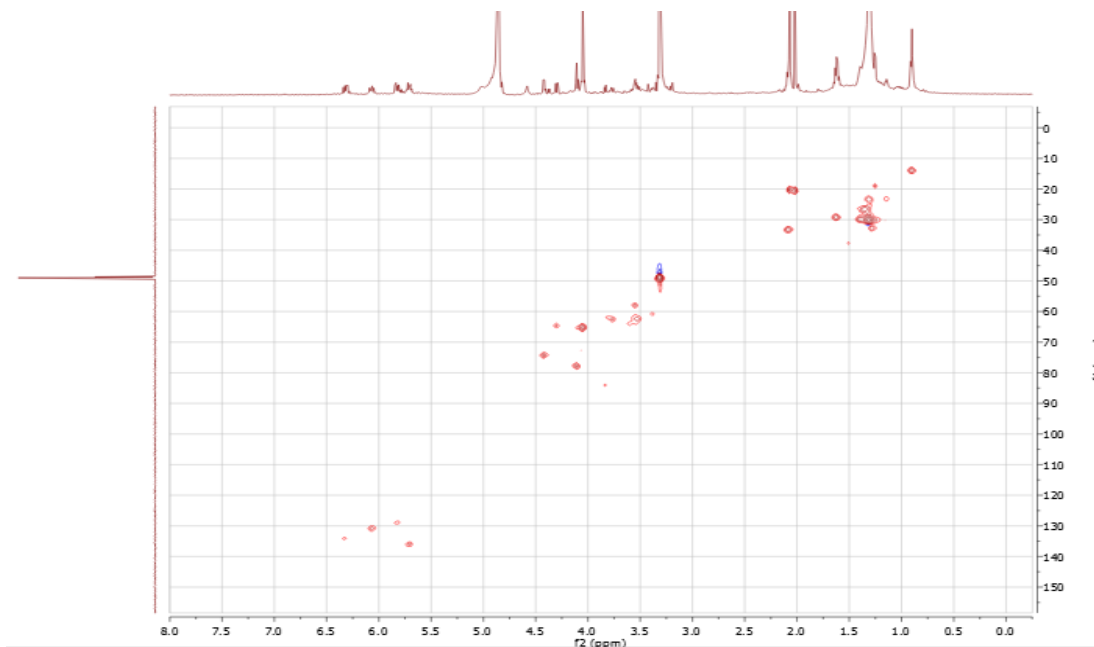
Figure S88. COSY (methanol-d_4) spectrum of compound **12**

49
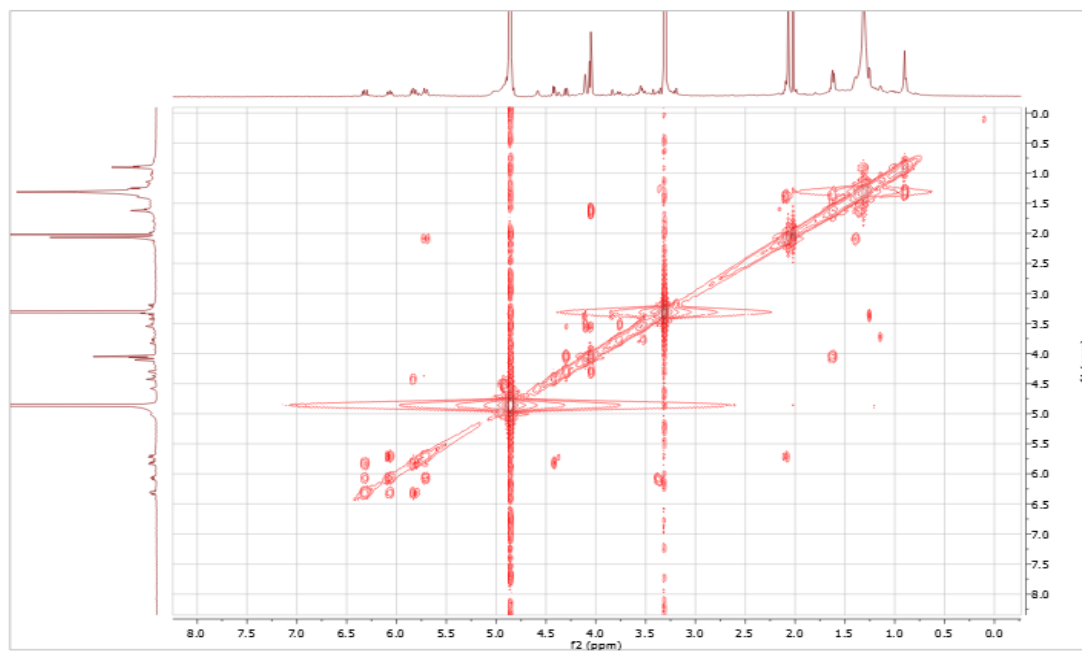
Figure S89. HMBC (methanol-d_4) spectrum of compound **12**
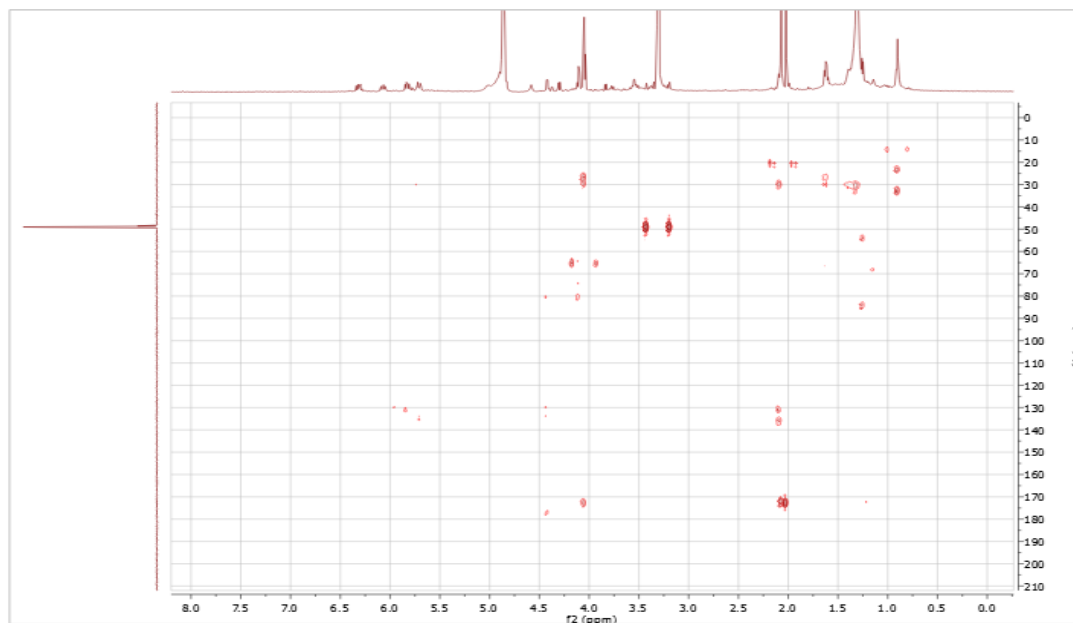
Figure S90. ROESY (methanol-d_4) spectrum of compound **12**

50
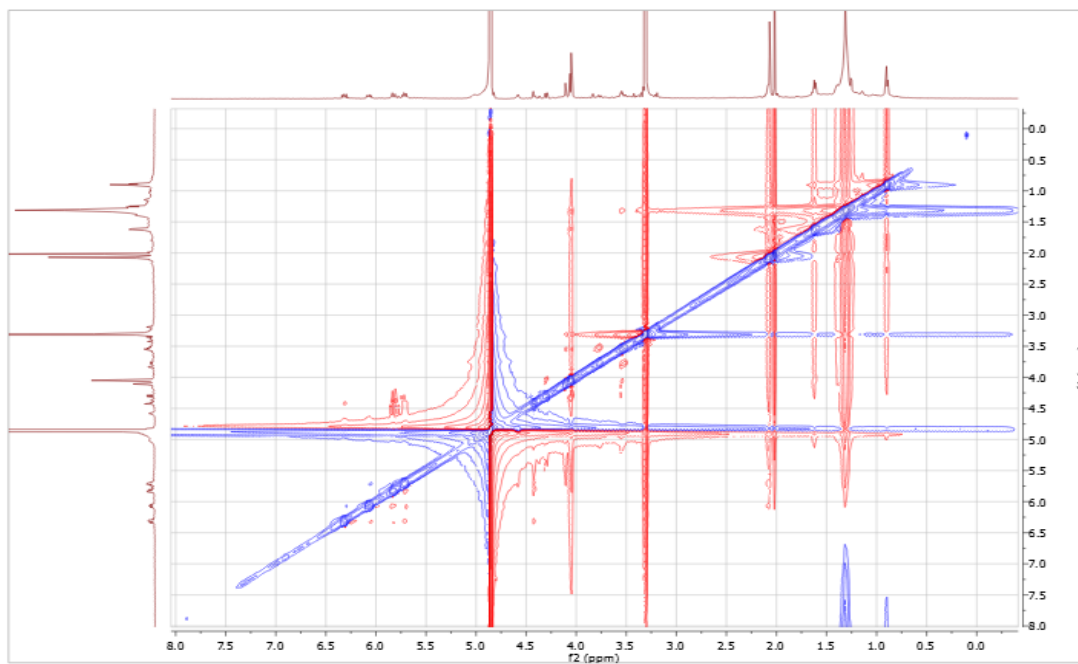
Figure S91. HRESIMS of compound **12**
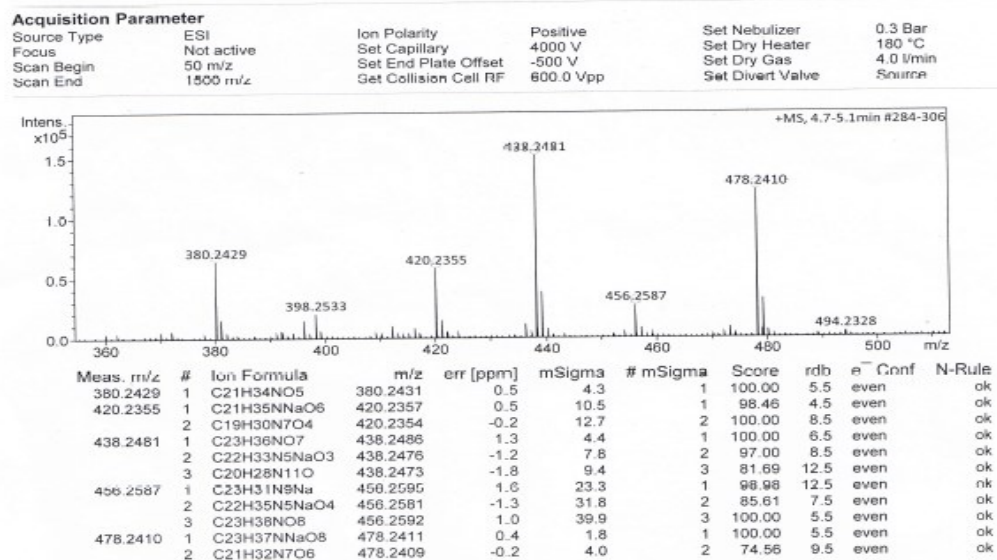
Figure S92. Low-energy conformers and populations of (3*S*,4*S*,5*S*)-**1mod** computed at the ωB97X/TZVP PCM/MeOH level of theory.
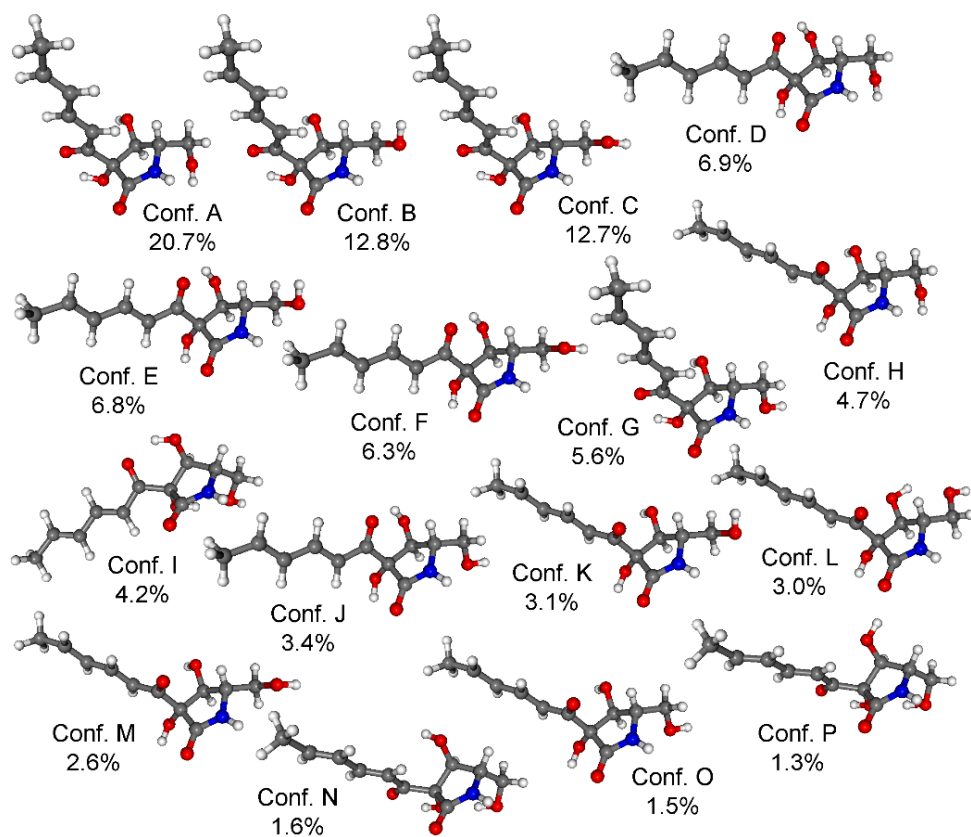
Figure S93. Low-energy conformers and populations of (3*R*,4*S*,5*S*,7*R*)-**2mod** computed at the B3LYP/6-31+G(d,p) level of theory.
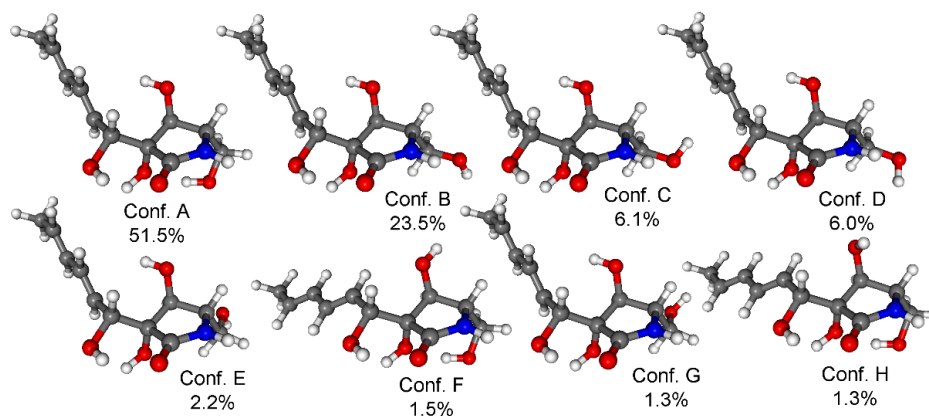
Figure S94. Low-energy conformers and populations of (3*R*,4*S*,5*S*,7*S*)-**2mod** computed at the B3LYP/6-31+G(d,p) level of theory.

53
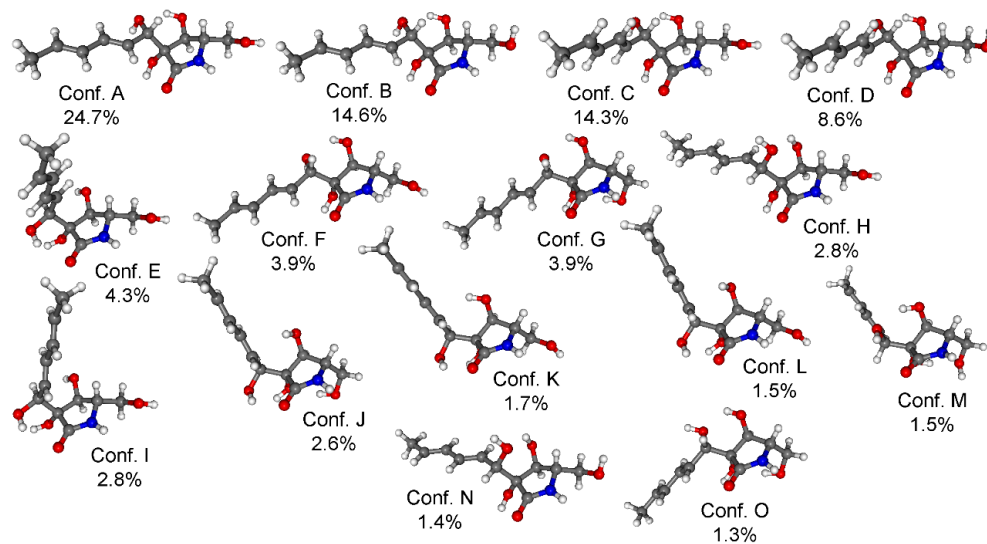
Figure S95. Experimental ECD spectrum of **2** in MeCN compared with the Boltzmann-weighted B3LYP/TZVP PCM/MeCN ECD spectrum of (3*R*,4*S*,5*S*,7*R*)-**2mod**.

Level of optimization: ωB97X/TZVP PCM/MeCN. Bars represent the rotatory strength values of the lowest-energy conformer. The experimental spectrum was scaled to the computed one.
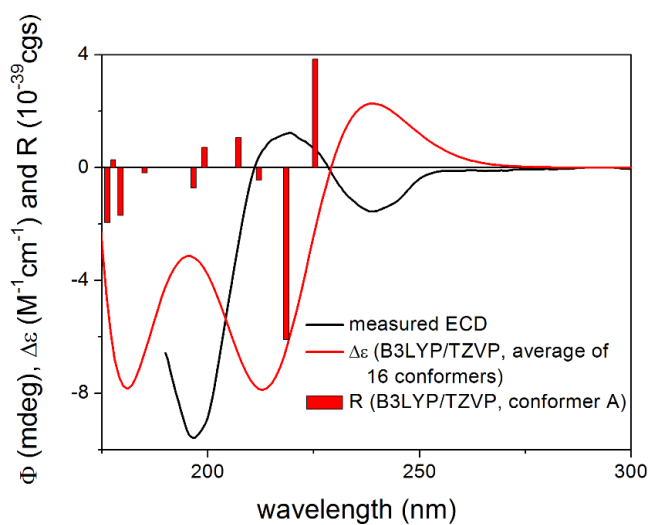
Figure S96. Low-energy conformers and populations of (3*R*,4*S*,5*S*,7*R*)-**2mod** computed at the ωB97X/TZVP PCM/MeCN level of theory.

55
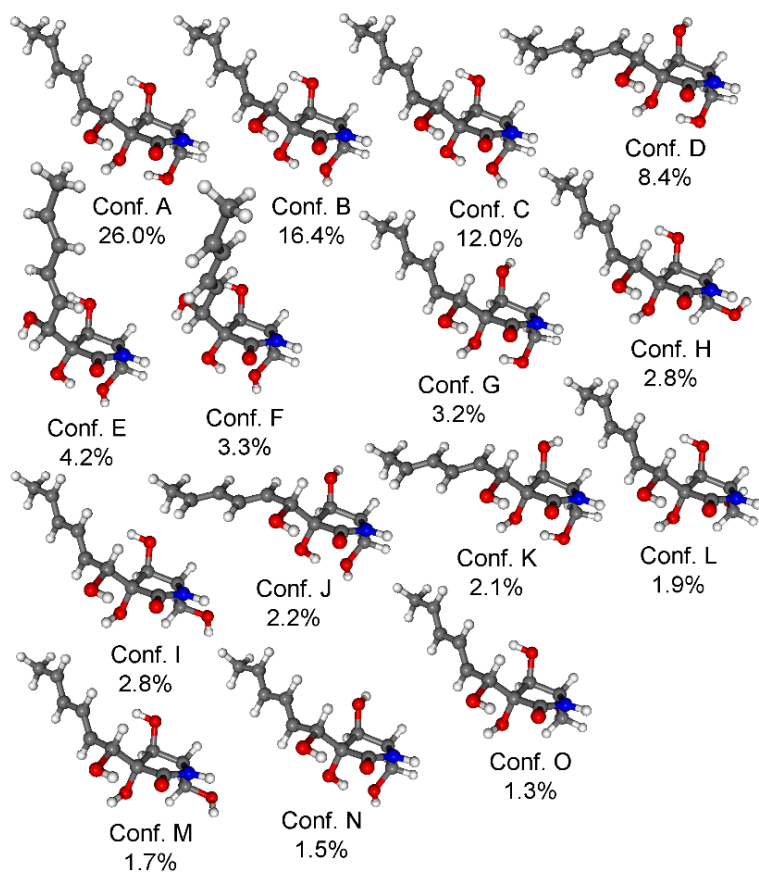
Figure S97. Low-energy conformers and populations of (3*R*,4*S*,5*S*,7*S*)-**2mod** computed at the ωB97X/TZVP PCM/MeCN level of theory.

56
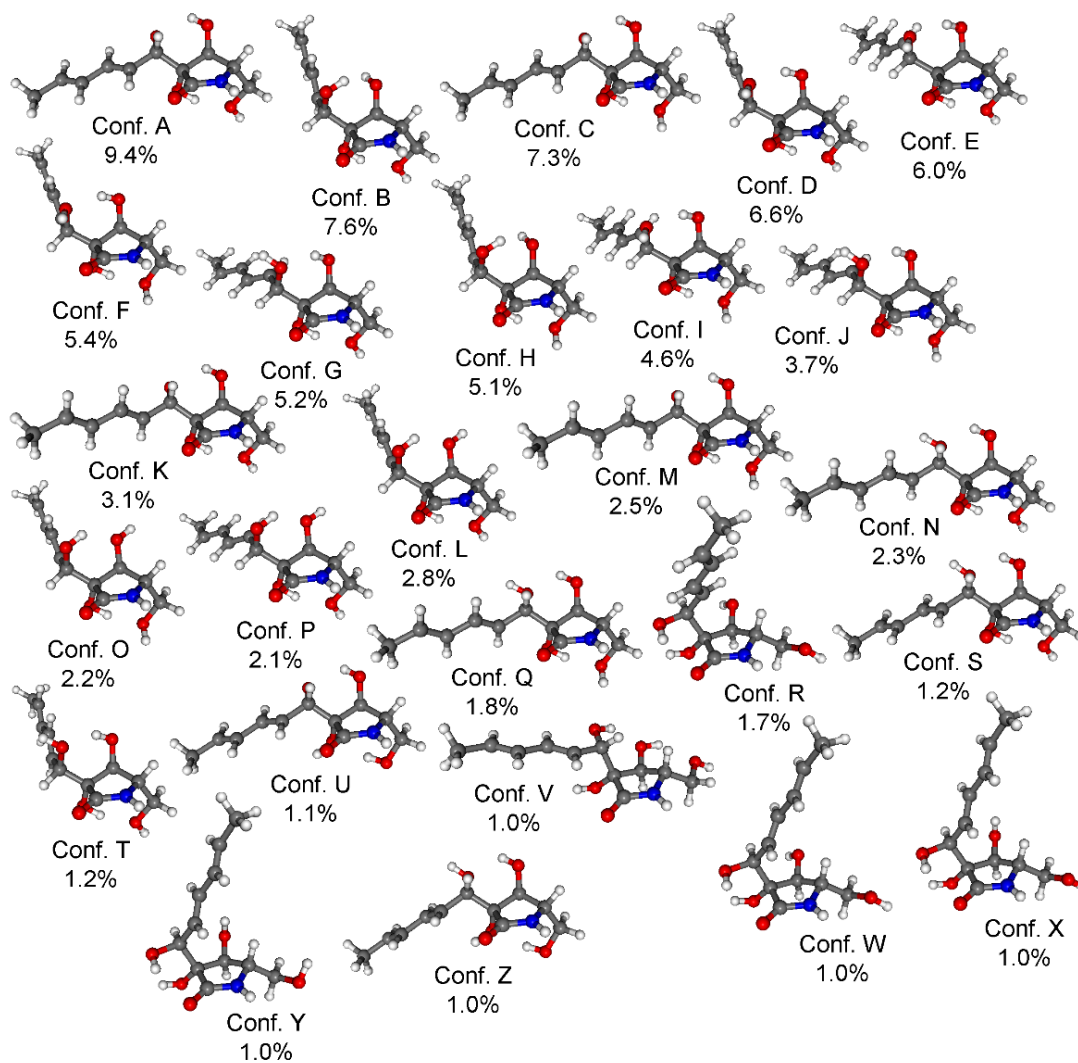
Table S1. Computed SOR values for (3*S*,4*S*,5*S*)-**1mod** at various levels.

Level of optimization	Boltzmann population (%)	ωB97X/TZVP PCM/MeOH			
Level of OR calculation		B3LYP/TZVP PCM/MeOH	BH&HLYP/TZVP PCM/MeOH	CAM-B3LYP/TZVP PCM/MeOH	PBE0/TZVP PCM/MeOH
Conf A	20.73	-60.03	-51.48	-58.60	-57.66
Conf B	12.79	-64.09	-64.99	-70.75	-62.59
Conf C	12.68	-49.89	-51.60	-56.93	-49.38
Conf D	6.88	-318.03	-212.93	-237.03	-295.78
Conf E	6.84	-339.21	-239.35	-263.70	-317.02
Conf F	6.34	-324.85	-225.96	-249.83	-303.68
Conf G	5.63	-70.64	-65.52	-72.08	-69.20
Conf H	4.74	-70.11	-65.06	-62.20	-64.43
Conf I	4.24	58.63	40.13	49.06	55.72
Conf J	3.41	-318.35	-215.63	-239.63	-296.42
Conf K	3.11	-98.38	-100.36	-97.64	-93.64
Conf L	3.02	54.80	31.22	43.09	57.26
Conf M	2.55	-88.36	-90.06	-86.62	-84.33
Conf N	1.60	69.08	50.40	51.91	74.14
Conf O	1.48	-71.23	-72.71	-68.89	-66.53
Conf P	1.31	-11.95	-17.24	-16.59	-11.74
BW Average		-115.13	-90.67	-98.66	-108.36

57

Table S2. Comparison of the experimental ^{13}C NMR data of the carbons of the **2** measured in MeOH-d_4 with the mPW1PW91/6-311+G(2d,p) // B3LYP/6-31+G(d,p) ones of the (3*R*,4*S*,5*S*,7*R*)-**2mod** and (3*R*,4*S*,5*S*,7*S*)-**2mod** stereoisomers.

Numbering	Exp	Calc$_{SSSR}$	Calc$_{SSSS}$	Δδ$_{SSSR}$	Δδ$_{SSSS}$
C-2	177.3	179.49	174.87	2.19	2.43
C-3	80.8	76.60	80.15	4.20	0.65
C-4	77.9	78.39	80.71	0.49	2.81
C-5	61.2	63.70	61.33	2.50	0.13
C-6	62.9	64.58	66.51	1.68	3.61
C-7	74.5	74.63	74.88	0.13	0.38
C-8	129.6	130.54	130.27	0.94	0.67
C-9	134.6	139.14	137.72	4.54	3.12
C-10	131.2	133.58	134.07	2.38	2.87
C-11	136.3	138.92	135.96	2.62	0.34
C-12	33.7	19.51	19.47	14.19	14.23
Average	N/A	N/A	N/A	3.26	2.84
Average without C-12	N/A	N/A	N/A	2.17	1.70

58

Table S3. Computed SOR values for (3*R*,4*S*,5*S*,7*R*)-**2mod** at various levels.

Level of optimization	Boltzmann population (%)	ωB97X/TZVP PCM/MeOH			
Level of OR calculation		B3LYP/TZVP PCM/MeOH	BH&HLYP/TZVP PCM/MeOH	CAM-B3LYP/TZVP PCM/MeOH	PBE0/TZVP PCM/MeOH
Conf A	26.54	-31.08	-19.24	-20.12	-30.61
Conf B	16.04	-45.15	-36.95	-37.62	-43.31
Conf C	11.70	-53.17	-40.90	-42.15	-51.37
Conf D	8.47	214.61	175.58	186.10	207.09
Conf E	4.21	193.76	164.87	172.43	191.92
Conf F	3.24	-28.52	-27.21	-24.12	-30.76
Conf G	3.21	-65.79	-55.78	-55.78	-61.12
Conf H	2.89	-103.64	-85.77	-90.43	-102.12
Conf I	2.85	-83.68	-70.92	-73.96	-83.06
Conf J	2.14	187.81	159.58	165.90	184.01
Conf K	2.06	208.76	176.86	183.19	203.53
Conf L	1.90	34.89	27.74	32.44	32.81
Conf M	1.76	-63.37	-48.68	-51.64	-63.37
Conf N	1.44	-29.30	-33.19	-29.44	-30.24
Conf O	1.29	6.38	4.40	9.01	6.30
BW Average		4.18	5.73	6.87	3.97

59

Table S4. Computed SOR values for (3*R*,4*S*,5*S*,7*S*)-**2mod** at various levels.

Level of optimization	Boltzmann population (%)	ωB97X/TZVP PCM/MeOH			
Level of OR calculation		B3LYP/TZVP PCM/MeOH	BH&HLYP/TZVP PCM/MeOH	CAM-B3LYP/TZVP PCM/MeOH	PBE0/TZVP PCM/MeOH
Conf A	9.40	-84.26	-75.84	-70.66	-85.35
Conf B	7.44	-64.78	-61.18	-57.65	-64.12
Conf C	7.36	-101.23	-88.55	-83.34	-102.01
Conf D	6.68	-84.84	-77.74	-77.61	-85.62
Conf E	6.06	172.44	139.47	148.03	164.32
Conf F	5.47	-93.73	-83.26	-83.85	-94.87
Conf G	5.14	80.73	55.68	64.12	75.91
Conf H	5.00	-70.29	-62.94	-59.72	-69.90
Conf I	4.65	148.52	119.58	128.45	140.59
Conf J	3.69	58.00	36.77	45.74	53.61
Conf K	3.13	-45.18	-36.87	-36.70	-43.87
Conf L	2.64	-68.47	-72.58	-67.38	-69.01
Conf M	2.45	-50.99	-41.29	-40.31	-50.26
Conf N	2.29	55.13	38.35	44.27	48.32
Conf O	2.11	-73.24	-73.82	-69.30	-74.16
Conf P	1.96	56.03	41.84	45.07	52.16

Conf Q	1.82	35.56	22.30	28.48	28.61
Conf R	1.75	-176.10	-151.82	-155.11	-172.35
Conf S	1.19	22.78	2.98	12.94	10.38
Conf T	1.16	-33.80	-41.39	-38.43	-38.72
Conf U	1.15	-30.50	-22.32	-17.68	-35.14
Conf V	1.06	-14.38	-4.92	-5.29	-15.06
Conf W	1.05	-103.87	-68.95	-73.87	-101.42
Conf X	1.05	5.62	5.71	6.32	3.19
Conf Y	1.01	-8.01	-5.83	-5.93	-9.62
Conf Z	0.99	107.71	85.88	94.45	92.45
BW Average		-20.08	-22.44	-18.19	-22.56

61

Chapter 5 Discussion

5.1 Endophytic fungus *Aplosporella javeedii* produces antifungal polyketides

Life-threatening fungal infections have become dramatically more common in human beings due to the increase in the immunocompromised population and aging societies (Barrett 2002). The extensive usage of antibacterial and antifungal drugs also leads to an increase in microbial resistance, which makes eradicating those infections even more challenging (Zacchino *et al.* 2017). Ironically, the number of antifungal drugs that have been used in clinical practice or newly introduced into the market is very limited (Deshmukh *et al.* 2018). Today, the most widely used and approved antifungal compounds are azoles, echinocandins, polyenes and flucytosine (Perfect 2017). Most of them were discovered decades ago. For example, hygromycin B which was developed in the 1950s inhibits protein synthesis and acts against both prokaryotic and eukaryotic cells. In addition, the limitations of these current drugs such as toxicity, fungistatic rather than fungicidal activity, poor pharmacokinetics, narrow spectrum of activity, drug-drug interactions, and emerging drug-resistant fungi restrict their application in clinical therapy (Aldholmi *et al.* 2019, Miller *et al.* 2019). A recent review of antifungal leads from natural products within the last decade revealed that endophytic fungi are the primary source of antifungal compounds (Aldholmi *et al.* 2019). The secondary metabolites of endophytic fungi can be used as antifungal agents directly or as precursor molecules to synthesize antifungal drugs due to their small molecular size and high structural diversity. Therefore, endophytic fungi are an essential source of potential antifungal compounds.

There are many natural products isolated from endophytic fungi exhibiting novel antifungal activities. For example, a novel phenolic compound 4-(2,4,7-trioxa-bicyclo[4.1.0]heptan-3-yl) phenol which was isolated from endophytic fungus

Pestalotiopsis mangiferae associated with *Mangifera indica* Linn, exhibited intense antifungal activity against *C. albicans* with MIC value of 0.039 μg/mL, while the positive control nystatin showed MIC 10.0 μg/mL (Subban *et al.* 2013). Nine oxygenated guaiane-type sesquiterpenes and three isopimarane diterpenes were isolated from endophytic fungus *Xylaria* sp. YM 311647 associated with *Azadirachta indica.* The antifungal results of these compounds revealed that they were moderately active against *Candida albicans* and *Hormodendrum compactum* with MIC values ranging from 16 to 256 μg/mL. One of the isopimaranes, the diterpene 9-deoxy-hymatoxin A, exhibited the most potent inhibitory activity against *C. albicans* and *Pyricularia oryzae* with MIC values of 16 μg/mL (Wu *et al.* 2014). A biphenyl derivative altenusin was isolated from the endophytic fungus *Alternaria alternata* Tche-153 of a Thai medicinal plant *Terminalia chebula* Rezt. The compound when used in combination with each of three azole drugs, ketoconazole, fluconazole or itraconazole at their low sub-inhibitory concentrations displayed potent synergistic activity against *C. albicans* with the fractional inhibitory concentration (FIC) index range of 0.078 to 0.188 (Phaopongthai *et al.* 2013). A new cyclodepsipeptide fusaripeptide A was isolated from the endophytic fungus *Fusarium* sp. associated with *Mentha longifolia.* It exhibited potent antifungal activity toward *C. albicans*, *C. glabrata*, *C. krusei*, and *A. fumigates* with IC_{50} values of 0.11, 0.24, 0.19, and 0.14 μM, respectively, whereas the results of positive control amphotericin B were 0.3, 0.6, 0.5, 0.7 μM, respectively (Ibrahim *et al.* 2018).

Although natural products have proven to be an excellent source of antifungal agents, there is still a long way to go from potential ingredients to clinical drugs. The compounds selected for further investigation need to follow certain criteria to lead to the final success: structurally novel, novel mechanism of action or potentially useful, good biological activity, the possibility of chemical modification (Barrett

2002). In the first publication (Chapter 2), aplojaveediin A which was isolated from the axenic culture of endophytic fungus *Aplosporella javeedii* exhibited potent antifungal activity against *Candida albicans* strain ATCC 24433. Based on its good fungicidal activity and lack of cytotoxicity against human cells, aplojaveediin A could be a promising candidate for the development of new antifungal drugs. Moreover, due to its small molecule weight and simple structure, it is possible to further study chemical modification of aplojaveediin A. Therefore, analyzing the structure-activity relationship (SAR) and identifying the essential structural requirements for its antifungal activity may help us to find novel analogues with enhanced chemical stability and antifungal efficacy.

Upon searching the literature, the structurally similar compound anguillosporal, which was isolated from the freshwater fungus *Anguillospora longissima* showed moderate antifungal activity against *Candida albicans* with MIC value of 58 μg/mL (Harrigan *et al.* 1995). 2,4-Dihydroxyacylophenones and related compounds exhibited antifungal activity against *Trichophyton* spp and other fungi. SAR studies showed that their antifungal activity was closely correlated to the length of the acyl and alkyl substituents attached to the 1,3-dihydroxybenzene moiety (Mizobuchi *et al.* 1985). The initial SAR studies of the antifungal agent 2,4-dihydroxy-5-methylacetophenone showed the importance of 2,4-dihydroxy groups for its antifungal activity against five plant fungal pathogens including *Cytospora* sp., *Glomerella cingulate*, *Pyricularia oryzaecar*, *Botrytis cinerea* and *Alternaria solani*. Moreover, the increased hydrophobicity of acetophenone derivatives can improve their antifungal activity. Among the synthetic acetophenone analogues, 1-(2,4-dihydroxy-5-methylphenyl)-2-methyl-1-propanone showed a remarkable in vitro antifungal activity against the tested organisms with IC$_{50}$ values of 17.28–32.32 μg/mL. The results suggested that an increase in chain length of linear alkyl ketones led to enhanced antifungal activity, whereas branched alkyl ketones exhibited

stronger activity than linear alkyl ketones in general (Shi *et al.* 2016). Acylphloroglucinol compound jensenone exhibited antifungal activity with an IC_{50} value of 5.5 μg/mL against *C. albicans*, while it was inactive against *C. neoformans* and *A. fumigatus*. However, its synthetic analogue 2,4,6-trihydroxy-3-(3-hydroxy-2-methyl-acryloyl)-benzaldehyde showed improved antifungal activity against *C. albicans* and *C. neoformans* with an IC_{50} of 2.0 and 2.5 μg/mL, respectively, and was fungicidal toward *C. albicans*. It seems that the length of the acyl side chain is the major contributing factor to its antifungal activity, and decrease in acyl chain length or replacement of an acyl with an alkyl substituent resulted in loss of activity (Bharate *et al.* 2007).

In our research, the co-isolated compounds aplojaveediin B-F, which were slightly different in their structures compared to aplojaveediin A, showed inactivity when tested against *C. albicans*. When comparing unique structural features of aplojaveediin A to its inactive derivatives, it occurs as obvious that the presence of polar groups attached to the side chain as well as shortening of the side chain may weaken the antifungal activity. It might refer that 2,6-dihydroxy-benzaldehyde moiety and the lipophilicity of the compounds are important for their antifungal activity. The hypothesis about the side chain is that the addition of the aliphatic side chains may increase the lipophilicity of the compounds, leading to better penetration across the fungi's plasmatic membrane and thus enhancing their antifungal activity. Therefore, it is believed that the structural modification of aplojaveediin A or synthesis of its analogues will provide more information on SAR to find enhanced antifungal drugs and be of interest in further research.

Aplojaveediin A

Aplojaveediin B

Aplojaveediin C

Aplojaveediin D

Aplojaveediin E

Aplojaveediin F

Anguillosporal

2,4-Dihydroxyacetophenone

2,4-Dihydroxy-5-methylacetophenone

1-(2,4-Dihydroxy-5-methylphenyl)-2-methyl-1-propanone

Jensenone

2,4,6-Trihydroxy-3-(3-hydroxy-2-methyl-acryloyl)-benzaldehyde
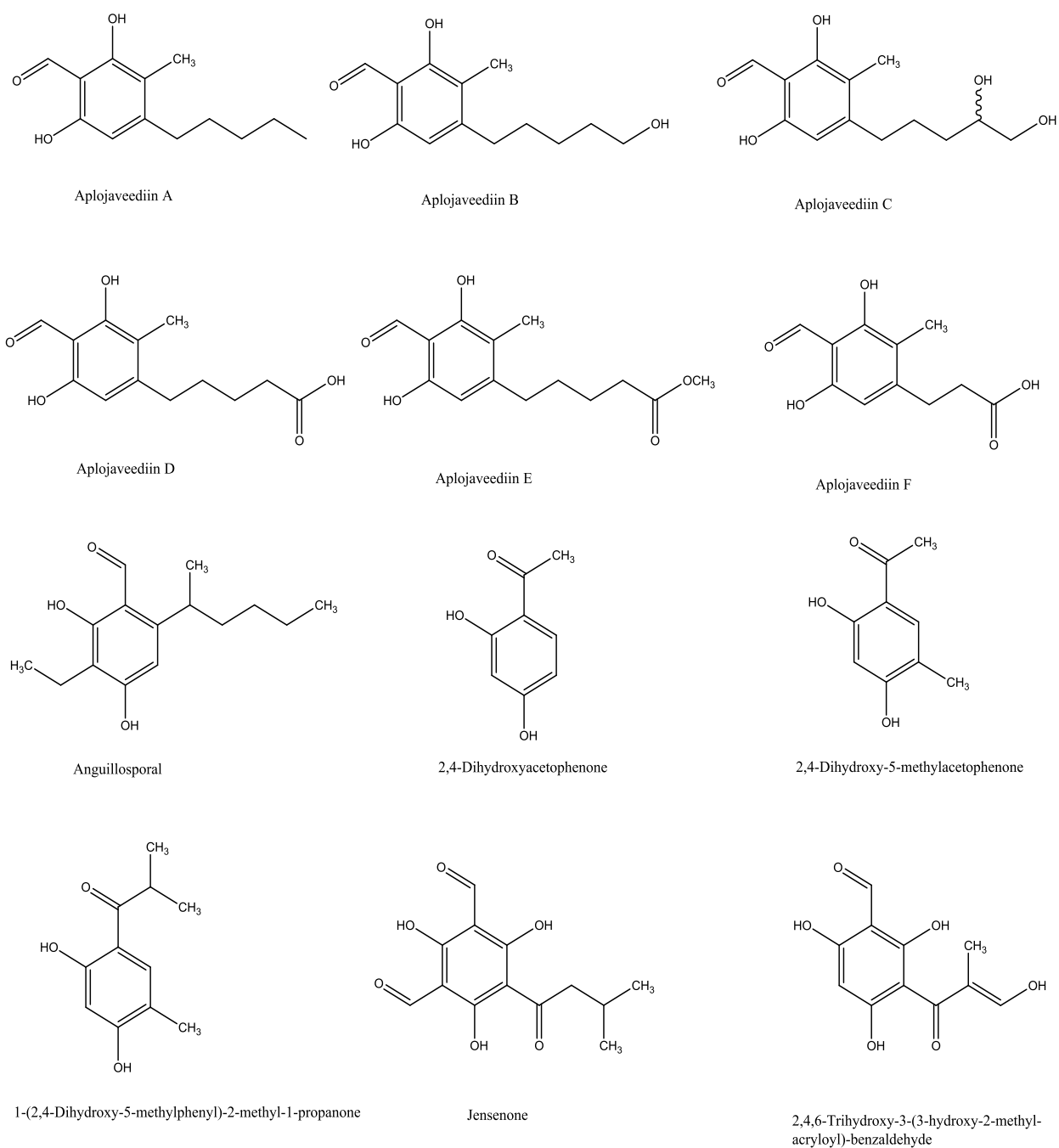
Figure 5.1 Structural analogues of aplojaveediin A

5.2 Endophytic fungus *Aplosporella javeedii* produces cytotoxic sesterterpenes and macrolide derivatives

5.2.1 Sesterterpene derivatives

Bicyclo-sesterterpenes terpestacin and fusaproliferin are well known mycotoxins which exhibit the same skeleton. Terpestacin was first isolated from *Arthriniuna* sp. and showed syncytium formation inhibitory activity during HIV infection (Oka, Iimura, Tenmyo*, et al.* 1993, Oka, Iimura, Narita*, et al.* 1993, Iimura *et al.* 1993). Later, it was also isolated as a phytotoxin from *Bipolaris cynodontis* (Lim 1995). Recent bioassay research revealed that terpestacin exhibits good antiangiogenic activity without affecting endothelial cell viability, which could make it suitable to be used as an anticancer agent (Jung *et al.* 2003, 2010, Park *et al.* 2013). The absolute configuration and biosynthetic pathway of terpestacin has been confirmed by NMR, X-ray crystallographic analysis (Oka, Iimura, Narita*, et al.* 1993) and total enantioselective synthesis (Chan *et al.* 2003, 2004, Berger *et al.* 2005, 2007).

Fusaproliferin, which is a primary acetate derivative of terpestacin, was isolated from a strain of the human pathogenic fungus *Fusarium proliferatum* (Ritieni *et al.* 1995). It was reported to exhibit potent and rapid cytotoxicity against both pancreatic and breast cancer cell lines (Hoque *et al.* 2018). In addition, it also showed teratogenic effects on chicken embryos (Ritieni *et al.* 1997) and toxicity on *Artemia salina*, insect cells and human B lymphocytes (Logrieco *et al.* 1996). The absolute configuration of fusaproliferin has been determined by single crystal X-ray diffraction analysis (Santini *et al.* 1996). Due to the structural novelty as well as intriguing biological activity of these two compounds, some key hemisynthetic derivatives were prepared and SAR was discussed regarding their antifungal activity against some ascomycetous fungi such as *Alternaria brassicicola*, *Botrytis cinerea*

and *Fusarium graminearum*. The results showed that these two compounds are allelopathic to other fungi, and the enolic hydroxyl group at C17 is a structural feature important to impart activity (Cimmino *et al.* 2016).

In the second publication (Chapter 3), fusaproliferin (FUS) was found to exhibit potent cytotoxicity against the L5178Y cell line after 72 h of incubation, whereas terpestacin was inactive in comparison. This implies that the presence of an acetyl function in fusaproliferin increases the cytotoxicity compared to the hydroxyl analogue terpestacin. Therefore, acetyl derivatives were prepared to explore the effect of acetyl groups on their cytotoxic activity. The diacetyl derivatives **a** and **b** and the triacetyl derivative **c** were prepared by acetylation of FUS. The cytotoxic effects against L5178Y cells were determined in the order of **b**<FUS=**c**<**a** after 72 h of incubation. Thus, acetylation of the hydroxyl group at C-17 increased the cytotoxicity against L5178Y cells relative to FUS. In the human lymphoma (Ramos) cell line the cytotoxic effects were determined in the order of **a**<FUS=**c**, whereas **b** was inactive, after 24 h of incubation. Meanwhile, the cytotoxic effects against the human leukemia (Jurkat J16) cell line were determined as **a** equipotent to **c**, whereas FUS and **b** were inactive. Hence **a** and **c** showed cytotoxicity against both human cell lines, while **b** was inactive ($IC_{50} > 20\,\mu M$) against both cell lines in comparison. In conclusion, compound **a** with acetyl functions at C-17 and C-24 is a favorable structure for cytotoxicity against human lymphoma (Ramos) and human leukemia (Jurkat J16) cell lines.

Terpestacin

Fusaproliferin

a

b

c
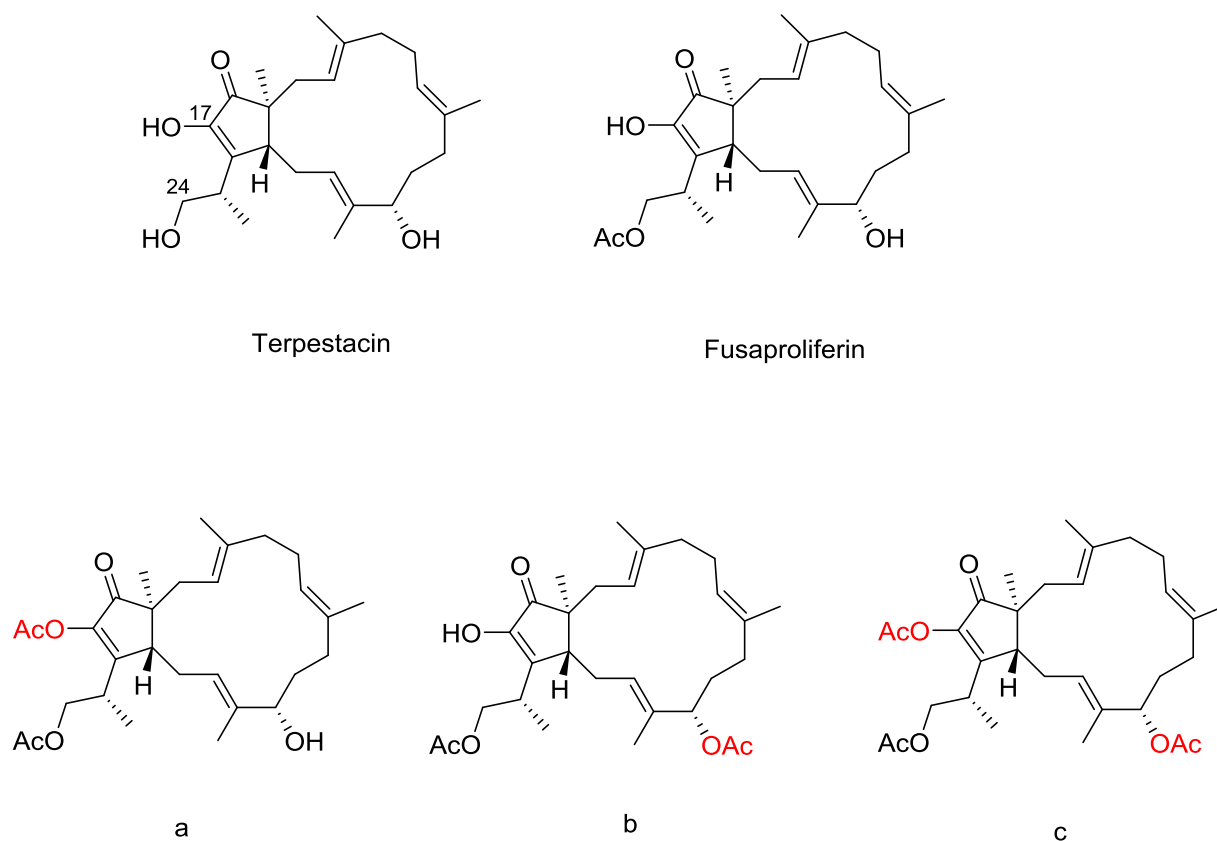
Figure 5.2 Terpestacin and its acetate derivatives

5.2.2 Macrolide derivatives

Two 14-membered macrolides were isolated from the endophytic fungus *Aplosporella javeedii*. The known macrolide mutolide was first discovered from a UV mutagenesis strain of the fungus *Sphaeropsidales* sp. Its absolute configuration was confirmed by the advanced Mosher's ester methodology, X-ray analysis and derivatisation. Feeding experiment proved that mutolide was generated from acetate/malonate only (Bode *et al.* 2000). More recently, mutolide was isolated from the coprophilous fungus *Lepidosphaeria* sp. and showed excellent anti-inflammatory activity. Mechanistic studies indicated that mutolide inhibits induced

NF‑κB activation and translocation from cytoplasm into the nucleus (Shah *et al.* 2015).

In our research (Chapter 3 Publication 2), the known macrolide mutolide was found to exhibit significant cytotoxicity against the L5178Y cell line, as well as against the human leukemia (Jurkat J16) and lymphoma (Ramos) cell lines. Mechanistic evaluations revealed that mutolide induces apoptotic cell death and thus could be considered as a candidate for an anticancer agent. However, the co-isolated new compound 6,7,9,10-tetrahydromutolide was inactive in cytotoxicity tests. 6,7,9,10-tetrahydromutolide is an epimer of pestalotioprolide C, with the only difference being the stereocenter at C-14, which is configured *R* in 6,7,9,10-tetrahydromutolide instead of *S* as in pestalotioprolides C. Pestalotioprolide C also showed no cytotoxicity against the L5178Y cell line in the research of Liu *et al.* 2016. It means that the double bonds at $\Delta^{6,7}$ and $\Delta^{9,10}$ in the 14-membered ring of mutolide are important for cytotoxicity compared to 6,7,9,10-tetrahydromutolide.

Furthermore, the cytotoxicity of 11 14-membered macrolides, which were isolated from endophytic fungus *Pestalotiopsis microspora,* was evaluated in the literature, which provided additional SAR information for 14-membered macrolides (Liu *et al.* 2016). It was discovered that the epoxy group at C-6/C-7 leads to the loss of cytotoxicity (seiricuprolide vs nigrosporolide), whereas the *O*-methylation of the hydroxyl group at C-8 (7-O-methylnigrosporolide vs nigrosporolide) or C-10 (pestalotioprolide H vs pestalotioprolide G) resulted in a strong increase of cytotoxicity. Meanwhile, the rearrangement of the double bond from C-3/C-4 to the C-4 ketone (pestalotioprolide E and pestalotioprolide F vs pestalotioprolide G) decreases the cytotoxicity, and the configuration at C-5 has little influence on the cytotoxicity (pestalotioprolide E vs pestalotioprolide F).

6,7,9,10-Tetrahydromutolide   Mutolide   Seiricuprolide

7-O-Methylnigrosporolide R=Me
Nigrosporolide   R=H

Pestalotioprolide E R=α-OH
Pestalotioprolide F R=β-OH

Pestalotioprolide G R=H
Pestalotioprolide H R=Me
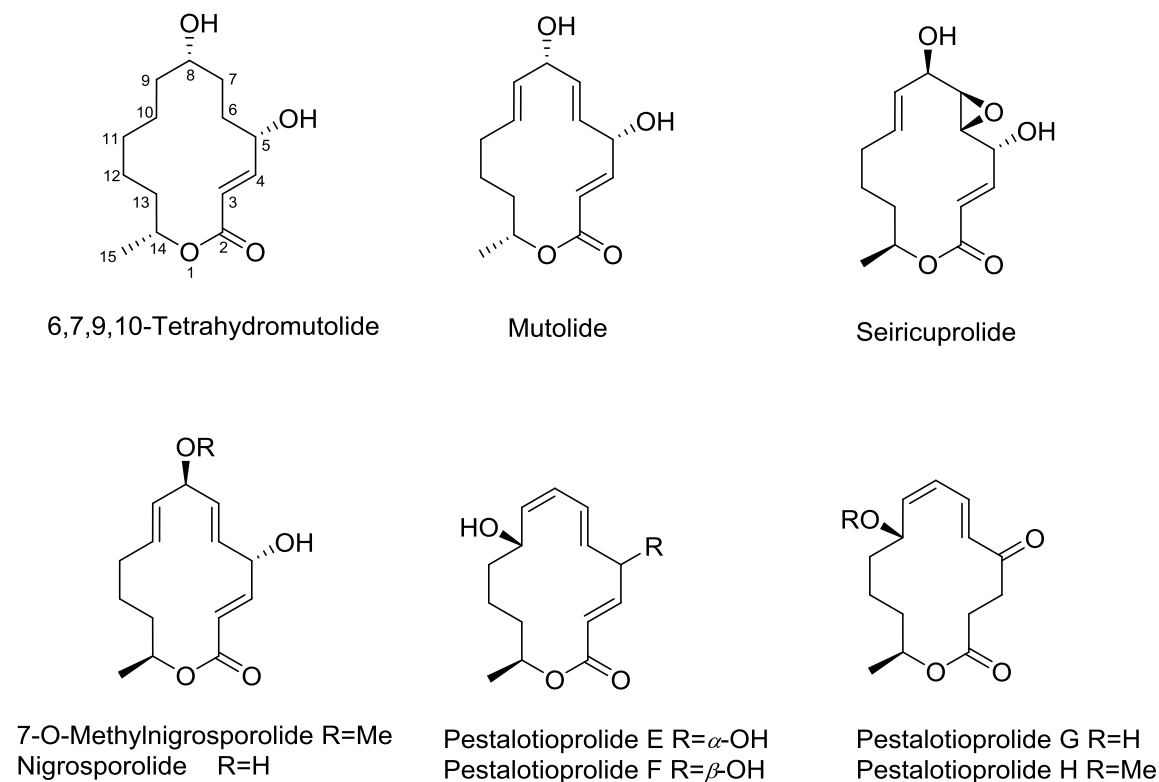
Figure 5.3 14-Membered macrolides

5.3 OSMAC approach diversified secondary metabolites of endophytic fungus *Aplosporella javeedii*

5.3.1 OSMAC is a powerful method to mine the chemical diversity of fungi

As a part of our ongoing study on searching new natural products from endophytic fungus *Aplosporella javeedii*, the OSMAC approach was used to diversify the chemical profile of secondary metabolites. The chemical profiles of *A. javeedii* were studied by adding different salts to solid rice medium, including 3.5% NaBr, 3.5% NaCl, 3.5% KCl, 3.5% NH_4Cl, 3.5% $(NH_4)_2SO_4$, 3.5% $C_5H_8NNaO_4\cdot H_2O$ (monosodium glutamate), 3.5% $NaNO_3$, 3.5%KH_2PO_4, 3.5% $K_2HPO_4\cdot 3H_2O$, 3.5% Na_2HPO_4, 3.5% NaF, 3.5% $FeSO_4$, 3.5%$ZnSO_4$, 3.5%$MgSO_4$. As a result, the fungus did not grow on rice medium in the presence of 3.5% Na_2HPO_4, 3.5% NaF, 3.5% $FeSO_4$, or 3.5% $ZnSO_4$, while the addition of 3.5% NaBr,

NaCl, KCl, NH$_4$Cl, (NH$_4$)$_2$SO$_4$, KH$_2$PO, K$_2$HPO$_4$·3H$_2$O, or MgSO$_4$ had no detectable influence. However, there are significant changes in the chromatographic profile when adding either 3.5% NaNO$_3$ or 3.5% C$_5$H$_8$NNaO$_4$·H$_2$O (monosodium glutamate) to solid rice medium compared to that of the fungus grown only on rice (**Figure 5.4**).
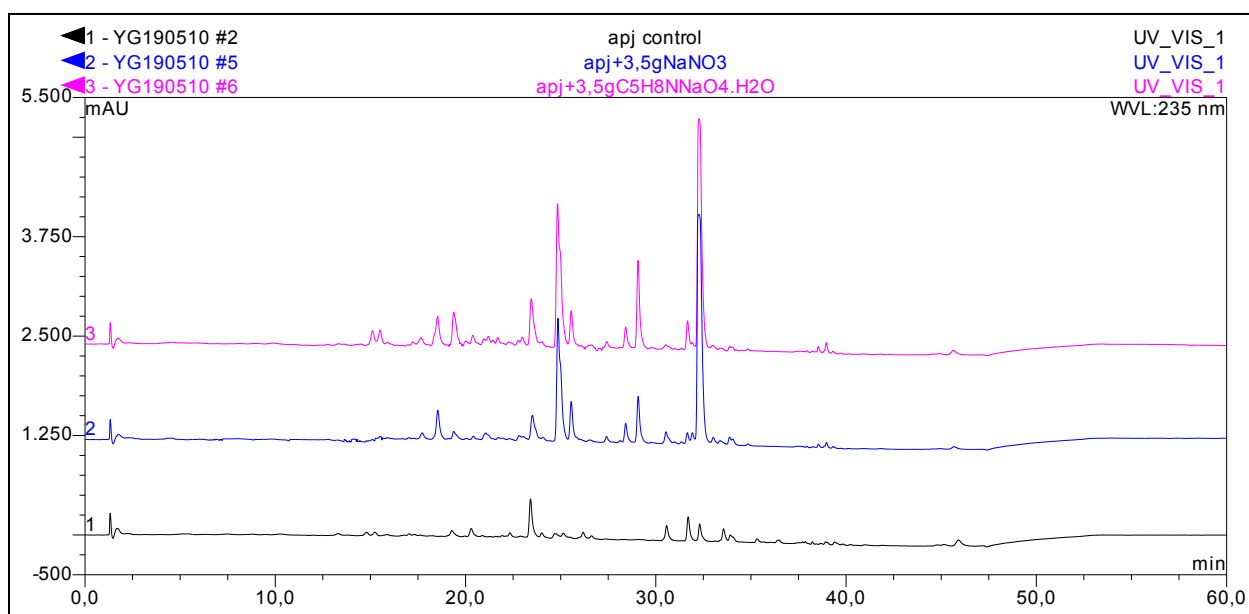
Figure 5.4 HPLC chromatograms of the EtOAc extracts from OSMAC experiments (3.5% NaNO$_3$ or 3.5% monosodium glutamate) detected at 235 nm: (1) *A. javeedii* control grown on solid rice medium; (2) *A. javeedii* cultured on solid rice medium with 3.5% NaNO$_3$; (3) *A. javeedii* cultured on solid rice medium with 3.5% monosodium glutamate.

Chemical investigation of fungal extracts obtained from the fermentation of *A. javeedii* in the presence of either 3.5% NaNO$_3$ or 3.5% monosodium glutamate led to the isolation of 12 lactam derivatives, including pramanicin A and 11 new pramanicin-like derivatives aplosporellins A–K. All of these lactam derivatives were not detected in fungal cultures without salt or with other salts. These results suggest that NaNO$_3$ and monosodium glutamate provide the fungus with additional nitrogen sources for the biosynthesis of these lactam derivatives.

Meanwhile, the addition of 3.5% NaI to the solid rice medium also induced new peaks with different UV spectra that were not detected in the control or other salt fermentations (**Figure 5.5**). The chemical investigation of this fungal extract is still ongoing at this time. Since the currently isolated compounds do not contain iodine atoms, the effect of NaI on fungal biosynthetic pathway is unknown. Iodide ions may activate silent gene clusters of *A. javeedii* without being substrates themselves.
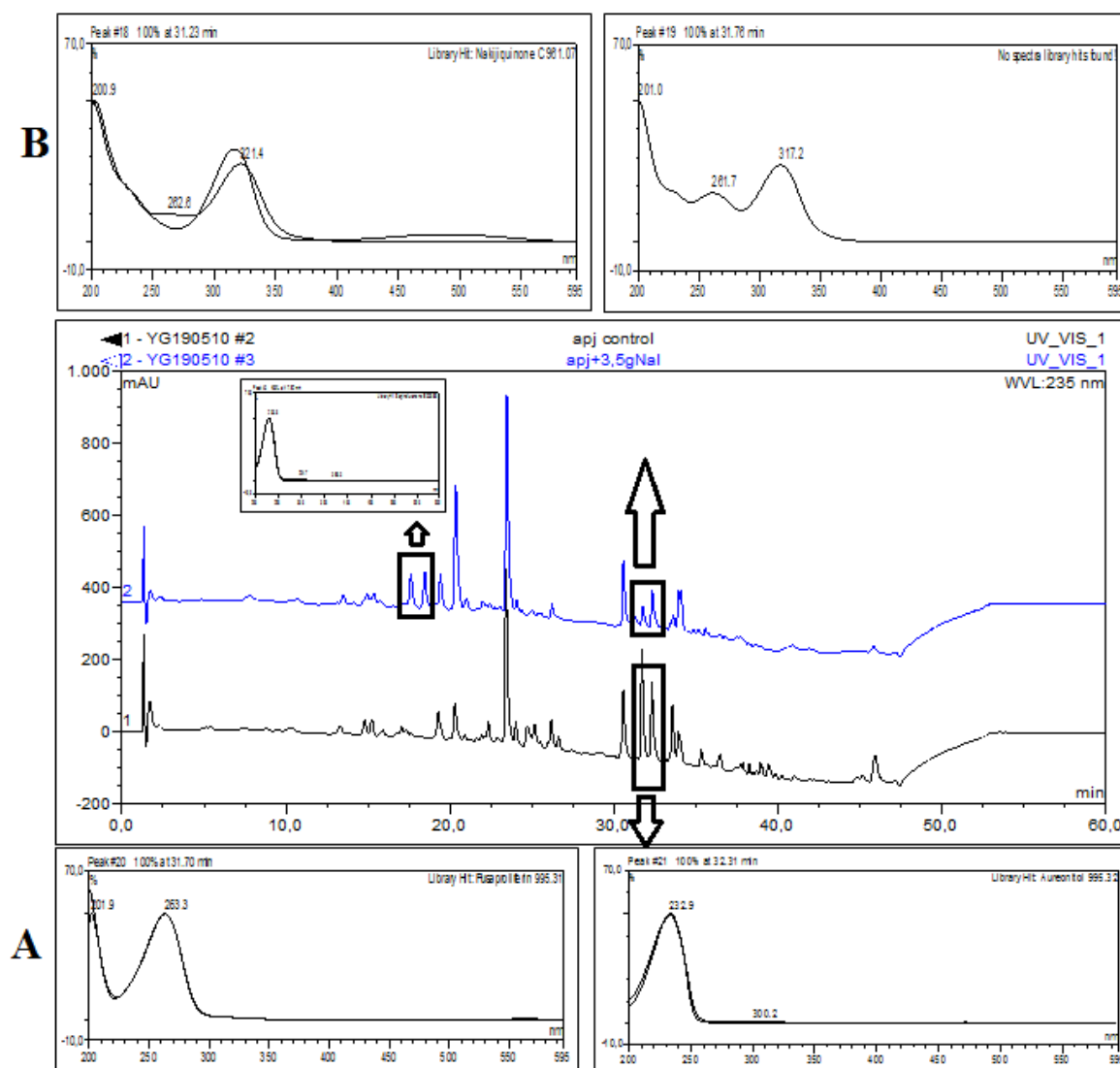
Figure 5.5 HPLC chromatogram of the EtOAc extract from OSMAC experiment

(3.5% NaI) detected at 235 nm: (A) UV spectra of two peaks around 31 min in *A. javeedii* control fermentation; (B) UV spectra of new peaks as well as two peaks around 31 min in *A. javeedii* cultured in the presence of 3.5% NaI.

5.3.2 Pramanicin-like derivatives

The antimicrobial agent pramanicin and pramanicin A, which contain a highly functionalized γ-lactam-based headgroup with a functionalized lipophilic side chain, were first isolated and reported from the fungus *Stagonospora* sp. (Schwartz *et al.* 1994). The difference between pramanicin and pramanicin A being the presence of an epoxide group at C-10/C-11 in the former instead of a double bond in the latter. Full confirmation of the absolute configuration of natural pramanicin came after the total synthesis of (+)-pramanicin was accomplished by Barrett and co-workers, as well as the synthesis of the fatty acid (Barrett *et al.* 1999a, b, Cow *et al.* 1997). (+)-Pramanicin is the enantiomer of the natural product pramanicin, and thus the ^{1}H and ^{13}C NMR spectra of both compounds are identical. However, the numerical value of the specific optical rotation of (+)-pramanicin is opposite to that of the natural one, thus establishing the absolute stereochemistry of natural product pramanicin through the total synthesis of (+)-pramanicin.

The biosynthesis of pramanicin has also attracted the attention of scientists. Duspara *et al.* added ^{13}C and ^{15}N labeled serine to production cultures, and it was shown that labeled L-serine as an intact entity was incorporated into pramanicin. It suggested that L-serine is the true biosynthetic precursor for pramanicin, and the absolute configuration at C-5 of pramanicin is 5S which is identical to that of C-2 of L-serine (Duspara *et al.* 1998). Harrison *et al.* incorporated the labeled acetates and serine into pramanicin in fungal cultures, and found that the carbon skeleton of pramanicin is produced by eight acetate units and a serine residue. They revealed

that acetate and L-serine were the probable precursors to pramanicin and consistent with a biosynthetic pathway of 3-acyltetramic acids (Harrison *et al.* 1998). Subsequently, Harrison and co-workers conducted the isotopically labeled feeding experiment by using ^{2}H, ^{13}C, ^{15}N, and ^{18}O isotopically labeled precursors in *Stagonospora* sp. They concluded that pramanicin originated from a starter acetate with six extender malonates to generate the aliphatic acyl tail, and L-serine interacts with one acetate to form the pyrrolidone ring, then acetylation of these two moieties to provide 3-acyltetramic acid, followed by a series of oxidation reduction reactions to form pramanicin. This experiment also elucidated details of the structure of pramanicin A which was a byproduct during the fermentation. It indicated that pramanicin A exibits the same stereochemistry as pramanicin. (Harrison *et al.* 2000) Meanwhile, other research demonstrated that proline and glutamate could not be precursors of the pyrrolidone moiety of pramanicin (Harrison *et al.* 1998).

However, in our study, the addition of 3.5% $NaNO_3$ or of 3.5% $C_5H_8NNaO_4 \cdot H_2O$ to solid rice medium was able to induce the production of pramanicin-like compounds, which may be due to the presence of the precursors required for the pyrrolidone ring formation. Otherwise, the yield of pramanicin-like compounds in addition of 3.5% $C_5H_8NNaO_4 \cdot H_2O$ medium is 1.2 times the yield of them in addition of $NaNO_3$ medium. It probably means that $C_5H_8NNaO_4 \cdot H_2O$ was an efficient precursor to pramanicin-like compounds. Therefore, the biosynthetic pathway of isolated pramanicin-like compounds using $C_5H_8NNaO_4 \cdot H_2O$ as precursor in Publication 3 can be hypothesized based on the above evidences (**Figure 5.6**). A feeding study using labeled glutamate as a potential precursor of pramanicin-like compounds would be of interest as a follow up investigation.
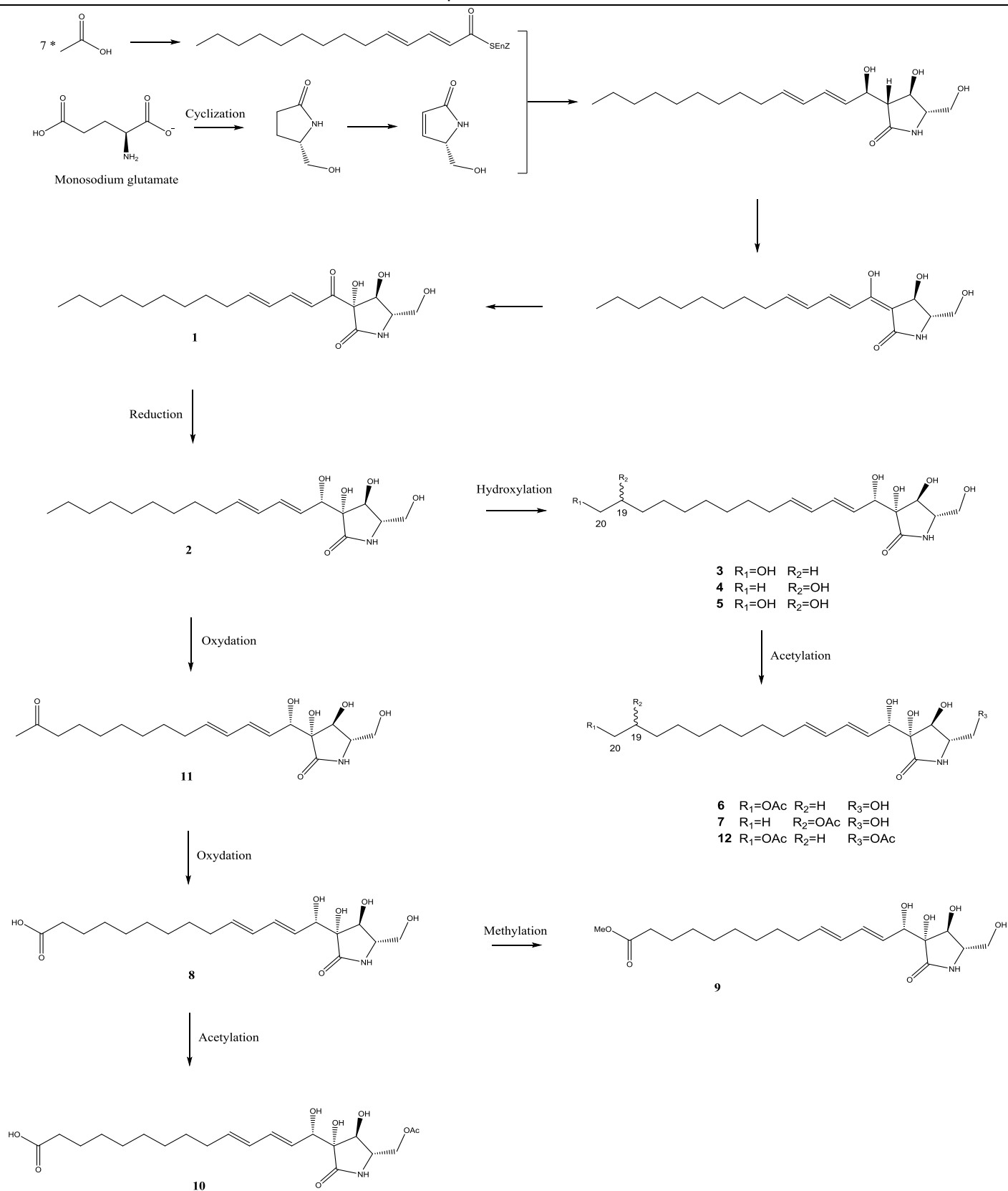
Figure 5.6 Proposed biosynthetic pathway of isolated pramanicin-like compounds in Chapter 4 Publication 3. Numbers refer to the compounds' numbers in publication 3.

In the bioactive research of pramanicin, it was first isolated as an inhibitor of *Cryptococcus neoformans* (MY2062), *Candida parapsilosis* (MY 1010) and *Bacillus subtilis* (MB 964) (Schwartz *et al.* 1994). In 2001, Kwan *et al.* found that pramanicin exhibited endothelium-dependent and NO-mediated vasorelaxant effects (Kwan *et al.* 2001). Two years later, they also found it was able to raise cytosolic Ca^{2+} and cause cell death in vascular endothelial cells. However, pramanicin A which possesses a C=C double bond instead of the epoxy group of pramanicin, as well as pramanicin B which reduce both double bonds of the diene system in pramanicin, caused little endothelial-dependent relaxation, indicating that the epoxy group between the aliphatic side chain moiety and the polar acyltetramic acid entity play an important role in the vasorelaxant effect (Kwan, Harrison*, et al.* 2003, Kwan, Zhang*, et al.* 2003).

In 2005, Kutuk *et al.* explored the pro-apoptotic effects in Jurkat T leukemia cells caused by pramanicin. Mechanistic research showed that pramanicin induced the release of cytochrome c as well as caspase-9 and caspase-3 activation, and also activated c-jun N-terminal kinase (JNK), p38 and extracellular signal-regulated kinases. These results suggested that pramanicin can be a potential pro-apoptosis agent in Jurkat T leukemia cells, and acts through a JNK- and p38-dependent apoptosis signaling pathway (Kutuk *et al.* 2005). Bodur *et al.* screened pramanicin and its analogues for their cytotoxicity against HCT116 human colon cancer cells in 2013. Pramanicin A was found to be a remarkably potent cytotoxic compound which led to apoptosis through activation of caspase-9 and caspase-3. Detailed mechanistic study revealed that p53-independent transcriptional Bcl-2 downregulation and p38 signaling are the key modulatory factors in pramanicin A induced apoptosis in HCT116 human colon cancer cells. Meanwhile, the SAR research in this experiment found that an acylated pyrrolidinone is the key pharmacophore for their pro-apoptosis activity (Bodur *et al.* 2013).

In our research (Charpter 4 Publication 3), pramanicin A exhibited pronounced cytotoxicity against human lymphoma (Ramos) and leukemia (Jurkat J16) cell lines which was due to the activation of caspase-3 and induction of apoptotic cell death. However, other analogues isolated in publication 3 showed no cytotoxicity against these cell lines, indicating that the ketone group at C-7 of pramanicin A which is α,β-unsaturated ketone functionality is the key pharmacophore for its cytotoxicity against human Ramos and Jurkat J16 cell lines. Furthermore, in the antimicrobial assay, pramanicin A showed weak antibacterial activities against *Staphylococcus aureus* ATCC 29213 and *Acinetobacter baumannii* (BAA1605+ Colistin 0.1 μM) with MICs of 100 μM, respectively. Other isolated compounds were inactive in these experiments. It means that the ketone group at C-7 of pramanicin A is also important for its antibacterial activities.

α,β-Unsaturated ketone groups have potential Michael acceptor activity which can add nucleophiles to the electrophilic β-position of the unsaturated system, leading to multiple biological activities, such as cytotoxicity, anti-inflammatory activity, anti-oxidant activity, radical scavenging activity, cyto-/chemoprotection and chemoprevention (Amslinger 2010). The cytotoxic property of α,β-unsaturated ketone groups could due to its Michael-addition reaction with a thiol group of cysteine amino acid of proteins or enzymes thus inducing apoptotic cell damage (Darsih *et al.* 2015). Therefore, α,β-unsaturated ketone compounds such as pramanicin A could be useful for the design of anticancer agents and irreversible enzyme inhibitors.

References

Abdelwahab, M. F., Kurtán, T., Mándi, A., Müller, W. E. G., Fouad, M. A., Kamel, M. S., et al. 2018. "Induced secondary metabolites from the endophytic fungus *Aspergillus versicolor* through bacterial co-culture and OSMAC approaches." *Tetrahedron Lett.* 59 (27):2647-2652. doi: 10.1016/j.tetlet.2018.05.067.

Aldholmi, M., Marchand, P., Ourliac-Garnier, I., Le Pape, P., and Ganesan, A. 2019. "A decade of antifungal leads from natural products: 2010-2019." *Pharmaceuticals (Basel)* 12 (4):182. doi: 10.3390/ph12040182.

Aly, A. H., Debbab, A., Kjer, J., and Proksch, P. 2010. "Fungal endophytes from higher plants: a prolific source of phytochemicals and other bioactive natural products." *Fungal Diversity* 41 (1):1-16. doi: 10.1007/s13225-010-0034-4.

Aly, A. H., Debbab, A., and Proksch, P. 2011. "Fungal endophytes: unique plant inhabitants with great promises." *Appl. Microbiol. Biotechnol.* 90 (6):1829-45. doi: 10.1007/s00253-011-3270-y.

Amslinger, S. 2010. "The tunable functionality of alpha,beta-unsaturated carbonyl compounds enables their differential application in biological systems." *ChemMedChem* 5 (3):351-6. doi: 10.1002/cmdc.200900499.

Araujo, O. E., Flowers, F. P., and King, M. M. 1990. "Griseofulvin: a new look at an old drug." *DICP* 24 (9):851-4. doi: 10.1177/106002809002400912.

Ariantari, N. P., Daletos, G., Mándi, A., Kurtán, T., Müller, W. E. G., Lin, W. H., et al. 2019. "Expanding the chemical diversity of an endophytic fungus *Bulgaria inquinans*, an ascomycete associated with mistletoe, through an OSMAC approach." *RSC Adv.* 9 (43):25119-25132. doi: 10.1039/c9ra03678d.

Barrett, A. G. M., Head, J., Smith, M. L., Stock, N. S., White, A. J. P., and Williams, D. J. 1999. "Fleming−tamao oxidation and masked hydroxyl functionality: total synthesis of (+)-pramanicin and structural elucidation of the antifungal

natural product (−)-pramanicin." *J. Org. Chem.* 64 (16):6005-6018. doi: 10.1021/jo9905672.

Barrett, A. G. M., Smith, M. L., and Stock, N. S. 1999. "Total synthesis of (+)-pramanicin and stereochemical elucidation of the natural product." *Chem. Commum.* (2):133-134. doi: 10.1039/A807988I.

Barrett, D. 2002. "From natural products to clinically useful antifungals." *Biochim. Biophys. Acta* 1587 (2-3):224-33. doi: 10.1016/s0925-4439(02)00085-6.

Bérdy, J. 2005. "Bioactive microbial metabolites." *J Antibiot (Tokyo)* 58 (1):1-26. doi: 10.1038/ja.2005.1.

Berger, G. O., and Tius, M. A. 2005. "Terpestacin core structure. control of stereochemistry." *Org. Lett.* 7 (22):5011-3. doi: 10.1021/ol052015d.

Berger, G. O., and Tius, M. A. 2007. "Total synthesis of (+/-)-terpestacin and (+/-)-11-epi-terpestacin." *J. Org. Chem* 72 (17):6473-80. doi: 10.1021/jo070923d.

Bharate, S. B., Khan, S. I., Yunus, N. A., Chauthe, S. K., Jacob, M. R., Tekwani, B. L., et al. 2007. "Antiprotozoal and antimicrobial activities of O-alkylated and formylated acylphloroglucinols." *Bioorg. Med. Chem.* 15 (1):87-96. doi: 10.1016/j.bmc.2006.10.006.

Bode, H. B., Walker, M., and Zeeck, A. 2000. "Secondary metabolites by chemical screening, 41 - Structure and biosynthesis of mutolide, a novel macrolide from a UV mutant of the fungus F-24'707." *Eur. J. Org. Chem.* 2000 (8):1451-1456.doi:10.1002/(sici)10990690(200004)2000:8<1451::Aidejoc1451>3.0.Co;2-f.

Bode, H. B., Bethe, B., Höfs, R., and Zeeck, A. 2002. "Big effects from small changes: possible ways to explore nature's chemical diversity." *Chembiochem.* 3 (7):619-627. doi: 10.1002/1439-7633(20020703)3:7<619::Aid-cbic619>3.0.Co;2-9.

Bodur, C., Kutuk, O., Karsli-Uzunbas, G., Isimjan, T. T., Harrison, P., and Basaga, H. 2013. "Pramanicin analog induces apoptosis in human colon cancer cells: critical roles for Bcl-2, Bim, and p38 MAPK signaling." *PLoS One* 8 (2):e56369. doi: 10.1371/journal.pone.0056369.

Böhler, P., Stuhldreier, F., Anand, R., Kondadi, A. K., Schlutermann, D., Berleth, N., et al. 2018. "The mycotoxin phomoxanthone A disturbs the form and function of the inner mitochondrial membrane." *Cell Death Dis.* 9 (3):286. doi: 10.1038/s41419-018-0312-8.

Calixto, J. B. 2019. "The role of natural products in modern drug discovery." *An Acad Bras Cienc* 91 Suppl 3:e20190105. doi:10.1590/0001-3765201920190105.

Chahine, E. B., and Nornoo, A. O. 2011. "Ceftobiprole: the first broad-spectrum anti–methicillin-resistant *Staphylococcus aureus* beta-lactam." *J. Exp. Clin. Med.* 3 (1):9-16. doi: 10.1016/j.jecm.2010.12.007.

Chan, J., and Jamison, T. F. 2003. "Synthesis of (-)-terpestacin via catalytic, stereoselective fragment coupling: siccanol is terpestacin, not 11-epi-terpestacin." *J. Am. Chem. Soc.* 125 (38):11514-5. doi: 10.1021/ja0373925.

Chan, J., and Jamison, T. F. 2004. "Enantioselective synthesis of (-)-terpestacin and structural revision of siccanol using catalytic stereoselective fragment couplings and macrocyclizations." *J. Am. Chem. Soc.* 126 (34):10682-91. doi: 10.1021/ja0470968.

Chaudhry, S. B., Veve, M. P., and Wagner, J. L. 2019. "Cephalosporins: a focus on side chains and beta-lactam cross-reactivity." *Pharmacy (Basel)* 7 (3):103. doi: 10.3390/pharmacy7030103.

Chavali, A. K, and Rhee, S. Y. 2017. "Bioinformatics tools for the identification of gene clusters that biosynthesize specialized metabolites." *Briefings Bioinf.* 19 (5):1022-1034. doi: 10.1093/bib/bbx020 %J Briefings in Bioinformatics.

Cimmino, A., Sarrocco, S., Masi, M., Diquattro, S., Evidente, M., Vannacci, G., et al. 2016. "Fusaproliferin, terpestacin and their derivatives display variable allelopathic activity against some ascomycetous fungi." *Chem. Biodivers* 13 (11):1593-1600. doi: 10.1002/cbdv.201600145.

Cow, C., Valentini, D., and Harrison, P. 1997. "Synthesis of the fatty acid of pramanicin." *Can. J. Chem.* 75 (6):884-889. doi: DOI 10.1139/v97-106.

Cragg, G. M., and Newman, D. J. 2013. "Natural products: a continuing source of novel drug leads." *Biochim Biophys Acta.* 1830 (6):3670-95. doi: 10.1016/j.bbagen.2013.02.008.

Darsih, C., Prachyawarakorn, V., Wiyakrutta, S., Mahidol, C., Ruchirawat, S., and Kittakoop, P. 2015. "Cytotoxic metabolites from the endophytic fungus *Penicillium chermesinum*: discovery of a cysteine-targeted Michael acceptor as a pharmacophore for fragment-based drug discovery, bioconjugation and click reactions." *RSC Adv.* 5 (86):70595-70603. doi: 10.1039/c5ra13735g.

Deshmukh, S. K., Gupta, M. K., Prakash, V., and Saxena, S. 2018. "Endophytic fungi: a source of potential antifungal compounds." *J. Fungi (Basel)* 4 (3):77. doi: 10.3390/jof4030077.

Duspara, P., Jenkins, S. I., Hughes, D. W., and Harrison, P. H. M. 1998. "The biosynthesis of pramanicin: intact incorporation of serine and absolute configuration of the antibiotic." *Chem. Commun.* (23):2643-2644. doi: DOI 10.1039/a807401a.

Egamberdieva, D., Wirth, S. J., Alqarawi, A. A., Abd_Allah, E. F., and Hashem, A. 2017. "Phytohormones and beneficial microbes: essential components for plants to balance stress and fitness." *Front. Microbiol.* 8 (2104):2104. doi:10.3389/fmicb.2017.02104.

Ekanayaka, A. H., Dissanayake, A. J., Jayasiri, S. C., To-anun, C., Jones, E. B. G., Zhao, Q., et al. 2016. "*Aplosporella thailandica*; a novel species revealing the

sexual-asexual connection in *Aplosporellaceae* (*Botryosphaeriales*)." *Mycosphere* 7 (4):440-447. doi: 10.5943/mycosphere/7/4/4.

Fan, X. L., Yang, Q., Cao, B., Liang, Y. M., and Tian, C. M. 2015. "New record of *Aplosporella javeedii* on five hosts in China based on multi-gene analysis and morphology." *Mycotaxon* 130 (3):749-756. doi: 10.5248/130.749.

Fouda, A. H., Hassan, S. E., Eid, A. M., and Ewais, E. E. 2015. "Biotechnological applications of fungal endophytes associated with medicinal plant *Asclepias sinaica* (Bioss.)." *Annals of Agricultural Sciences* 60 (1):95-104. doi: 10.1016/j.aoas.2015.04.001.

Gomez, H. J., Cirillo, V. J., and Irvin, J. D. 1985. "Enalapril: a review of human pharmacology." *Drugs* 30 Suppl 1 (1):13-24. doi: 10.2165/00003495-198500301-00004.

Gouda, S., Das, G., Sen, S. K., Shin, H. S., and Patra, J. K. 2016. "Endophytes: a treasure house of bioactive compounds of medicinal importance." *Front. Microbiol.* 7:1538. doi: 10.3389/fmicb.2016.01538.

Grabowski, K., Baringhaus, K. H., and Schneider, G. 2008. "Scaffold diversity of natural products: inspiration for combinatorial library design." *Nat Prod Rep* 25 (5):892-904. doi: 10.1039/b715668p.

Hameed, T. K., and Robinson, J. L. 2002. "Review of the use of cephalosporins in children with anaphylactic reactions from penicillins." *Can J Infect Dis* 13 (4):253-8. doi: 10.1155/2002/712594.

Hamill, R. J. 2013. "Amphotericin B formulations: a comparative review of efficacy and toxicity." *Drugs* 73 (9):919-34. doi: 10.1007/s40265-013-0069-4.

Harrigan, G. G., Armentrout, B. L., Gloer, J. B., and Shearer, C. A. 1995. "Anguillosporal, a new antibacterial and antifungal metabolite from the freshwater fungus *Anguillospora longissima*." *J. Nat. Prod.* 58 (9):1467-9. doi: 10.1021/np50123a022.

Harrison, P. H. M., Duspara, P. A., Jenkins, S. I., Kassam, S. A., Liscombe, D. K., and Hughes, D. W. 2000. "The biosynthesis of pramanicin in *Stagonospora* sp ATCC 74235: a modified acyltetramic acid." *J. Chem. Soc., Perkin Trans. 1* (24):4390-4402. doi: 10.1039/b006007k.

Harrison, P. H. M., Hughes, D. W., and Riddoch, R. W. 1998. "The biosynthesis of pramanicin: origin of the carbon skeleton." *Chem. Commun.* (2):273-274. doi: 10.1039/A706799B.

Hoque, N., Hasan, C. M., Rana, M. S., Varsha, A., Sohrab, M. H., and Rahman, K., M. 2018. "Fusaproliferin, a fungal phytotoxin shows rapid and potent cytotoxicity against pancreatic cancer cell lines." *Molecules* 23: 3288. doi: 10.20944/preprints201810.0375.v1

Hu, H., Wang, Q., and Liu, J. Q. 2014. "Recent advances and future prospects of the important resource plant *Orychophragmus*." 32 (2):189-198. doi: 10.3724/sp.J.1142.2014.20189.

Huo, X., Liu, C., Gao, L., Xu, X., Zhu, N., and Cao, L. 2017. "Hepatoprotective effect of aqueous extract from the seeds of *Orychophragmus violaceus* against liver injury in mice and HepG2 cells." *Int J Mol Sci* 18 (6):1197. doi: 10.3390/ijms18061197.

Ibrahim, S. R. M., Abdallah, H. M., Elkhayat, E. S., Al Musayeib, N. M., Asfour, H. Z., Zayed, M. F., et al. 2018. "Fusaripeptide A: new antifungal and anti-malarial cyclodepsipeptide from the endophytic fungus *Fusarium* sp." *J Asian Nat Prod Res* 20 (1):75-85. doi: 10.1080/10286020.2017.1320989.

Iimura, S., Oka, M., Narita, Y., Konishi, M., Kakisawa, H., Gao, Q., et al. 1993. "Terpestacin, a novel syncytium formation inhibitor, isolated from *Arthrinium* species." *Tetrahedron Lett.* 34 (3):493-496. doi: 10.1016/0040-4039(93)85110-I.

Jami, F., Slippers, B., Wingfield, M. J., and Gryzenhout, M. 2014. "Botryosphaeriaceae species overlap on four unrelated, native South African hosts." *Fungal Biol* 118 (2):168-79. doi: 10.1016/j.funbio.2013.11.007.

Jia, H. Q., Liu, Z. X., Sungbom, O., Yao, C. H., Chen, J., Dong, A. R., et al. 2019. "First report of *Aplosporella javeedii* causing branch blight disease of *Mulberry* (*Morus alba*) in China." *J. Plant Dis. Prot.* 126 (5):475-477. doi: 10.1007/s41348-019-00245-5.

Jia, M., Chen, L., Xin, H. L., Zheng, C. J., Rahman, K., Han, T., et al. 2016. "A friendly relationship between endophytic fungi and medicinal plants: A systematic review."*Front. Microbiol.* 7:906. doi: 10.3389/fmicb.2016.00906.

Jordan, M. A., and Wilson, L. 2004. "Microtubules as a target for anticancer drugs." *Nat Rev Cancer* 4 (4):253-65. doi: 10.1038/nrc1317.

Jung, H. J., Lee, H. B., Kim, C. J., Rho, J. R., Shin, J. H., and Kwon, H. J. 2003. "Anti-angiogenic activity of terpestacin, a bicyclo sesterterpene from *Embellisia chlangdospora*." *J. Antibiot.* 56 (5):492-496. doi: 10.7164/antibiotics.56.492.

Jung, H. J., Shim, J. S., Lee, J., Song, Y. M., Park, K. C., Choi, S. H., et al. 2010. "Terpestacin inhibits tumor angiogenesis by targeting UQCRB of mitochondrial complex III and suppressing hypoxia-induced reactive oxygen species production and cellular oxygen sensing." *J Biol Chem* 285 (15):11584-95. doi: 10.1074/jbc.M109.087809.

Kanoh, K., Kohno, S., Asari, T., Harada, T., Katada, J., Muramatsu, M., et al. 1997. "(−)-Phenylahistin: A new mammalian cell cycle inhibitor produced by *aspergillus ustus*." *Bioorg. Med. Chem. Lett.* 7 (22):2847-2852. doi: 10.1016/s0960-894x(97)10104-4.

Khan, R. A. 2018. "Natural products chemistry: The emerging trends and prospective goals." *Saudi Pharm J* 26 (5):739-753. doi: 10.1016/j.jsps.2018.02.015.

Khare, E., Mishra, J., and Arora, N. K. 2018. "Multifaceted interactions between endophytes and plant: Developments and prospects." *Front. Microbiol.* 9:2732. doi: 10.3389/fmicb.2018.02732.

Khiralla, A., Rosella, S., Yagi, S., Mohamed, I., and Dominique L. M. 2016. "Endophytic fungi: occurrence, classification, function and natural products." In. editor, Evelyn Hughes. New York : Nova Science Publisher's, Inc., ISBN 9781536103588

Kishore, S. P., Blank, E., Heller. D. J., Patel, A., Peters, A., Price, M., et al. 2018. "Modernizing the World Health Organization list of essential medicines for preventing and controlling cardiovascular diseases." *J Am Coll Cardiol* 71 (5):564-574. doi: 10.1016/j.jacc.2017.11.056.

Klayman, D. L. 1985. "Qinghaosu (artemisinin): an antimalarial drug from China." *Science* 228 (4703):1049-55. doi: 10.1126/science.3887571.

Kumar, A., Patil, D., Rajamohanan, P. R., and Ahmad, A. 2013. "Isolation, purification and characterization of vinblastine and vincristine from endophytic fungus *Fusarium oxysporum* isolated from *Catharanthus roseus*." *PLoS One* 8 (9):e71805. doi: 10.1371/journal.pone.0071805.

Kusari, S., Zuhlke, S., and Spiteller, M. 2009. "An endophytic fungus from *Camptotheca acuminata* that produces camptothecin and analogues." *J Nat Prod* 72 (1):2-7. doi: 10.1021/np800455b.

Kutuk, O., Pedrech, A., Harrison, P., and Basaga, H. 2005. "Pramanicin induces apoptosis in Jurkat leukemia cells: a role for JNK, p38 and caspase activation." *Apoptosis* 10 (3):597-609. doi: 10.1007/s10495-005-1894-z.

Kwan, C. Y., Harrison, P. H., Duspara, P. A., and Daniel, E. E. 2001. "Vasorelaxant effects of pramanicin, an anti-fungal agent: selective action on endothelial cells." *Jpn J Pharmacol* 85 (3):234-40. doi: 10.1254/jjp.85.234.

Kwan, C. Y., Harrison, P. H., and Kwan, T. K. 2003. "Pramanicin, an antifungal agent, raises cytosolic Ca^{2+} and causes cell death in vascular endothelial cells." *Vascul Pharmacol* 40 (1):35-42. doi: 10.1016/s1537-1891(02)00314-2.

Kwan, C. Y., Zhang, W. B., Miller, J., Harrison, P. H., Kassan, S., and Liscombe, D. 2003. "The epoxy group of pramanicin is required for the optimal endothelium-dependent relaxation of rat aorta." *J Pharmacol Sci* 92 (3):203-8. doi: 10.1254/jphs.92.203.

Li, L., Jiang, W., and Lu, Y. 2017. "New strategies and approaches for engineering biosynthetic gene clusters of microbial natural products." *Biotechnol Adv* 35 (8):936-949. doi: 10.1016/j.biotechadv.2017.03.007.

Li, W., Ding, L., Wang, N., Xu, J., Zhang, W., Zhang, B.,et al. 2019. "Isolation and characterization of two new metabolites from the sponge-derived fungus *Aspergillus* sp. LS34 by OSMAC approach." *Mar Drugs* 17 (5):283. doi: 10.3390/md17050283.

Lim, C. M. 1995. "Isolation and structure elucidation fo terpenoid phytotoxins produced by the plant pathogenic fungus *Bipolaris cynodontis*." *Abstracts of Papers of 37th Symposium on the Chemistry of Natural Products.*:325-330.

Liu, S., Dai, H., Makhloufi, G., Heering, C., Janiak, C., Hartmann, R., et al. 2016. "Cytotoxic 14-membered macrolides from a mangrove-derived endophytic fungus, *Pestalotiopsis microspora*." *J Nat Prod* 79 (9):2332-40. doi: 10.1021/acs.jnatprod.6b00473.

Lobanovska, M., and Pilla, G. 2017. "Penicillin's discovery and antibiotic resistance: lessons for the future?" *Yale J Biol Med* 90 (1):135-145.

Logrieco, A., Moretti, A., Fornelli, F., Fogliano, V., Ritieni, A., Caiaffa, M. F., et al. 1996. "Fusaproliferin production by *Fusarium subglutinans* and its toxicity to *Artemia salina*, SF-9 insect cells, and IARC/LCL 171 human B lymphocytes." *Appl Environ Microbiol* 62 (9):3378-84. doi: 10.1128/AEM.62.9.3378-3384.1996.

Medicinal Plant Images Database. 2007. School of Chinese Medicine. Hong Kong Baptist University. http://libproject.hkbu.edu.hk.

Miller, A. S., and Wilmott, R. W. 2019. "31 - The Pulmonary Mycoses." In *Kendig's Disorders of the Respiratory Tract in Children (Ninth Edition)*, edited by Wilmott, R. W., Deterding, R., Li, A., Ratjen, F., Sly, P., Zar, H. J. and Bush, A. 507-527.e3. Philadelphia: Content Repository

Miller, E. L. 2002. "The penicillins: a review and update." *J Midwifery Womens Health* 47 (6):426-34. doi: 10.1016/s1526-9523(02)00330-6.

Mizobuchi, S., and Sato, Y. 1985. "Antifungal activity of 2,4-dihydroxyacylophenones and related-compounds." *Agric. Biol. Chem.* 49 (5):1327-1333. doi: 10.1080/00021369.1985.10866924.

Newman, D. J., and Cragg, G. M. 2020. "Natural products as sources of new drugs over the nearly four decades from 01/1981 to 09/2019." *J Nat Prod* 83 (3):770-803. doi: 10.1021/acs.jnatprod.9b01285.

Newman, D. J., Cragg, G. M., and Grothaus, P. G. 2017. "Natural products of the rhizosphere and its microorganisms." *Chem. Biol. Nat. Prod.*, 285-331. doi: 10.1201/9781315117089-9

Nicholson, B., Lloyd, G. K., Miller, B. R., Palladino, M. A., Kiso, Y., Hayashi, Y., et al. 2006. "NPI-2358 is a tubulin-depolymerizing agent: in-vitro evidence for activity as a tumor vascular-disrupting agent." *Anticancer Drugs* 17 (1):25-31. doi: 10.1097/01.cad.0000182745.01612.8a.

Noor, A. O., Almasri, D. M., Bagalagel, A. A., Abdallah, H. M., Mohamed, S. G. A., Mohamed, G. A., et al. 2020. "Naturally occurring isocoumarins derivatives from endophytic fungi: sources, isolation, structural characterization, biosynthesis, and biological activities." *Molecules* 25 (2):395. doi: 10.3390/molecules25020395.

Oka, M., Iimura, S., Narita, Y., Furumai, T., Konishi, M., Oki, T., et al. 1993. "Stereochemistry and biosynthesis of terpestacin, a new syncytium formation inhibitor." *J. Org. Chem.* 58 (7):1875-1881. doi: 10.1021/jo00059a045.

Oka, M., Iimura, S., Tenmyo, O., Sawada, Y., Sugawara, M., Ohkusa, N., et al. 1993. "Terpestacin, a new syncytium formation inhibitor from *Arthrinium* sp." *J Antibiot (Tokyo)* 46 (3):367-73. doi: 10.7164/antibiotics.46.367.

Opie, L. H., and Kowolik, H. 1995. "The discovery of captopril: from large animals to small molecules." *Cardiovasc Res* 30 (1):18-25. doi: 10.1016/s0008-6363(95)00006-2.

Pan, R., Bai, X., Chen, J., Zhang, H., and Wang, H. 2019. "Exploring structural diversity of microbe secondary metabolites using OSMAC strategy: a literature review." *Front. Microbiol.* 10:294. doi: 10.3389/fmicb.2019.00294.

Park, K. C., and Choi, S. H. 2013. "Effects of endostatin and a new drug terpestacin against human neuroblastoma xenograft and cell lines." *Pediatr Surg Int* 29 (12):1327-40. doi: 10.1007/s00383-013-3398-1.

Patil, R. H., Patil, M. P., and Maheshwari, V. L. 2016. "Bioactive secondary metabolites from endophytic fungi." In *Studies in Natural Products Chemistry*, Volume 49, edited by Rahman Atta ur, 189-205. Elsevier.

Perfect, J. R. 2017. "The antifungal pipeline: a reality check." *Nat Rev Drug Discov* 16 (9):603-616. doi: 10.1038/nrd.2017.46.

Phaopongthai, J., Wiyakrutta, S., Meksuriyen, D., Sriubolmas, N., and Suwanborirux, K. 2013. "Azole-synergistic anti-candidal activity of altenusin,

a biphenyl metabolite of the endophytic fungus *Alternaria alternata* isolated from *Terminalia chebula* Retz." *J Microbiol* 51 (6):821-8. doi: 10.1007/s12275-013-3189-3.

Rehberg, N., Akone, H. S., Ioerger, T. R., Erlenkamp, G., Daletos, G., Gohlke, H., et al. 2018. "Chlorflavonin targets acetohydroxyacid synthase catalytic subunit IlvB1 for synergistic killing of *Mycobacterium tuberculosis*." *ACS Infect Dis* 4 (2):123-134. doi: 10.1021/acsinfecdis.7b00055.

Ritieni, A., Fogliano, V., Randazzo, G., Scarallo, A., Logrieco, A., Moretti, A., et al. 1995. "Isolation and characterization of fusaproliferin, a new toxic metabolite from *Fusarium proliferatum*." *Nat Toxins* 3 (1):17-20. doi: 10.1002/nt.2620030105.

Ritieni, A., Monti, S. M., Randazzo, G., Logrieco, A., Moretti, A., Peluso, G., et al. 1997. "Teratogenic effects of fusaproliferin on chicken embryos." *J. Agric. Food Chem.* 45 (8):3039-3043. doi:10.1021/jf960890v.

Rönsberg, D., Debbab, A., Mándi, A., Vasylyeva, V., Böhler, P., Stork, B., et al. 2013. "Pro-apoptotic and immunostimulatory tetrahydroxanthone dimers from the endophytic fungus *Phomopsis longicolla*." *J Org Chem* 78 (24):12409-25. doi: 10.1021/jo402066b.

Santini, A., Ritieni, A., Fogliano, V., Randazzo, G., Mannina, L., Logrieco, A., et al. 1996. "Structure and absolute stereochemistry of fusaproliferin, a toxic metabolite from *Fusarium proliferatum*." *J Nat Prod* 59 (2):109-12. doi: 10.1021/np960023k.

Saxena, S., Chhibber, M., and Singh, I. P. 2019. "Fungal bioactive compounds in pharmaceutical research and development." *Curr. Bioact. Compd.* 15 (2):211-231. doi: 10.2174/1573407214666180622104720.

Schwartz, R. E., Helms, G. L., Bolessa, E. A., Wilson, K. E., Giacobbe, R. A., Tkacz, J. S., et al. 1994. "Pramanicin, a novel antimicrobial agent from a fungal

fermentation." *Tetrahedron* 50 (6):1675-1686. doi:10.1016/S0040-4020(01)80843-7.

Shah, M., Deshmukh, S. K., Verekar, S. A., Gohil, A., Kate, A. S., Rekha, V., et al. 2015. "Anti-inflammatory properties of mutolide isolated from the fungus *Lepidosphaeria species* (PM0651419)." *Springerplus* 4 (1):706. doi: 10.1186/s40064-015-1493-6.

Shi, W., Dan, W. J., Tang, J. J., Zhang, Y., Nandinsuren, T., Zhang, A. L., et al. 2016. "Natural products as sources of new fungicides (III): Antifungal activity of 2,4-dihydroxy-5-methylacetophenone derivatives." *Bioorg Med Chem Lett* 26 (9):2156-8. doi: 10.1016/j.bmcl.2016.03.073.

Shukla, S., Habbu, P., Kulkarni, V. H., Jagadish, K., Pandey, A., and Sutariya, V. 2014. "Endophytic microbes: A novel source for biologically/pharmacologically active secondary metabolites." *Asian Journal of Pharmacology and Toxicology* 02:1-16.

Slippers, B., Boissin, E., Phillips, A. J., Groenewald, J. Z., Lombard, L., Wingfield, M. J., et al. 2013. "Phylogenetic lineages in the *Botryosphaeriales*: a systematic and evolutionary framework." *Stud Mycol* 76 (1):31-49. doi: 10.3114/sim0020.

Slippers, B., and Wingfield, M. J. 2007. "*Botryosphaeriaceae* as endophytes and latent pathogens of woody plants: diversity, ecology and impact." *Fungal Biology Reviews* 21 (2-3):90-106. doi: 10.1016/j.fbr.2007.06.002.

Stierle, A., Strobel, G., and Stierle, D. 1993. "Taxol and taxane production by *Taxomyces andreanae*, an endophytic fungus of *Pacific yew*." *Science* 260 (5105):214-6. doi: 10.1126/science.8097061.

Strobel, G. 2018. "The emergence of endophytic microbes and their biological promise." *J. Fungi* 4 (2):57. doi:10.3390/jof4020057.

Strobel, G., and Daisy, B. 2003. "Bioprospecting for microbial endophytes and their natural products." *Microbiol. Mol. Biol. Rev.* 67 (4):491-502. doi: 10.1128/Mmbr.67.4.491-502.2003.

Subban, K., Subramani, R., and Johnpaul, M. 2013. "A novel antibacterial and antifungal phenolic compound from the endophytic fungus *Pestalotiopsis mangiferae*." *Nat Prod Res* 27 (16):1445-9. doi: 10.1080/14786419.2012.722091.

Thomford, N. E., Senthebane, D. A., Rowe, A., Munro, D., Seele, P., Maroyi, A., et al. 2018. "Natural products for drug discovery in the 21st century: Innovations for novel drug discovery." *Int J Mol Sci* 19 (6):1578. doi: 10.3390/ijms19061578.

Tobert, J. A. 2003. "Lovastatin and beyond: the history of the HMG-CoA reductase inhibitors." *Nat Rev Drug Discov* 2 (7):517-26. 10.1038/nrd1112.

Torres, M., and White, J. 2012. "Endophytic Fungi." doi: 10.13140/2.1.3835.2169

Tran-Cong, N. M., Mándi, A., Kurtán, T., Müller, W. E. G., Kalscheuer, R., Lin, W. H., et al. 2019. "Induction of cryptic metabolites of the endophytic fungus *Trichocladium* sp. through OSMAC and co-cultivation." *RSC Adv.* 9 (47):27279-27288. doi: 10.1039/c9ra05469c.

Van Lanen, S. G., and Shen, B. 2006. "Microbial genomics for the improvement of natural product discovery." *Curr Opin Microbiol* 9 (3):252-60. doi: 10.1016/j.mib.2006.04.002.

Venieraki, A., Dimou, M., and Katinakis, P. 2017. "Endophytic fungi residing in medicinal plants have the ability to produce the same or similar pharmacologically active secondary metabolites as their hosts." *Hellenic Plant Protection Journal* 10 (2):51-66. doi: 10.1515/hppj-2017-0006.

Verma, V. C., Kharwar, R. N., and Strobel, G. A. 2009. "Chemical and functional diversity of natural products from plant associated endophytic fungi." *Nat Prod Commun* 4 (11):1511-32.

Wang, C. Y., Engelke, L., Bickel, D., Hamacher, A., Frank, M., Proksch, P., et al. 2019. "The tetrahydroxanthone-dimer phomoxanthone A is a strong inducer of apoptosis in cisplatin-resistant solid cancer cells." *Bioorg. Med. Chem.* 27 (19):115044. doi:10.1016/j.bmc.2019.115044.

Wang, H., Eze, P. M., Höfert, S. P., Janiak, C., Hartmann, R., Okoye, F. B. C., et al. 2018. "Substituted L-tryptophan-L-phenyllactic acid conjugates produced by an endophytic fungus *Aspergillus aculeatus* using an OSMAC approach." *RSC Adv.* 8 (14):7863-7872. doi: 10.1039/c8ra00200b.

Wu, S. H., He, J., Li, X. N., Huang, R., Song, F., Chen, Y. W., et al. 2014. "Guaiane sesquiterpenes and isopimarane diterpenes from an endophytic fungus *Xylaria* sp." *Phytochemistry* 105:197-204. doi: 10.1016/j.phytochem.2014.04.016.

Yan, L., Zhu, J., Zhao, X., Shi, J., Jiang, C., and Shao, D. 2019. "Beneficial effects of endophytic fungi colonization on plants." *Appl Microbiol Biotechnol* 103 (8):3327-3340. doi: 10.1007/s00253-019-09713-2.

Yu, H. F., Qiu, F. J., Wang, Y. J., Li, Y. Y., Fang, L., Yao, J. B., et al. 2018. "Induced production of furan derivatives in a fungal endophyte *Ceriporia lacerate* HS-ZJUT-C13A by the Osmac method." *Chem. Nat. Compd.* 54 (3):450-454. doi: 10.1007/s10600-018-2377-0.

Yuan, H., Ma, Q., Ye, L., and Piao, G. 2016. "The traditional medicine and modern medicine from natural products." *Molecules* 21 (5):559. doi: 10.3390/molecules21050559.

Zacchino, S. A., Butassi, E., Liberto, M. D., Raimondi, M., Postigo, A., and Sortino, M. 2017. "Plant phenolics and terpenoids as adjuvants of antibacterial and

antifungal drugs." *Phytomedicine* 37:27-48. doi:10.1016/j.phymed. 2017.10.018.

Zhang, M. M., Qiao, Y., Ang, E. L., and Zhao, H. 2017. "Using natural products for drug discovery: the impact of the genomics era." *Expert Opin Drug Discov* 12 (5):475-487. doi: 10.1080/17460441.2017.1303478.

Zheng, Y. G., Wu, J., Chen, Z., and Goodman, M. 2008. "Chemical regulation of epigenetic modifications: opportunities for new cancer therapy." *Med Res Rev* 28 (5):645-87. doi: 10.1002/med.20120.

Zhou, L. R., Wu, J., and Wang, S. 2011. "Orychophragmus." In *Wild Crop Relatives: Genomic and Breeding Resources*, edited by Chittaranjan Kole, 199-225. Berlin, Heidelberg: Springer Berlin Heidelberg.

Zhu, H. Y., Tian, C. M., and Fan, X. L.. 2018. "Studies of botryosphaerialean fungi associated with canker and dieback of tree hosts in Dongling Mountain of China." *Phytotaxa* 348 (2):63-76. doi: 10.11646/phytotaxa.348.2.1.

List of abbreviations

$(NH_4)_2SO_4$	Ammonium sulfate
$[\alpha]_D$	Specific rotation at the sodium D-line
br	Broad
$C_5H_8NNaO_4 \cdot H_2O$	Monosodium glutamate
CD_3OD	Deuterated methanol
$CDCl_3$	Deuterated chloroform
CH_2Cl_2	Dichloromethane
COSY	Correlation spectroscopy
d	Doublet signal
dd	Doublet of doublet signal
ddd	Doublet of doublet of doublet signal
DFT	Density functional theory
DMSO	Dimethyl sulfoxide
DNA	Deoxyribonucleic acid
e. g.	Exempli gratia (for the sake of example)
ECD	Equivalent circulating density
et al.	et altera (and others)
EtOAc	Ethyl acetate
FDA	Food and drug administration
$FeSO_4$	Iron(II) sulfate
FUS	Fusaproliferin
h	Hour
HMBC	Heteronuclear multiple bond connectivity
HPLC	High performance liquid chromatography
HRESIMS	High resolution electrospray ionisation mass
HSQC	Heteronuclear single quantum coherence spectroscopy
IC_{50}	Half maximal inhibitory concentration
JNK	C-jun N-terminal kinase
$K_2HPO_4 \cdot 3H_2O$	Potassium phosphate dibasic trihydrate
KCl	Potassium chloride
KH_2PO_4	Potassium dihydrogen phosphate
L	Liter
m	Multiplet signal
M	Mole
m/z	Mass per charge
MeCN	Acetonitrile
MeOH	Methanol

mg	Milligram
$MgSO_4$	Magnesium sulfate
MHz	Mega Herz
MIC	Minimum inhibitory concentration
min	Minute
mL	Milliliter
mm	Millimeter
MMFF	Merck molecular force field
MRSA	Methicillin-resistant *Staphylococcus aureus*
MS	Mass spectrometry
MW	Molecular weight
Na_2HPO_4	Sodium phosphate dibasic
NaBr	Sodium bromide
NaCl	Sodium chloride
NaF	Sodium fluoride
NaI	Sodium iodide
$NaNO_3$	Sodium nitrate
NaOH	Sodium hydroxide
NH_4Cl	Ammonium chloride
nm	Nanometer
NMR	Nuclear magnetic resonance spectrometry
OSMAC	One Strain MAny Compounds
PARP1	Poly [ADP-ribose] polymerase 1
PDB	Potato dextrose broth
ppm	Parts per million
ROESY	Rotating frame overhauser effect spectroscopy
RP 18	Reversed phase C18
s	Singlet signal
SAR	structure-activity relationship
SOR	Specific optical rotation
sp.	Species
t	Triplet signal
TCM	Traditional chinese medicine
TDDFT-ECD	Time-dependent density functional theory electronic circular dichroism
TLC	Thin layer chromatography
UV	Ultra-violet
VLC	Vacuum liquid chromatography
$ZnSO_4$	Zinc sulfate
μM	Micromolar

Acknowledgements

First of all, I would like to express my deepest appreciation to Prof. Dr. Dres. h.c. Peter Proksch for giving me this precious opportunity to pursue my doctoral research on fungal secondary metabolites in such excellent working conditions and good facilities at the Institute of Pharmaceutical Biology and Biotechnology of Heinrich Heine University, Düsseldorf. His profound knowledge, patient guidance, scientific advice and comprehensive support have greatly helped me successfully complete the research and learn a lot of new knowledge. Moreover, his serious and responsible work attitude, meticulous scientific research spirit, and sincere belief in the pursuit of truth are the models for me to learn throughout my life.

I would like to express my sincere gratitude to Prof. Dr. Rainer Kalscheuer (Institute of Pharmaceutical Biology and Biotechnology, Heinrich Heine University, Düsseldorf) as my co-supervisor to provide the support for antimicrobial assays. I want to thank Mrs. Heike Goldbach-Gecke and Mr. Lin Wang for their helping in performing antimicrobial experiments.

I am heavily indebted to postdoctoral Dr. Yang Liu (Institute for Insect Biotechnology, Justus-Liebig-University of Giessen) for introducing me to Prof. Dr. Dres. h.c. Peter Proksch and for her scientific guidance and kind help during my study. She is not only a former colleague but also a best friend of all my family.

My deep thanks to postdoctoral Dr. Zhen Liu for his valuable suggestion, fruitful discussion and rich knowledge in the experimental operation, structure elucidation and manuscript preparation.

My special thanks to postdoctoral Dr. Marian Frank for his extensive knowledge, scientific guidance and his kind help on German communication with other research groups. At the same time, I am deeply grateful to him for his suggestions and revisions to my dissertation.

I wish to appreciate Dr. Haiqian Yu, Dr. Hao Wang, Dr. Georgios Daletos, Dr. Nam Michael Tran-Cong, Ms. Xiaoqin Yu, for their generous help and fruitful discussions.

I would like to convey my cordial thanks to Ms. Claudia Eckelskemper, Mrs. Simone Miljanovic, Mrs. Katja Friedrich, Mrs. Eva Müller, Mrs. Simone Mönninghoff-Pützer, Ms. Linda Weigand, Mrs. Waltraud Schlag, and Mrs. Maryam Masrouri, for their warm-hearted help and friendly support.

I would like to sincerely thank all my colleagues and friends for their meticulous care and enthusiastic help, as well as the warm atmosphere that we have formed in our work: Dr. Elena Ancheeva, Dr. Ni Putu Ariantari, Dr. Harowoko, Dr. Mariam Moussa, Dr. Daowan Lai, Prof. Han Xiao, Dr. Chenyin Wang, Dr. Ramsay Kadeem, Dr. Sergi Herve Akone, Dr. Weaam Ebrahim, Dr. Shuai Liu, Dr. Amin Mokhlesi, Dr. Feng Pan, Dr. Ferhat Oezkaya, Dr. Festus Okoye, Dr. Peter Eze, Ms. Dina Elkashef, Ms. Kim Thao Lee, Mr. Lei Wang, Ms. Miada Sakr, Ms. Nada Mohamed, Ms. Nihal Aktas, Mr. Tino Seidemann.

My sincere thanks to the Jürgen Manchot Foundation for the financial support during my study.

In the end, I would like to express my heartfelt thanks to my family for their encouragement, understanding and full support. Thanks to my husband for his continuous support and encouragement. Thank my dear parents and parents-in-law for their understanding and dedication. Finally, I want to dedicate this achievement to my daughter. She is my little sun and inspires me to keep going.

Curriculum vitae

- **Name:** Ying Gao

- **Nationality:** Chinese

- **Address**: Institute of Pharmaceutical Biology and Biotechnology, Heinrich Heine University, 40225, Düsseldorf,

- **E-mail Address**: Ying.Gao@hhu.de, gaoying446@gmail.com

- **Educational Backgrounds**

  - 02.2017-present: Doctoral candidate in Pharmacy, Pharmaceutical Biology and Biotechnology Institute, Heinrich Heine University Düsseldorf, Germany. Supervisor: Prof. Dr. Dres. h.c. Peter Proksch

  - 09.2007-07.2010: Master in Pharmaceutics of Chinese Materia Medica, School of Chinese Materia Medica, Beijing University of Chinese Medicine. Supervisor: Prof. Dr. Shouying Du

  - 09.2003-07.2007: Bachelor in Chinese Materia Medica, School of Chinese Materia Medica, Beijing University of Chinese Medicine. Supervisor: Prof. Dr. Shouying Du

- **Employment Record**

  - 08.2010-12.2017: Pharmacy Department of Shunyi Hospital, Beijing Traditional Chinese Medicine Hospital

- **Publications:**

1. **Ying Gao**, Fabian Stuhldreier, Laura Schmitt, Sebastian Wesselborg, Zhiyong Guo, Kun Zou, Attila Mándi, Tibor Kurtán, Zhen Liu, and Peter Proksch (2020) Induction of New Lactam Derivatives from the Endophytic Fungus *Aplosporella javeedii* through an OSMAC Approach. *Frontiers in Microbiology,* 11, 600983.

2. **Ying Gao**, Lin Wang, Rainer Kalscheuer, Zhen Liu, and Peter Proksch (2020) Antifungal polyketide derivatives from the endophytic fungus *Aplosporella javeedii*. *Bioorganic & Medicinal Chemistry*, 28, 115456.

3. **Ying Gao**, Fabian Stuhldreier, Laura Schmitt, Sebastian Wesselborg, Lin Wang, Werner E. G. Müller, Rainer Kalscheuer, Zhiyong Guo, Kun Zou, Zhen Liu, Peter Proksch (2020) Sesterterpenes and macrolide derivatives from the endophytic fungus *Aplosporella javeedii*. *Fitoterapia*, 146, 104652.

4. Xiaoqin Yu, **Ying Gao**, Marian Frank, Attila Mándi, Tibor Kurtán, Werner E. G. Müller, Rainer Kalscheuer, Zhiyong Guo, Kun Zou, Zhen Liu, Peter Proksch (2020) Induction of ambuic acid derivatives by the endophytic fungus *Pestalotiopsis lespedezae* through an OSMAC approach. *Tetrahedron*, 79, 131876.

5. Zhen Liu, Marian Frank, Xiaoqin Yu, Haiqian Yu, Nam M. Tran-Cong, **Ying Gao**, Peter Proksch (2020) Secondary Metabolites from Marine-Derived Fungi from China. In: Kinghorn A., Falk H., Gibbons S., Kobayashi J., Asakawa Y., Liu JK. (eds) Progress in the Chemistry of Organic Natural Products 111. *Progress in the Chemistry of Organic Natural Products*, vol 111. Springer, Cham.

- **Honors:**

  Granted a doctoral scholarship from the Jürgen Manchot Foundation in Germany